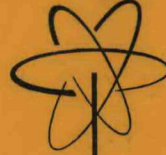RECEIVED BY DTIE MAY 27 1970

GEAP-13588
AEC RESEARCH AND
DEVELOPMENT REPORT
MARCH 1970

MASTER

RESULTS OF SEFOR ZERO POWER EXPERIMENTS

U.S. ATOMIC ENERGY COMMISSION
CONTRACT AT(04-3)-540

GENERAL ⊕ ELECTRIC

DISCLAIMER

This report was prepared as an account of work sponsored by an agency of the United States Government. Neither the United States Government nor any agency Thereof, nor any of their employees, makes any warranty, express or implied, or assumes any legal liability or responsibility for the accuracy, completeness, or usefulness of any information, apparatus, product, or process disclosed, or represents that its use would not infringe privately owned rights. Reference herein to any specific commercial product, process, or service by trade name, trademark, manufacturer, or otherwise does not necessarily constitute or imply its endorsement, recommendation, or favoring by the United States Government or any agency thereof. The views and opinions of authors expressed herein do not necessarily state or reflect those of the United States Government or any agency thereof.

DISCLAIMER

Portions of this document may be illegible in electronic image products. Images are produced from the best available original document.
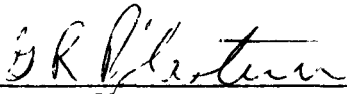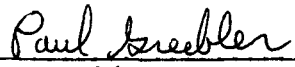
RESULTS OF SEFOR ZERO POWER EXPERIMENTS

AUTHORS

L. D. Noble
F. Mitzel*
B. Sarma
D. Wintzer*
Y. S. Lu
G. Kessler*
G. R. Pflasterer
R. A. Becker
L. Mansur+

APPROVED:

G. R. Pflasterer, Project Engineer
SEFOR Research and Development Program
Breeder Reactor Development Operation

P. Greebler, Manager
Nuclear Engineering Subsection

LEGAL NOTICE

ABSTRACT

The SEFOR experimental program is comprised of a series of tests
beginning with low power tests, proceeding through static and frequency
response tests at various power levels up to full power, and culminating
in a series of sub-prompt and super-prompt critical transients.

The results of the low (zero) power tests are reported here and
are compared with calculations. The agreement between experiment and
calculation is generally good. The tests were conducted at low power
and included such experiments as the approach to the minimum critical
core size, calibration of the reflector control, measurement of fission
rate distributions, material reactivity worth measurements, uniform
non-nuclear heating of the reactor to determine the reactivity temp-
erature coefficient, and the measurement of the ratio (ℓ/β) of the
prompt neutron lifetime to the effective delayed neutron fraction.

CONTENTS

CONTENTS (Continued

CONTENTS (Continued)

LIST OF ILLUSTRATIONS

LIST OF ILLUSTRATIONS (Continued)

LIST OF ILLUSTRATIONS (Continued)

LIST OF ILLUSTRATIONS (Continued)

LIST OF ILLUSTRATIONS (Continued

LIST OF TABLES

LIST OF TABLES (Continued)

LIST OF TABLES (Continued)

LIST OF TABLES (Continued)

INTRODUCTION, SUMMARY OF RESULTS, AND SEQUENCE OF MEASUREMENTS

1.1 INTRODUCTION

The Southwest Experimental Fast Oxide Reactor (SEFOR) is a 20 MW(t) fast spectrum reactor fueled with mixed PuO_2 - UO_2 and cooled with sodium. SEFOR has characteristics similar to large, soft spectrum, fast breeder reactors fueled with mixed PuO_2 - UO_2 for economic electrical power generation. SEFOR will be used to obtain physics and engineering data at fuel compositions, temperatures, and crystalline states characteristic of power reactor operating conditions. SEFOR is particularly designed for the systematic determination of the Doppler coefficient of reactivity at temperatures up to the vicinity of fuel melting.

The SEFOR Project consists of two major parts: the design and construction of the reactor and a related research and development program. Funds for the design and construction of the facility are being provided by the Southwest Atomic Energy Associates (a group of seventeen investor-owned utility companies located in the South and Southwest part of the United States), together with the Karlsruhe Laboratory of the Federal Republic of Germany, Euratom, and the General Electric Company.

The United States Atomic Energy Commission is supporting the research and development program. The R and D Program consists of two phases:

        Phase I   - Pre-Operational Research and Development
        Phase II - Post Construction Research and Development

Work performed in Phase I of the program under Task 1, planning the

experimental program, has been reported in references 1 through 4.
The SEFOR facility is described in references 5 and 6, and the physics
design of the core is described in references 6 through 9.

This report describes work performed in Phase II of the program
under Task 10.3, Wet Critical Tests. The purpose of Task 10.3 is to
determine such information as the minimum critical mass of the core,
reflector control calibration data, material reactivity worths at
various radial distances from the core center, and low power reactivity
temperature coefficients.

1.2   SUMMARY OF RESULTS

Agreement between experiment and calculation is generally good.
Representative results are summarized in Table 1-1. The minimum
critical core fuel loading (284 Kg fissile Pu) was predicted[10] to
within 0.2% (1 fuel rod), and the magnitude of the reflector control
strength ($\sim$10$) is within the predicted[10] range of 11.2 $\pm$ 1.8$.
The measured ratio of ℓ/β, 2.0 X 10^{-4} seconds, is about 10% higher than
the calculated value and is in agreement with similar comparisons of
experiment and calculation in the SEFOR critical assembly mockup in
ZPR-III[11]. Measured and calculated reactivity worths of fuel and
B_4C rods agreed within 10 to 15%, with the largest disparities
occurring near the core center, while the experimental fission rate
distributions agree with the calculations throughout most of the core,
but show deviations as large as 25% near the core boundaries. These
disparities indicate that the flux distributions (and consequently
the temperature distributions which will occur during operation at
power) may be somewhat flatter than calculated. The Doppler coefficient
is relatively insensitive[8,12] to the spatial temperature and flux
distribution however, and calculations which might give better agreement

TABLE 1-1

REPRESENTATIVE ZERO POWER TEST RESULTS

Experiment	Measured	Calculated
Minimum Critical Core Size (Mass of Pu-239 + Pu-241)	284.3 Kg	284.9 Kg
Reflector Control Strength	9.7\$	11.2\$
Ratio (ℓ/β) of neutron lifetime-to effective delayed neutron fraction.	2.0×10^{-4} sec	1.8×10^{-4} sec
Fuel Rod Worth near core center	+35¢	+40¢
B_4C Rod Worth near core center	−71¢	−82¢
Fission Ratios near Core Center		
$\sigma_f^{238}/\sigma_f^{235}$	0.0252	0.0256
$\sigma_f^{239}/\sigma_f^{235}$	0.905	0.894
Flow and pressure coefficients of reactivity	0	0
Uniform Temperature coefficient of reactivity in the following temperature ranges		
350°F to 450°F	−0.67¢/°F	−0.66¢/°F*
450°F to 550°F	−0.64¢/°F	−0.63¢/°F*
550°F to 650°F	−0.60¢/°F	−0.61¢/°F*
650°F to 760°F	−0.57¢/°F	−0.58¢/°F*

---

*The calculated total non Doppler effect is a constant −0.36¢/°F throughout this temperature range.

with experiment should have only a small ($\lesssim$ 3%) effect on the calculated Doppler coefficient.

The measurement of reactivity feedback effects of flow, pressure, and temperature are in very good agreement with calculation. As expected, the reactivity effects of sodium flow and cover gas pressure are essentially zero over the entire operating range of these variables. The measured temperature reactivity feedback data between 350°F and 760°F at zero power are in very good agreement with the calculations (within about 2% over this entire temperature range) using the predicted[13] Doppler T $\frac{dk}{dT}$ of -0.0082 and total expansion coefficient of -0.36¢/°F. Since the Doppler effect contributes about 40% of the calculated uniform temperature coefficient in the 350°F to 760°F temperature range, the close agreement between the calculated and the measured temperature coefficient is an indication that the Doppler effect is not drastically different from its predicted value.

1.3   SEQUENCE OF MEASUREMENTS

During the zero power tests which are reported here, experiments were performed on 5 major different core loadings, or arrangements, of fuel, BeO, and B_4C rods within the core. These 5 different core loadings have been designated Assembly I-A, through Assembly I-E, and the core loadings are illustrated in Figures 1-1 through 1-5. In addition, a fine reflector was calibrated on another loading, Assembly I-F, and a portion of the reactivity flow coefficient measurements were performed on Assembly I-I. The latter two loadings are shown in Figures 1-6 and 1-7.

The first critical loading was Assembly I-A shown in Figure 1-1 which contained 550 fuel rods, 96 BeO tightener rods and no B_4C rods.

The excess reactivity of this assembly with all reflectors raised was nine cents at a sodium temperature of 350°F.

After measurements to evaluate the inherent neutron source strength were performed in Assembly I-A (see Appendix VII), 13 fuel rods and 4 BeO tightener rods were added on the core periphery to provide enough excess reactivity for calibration of the reflectors. This loading was designated Assembly I-B and is illustrated in Figure 1-2. This loading was critical with one reflector completely lowered and a fine reflector raised about 87% of its stroke. The estimated excess reactivity of this assembly with all reflectors raised was $1.35 at a temperature of 350°F. In addition to the reflector calibrations, the reactivity worth of fuel, B_4C, and stainless steel rods were measured at different locations in the core. Fuel rod reactivity worth measurements in this assembly revealed that a number of fuel rods were low (by as much as 40%) in reactivity worth when compared to a standard rod. An extensive investigation, which is reported in reference 14, demonstrated that these rods were deficient in plutonium.

The very low worth rods in Assembly I-B were removed and replaced with rods from the core periphery. A minimum critical loading of 522 fuel rods and 100 BeO tightener rods that is shown in Figure 1-3 was attained. This loading, Assembly I-C, was less than 1 cent super-critical with all reflectors raised at 350°F.

Some of the fuel rods in Assembly I-C were moved to the core periphery and B_4C rods, as well as additional fuel rods and BeO tightener rods, were added to the core to completely fill the 108 fuel channels. The adjustment in loading was performed in incremental steps and critical checks were performed at the end of each step. The resulting full size core loading was designated Assembly I-D and is illustrated in

Figure 1-4. This assembly was critical at 350°F with one fine re-
flector completely lowered and the other fine reflector raised about
half way. The estimated excess reactivity at 350°F with all reflectors
raised was $1.8. Experiments which were performed in Assembly I-D
included control rod calibrations, material worth measurements, noise
measurements to determine ℓ/β, measurement of the inherent neutron
source, fission rate distribution measurements, and a measurement
of the temperature dependent feedback between 350°F and 400°F.

In order to provide enough excess reactivity to compensate the
expected reactivity feedback upon heating the reactor to 760°F, and
to accomodate the loading of guinea pig rods which contain 33% more
Pu than a standard fuel rod, the fuel and B_4C distribution within the
core was changed. The resulting core loading was called Assembly
I-E and is illustrated in Figure 1-5. At 350°F this assembly was
critical with two reflectors lowered and one fine reflector approx-
imately 40% raised. The estimated excess reactivity with all re-
flectors raised at 350°F was about $3.4. Measurements in this assembly
included reflector calibrations at two different temperatures (i.e.
with two different critical reflector configurations for the same
core loading), measurement of the flow and pressure coefficients of
reactivity, and reactivity temperature effects between 350°F and 760°F.

A symmetrical loading of B_4C, and guinea pig rods was arranged
within the core to provide enough excess reactivity for the approach
to full power operation. This loading, Assembly I-F that is shown in
Figure 1-6, was critical at 350°F with three reflectors lowered and one
fine reflector raised approximately one third of its complete stroke.
A fine reflector was calibrated with this loading.

A final core loading was Assembly I-I. This loading was obtained
by removing two standard fuel rods and one tightener rod from each of

two different fuel channels in Assembly I-F and replacing them with
Instrumented Fuel Assemblies (IFA's). Each IFA, which contains two
temperature-instrumented fuel rods and a central tightener rod, as
well as sodium temperature thermocouples and a flow meter, are
described in detail in reference 15. A portion of the reactivity flow
coefficient measurements were then performed on this core. The loading
for this core is shown in Figure 1-7.
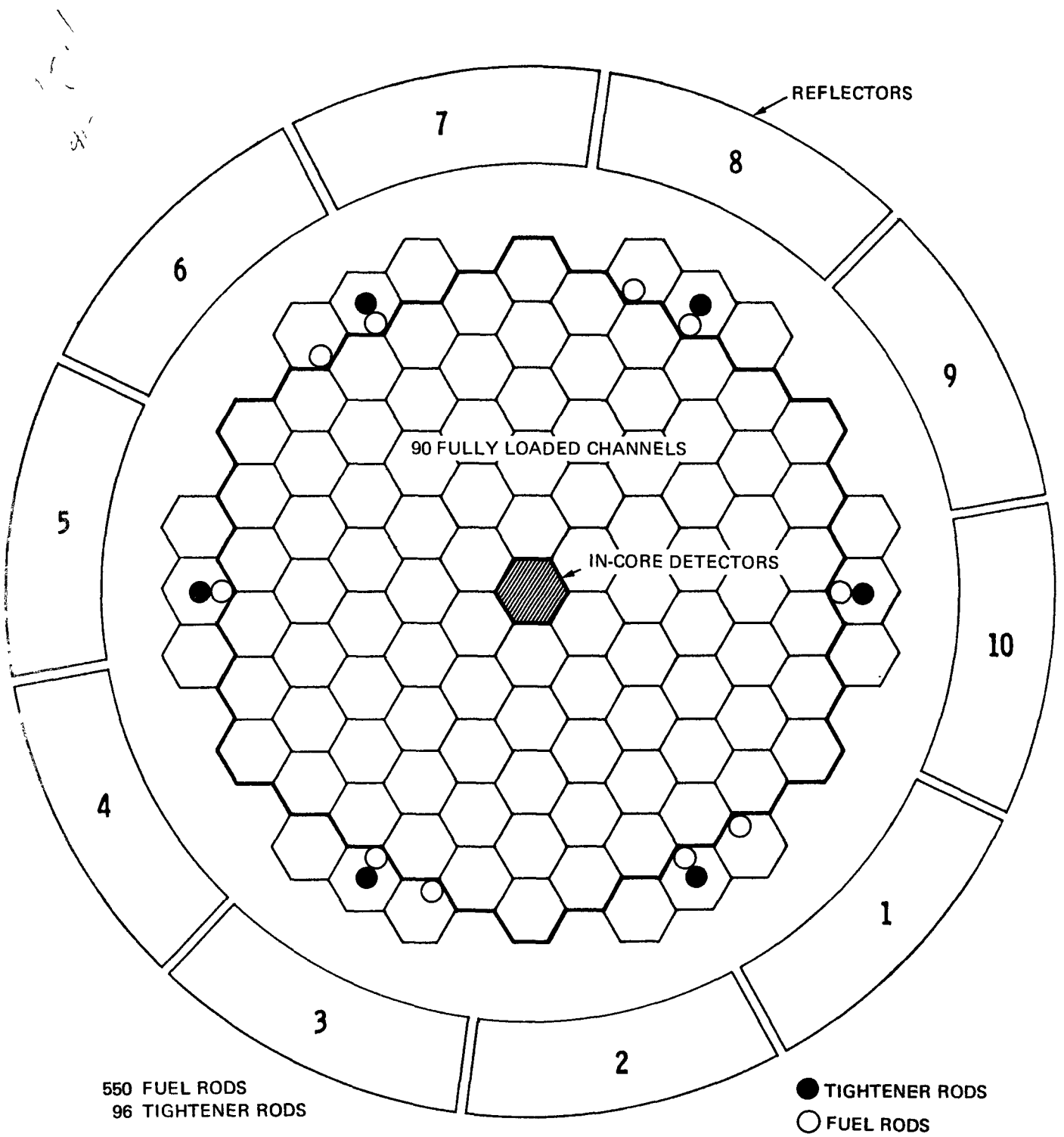
FIGURE 1-1. SEFOR INITIAL CRITICAL CORE LOADING (ASSEMBLY I-A)
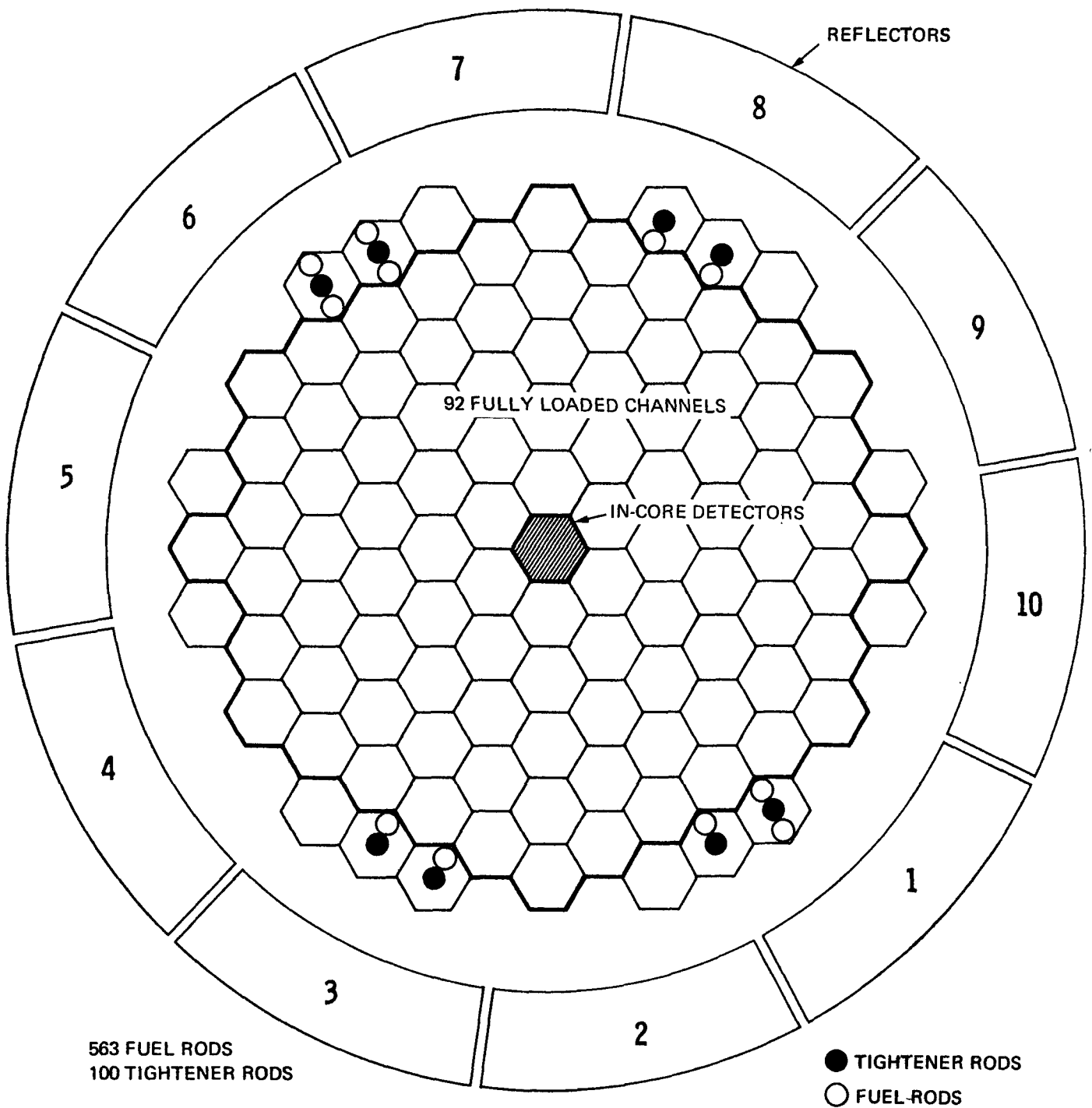
FIGURE 1-2. SEFOR CORE LOADING (ASSEMBLY I-B)
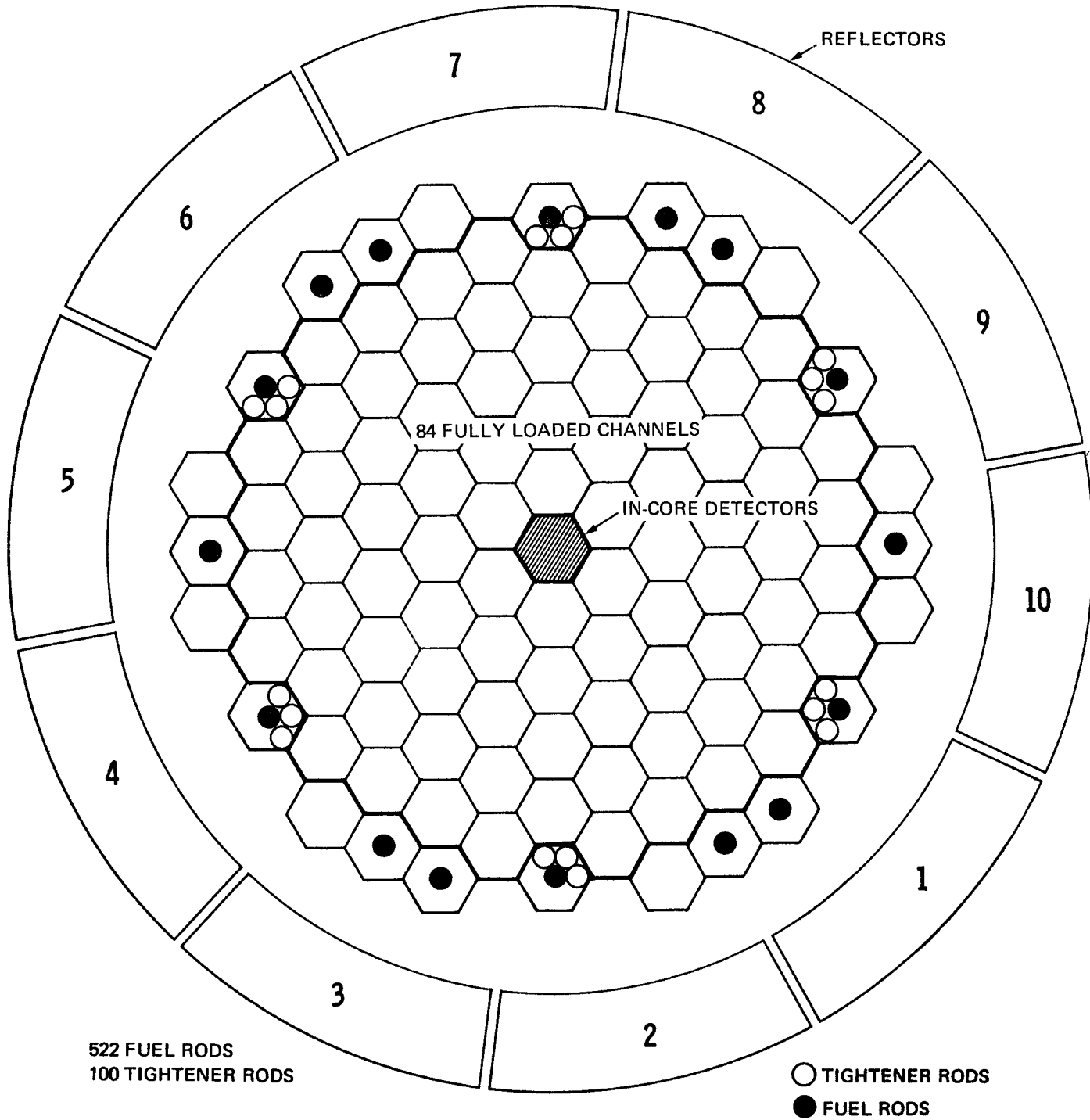
FIGURE 1-3. SEFOR MINIMUM CRITICAL LOADING (ASSEMBLY I-C)
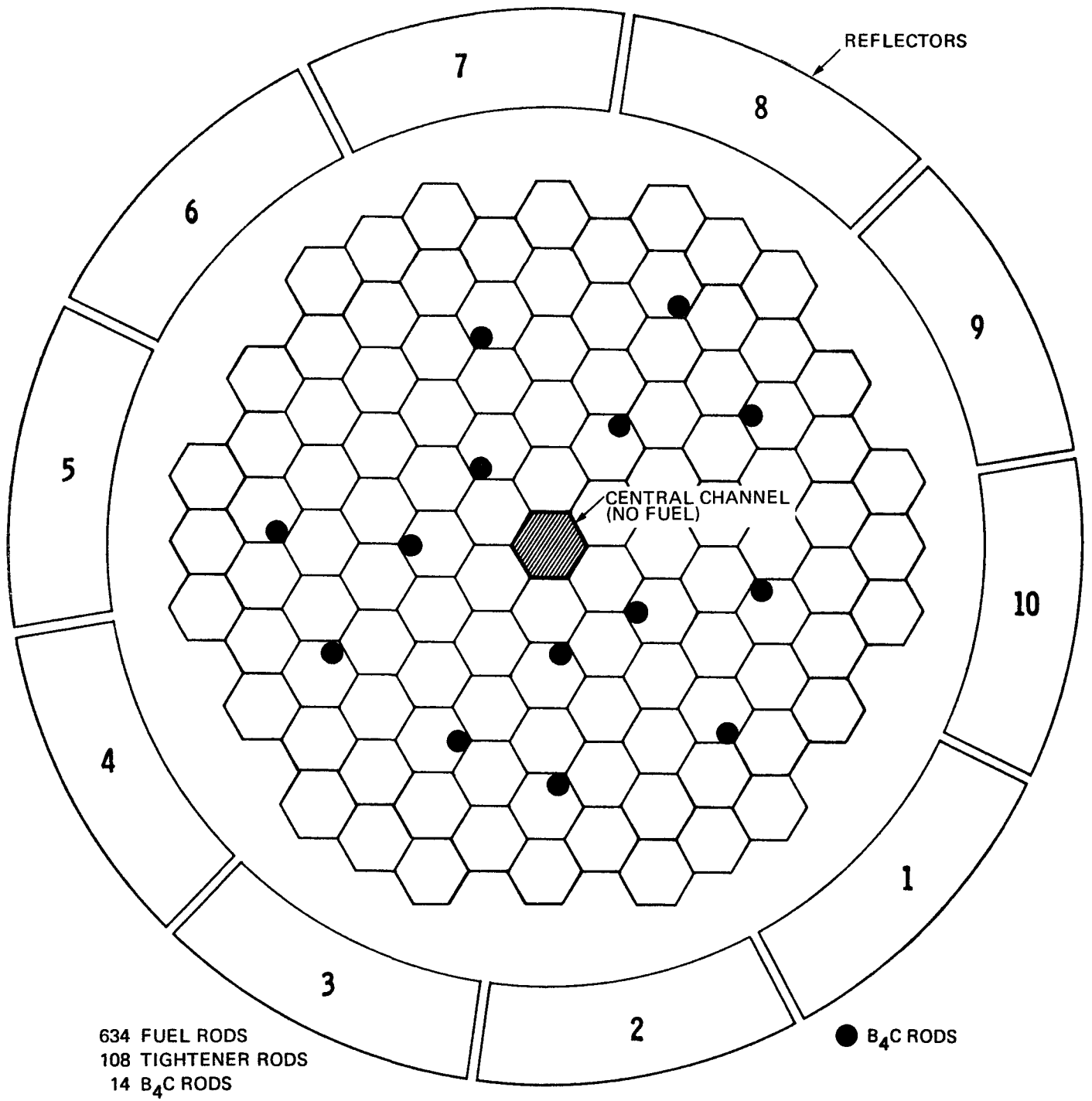
FIGURE 1-4. CORE LOADING FOR ASSEMBLY I-D

REFLECTORS

7

8

6

9

5

10

CENTRAL CHANNEL
(NO FUEL)

4

1

3

2

627 FUEL RODS
108 TIGHTENER RODS
14 B$_4$C RODS
7 GUINEA PIG RODS

● B$_4$C RODS
○ GUINEA PIG RODS
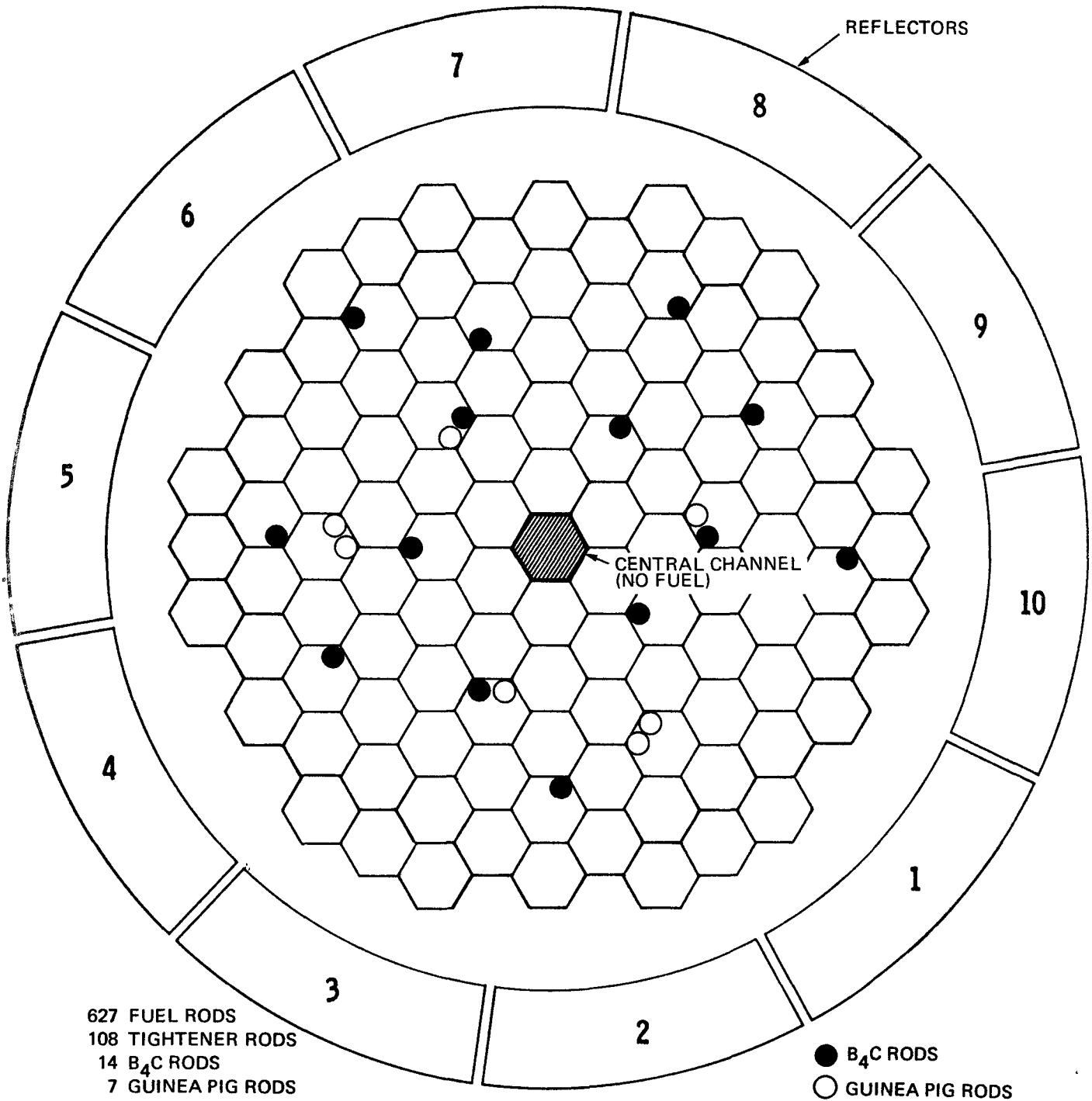
FIGURE 1-5. CORE LOADING FOR ASSEMBLY I-E

REFLECTORS

7

8

6

9

5

10

CENTRAL CHANNEL
(NO FUEL)

4

1

3

2

629 FUEL RODS
108 TIGHTENER RODS
 12 B$_4$C RODS
  7 GUINEA PIG RODS

● B$_4$C RODS
○ GUINEA PIG RODS
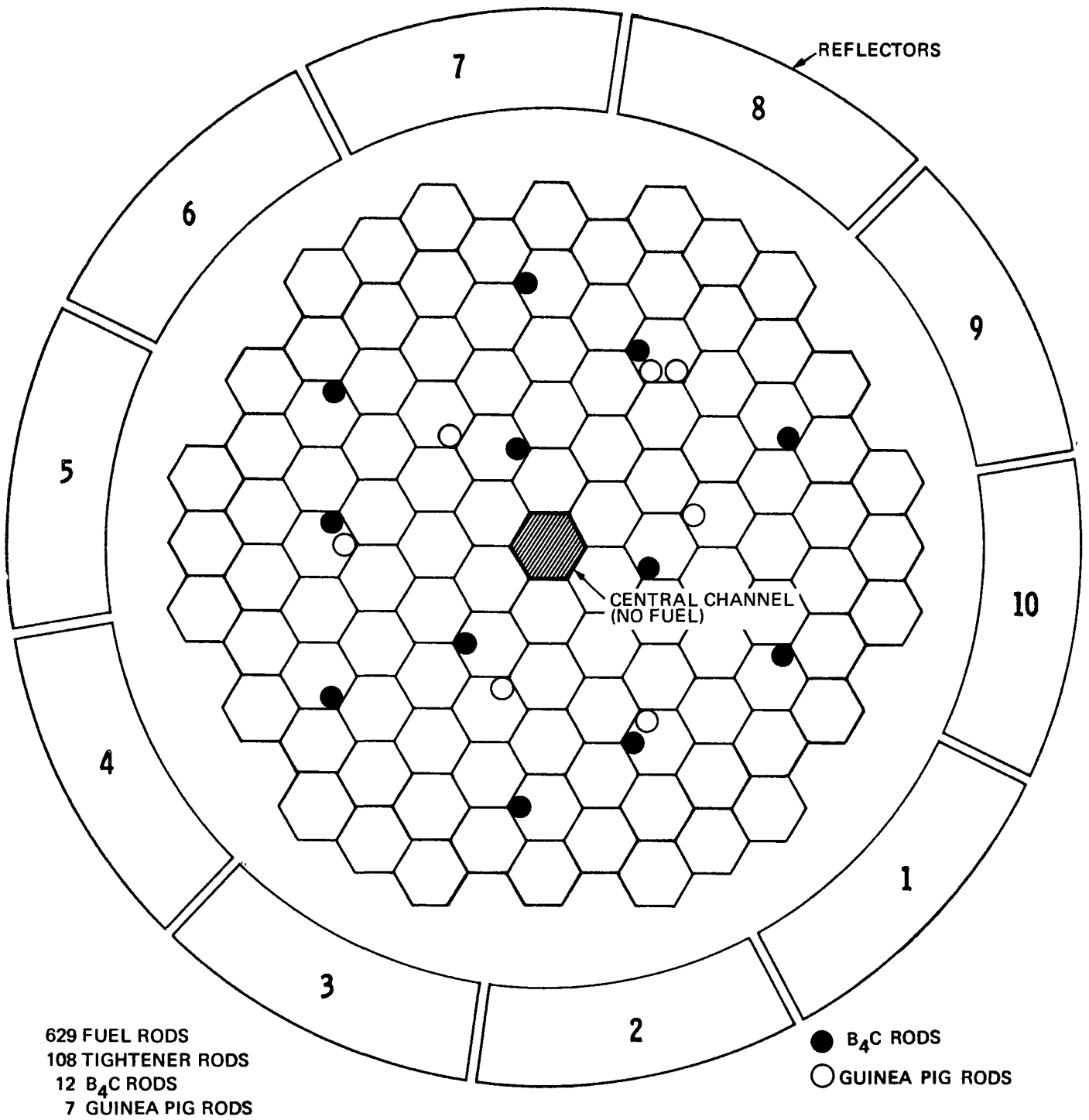
FIGURE 1-6. CORE LOADING FOR ASSEMBLY I-F

REFLECTORS

DRY-WELL
(NO FUEL)

625 STANDARD FUEL RODS
4 IFA FUEL RODS
106 STANDARD TIGHTENER RODS
2 IFA TIGHTENER RODS
12 B$_4$C RODS
7 GUINEA PIG RODS

● – B$_4$C ROD
○ – GUINEA PIG ROD
⬭ – INSTRUMENTED FUEL ASSEMBLY
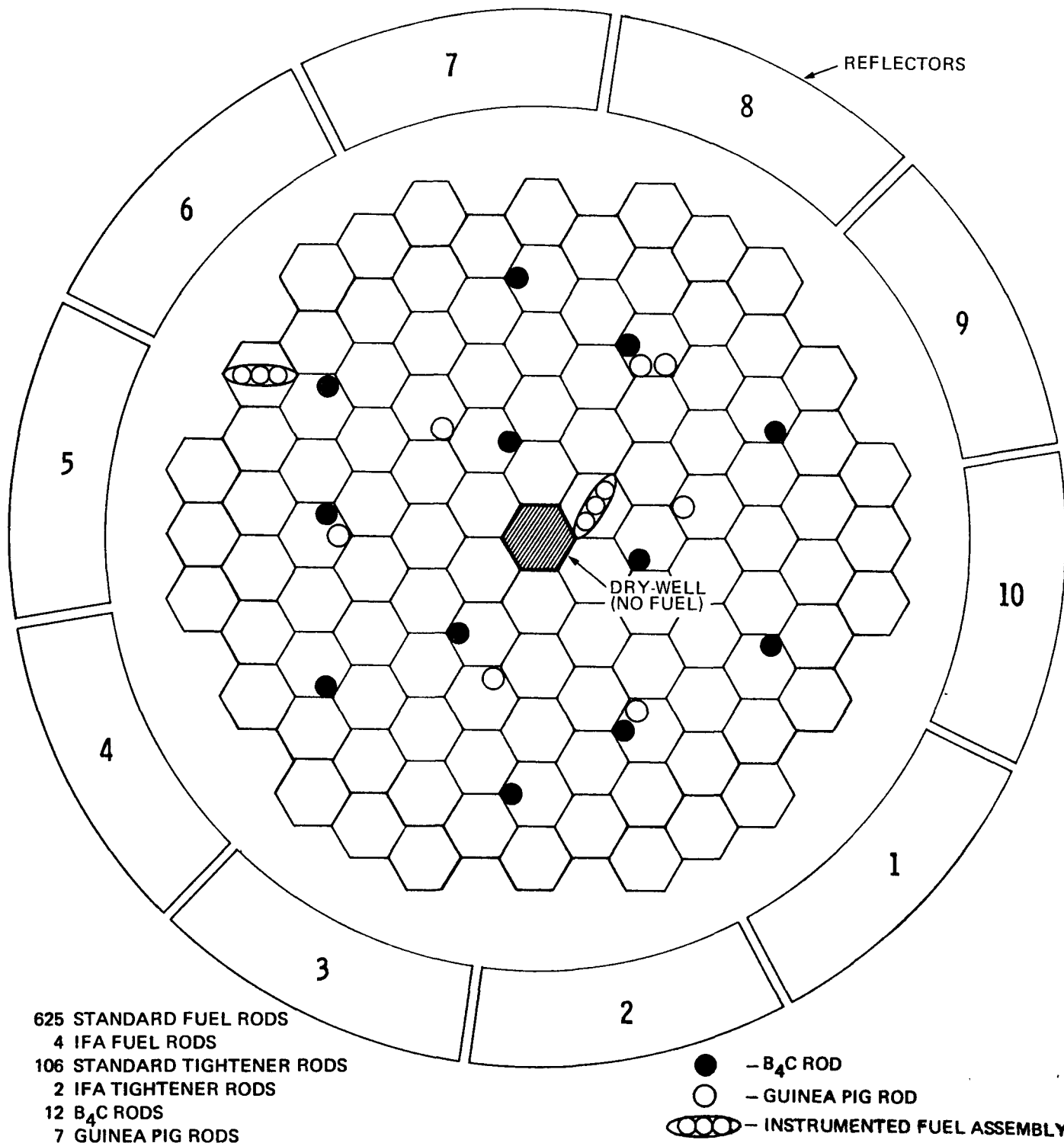
FIGURE 1-7. CORE LOADING FOR ASSEMBLY I-I
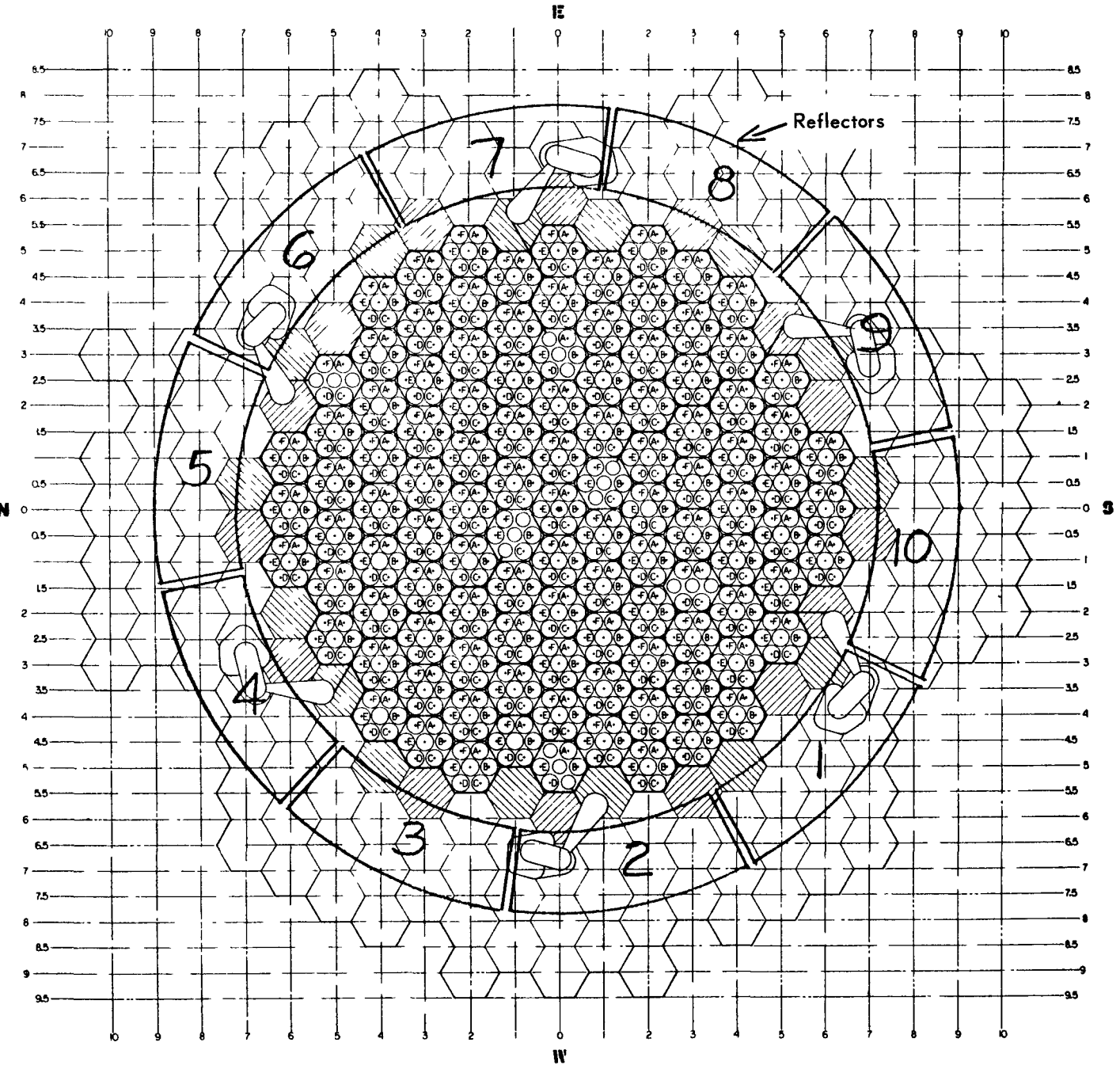
FIGURE 1-8. CORE LOADING LOCATIONS

.

SECTION II

MINIMUM CRITICAL CORE SIZE

2.1 PREDICTION OF THE MINIMUM CRITICAL SIZE

2.1.1 Calculated Results

Calculations were performed prior to the initial SEFOR fuel loading to predict the minimum critical core size for the Southwest Experimental Fast Oxide Reactor (SEFOR). The predicted minimum critical loading was 519 PuO_2 - UO_2 fuel rods containing 285 kg of fissile (Pu-239 + Pu-241) plutonium, with one beryllium oxide tightener rod for each six fuel rods. The expected range of the minimum critical size was 265 to 307 kg (482 to 559 rods) corresponding to an estimated uncertainty of $\pm$0.017 in reactivity. The actual minimum critical loading was equivalent to a core containing 518 standard fuel rods and the nominal 6-to-1 ratio of fuel-to-tightener rods.

The prediction was based on calculations which included a number of SEFOR core sizes ranging between approximately 65% and 100% of the fully loaded core, as well as the ZPR-3 Assembly 47 critical mockups[1,2] of two SEFOR designs. One of these mockups was a one-fuel-segment design with no axial gaps between fuel pellets, while the other was the two-segment design used in the SEFOR reactor to decrease the reactivity effect of fuel axial expansion.

The calculated results are shown in Table 2-1. The multiplication factors of the various reactor models are shown both before and after normalization to an average of the calculated values for the ZPR-3 one- and two-segment mockups. The multiplication factors were normalized by adding to the calculated values a constant chosen so that the average of the normalized multiplication factors for the one-and two-segment ZPR-3 Assembly 47 mockups were equal to unity. The predicted minimum critical core loading was then obtained by interpolation among the normalized multiplication factors.

Comparison of the normalized and calculated multiplication factors shown in the table indicates that the cross section data and methods used for these calculations are under-reactive by about 1%. Hence, as indicated in the table, the predicted SEFOR minimum critical core size would have been 541 fuel rods (302 kg of fissile Pu) if the calculations had not been normalized to the results for the ZPR-3 SEFOR mockups. Although the method of calculation for systems as complex as the SEFOR reactor and critical assembly mockups tends to obscure the amount of reactivity deficiency which may actually be present in the cross section data, the under-prediction of k is consistent with other comparisons between calculation and experiment made for critical assemblies in SNEAK, [3] ZPR-6[4], and ZPR-3[5] facilities.

It is noted from a comparison of the ZPR-III one-segment and the ZPR-III two-segment values that the calculations appear to over-predict the negative reactivity due to the gap by about 0.01. (A 0.007 over-prediction of the negative gap effect was noted in the earlier calculations – see 2-dimensional results in Table 4-1 of Reference 2). The more highly negative gap effect in the present calculation may be due in part to the shift in the adjoint flux spectrum associated

with the higher Pu-239 alpha in the current data, since there is an appreciable leakage of high energy neutrons from the core into the gap and a reverse leakage of low energy neutrons.

The curve of Figure 2-1 is a plot of the normalized multiplication factors of Table 2-1 versus number of loaded fuel rods (648 rods are in the fully loaded core). The projected minimum critical configuration of 519 fuel rods is the point where the curve crosses k = 1.0. The basis for the expected range of 265 to 307 Kg Pu is discussed in Section 2.1.3 below.

The above calculated multiplication factors for the ZPR-3 mockups are in about the same range as those calculated earlier (see 2-dimensional, 4-group results in Table 4-1 of Reference 2). However, the k values listed in Table 2-1 include about a 1% (0.01) reactivity increment as a transport theory correction for the diffusion theory over-estimate of leakage plus a correction for the ZPR-3 plate lattice heterogeneity effects (mainly the high energy self-multiplication effect in the fuel plates, which is reduced by a smaller low energy "smooth" shielding effect and a small leakage effect, see Section 2.1.2); and no corrections were estimated for these effects in the earlier calculations. Thus, the cross section data used for the current calculations (Appendix I) are less reactive than those used for the earlier calculations by about 1%. The higher Pu-239 alpha values in the present data (ORNL-RPI data) accounts for about a 1.4% reactivity loss; but this is partially compensated by a higher Pu-239 fission cross section between 20 and 60 keV in the present data. Several other differences in the data (See Appendix I) nearly cancel in their net reactivity effect. The difference in cross section

TABLE 2-1

CALCULATED K FOR SEFOR AND ZPR-3 ASSEMBLY 47 MOCKUPS

Reactor Model	Calculated k[d]	Normalized k[a]
ZPR-3, 1 Segment	0.995	1.005
ZPR-3, 2 Segment	0.985	0.995
SEFOR, 419 Fuel Rods	0.941	0.951
SEFOR, 464 Fuel Rods	0.966	0.976
SEFOR, 512 Fuel Rods	0.988	0.998
SEFOR, 519 Fuel Rods[b]	--	1.000[b]
SEFOR, 541 Fuel Rods[c]	1.000[c]	--
SEFOR, 554 Fuel Rods	1.006	1.016
SEFOR, 600 Fuel Rods	1.022	1.032
SEFOR, 648 Fuel Rods (Full Core)	1.038	1.048

(a). 0.01 added to calculated k values to make the average k of the ZPR-3 assembly 47 mockups equal to unity.

(b). SEFOR minimum critical core size predicted by interpolation.

(c). Minimum critical size that would have been predicted without normalization to the ZPR-3 Assembly 47 mockups.

(d). The correction factors of Table 2-3 are included.
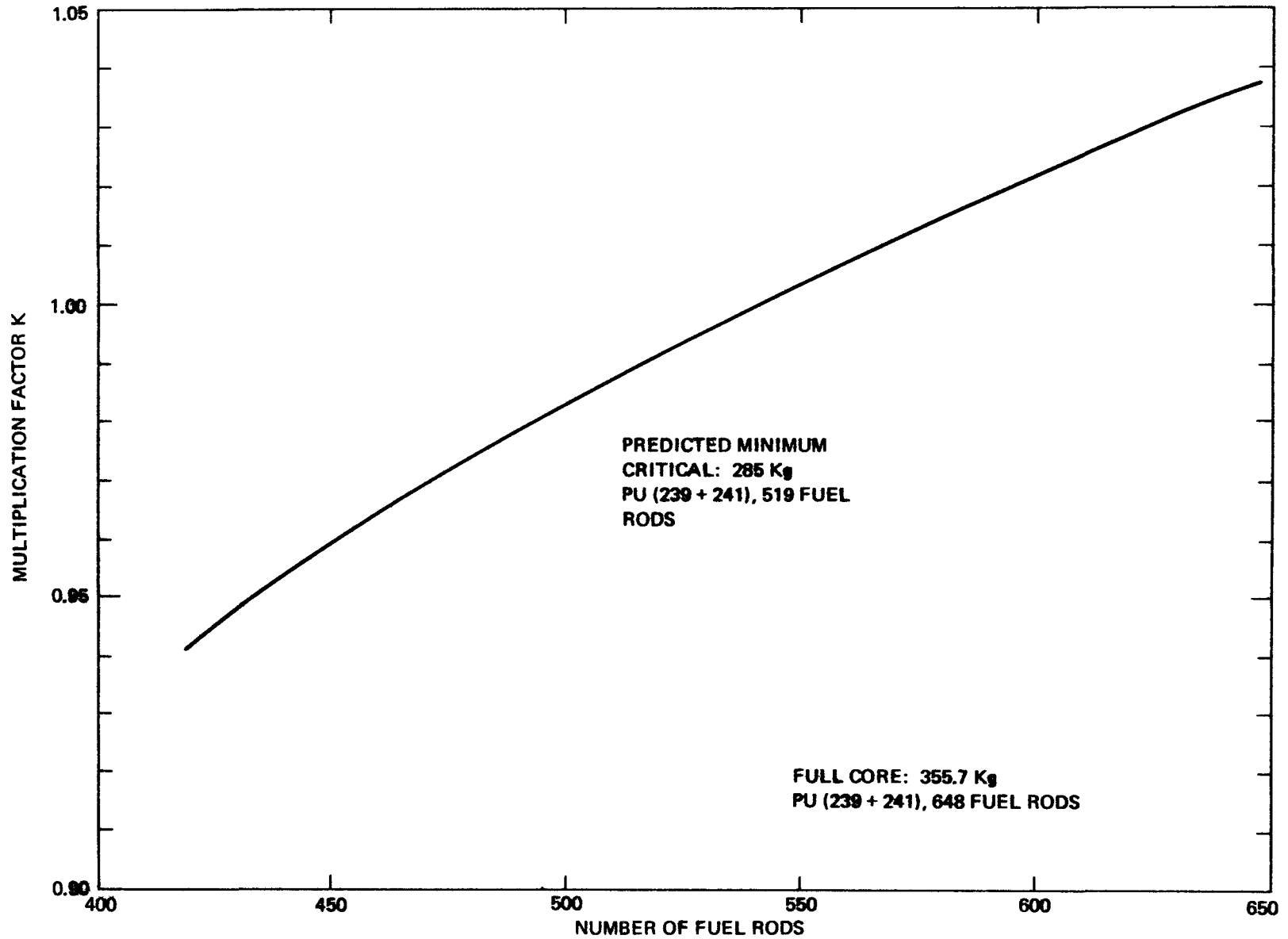
FIGURE 2-1. K VERSUS NUMBER OF LOADED FUEL RODS

data used between the present and the earlier calculations might have
a small effect on the critical mass prediction with respect to the
contributions made by geometry or composition variations between the
SEFOR reactor and the critical assembly mockup (e.g., the reactivity
effect of the replacement of the BeO side rods with steel would be
expected to be sensitive to the change in the Pu-239 alpha).

2.1.2   Calculational Methods

The ZPR-3 and SEFOR reactor geometries were approximated by
right circular cylinders of volumes equal to those of the reactors.
The compositions of the different SEFOR core designs were assumed to
be constant and the same as that of a standard fuel channel containing
six fuel rods and one BeO tightener rod. The details of the ZPR-3
geometries are given in References 1 and 2, and a detailed des-
cription of the SEFOR geometry is given in Appendix I.

The cross sections used in the analysis were essentially those
in the ENDF/B file, Version 1, distributed by Brookhaven National
Laboratory in the summer of 1968,[6] with the exception of modifications
to the fuel cross sections as noted in Appendix I.

The computational methods which were used included two-dimen-
sional diffusion theory calculations[7] with four and thirteen energy
groups and two-dimensional synthesis calculations[8] that combined
one-dimensional flux and adjoint solutions performed along the ortho-
gonal coordinates. In addition, transport theory was used to obtain
correction factors which were applied to the diffusion theory cal-
culations. The results of the two-dimensional and synthesis

TABLE 2-2

RESULTS OF SYNTHESIS AND DIFFUSION THEORY CALCULATIONS

Reactor Model	2-Dimensional Diffusion[b]		2-Dimensional[b] Synthesis	Normalized k[a,b]
	4 Groups	13 Groups	13 Groups	
ZPR-III, 1 Segment	.989	.995	.985	1.005
ZPR-III, 2 Segment	.981	.984	.976	.995
SEFOR, 419 Fuel Rods	–	–	.931	.951
SEFOR, 464 Fuel Rods	–	–	.956	.976
SEFOR, 512 Fuel Rods	.988	–	.978	.998
SEFOR, 554 Fuel Rods	–	–	.996	1.016
SEFOR, 600 Fuel Rods	–	–	1.012	1.032
SEFOR, 648 Fuel Rods	–	1.039	1.028	1.048

(a) Normalized so that the average of the multiplication factors for the one and two segment ZPR-3 Assembly 47 mockups is equal to unity.

(b) The correction factors listed in Table 2-3 are included.

calculations are compared in Table 2-2. These multiplication factors
listed in the table include the corrections of Table 2-3 which are
discussed below.

The two-dimensional, 13-group diffusion theory results are the
most reliable while the 4-group results are the most sensitive to
approximations made to obtain the neutron spectra used for con-
densation of the group constants. The 13-group 2-dimensional synthesis[8]
consistently gave about a 0.01 lower multiplication factor than the
13-group direct 2-dimensional diffusion calculation. Because of this
consistency, the 13-group synthesis results can be used to obtain
differences in k between the various SEFOR cases and the ZPR-III
mockups, and only minor adjustments in these differences are required
in order to give good agreement with similar differences calculated
using the direct 13-group 2-dimensional computation. The "calculated
K" values of Table 2-1 were therefore obtained by using the results
of synthesis calculations (including the corrections of Table 2-3)
to interpolate to SEFOR core sizes for which a true two-dimensional
calculation had not been performed.

The correction factors which were applied to the diffusion theory
calculations are summarized in Table 2-3. The corrections are for the
following effects:

a)   Estimated over-prediction of core leakage by diffusion theory
     (based on comparisons between two-dimensional, 4-energy-group
     S_4 transport calculations, and two-dimensional, 4-group diffusion
     calculations using the DOT2DB[7] code).

     The over-prediction of core leakage with diffusion theory was
     calculated for the ZPR-III 2-segment core using 4-group,

TABLE 2-3

CORRECTIONS TO DIFFUSION THEORY CALCULATIONS

Correction Factor	ZPR-III 1-Segment	ZPR-III 2-Segment	SEFOR 512 Rods	SEFOR 648 Rods
a) Transport Core Leakage Effect	+0.0086	+0.0089	+0.0097	+0.0089
b) Cell Heterogeneity High Energy	+0.0067	+0.0067	+0.0042	+0.0042
Low Energy	−0.0017	−0.0017	−0.0004	−0.0004
Leakage	−0.002	−0.002	−0.001	−0.001
c) Excess Reactivity in ZPR-III Mockup Models	−0.0073	−0.0042	−	−
d) Non-cylindrical Outer Periphery	−	−	−0.003	−0.003
e) Doppler Effect (80 → 350°F)	−	−	−0.003	−0.0033
f) Overshielding Nickel Reflector	+0.001	+0.001	+0.001	+0.001
Total Correction	+0.0053	+0.0087	+0.0075	+0.0064

2-dimensional S_4 transport calculations and 4-group, 2-
dimensional diffusion calculations with the DOT2DB[7]
code. The transport reactivity corrections for the
full SEFOR core listed in Table 2-3 (+0.0089) was made
the same as that calculated for the ZPR-III, 2-segment
mockup. A slightly higher transport correction (+0.0097)
was calculated for the smaller (512 rod) core. Corrections
for SEFOR cores containing other than 512 or 648 rods were
obtained by interpolation. The calculated transport
correction for the ZPR-III, 1-segment core (+0.0086) was not
significantly different than that of the two-segment core.
It is noted that the above transport effects obtained with
two-dimensional calculations are nearly twice as large as
those which would be estimated from results of earlier
transport S_4 and diffusion calculations which used one-
dimensional spherical reactor models [9].

b. High energy and low energy heterogeneity effects (over-and-
above resonance self-shielding) of the ZPR-III plate lattice
cells and the SEFOR rod lattice cell (based on one-dimensional,
24-group S_{16} transport cell calculations using the SN1D code,[10]
and confirmed using an independent analytical model). Also
included are estimated negative reactivity effects due to in-
creased leakage associated with the lattice heterogeneity.

Clumping of the fuel plates in the ZPR-III mockups produces
a fuel flux advantage factor at high energies (the energy region
of the fission source) which results in a significant positive
reactivity. At lower energies, this heterogeneity in the
ZPR-III lattice cells produces a flux disadvantage factor in
the fuel plates which results in a negative reactivity with
magnitude appreciably smaller than the positive high energy

effect. (This low energy effect is in addition to the usual
correction on the effective potential scattering cross section
used to account for cell heterogeneity). The rodded SEFOR fuel
has similar heterogeneity effects, even though all the uranium,
plutonium and most of the oxygen is homogeneous, because of
the large rod diameters and correspondingly large spaces of
BeO, steel, and sodium between the rods.

For ZPR-III Assembly 48, one-dimensional cell transport
calculations using up to 16-angles (S_{16} method) with
anisotropic scattering done at PNL[11] gave a positive
reactivity of about +0.014 for the high energy effect and
about -0.003 for the low energy effect. ZPR-III Assembly 47 -
the SEFOR mockup - has a much more complex lattice arrangement
than did Assembly 48 - in fact there are several different
lattice arrangements in Assembly 47 which were made necessary,
in part, because of the use of the new mixed U-Pu plates in
the central region of the core and the old Pu plates in the
outer region. Previous studies of the ZPR-III Assembly 48
high energy heterogeneity effect by Wintzer[12] yielded
simplified mathematical relationships for estimating flux
advantage factors which were found to give good agreement with
actual cell transport calculations. The estimates of the high
energy heterogeneity effect for the ZPR-III mockups and for the
SEFOR rod cell based on Wintzer's analysis are given in
Appendix II.

The results of cell transport theory calculation using 24
energy groups, 16 angles and anisotropic scattering to determine

the heterogeneity effects of Table 2-3 are also described
in Appendix II.

c. Reactivity reduction due to partially withdrawn control
drawer or nickel reflector segment in the ZPR-III critical
configurations.[1] Such withdrawn control elements were not
taken into account in the calculational model.

d. Reactivity reduction due to the non-cylindrical outer
periphery of the SEFOR full core and in the less predict-
able loading patterns during the approach to the minimum
critical configuration.

The computations performed for this analysis were based on
cylindrical approximations of the reactor geometry in which
the core volume is preserved. The two ZPR-III mockups were
loaded in a manner which simulates a cylinder, while the fully
loaded SEFOR core has a highly irregular hexagonal boundary
which departs considerably from a true cylinder. It was
assumed that the minimum critical configuration in SEFOR
would be approached in a sequence that would maintain as closely
as possible a cylindrical surface; but considerable surface
irregularities were expected to occur. Earlier calculations
of the fully loaded SEFOR core using an equal volume cylinder
resulted in multiplication factor which was 0.003 higher than
that obtained with the outer-most radial fuel pins homogenized
with material just outside the core.[13] The correct value
is expected to lie between these two cases, probably closer
to the model using the homogenized core sodium interface
region for the fully loaded SEFOR core. The full 0.003
reduction was applied to the cylindrical equal-area model
used for all the SEFOR reactor cases calculated, and no
correction was applied to the ZPR-III critical assembly cases.

e. SEFOR Doppler reactivity effect from 300°K to 350°F. The
    Doppler broadened fuel material cross sections were computed
    at a temperature of 300°K because of limitations in the
    cross-section generation code. For this correction a
    value of -0.008 was used for the Doppler coefficient
    $T \frac{dk}{dT}$.

f. The estimated effect caused by the overshielding of the
    nickel reflector cross sections. The radial reflector
    zones used in this analysis were dimensioned to include
    the movable nickel reflectors in a separate zone. Resonance
    self-shielding factors were determined for this nickel
    from tables in Bondarenko[14] and from factors generated
    with the ENDRUN code.[15] A σ_o value of 0.1, estimated from
    the total cross sections of other materials in the zone,
    was used to compute the self-shielding factors. An
    additional surface effect will lessen the degree of self-
    shielding and improve the computed reflector worth. An
    estimated correction to the multiplication factor for this
    surface effect has been included in Table 2-3.

2.1.3   Uncertainty Estimates

The predicted minimum critical configuration of 285 Kg Pu (239 + 241) (see Figure 2-1) had an expected range corresponding to ±0.017 in reactivity – which was considered to be one standard deviation. The ±0.017 reactivity range was calculated from the following estimated components:

a. Geometry defects in SEFOR computational model.   ±0.005
The treatment of the departure of the outer core periphery from a cylindrical surface appears to be the main defect.

b. Uncertainty in effect of BeO reduction. The   ±0.003
ZPR-3 assemblies were mockups of SEFOR cores containing BeO side rods. These rods were replaced with stainless steel in the actual SEFOR core. The effect of this reduction on the multiplication factor was not measured in the ZPR-3 mockups.

c. Uncertainty in fissile weight of fabricated   ±0.002
fuel. (The anticipated "grand average" fissile plutonium (Pu-239 + Pu-241) weight was 548.9 ± 2 grams per rod.

d. Uncertainty in effect of central FRED   ±0.003
channel (not present in the ZPR-3 mockups) and in the spacing between fuel channels (believed to be 10 mils in SEFOR).

e. Uncertainty in lattice heterogeneity effect differences between the SEFOR rod system and the ZPR-III plate system. (This uncertainty has been appreciably reduced as a result of transport cell calculations - see Section 2.1.2). +0.004

f. Uncertainties in differential neutron leakage (and other gap effects) between SEFOR and the ZPR-3 two-segment mockup. (This uncertainty is accentuated by the persistent over-prediction of the negative reactivity of the fuel gap in going from the one-segment to the two-segment critical assembly - even with 2-dimensional transport theory calculations.) +0.006

g. Sensitivity of the difference in k_{eff} between the SEFOR cores and the ZPR-III critical assemblies to the specific multigroup calculation scheme used. +0.005

Correlating the three effects above dependent mainly on neutron leakage-items a, d, and f - leads to a propagated uncertainty of +0.017.

Item f above is one of the largest uncertainties and, as noted above, its magnitude is influenced by the apparent over-prediction of the negative reactivity effect of the fuel gap in the ZPR-3 mockup. It is possible that the 2-dimensional, 4-group transport calculations used

did not adequately reduce the difference in multiplication factor between the one-segment and the two-segment critical assemblies because of the inadequacy of a 4-energy group approximation for accurate treatment of the high energy leakage effects; or gap heterogeneity effects not properly taken into account in the calculational model may be responsible for a large part of the persistent over-prediction of the negative reactivity due to the fuel gap. (A 50% reduction in the U-238 capture in the gap would account for only 0.003 of the 0.01 reactivity defect.) Nevertheless, the over-prediction remained substantial and was not accounted for. For that reason, it appeared that complete reliance for the prediction of k in SEFOR should not be placed on normalization to only the ZPR-III, 2-segment experiment, which would assume that the calculation is entirely in error in its apparent over-prediction of the negative reactivity produced by the fuel gap. Rather it appeared highly possible that some other unidentified factors in the 1-segment and/or 2-segment mockups might not have been properly accounted for in the computational model; and, hence, the normalization of SEFOR k values was made to both the 1-segment and the 2-segment critical assemblies.

2.2   EXPERIMENTAL FUEL LOADING RESULTS

2.2.1 Initial Critical Core (Assembly I-A)

Initial criticality in SEFOR was attained with a core loading of 550 fuel rods. The core arrangement for this loading (Assembly I-A) is shown in Figure 1-1. The excess reactivity of the system was 9.5¢ at a sodium temperature of 350°F. Later investigations revealed that a

number of the fuel rods in this core were low in reactivity worth as
compared to a standard rod. After calibration of the reflector control
system and performance of a few experiments, the low worth rods were
removed and a minimum critical loading of 522 fuel rods and 100 tightener
rods (Assembly I-C) was obtained. A description of this core is given
in Section 1.3.

2.2.2   Critical Approach

The initial critical approach in SEFOR was performed in a con-
ventional manner. Fuel was loaded in a roughly cylindrical pattern
about the core center with the reflector control in the lowered least-
reactive-position. Steady state count rates on two He-3 detectors
located in the central channel and on two source range monitors (BF_3
detectors) located below the core were recorded. The reflectors were
raised and the observed steady state count rates were recorded again.
The data was used to estimate the critical size and to determine the
next fuel loading increment. More fuel was then loaded, and the
counting-estimating-loading process was repeated until criticality was
attained with all reflectors in the raised (most reactive) position.
Usually, each channel of the core was completely filled with six fuel
rods and secured with a tightener rod prior to proceeding to the next
channel of the core. However, after loading of a total of 504 fuel
rods, single rods were placed in circumferential channels to maintain,
as near as possible, cylindrical symmetry in the near-critical core.

A total of 19 incremental loading steps were used in the initial
approach to critical. A total of 36 fuel rods and 6 tightener rods
were loaded as a part of the first step and each of the Helium-3
detectors, preassembled in its individual tube, was then loaded into
the center of the core. Due to the length of these tubes and the

width of the fuel grapple head, six channels immediately surrounding the central channel were completely loaded with fuel prior to insertion of the detectors.

The data obtained during the 19 loading steps are summarized in Table 2-4. The tabulated count rate data include the dead time corrections described in Appendix III. The corrections for the count rates in the in-core detectors became quite large with the reflectors raised after approximately 520 rods had been loaded, and they were switched to the current mode of operation for loading step thirteen. The count rates on each in-core counting channel were repeated at least five times to accumulate a total of at least 10,000 counts, in order to obtain better than 1% statistical accuracy. The count rate data was statistically analyzed to obtain the standard deviations and probable error in order to establish the consistency of the data. Chi-squared testing was also done to ensure the proper operation of the counting equipment throughout the fuel loading.

The count rate data adjusted for the dead time corrections discussed in Appendix III, is shown in Figures 2-2 through 2-4. The solid lines in Figures 2-3 and 2-3 represent a best fit of a one energy group fundamental mode description (see Appendix IV) of the flux at the core center to the experimental count rate data observed on the centrally located in-core detectors. The upper curves describe the data obtained when all the reflectors were lowered, while the lower curves correspond to data obtained when the reflectors were in the raised (most reactive) position. Except for deviations at very small core loadings, the data indicated an essentially linear relationship

TABLE 2-4

COUNT RATES ON START UP CHANNELS

Loading Step Number	Number of Fuel Rods in Core	Reflectors Down			Reflectors Up		
		In-core Detector No. 1 (counts/sec)	In-Core Detector No. 2 (counts/sec)	Average SRM* Count Rate (counts/min)	In-Core Detector No. 1 (counts/sec)	In-Core Detector No. 2 (counts/sec.)	Average SRM* Count Rate (counts/min)
1a	36	113.4	134.0	18	138.8	164.6	24
1b	108	347.5	418.4	73	394.3	471.5	103
2	216	936.8	1131	202	1081	1302	316
3	282	1442	1735	314	1742	2099	518
4	348	2310	2788	498	3031	3655	903
5	402	3210	3865	687	4684	5636	1396
6	456	4676	5657	1005	8336	10070	2524
7	486	5999	7275	1297	13400	16160	4052
8	504	7212	8686	1530	20730	24870	6108
9	516	8385	10080	1775	32080	38460	9361
10	524	8997	10800	1896	41460	50100	12370
11	531	9543	11390	2007	--	--	16480
12	534	9742	11670	2054	--	--	18950
13	540	--	--	2117	--	--	26870
14	545	--	--	2316	--	--	80660
15	546	--	--	2337	--	--	97800
16	547	--	--	2369	--	--	145600
17	548	--	--	2340	--	--	276500
18	549	--	--	2577	--	--	721900
19	550	--	--	--	--	--	Critical

* Source Range Monitor - located below the core
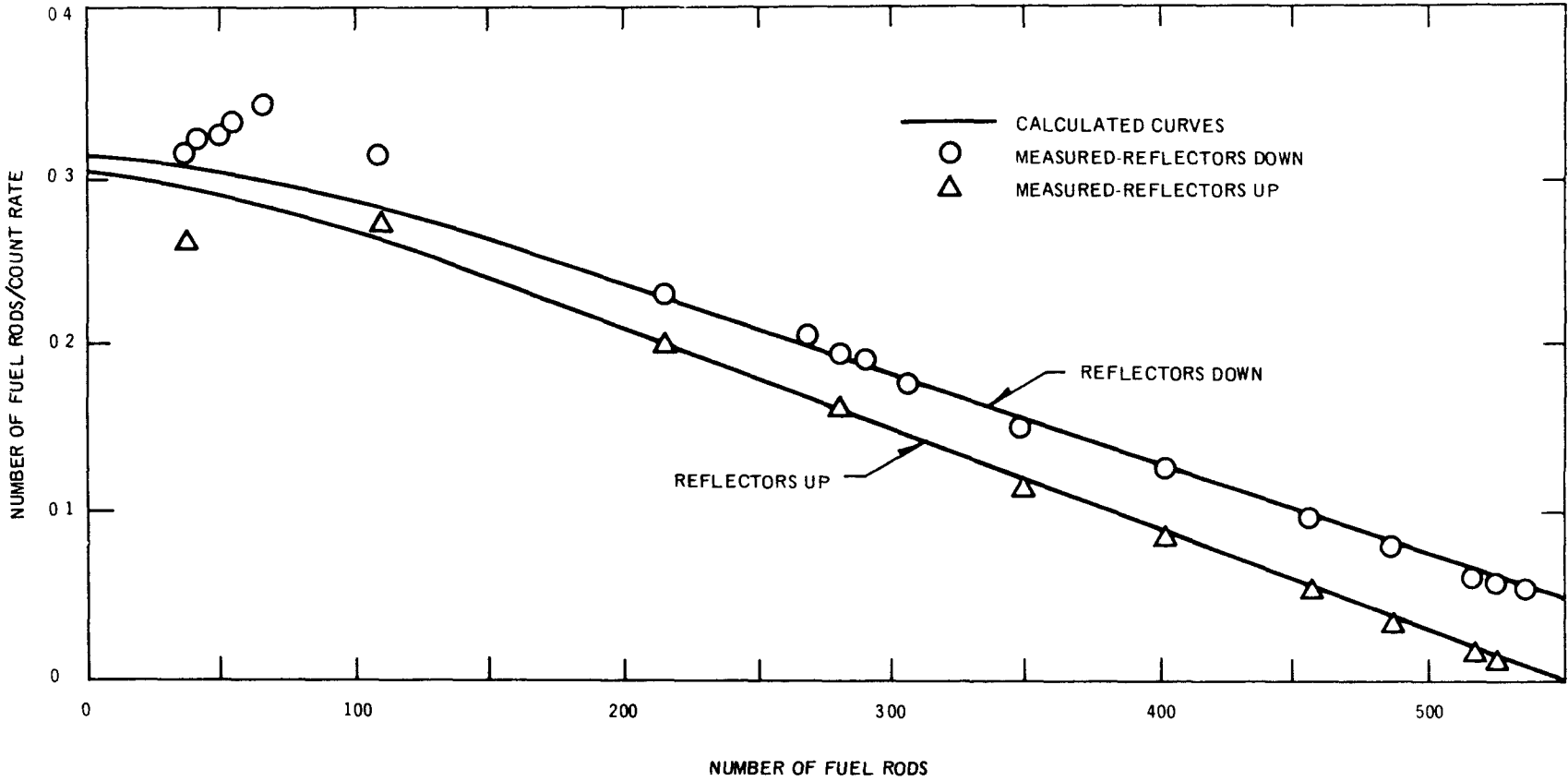
FIGURE 2-2. CRITICAL APPROACH USING IN-CORE DETECTOR NO. 1
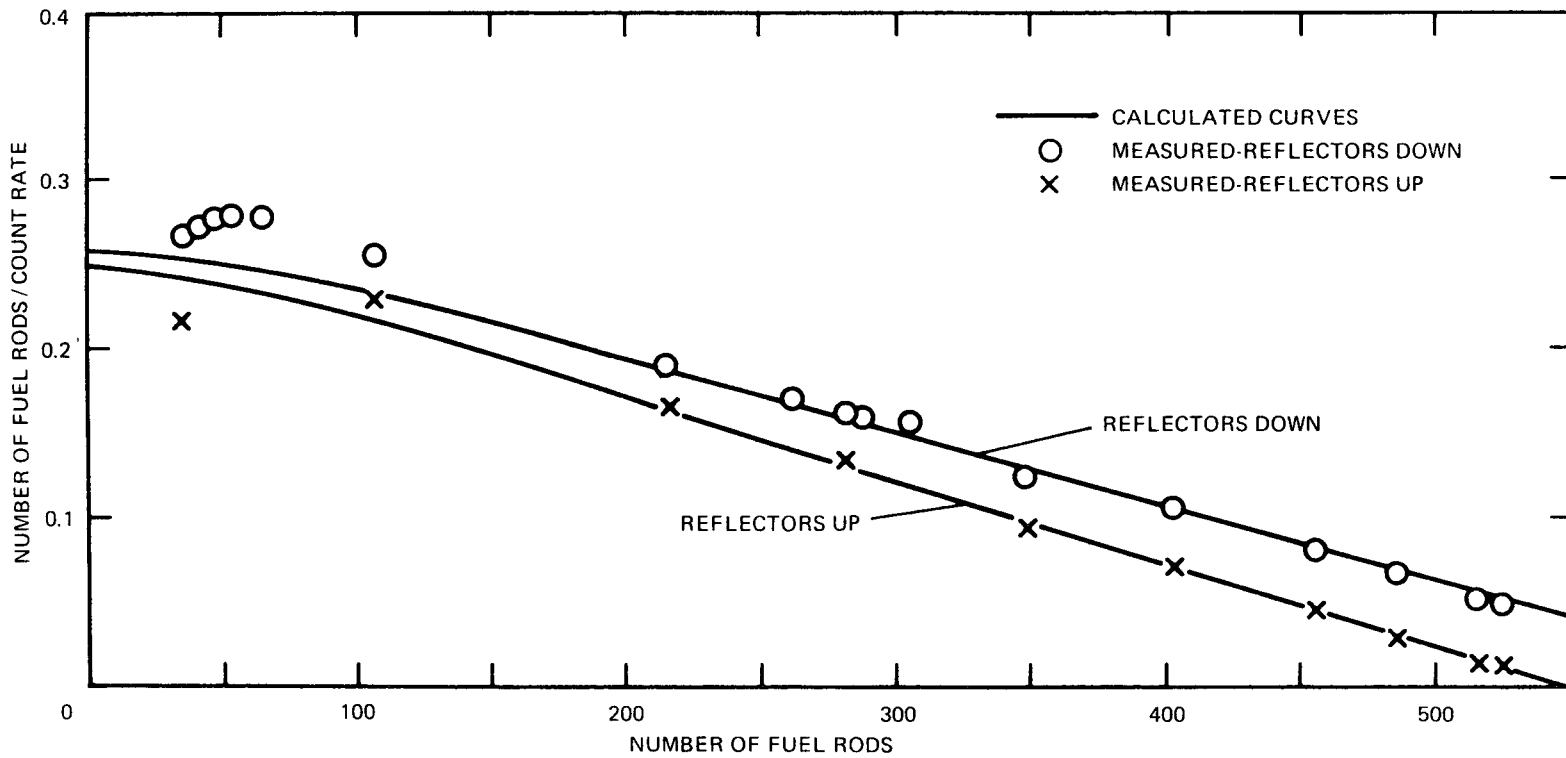
FIGURE 2-3. CRITICAL APPROACH USING IN-CORE DETECTOR NO. 2
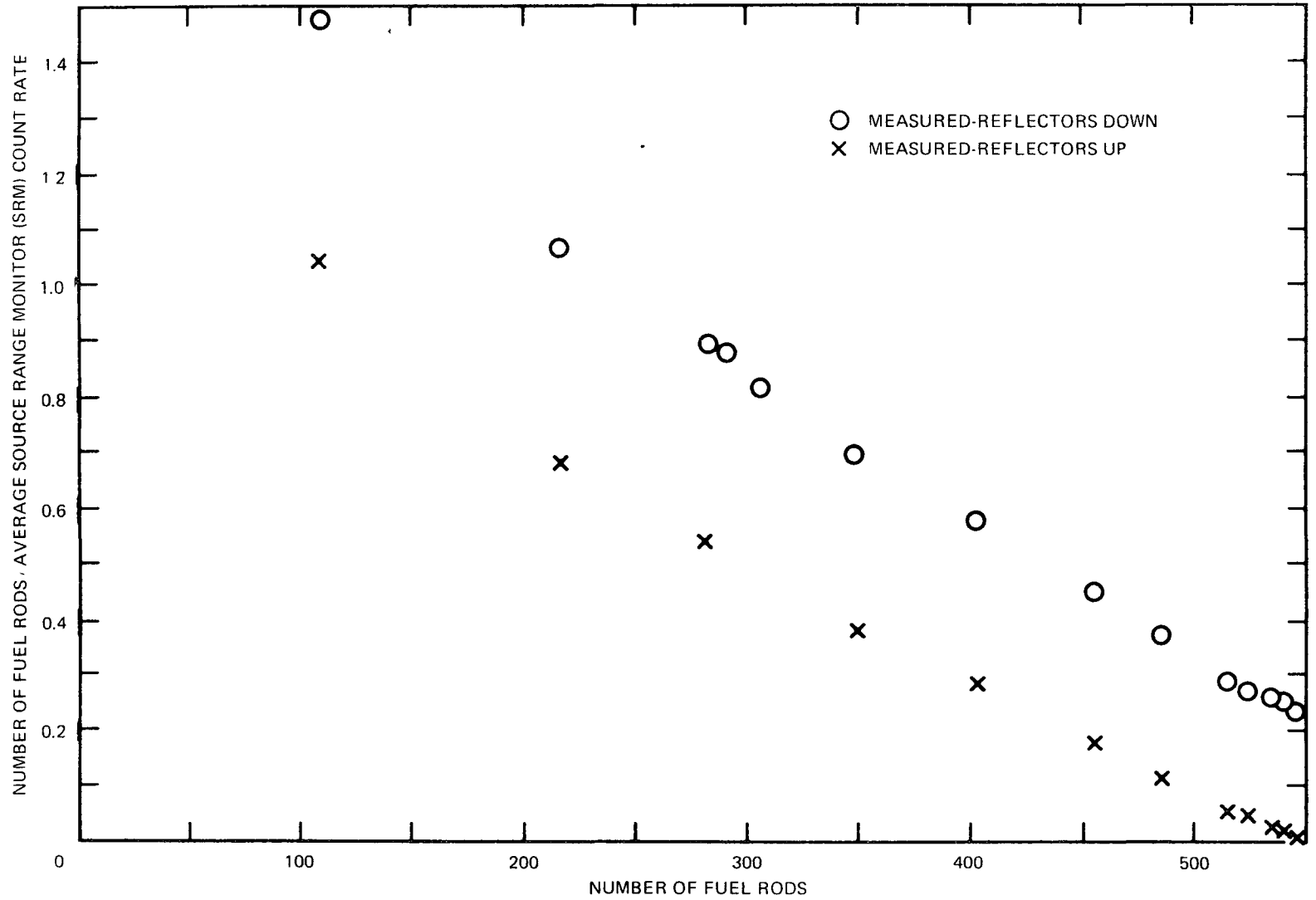
FIGURE 2-4. CRITICAL APPROACH USING THE AVERAGE COUNT RATES FROM TWO SOURCE RANGE MONITORS

between: (1) the ratio of the number of fuel rods divided by the count rate, and (2) the number of fuel rods in the core. The agreement between experiment and calculation is better than might be expected in view of the inability of this simple model (Appendix IV) to account for spectral changes with core size and reflector position, the non-cylindrical loading patterns, and the multidimensional spatial effects.

As Figures 2-2 through 2-4 indicate, it was thus clear, even before initial criticality was achieved, that the initial critical size would exceed the predicted value by some 30 fuel rods. The actual initial critical loading in SEFOR was 550 fuel rods. Subsequent investigations[16] revealed that a number of the fuel rods in this core were as much as 40% low in reactivity worth when compared to a standard rod. The very low worth fuel rods were replaced and the core size was reduced by removing fuel from the core boundary.

2.3   COMPARISON OF EXPERIMENTAL RESULTS WITH PREDICTION

The actual SEFOR minimum critical core loading was 522 PuO_2-UO_2 fuel rods and 100 BeO tightener rods. The core arrangement for this loading is shown in Figure 1.3. The excess reactivity of this nearly cylindrically loaded assembly was approximately 0.9¢ with all reflectors raised at a sodium temperature of 350°F.

In order to compare the experiment with prediction, the following two effects had to be accounted for:

1. The experimental assembly contained 13 BeO tightener rods over and above the standard fuel channel composition of one tightener rod for each six fuel rods. These extra tightener rods were not accounted for in the original prediction.

2. The core contained approximately 50 fuel rods near
the core center whose average reactivity worth was
slightly lower ($\sim$4%) than that of the reference rods.

The estimated corrections to the minimum critical core size which
could in principal have been made to offset the effects noted above are
summarized in Table 2-5. The addition of four fuel rods to compensate
the postulated removal of the excess tightener rods is based on mat-
erial reactivity worths in this assembly of 12¢ for a peripheral fuel
rod and 4¢ for a peripheral BeO tightener rod. (The measured values
of these worths agree with the calculated values.) The corresponding
correction for the replacement of the slightly low worth rods by
standard rods near the core center would be 8 fuel rods on the core
periphery. The multiplication factor for the actual minimum critical
core is thus equivalent to that of a core containing 518 standard fuel
rods and the nominal 6-to-1 ratio of fuel-to-tightener rods.

Both the prediction based on results of a critical experiment
mockup (519 rods), and the value which would have been predicted by
calculation alone (541 rods) are in reasonable agreement with ex-
perimental results (518 rods). Although the correction in prediction
caused by normalization to the critical assembly mockup was small
(22 rods or about 1% in k) in this case, it was not insignificant.
In view of their dissimilarities, it is highly encouraging, in fact,
that such a close prediction can be made of the critical fuel loading
for a rod-type core based on normalization of calculations to a plate-
type critical assembly mockup.

TABLE 2-5

COMPARISON OF PREDICTED AND
EXPERIMENTAL MINIMUM CRITICAL CORE

.

Predicted Core Size (6-to-1 ratio of fuel-to-tightener rods)	519 Fuel Rods
Experimental Core Loading (with 100 BeO tightener rods)	522 Fuel Rods
Correction for Excess Tightener Rods	(+4) Fuel Rods
Correction for Low Worth Fuel	(-8) Fuel Rods
Equivalent Experimental Core Loading (with composition used in prediction)	518 Fuel Rods

SECTION III

REFLECTOR CALIBRATIONS

3.1   CALCULATED REFLECTOR STRENGTH

Total reflector control worth for the minimum critical core[1]
was calculated using 4-energy-group, 2-dimensional, S_4 transport theory.
These calculations were compared with the earlier prediction of the
control worth[2] which was based on diffusion theory calculations using
modified boundary conditions to treat the voided region left when the
reflectors are lowered. The latter calculation also relied on extrapo-
lation of experimental results obtained from the single-rod and the
quadrant-rod measurements done in the ZPR-III critical assembly mockup
of the full core.[3] With transport theory the voided region with
reflectors down was incorporated directly into the multigroup computa-
tional model, thereby providing a check of the earlier diffusion theory
calculations by use of an appreciably different method.

The transport calculations gave a total reflector reactivity control
worth of 0.036 for the minimum critical core. The calculation was
performed for a core containing 512 fuel rods instead of the actual
minimum critical core (see Section 2.3). The calculated results (Table
3-1) indicate that this difference should have an insignificant effect
on the prediction. This is in very good agreement with the earlier
predicted value of 0.035 (11$).

Reflector-in and reflector-out 4-group cross section sets were
obtained from a 60-group condensation, with one-dimensional diffusion
calculations used to obtain the region-dependent spectra. The 60-group,
reflector-out case used for the cross section condensation was approx-
imated by reducing the reflector region density to only one-fourth of

the reflector-in density. This permitted the use of diffusion theory to obtain the condensation spectrum. The DOT2DB code[4] was used for the transport calculations.

The 0.036 Δk includes a correction of -0.0015 since the control segments in the reflector-out calculational model were dropped to a position 4-inches below the bottom of the core, instead of 1-inch above the bottom of the core. The 0.0015 reduction was estimated from the curve of reflector worth versus axial position (figure 4-17 of Reference 5).

Table 3-1 lists several values of total reflector control worth calculated earlier for the full core using different diffusion theory approximations and extrapolation from the ZPR-III critical assembly measurements.[3] Also listed are the total reflector control worths for the minimum critical core calculated using modified-boundary diffusion theory (earlier calculation) and transport theory (present calculation). The calculated worths are all nearly the same. The calculations also indicate that the control worth does not change very much in going from the full core condition to the minimum critical (i.e., the higher leakage of the minimum critical core, and hence, its greater sensitivity to reflector effectiveness relative to that of the full core appears to compensate the decrease in the reflector control worth due to increasing the downcomer region thickness in going from the full core to the minimum critical).

The predicted total reflector reactivity control worth, based on the values listed in Table 3-1 and a consideration of the uncertainties in the calculations is 0.036 $\pm$ 0.006 (11.2\$ $\pm$ 1.8\$). The $\pm$ 0.006 is an

TABLE 3-1

CALCULATED REFLECTOR CONTROL REACTIVITY WORTHS

Case	Reactor Model	Method of Calculation	Total Control[c] Reactivity Worth
1	SEFOR full core (648 fuel rods)	Extrapolation of ZPR-III experimental results on removal of nickel segments, using 4-group, 2-dimensional diffusion theory.[a,b]	0.036 (11.2$)
2	SEFOR full core (648 fuel rods)	4-group, one-dimensional diffusion theory with modified boundary condition to account for voided region with reflectors down.[a]	0.037 (11.6$)
3	SEFOR 512 fuel rods	Same as Case 2.	0.035 (10.9$)
4	SEFOR 512 fuel rods	4-group, 2-dimensional, S_4 transport theory.	0.036 (11.2$)

(a) See Reference 3, Sections 6.2 and 6.3 for details.

(b) It was possible to use diffusion theory to calculate the "nickel-out" condition since a relatively large amount of steel and aluminum remained in the region after removal of the nickel.

(c) Conversion from Δk to dollars is based on a β of 0.0032.

estimated standard deviation arising from possible consistent errors in the different calculations indicated in Table 3-1.* These include uncertainties in the method used for condensation from the 60-group to the 4-group cross sections (see above); differences between the idealized cylindrical geometry of the computational model and that of the real reactor (and also some small composition differences); uncertainties in the treatment of nickel self-shielding (including the surface effect); and possible nuclear data errors (due to data uncertainties) that may be sensitive to the difference in spectrum between the reflector-in and the reflector-out conditions.

The full core reflector worth was also predicted to be 0.036 $\pm$ 0.006. The 0.036 value is about twice the amount of calculated control required for operation.

---

*The method of extrapolation of the ZPR-III experimental results is subject to many of the same potential errors as the other methods indicated in Table 3-1. This is because the nickel was removed from only one-tenth of the ZPR-3 reflector (and also one-fourth in the ZPR-III one-segment critical assembly) and fairly elaborate diffusion theory calculations were required to extrapolate from the measured values in the critical assembly environment to the total reflector worth in SEFOR.

3.2   MEASURED TOTAL REFLECTOR STRENGTH

The total strength of the entire reflector system (i.e. - the
reactivity worth of simultaneously moving all the reflectors from the
completely raised to the completely lowered position) is estimated
to be 3% Δk/k or $10, for both the partially loaded and the fully
loaded critical cores. The estimated value for the 550 rod core
Assembly I-A is based on the normalized one group model for the critical
loading that is discussed in Appendix IV and the calculated radial
leakage for the critical assembly, while the extrapolation to other
core sizes is based on the calculations described above which indi-
cated that the total reflector strength is relatively insensitive
to core sizes in the range between the minimum critical and the
full size core.

For the model described in Appendix IV, the initial loading data
described in Section 2.2.2 indicates that the fundamental mode buckling
of the 550 rod core with reflectors lowered is 10.7% larger than the
corresponding (critical) buckling with reflectors raised. (i.e. the
data indicates that the leakage is increased by 10.7% when the re-
flectors are lowered.) Multigroup, two-dimensional synthesis calcula-
tions indicate that in the 550 rod core the radial leakage from the
core and that portion of the axial reflectors within the height of
the radial reflectors is 29%. Based on these two results the worth
of the ten reflector segments is then (0.107) (.29) = .031 ΔK/K, or
$9.7. This compares with the predicted[1] value of $11.2 ± $1.8
discussed in Section 3.1 above. Although the maximum upper limit
for the worth of the total system (i.e., the change in reactivity
when all ten segments are lowered simultaneously) is ten times the

average value per segment in Assembly I-B, or $12.7, it is known
from the experimental results described below that the worth of
an individual reflector is less when its immediate neighbors are
lowered. The total strength of the system is therefore less than
this maximum value.

3.3   REFLECTOR CALIBRATIONS

3.3.1   Summary of Experimental Results

Reflectors have been calibrated for four different core loadings;
the 563 rod partially loaded core - Assembly I-B, and three fully
loaded cores - Assemblies I-D, I-E, and I-F. In Assembly I-E the
reflectors were calibrated with the reactor at a temperature of 350°F,
and again with the reactor at 650°F. Calibrations on the other cores
were performed only at 350°F. In each case, with the exception of
Assembly I-F where only fine reflector #8 was calibrated, the two
fine reflectors (#3 and #8) were calibrated in increments by means
of period measurements with approximately 1% accuracy (see below)
and the worth of each of the eight coarse reflectors was obtained
by the rod-swap technique discussed below. As will be shown below,
the worth of a reflector is influenced ("shadowed") by the position
of its neighbors. Since the fine reflectors are used to determine
the reactivity effects associated with changes in temperature, core
loading, etc. the details of the calibrations and the associated
reflector configurations are described in some detail below.

The "shadowing effects" appear to be localized, and the worth of

a reflector is nearly independent of the position of non-adjacent reflectors provided the immediately adjacent reflectors are up. As indicated below, however, the worth of a reflector may be influenced (by up to ~4%) by the position of a neighbor which is only two reflectors removed; and the worth is strongly dependent on the position of immediately adjacent reflectors. The results show that the fine reflectors which are used to determine feedback effects should be calibrated with both adjacent reflectors completely raised and, insofar as practical, they should be calibrated with a coarse reflector configuration similar to that which will be used during the experimental program at power.

3.3.2   Calibration Procedures

The coarse reflector worths were determined in the following manner: A critical reflector configuration was attained with the coarse reflector to be calibrated completely raised; all other coarse reflectors either completely raised or completely lowered - not at intermediate positions; fine reflector number 3 completely lowered; and fine reflector #8 at an intermediate position as required for criticality. A second critical configuration was attained with fine reflector #3 completely raised, the coarse reflector to be calibrated completely lowered, the other coarse reflectors in their original positions, and fine reflector #8 at an intermediate position as required for criticality. The worth of the coarse reflector was then determined from the worth of the reflector (#3) for which it was "swapped" and the change in position of reflector #8.

The fine reflector calibrations are performed in the following
manner: The reactor was brought to critical with the fine reflector
to be calibrated in the completely lowered position and the other fine
reflector completely raised. A coarse reflector configuration was
selected to maintain criticality and to minimize the influence of a
lowered coarse reflector on the fine reflector calibration (i.e.,
the coarse reflectors immediately adjacent to the fine reflectors were
maintained in the completely raised position.). The reflector to
be calibrated was raised a few centimeters to produce a period of the
order of 100 seconds, the period was measured, and the other fine
reflector was then lowered to bring the reactor back to critical at
the original flux level. This process was repeated until the entire
length of a fine reflector had been calibrated.

In Assemblies I-B and I-D the reactor was critical at 350°F with
slightly more than one reflector lowered. The fine reflectors were
thus calibrated in these assemblies with one coarse reflector(#10)
in a partially raised position. Since Assembly I-E was critical at
350°F with 2 1/2 reflectors lowered, fine reflector #3 was calibrated
with reflector #5 lowered, #10 raised 40%, and the other coarse re-
flectors completely raised, while #8 was calibrated with #10 down and
#5 raised 35%. At 650°F the reactor was critical with slightly more
than one reflector lowered and #3 was calibrated with #10 raised 85%
while #8 was calibrated with #5 raised 75%. The calibration of
reflector #8 in Assembly I-F at 350°F was performed with coarse re-
flector #5 and #10 completely lowered and with #6 nearly down.

The delayed neutron parameters which were used in the in-hour
equation to convert measured periods to reactivities in units of
cents were taken from Keepin's[6] data and are listed for convenience
along with the calculated effective delayed neutron fractions in
Appendix V.

3.3.3   Calibration Results

The worths of the two fine reflectors (#3 and #8) are shown as
a function of reflector position for different assemblies in Figures
3-1 through 3-8, and the values for all the measurements are tabulated
in Appendix VI. These curves have the expected "S" shape, and the
total worth of each of the fine reflectors is in the expected range.
The values of the total worth of each reflector (coarse as well as
fine reflector segments) are summarized in Tables 3-2 and 3-3. Other
than as indicated in the tables, the measurements were performed
with all reflectors raised.

The data shows that the worth of fine reflector number 8 is
nearly the same as the worth of number 3 in Assembly I-B as well as
in I-D. In addition, the fine reflector worths are essentially the
same in both cores. In Assembly I-E, however, there is a difference
of about 10 percent in the worths of the two fine reflectors at
350°F, even though the total combined worth of the two reflectors
is the same as in Assembly I-B and I-D (about $2.52). The difference
in worths, combined with an inspection of the core loadings in the
different assemblies (Figures 1-2, 1-4, and 1-5) indicates that the
B_4C rod and guinea-pig rod distribution in Assembly I-E may have
caused an asymmetrical flux distribution with an increase toward
the W-side of the core relative to the E-side (see Figure 1-8 for
a diagram of the core). The loading in Assembly I-D, for example,
appears to be more uniform, although the N-E section of the core
in Assembly I-D may be somewhat deficient in B_4C relative to the
remainder of the core.
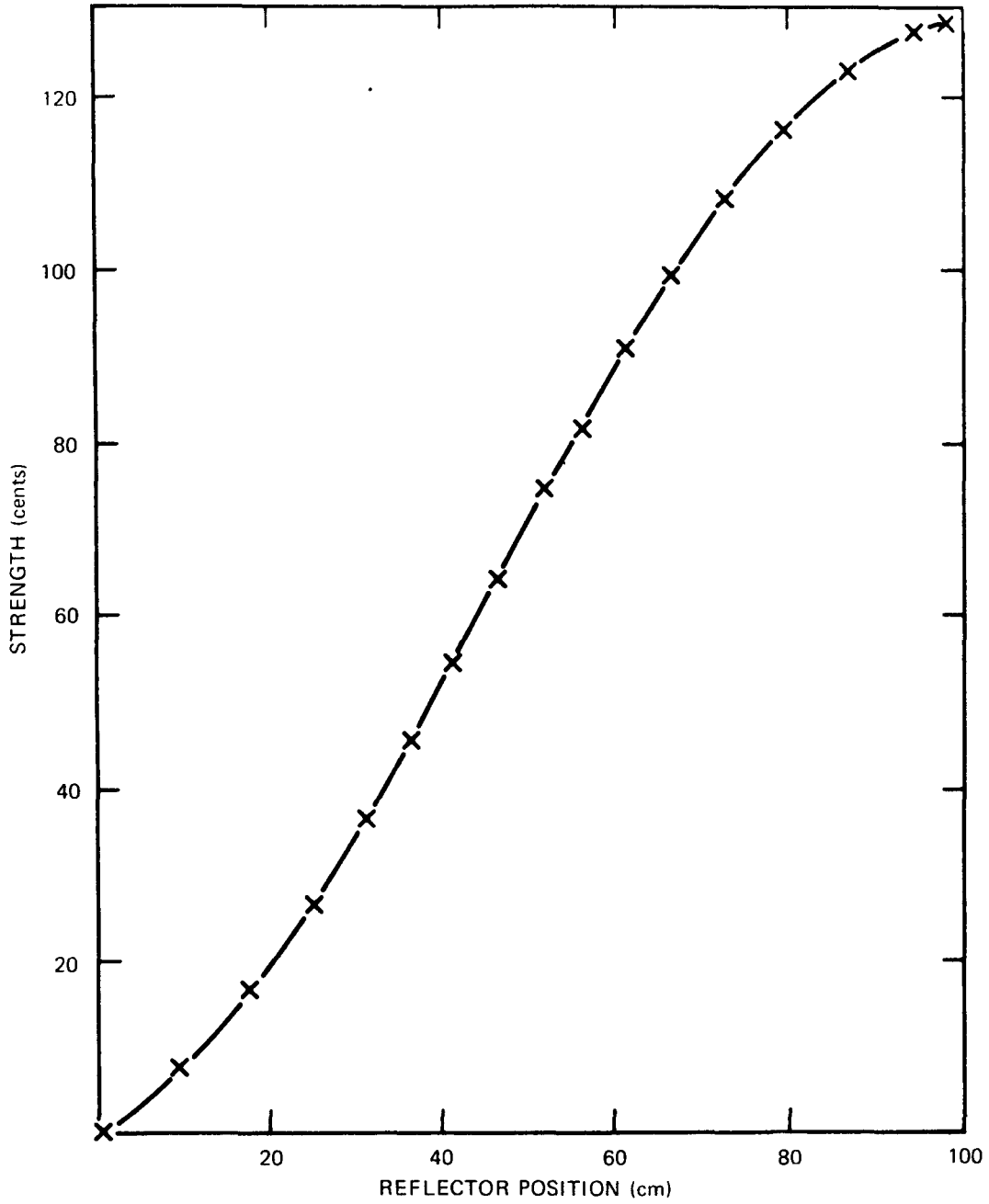
FIGURE 3-1. FINE REFLECTOR NO. 3 CALIBRATION CURVE (ASSEMBLY I-B)
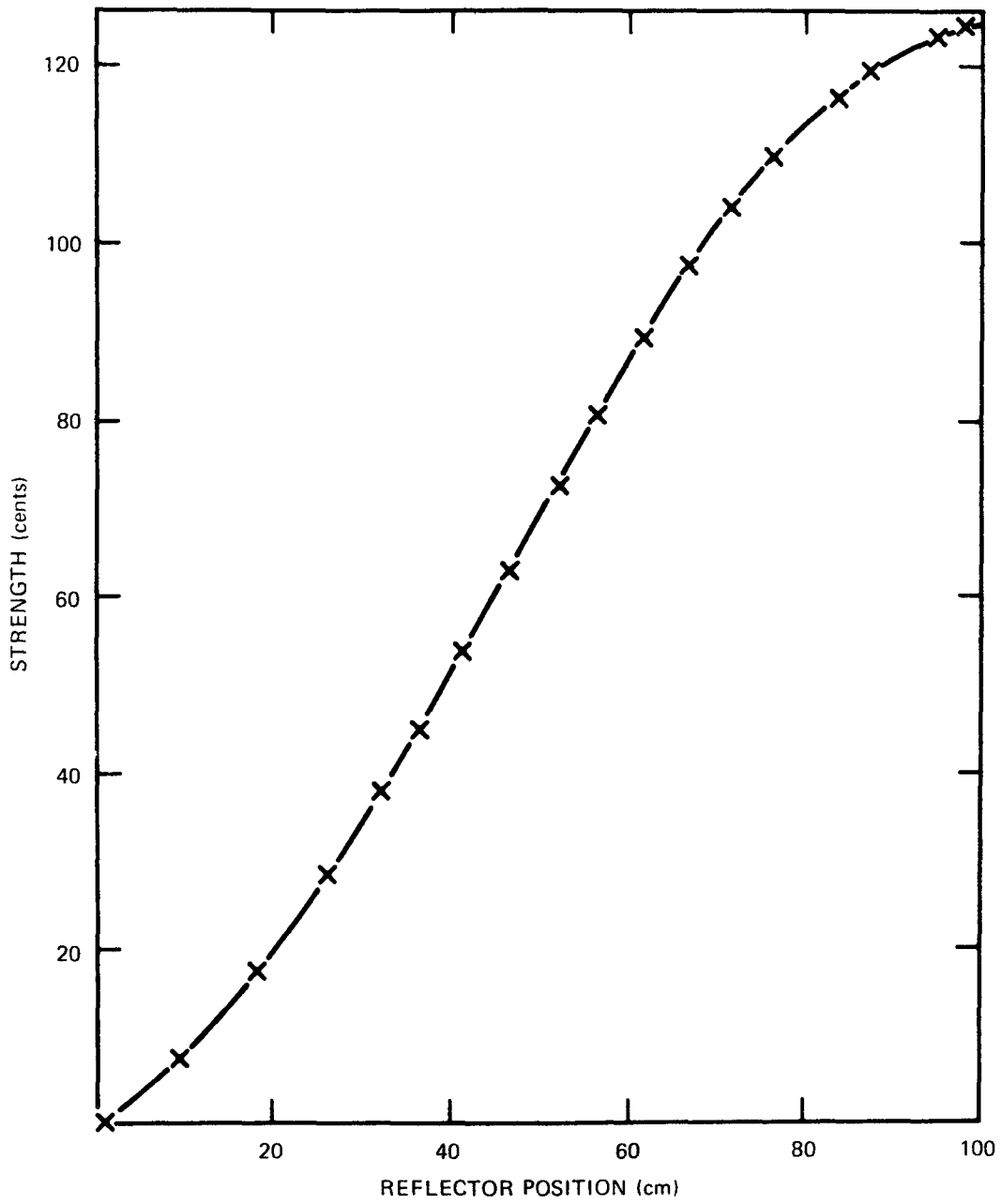
FIGURE 3-2. FINE REFLECTOR NO. 8 CALIBRATION CURVE (ASSEMBLY I-B)
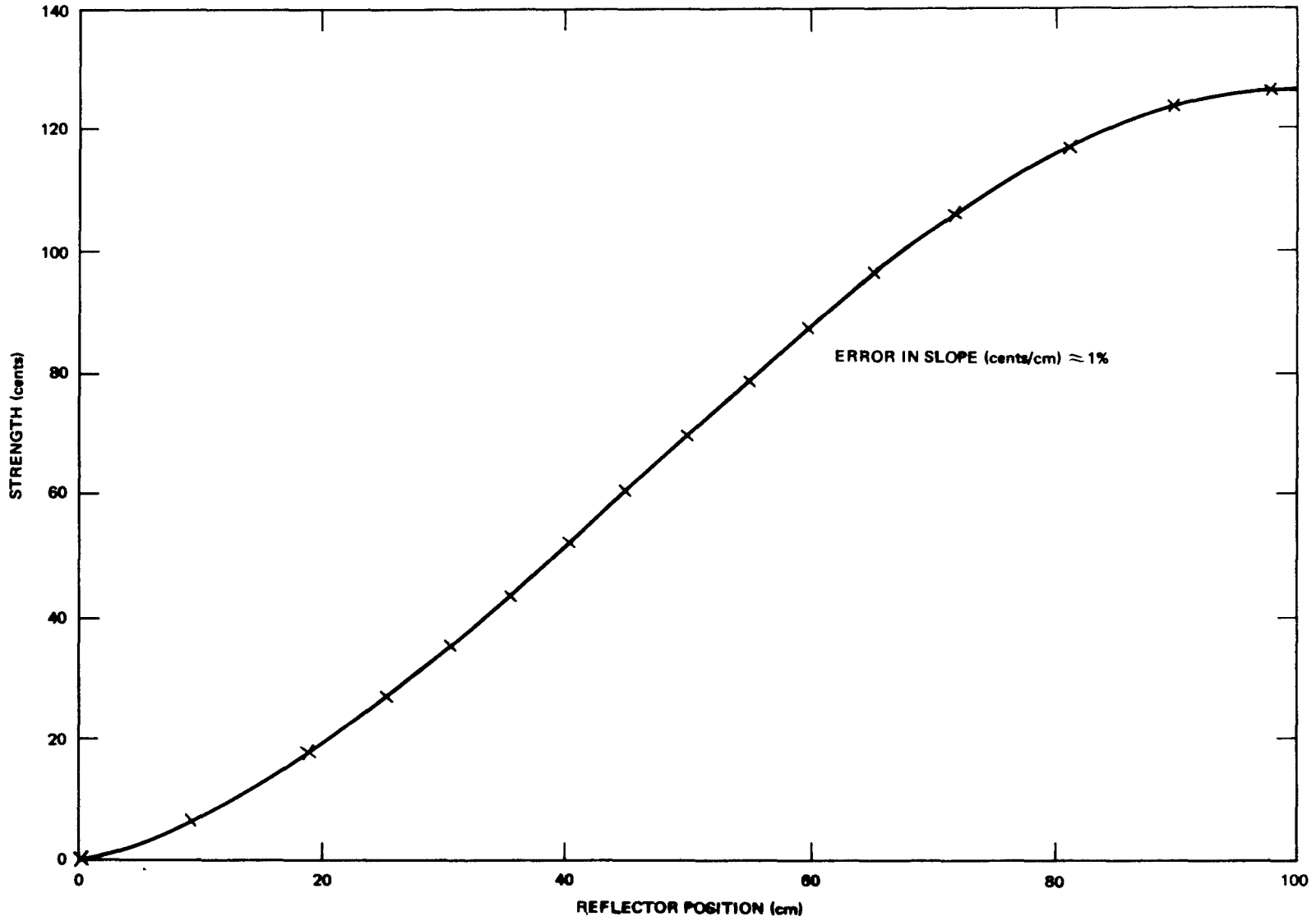
FIGURE 3-3. FINE REFLECTOR NO. 3 CALIBRATION CURVE (ASSEMBLY I-D)
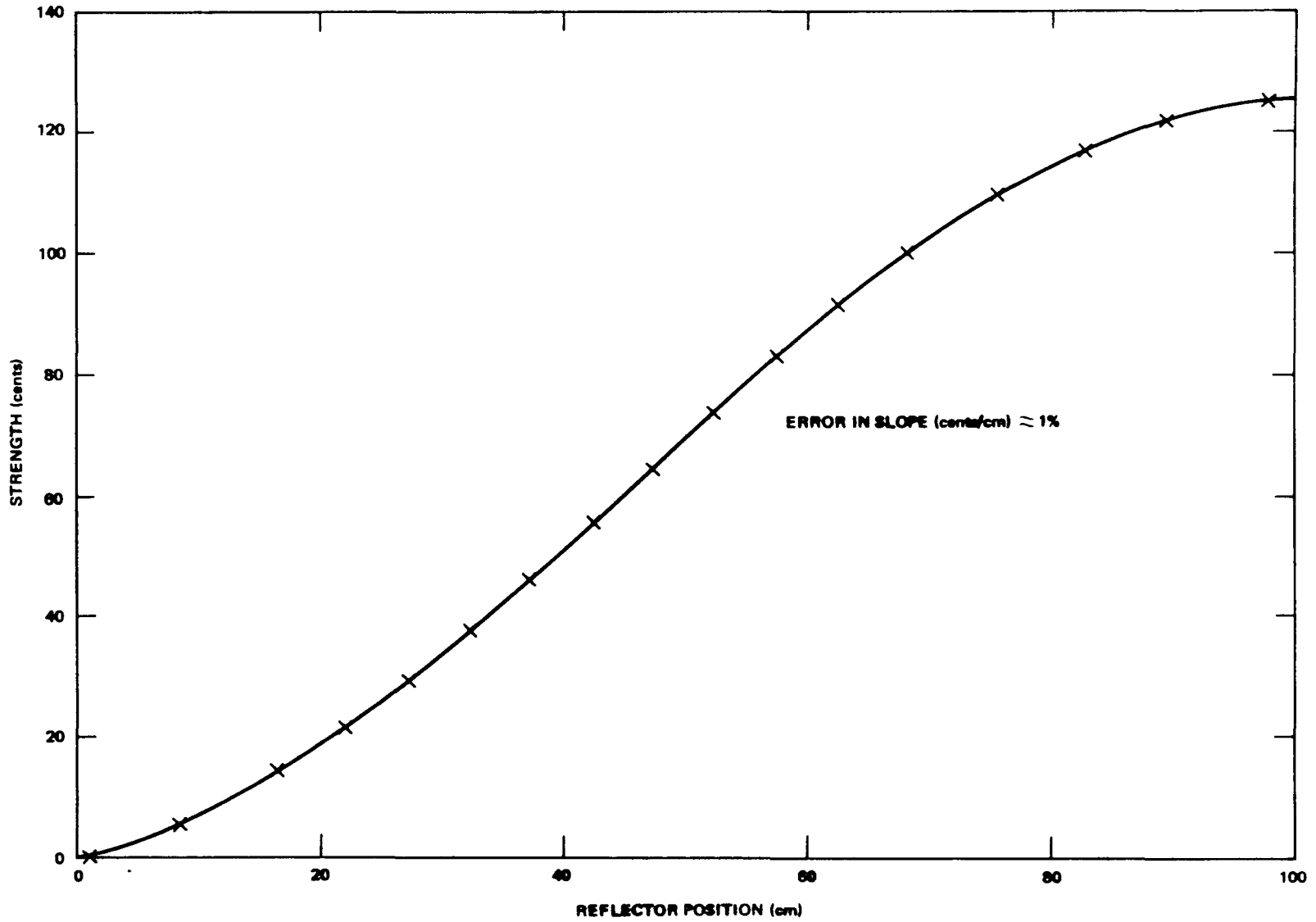
FIGURE 3-4. FINE REFLECTOR NO. 8 CALIBRATION CURVE (ASSEMBLY I-D)

ERROR IN SLOPE (cents/cm) $\simeq 1\%$
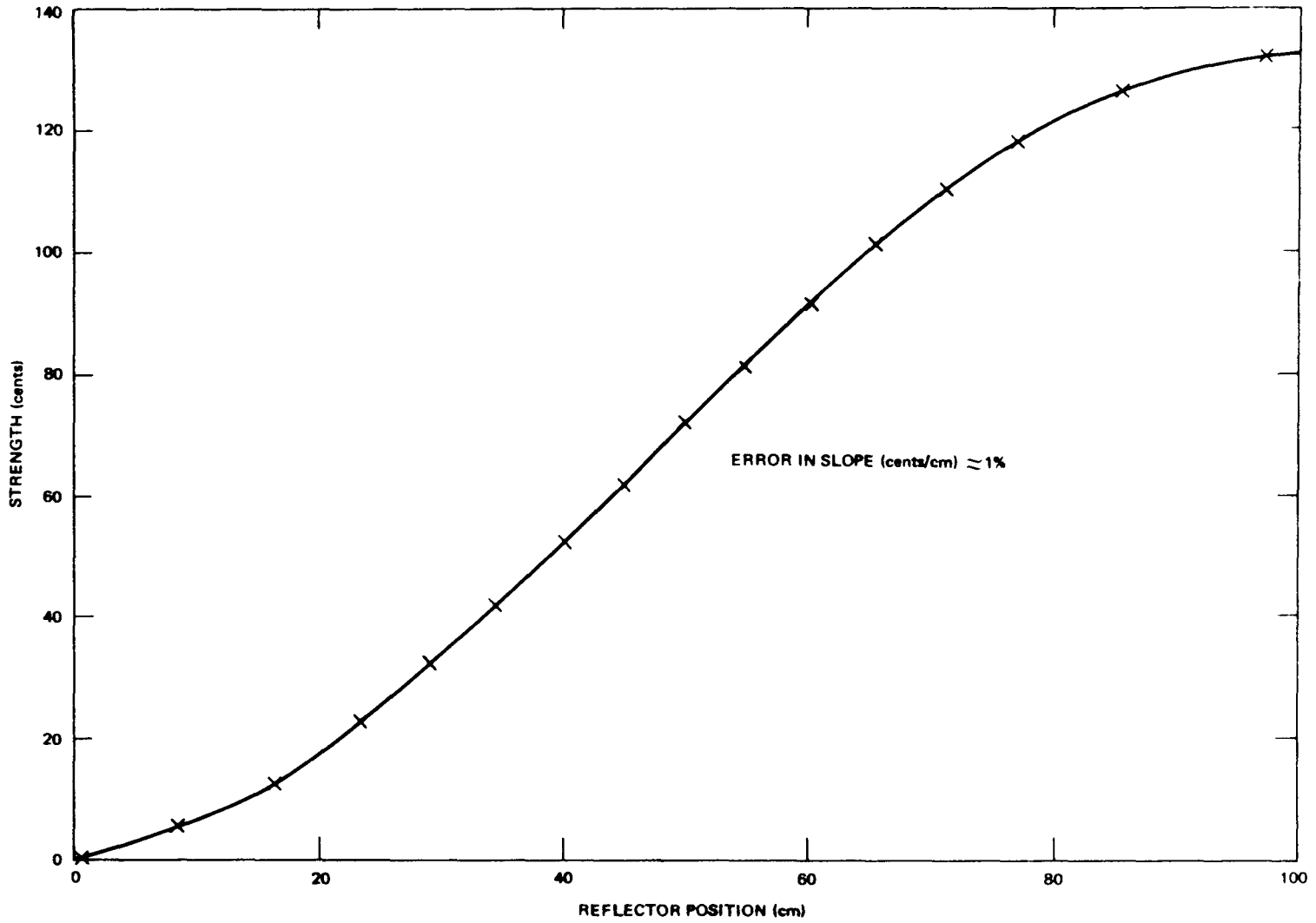
FIGURE 3-5. FINE REFLECTOR NO. 3 CALIBRATION CURVE AT 350°F (ASSEMBLY I-E)
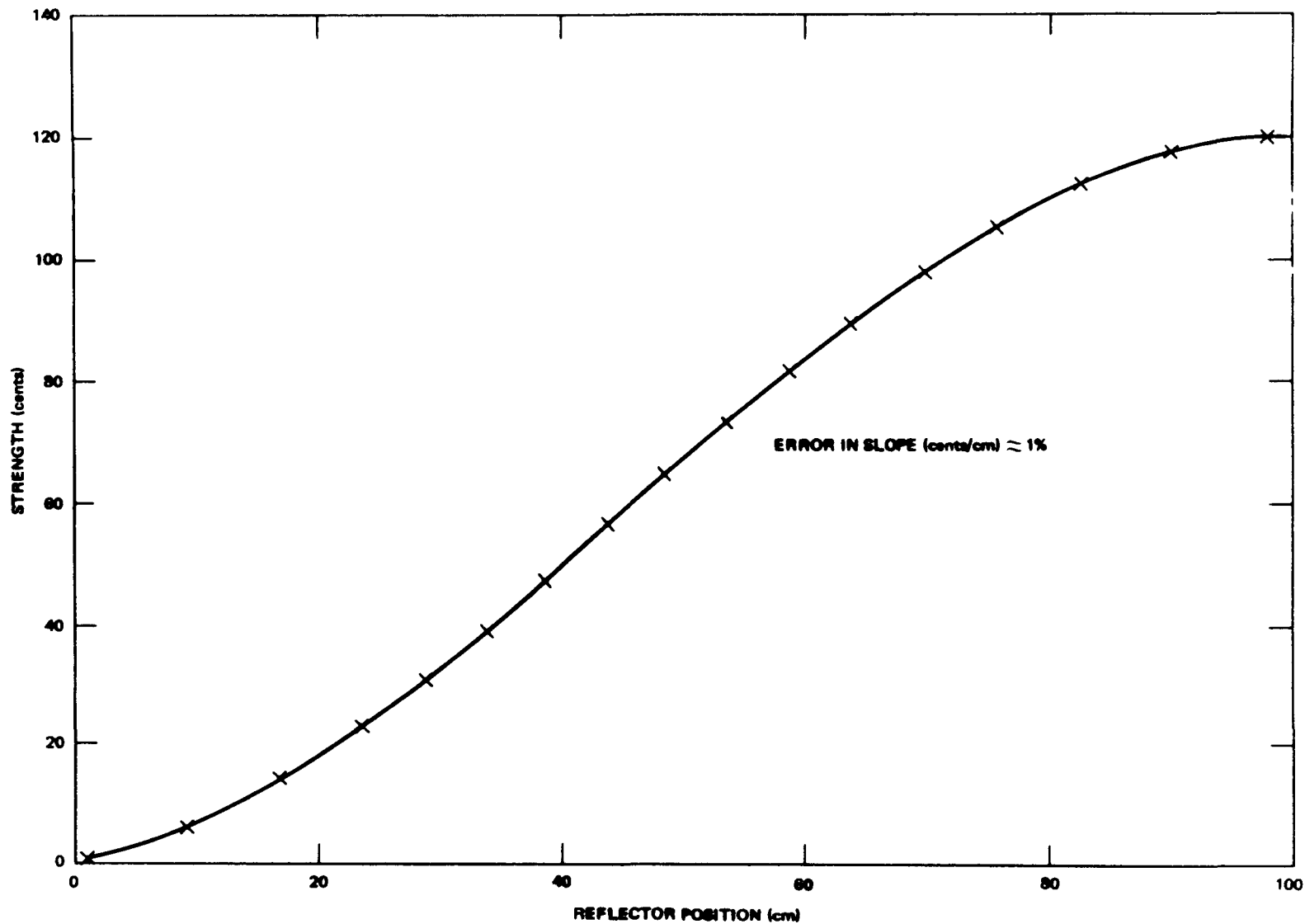
FIGURE 3-6. FINE REFLECTOR NO. 8 CALIBRATION CURVE AT 350°F (ASSEMBLY I-E)
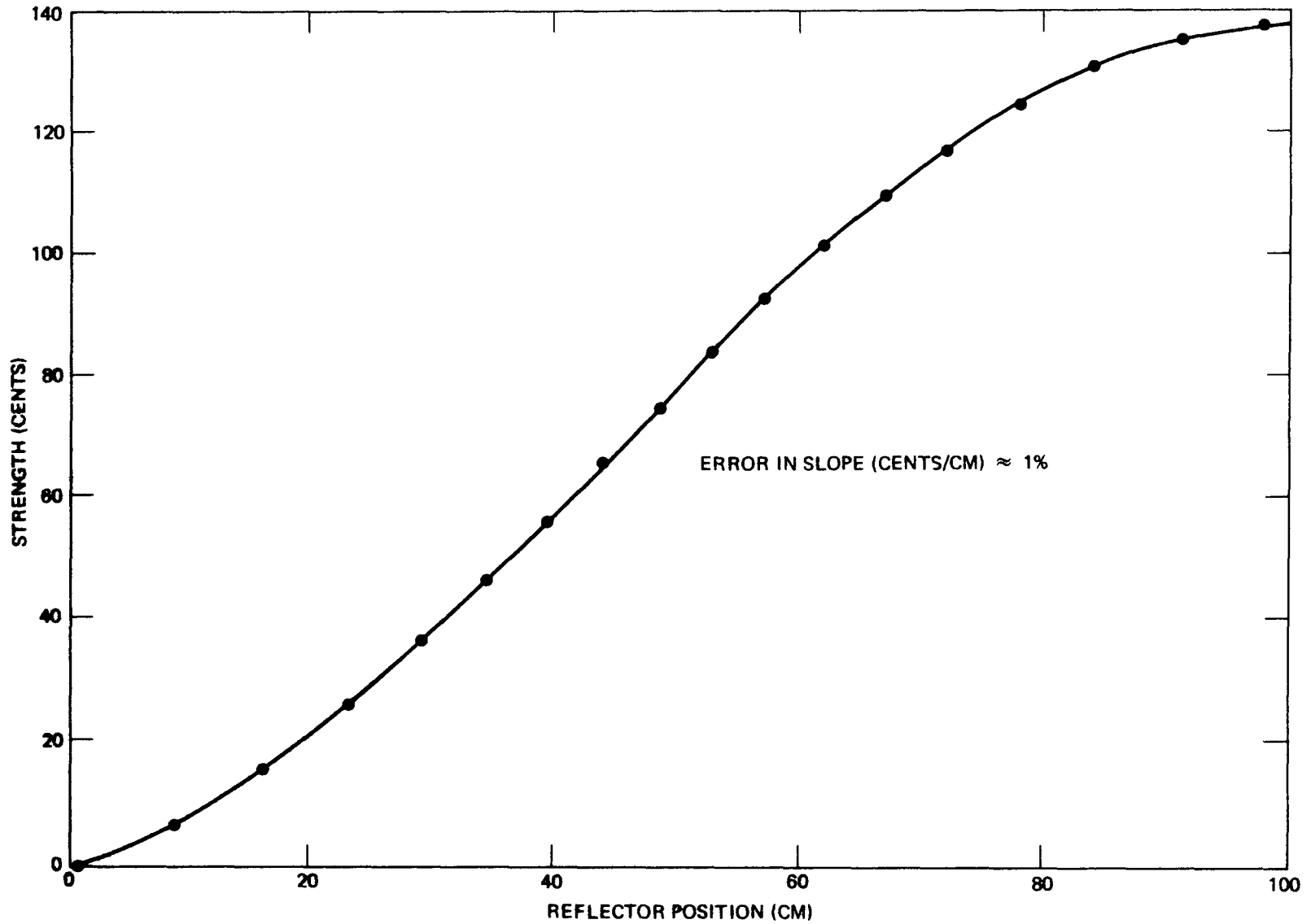
FIGURE 3-7. FINE REFLECTOR NO. 3 CALIBRATION AT 650°F (ASSEMBLY I-E)
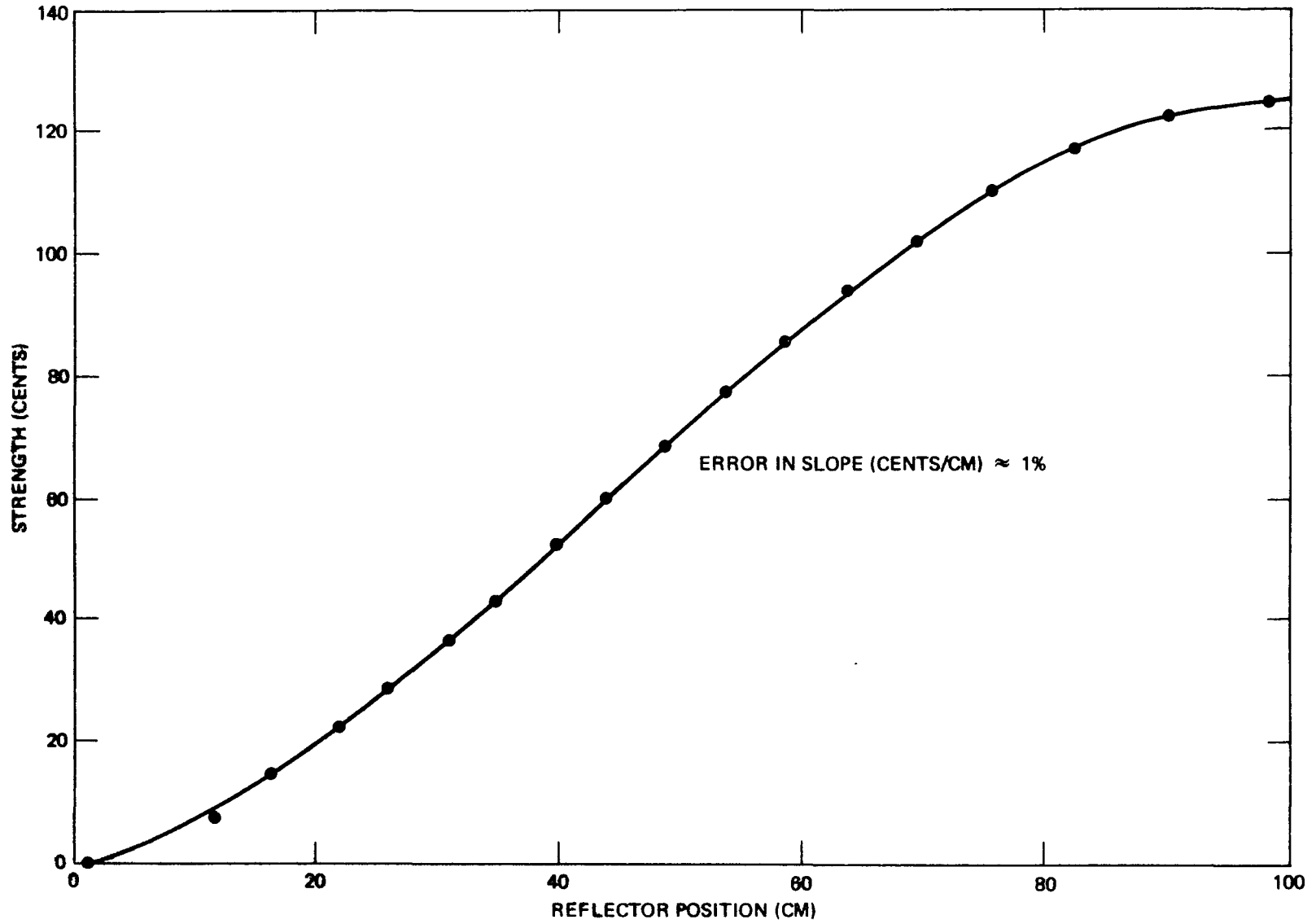
FIGURE 3-8. FINE REFLECTOR NO. 8 CALIBRATION AT 650°F (ASSEMBLY I-E)

TABLE 3-2

REFLECTOR WORTHS FOR ASSEMBLIES I-B and I-D

Worth (dollars)*

Reflector Number	Assembly I-B	Assembly I-D	
	(swapped with #3) (#8 at $\sim$ 85 cm)*** (#10 at $\sim$ 90 cm)***	Set 1 (swapped with #3) (#8 at $\sim$ 50 cm)***	Set 2 (swapped with #8) (#3 at $\sim$ 50 cm)***
1	1.22	1.25	
2	1.26	1.28	1.02
3	1.28**	1.27**	
4	1.28	1.24	0.99
5	1.34	1.25	1.20
6	1.32	1.28	
7	1.29	1.14	1.29
8	1.25**	1.25**	
9	1.20	1.09	1.24
10	1.28	1.26	
Average	1.27		

*The estimated standard deviation in the difference between two values for the same assembly is ±0.01 dollars. - Measurements were made with all reflectors, other than those indicated, in the raised position.

**Worths obtained from period measurements.

***Completely raised position is about 98 cm.

TABLE 3-3

REFLECTOR WORTHS IN ASSEMBLY I-E

Reflector Number	Calibration at 350°F (reflector #5 down)		Calibration at 650°F	
	Worth[++] ($) (swapped with #3)	Position[+] of Reflector #8 (cm)	Worth[++] ($) (swapped with #3)	Position[+] of Reflector #8 (cm)
1	1.42	44	1.39	84
2	1.44	45	1.43	88
3	1.32*	39	1.38*	82
4	1.00	17	1.30	75
5	1.23**	40	1.27	71
6	0.87	2	1.24	70
7	0.88	3	1.16	64
8	1.20*	--	1.25*	--
9	1.00	17	1.18	66
10	1.34	40	1.33	78

*Worth obtained from period measurements

** Worth measured with reflector #10 lowered.

+ Position of reflector #8 when the indicated reflector was lowered.

++ The estimated standard deviation in the difference between two values at the same temperature is ±0.01 dollars

GEAP-13588

In addition to demonstrating the asymmetry in worth that is congruous with an asymmetric core loading, the tabulated worths for both* assemblies I-D and I-E show that the worth of a reflector is influenced by the position of its neighbors. In particular, the total worth of a reflector is less when an adjacent reflector is lowered, or partially lowered, than when both adjacent reflectors are completely raised. For example, in the first set of measurements (Set 1 of Table 3-2) for Assembly I-D, fine reflector #3 was swapped with the coarse reflector to be calibrated, while fine reflector #8 was adjusted to maintain criticality. For these measurements, reflector #8 was only partially raised (approximately halfway) during the "swap". The reflectors adjacent to number eight (#7 and #9) are consequently lower in worth than the others. In the second set of measurements in Table 3-2, the functions of the two fine reflectors were interchanged. This caused a decrease in the worth of Reflector #2 and #4. Similarly, the data in Table 3-3 for Assembly I-E demonstrates this "shadowing" effect. For the measurements at 350°F, reflector #5 was lowered and #8 was either partially or almost completely lowered. The worths of reflectors #6 and #7 are thus considerably less in this configuration than the worths of the other reflectors. The worths of #4 and #9 demonstrate the same "shadowing" effect, although to a lesser extent, since their worths were determined with only one completely lowered neighboring reflector.

---

*The results for Assembly I-B also demonstrate this effect, although to a smaller extent, in that reflector #9 has a slightly smaller worth than the other reflectors (and also a slightly smaller worth than the worth of #9 in Assembly I-D) due to its two slightly lowered neighbors.

A comparison of the Assembly I-E calibrations at 650°F, which were performed with all coarse reflectors raised, with those at 350°F clearly demonstrates the influence of the lowered reflector #5 and partially lowered reflector #8 on other reflector worths. The worths of reflectors #1, #2, and #10 are essentially unchanged and #5 is only slightly changed, while the worths of #4, #6, #7, and #9 are from 18 to 43% larger at 650°F where #5 is completely raised and #8 is raised more than at 350°F. The worths of #3 and of #8 are both about 4% larger at 650°F than at 350°F. This is probably due to the influence of reflector #5 on the calibration of #3 and the influence of reflector #10 on the calibration of #8 (see above).

The "shadowing effects" thus appear to be somewhat localized although the worth of a reflector may be influenced by as much as 4% by the position of a neighbor which is only two reflectors removed.

3.3.4   Calibration Accuracy

The accuracy of the calibrations for measurements of the fine-reflector period is indicated by the data in Tables 3-4 and 3-5. The reactivity values under the second column of the tables were calculated with the in-hour equation using periods obtained from visual observation of flux changes and doubling-time measurements made with a stop watch. The values in the third column were calculated on-line from the neutron-flux signal input to a computer. These data provide two independent checks on the calibration and are in very good agreement. With the small reactivity values (large periods) excepted, the mean-squared deviation is approximately 0.9 percent for reactivity increments of the order of 9 cents. Similar deviations also occur in six repeated

TABLE 3-4

FINE REFLECTOR #8 CALIBRATION IN ASSEMBLY I-D

| Step No. | Reactivity | | %Deviation |
	Doubling-time Measurement (cents)	On-line Reactivity Meter(cents)	
1	5.58	5.65	-1.3
2	8.46	8.5	-0.5
3	7.66	7.75	-1.2
4	7.57	7.5	0.9
5	8.59	8.6	-0.1
6	8.68	8.7	-0.2
7	9.10	9.1	0.0
8*	9.41	9.45	-0.4
8A*	9.40	9.3	1.1
8B*	9.35	9.3	0.5
8C*	9.46	9.3	1.7
8D*	9.38	9.3	0.9
8E*	9.12	9.2	-0.9
9	9.24	9.25	-0.1
10	9.33	9.2	1.4
11	7.88	7.9	-0.3
12	8.55	8.6	-0.6
13	9.84	9.75	0.9
14	6.87	6.95	-1.2
15	5.16	5.3	-2.7
16	3.36	3.5	-4.2

*Repeated measurements of the reactivity associated with the movement of reflector #8 between 42.10 cm and 47.14 cm.

TABLE 3-5

PORTION OF FINE REFLECTOR #3 CALIBRATION
IN ASSEMBLY I-D

| | Reactivity | | |
Step No.	Doubling-time Measurement (cents)	On-line reactivity Meter (cents)	%Deviation
6	8.72	8.65	0.8
7	8.60	8.5	1.1
8	9.24	9.2	0.4
9	8.51	8.5	0.1
10	8.97	8.8	1.9
11	9.04	9.1	-0.7
12	9.56	9.6	-0.4
13	10.75	10.7	0.5
14	6.45	6.5	-0.8
15	2.87	3	-4.5

measurements (Step No. 8 through Step No. 8E) listed in Table 3-4.
Thus a ± 1 percent uncertainty is assigned to the slope of the reflector-
worth calibration curve (see Figures 3-1 through 3-8). The effects
of these deviations on measured reactivity changes are discussed in
Section 4.4.

SECTION IV

MATERIAL REACTIVITY WORTH MEASUREMENTS

4.1 SUMMARY OF RESULTS FOR ASSEMBLIES I-B AND I-D

The reactivity worth of numerous materials, such as fuel, B_4C, depleted UO_2, BeO, etc. were measured at different locations in the core of the 563 rod partially loaded core Assembly I-B and in the fully loaded core Assembly I-D. All materials were in rods which were identical, except for identification markings, to normal fuel rods, or in the case of BeO to tightener rods. The compositions of the various rods are given in Appendix I.

Generally acceptable agreement between experimental and calculated material reactivity worths was obtained. However, the consistent over-estimate (by 10 to 15%) of material worths in the center of Assembly I-D, (see Section 4.3) combined with the reaction rate discrepancies discussed in Section V, indicates that the spatial dependence of the flux is flatter than predicted, and analysis (Section 4.3) indicates that the calculations are sensitive to the axial flux shapes near the radial core boundaries. Comparison of two-dimensional S-4 transport and diffusion theory calculations in four energy groups indicated only a small effect due to the underprediction of core leakage by diffusion theory calculations. Generally better agreement between calculated and measured values can be obtained for both Assemblies I-B and I-D by increasing the calculated effective delayed neutron fraction, β, which is approximately 90% of the true delayed neutron fraction, by 6 to 10 percent.

4.2   WORTH MEASUREMENTS IN ASSEMBLY I-B

The reactivity worth of fuel (18.7% fissile Pu), B_4C, and stainless steel rods were measured at four different radial core locations in the 563 rod partially loaded core Assembly I-B as part of the planned experimental program. In addition, the reactivity worth of four BeO tightener rods on the core periphery were measured. During the measurements a fuel rod that was substantially low (approximately 40%) in worth was found and an extensive investigation was undertaken to determine the extent of the problem. The investigation, which is reported in Reference 1, showed that a number of rods were low in worth. As discussed in Section 2.2, the very low worth rods were removed after completion of the experiments on Assembly I-B. The results of the originally planned measurements are given here. The results of the additional reactivity worth measurements performed during the investigation of the low worth rods are given in Reference 1.

The reactivity worth of fuel, B_4C, and stainless steel rods at a given location were measured by recording the reactor temperature and the critical reflector positions with the following core arrangements; the core loading with the original fuel rod in place; the original fuel rod removed – the fuel rod location thus being filled with liquid sodium; the original fuel rod replaced by the reference fuel rod, the B_4C rod, or the stainless steel rod; and finally the core with the original rod re-inserted. The worth of the peripheral BeO tightener rods in Assembly I-B was determined from the critical reflector configurations occurring before and after insertion of four rods into sodium filled tightener rod locations.

The positions within the core at which measurements were made
are illustrated in Figure 4-1, and measured results are shown in
Figures 4-2 through 4-4 along with the curves obtained using per-
turbation calculations of 13 group two-dimensional synthesis solutions,
and the calculated effective delayed neutron fraction, β, for this
assembly of 0.00323. The measured results are also tabulated in
Table 4-1 along with the calculated values.

It is evident that the worth of fuel rod No. 874 is considerably
less than the worth of the reference rod No. 781. The relatively large
discrepancy between calculated and measured fuel rod worths at location
W1.0 - S2.0-B (in measurement set number 3) may be the result of a
number of very low worth rods in this region which were not taken into
account in the calculation. A portion of this disparity may also be
attributable to an over-estimate or rod worths near the core center
by the two-dimensional synthesis calculations, as evidenced by the
disparities in Assembly I-D (see below). The apparent close agreement
between calculated and measured fuel (if not B_4C) rod worths at location
N1.0 - N2.0-B would appear to refute the latter explanation; however,
it is possible that the very low worth rods in the vicinity of W1.0 -
S2.0-B may have caused an increase in measured worth on the opposite
side of the core near location E1.0 - N2.0-B to bring closer agreement
between measurement and calculation at this point than would otherwise
have occurred.

It is worthy of note that better agreement between the experimental
and calculated values is obtained by increasing the calculated effective
delayed neutron fraction (β) by 6% so that the calculated worths, in
cents, are decreased by 6%.
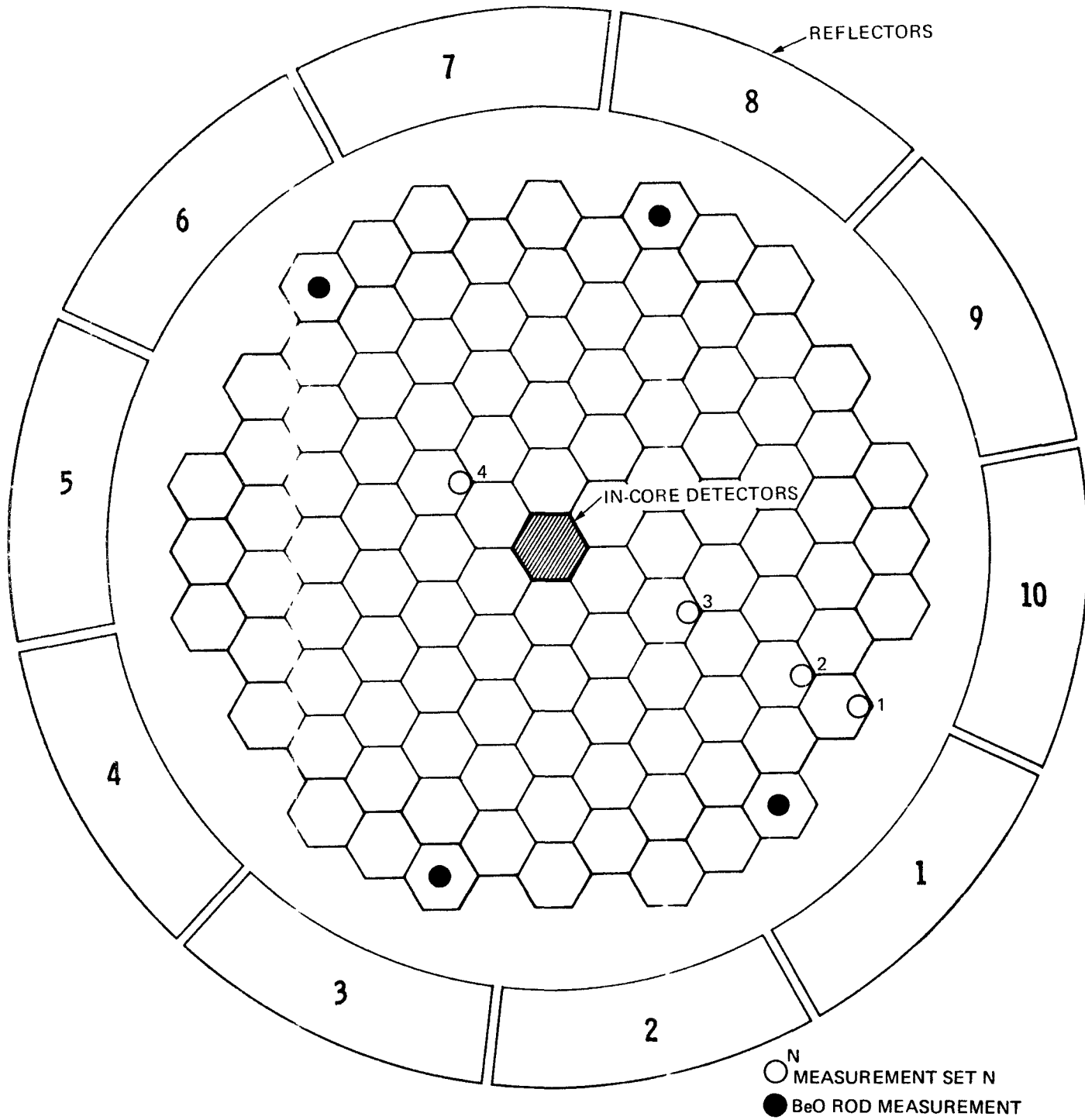
FIGURE 4-1. LOCATION OF MATERIAL WORTH MEASUREMENTS IN ASSEMBLY I-B
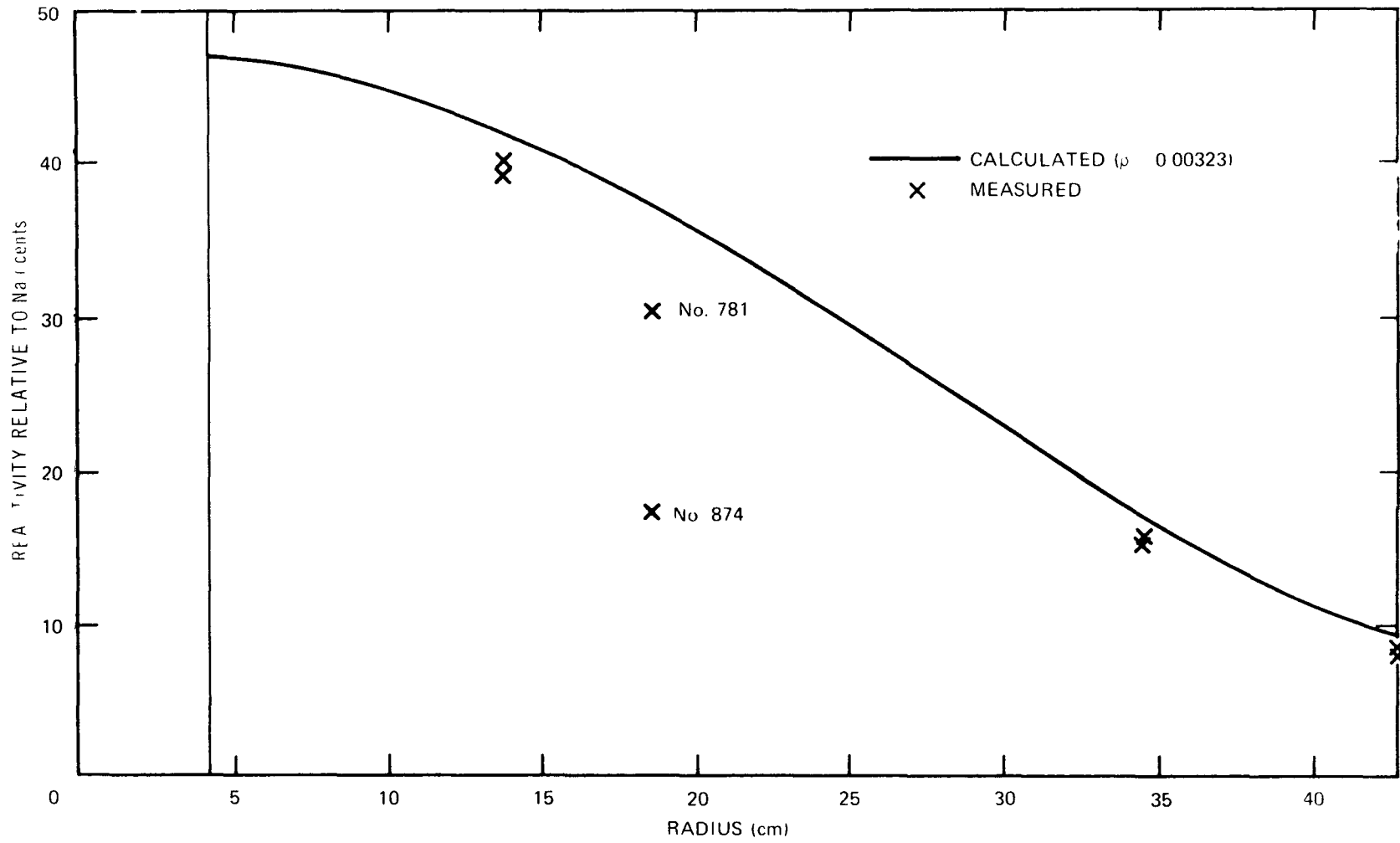
FIGURE 4-2. RADIAL DEPENDENCE OF FUEL ROD WORTH (ASSEMBLY I-B)
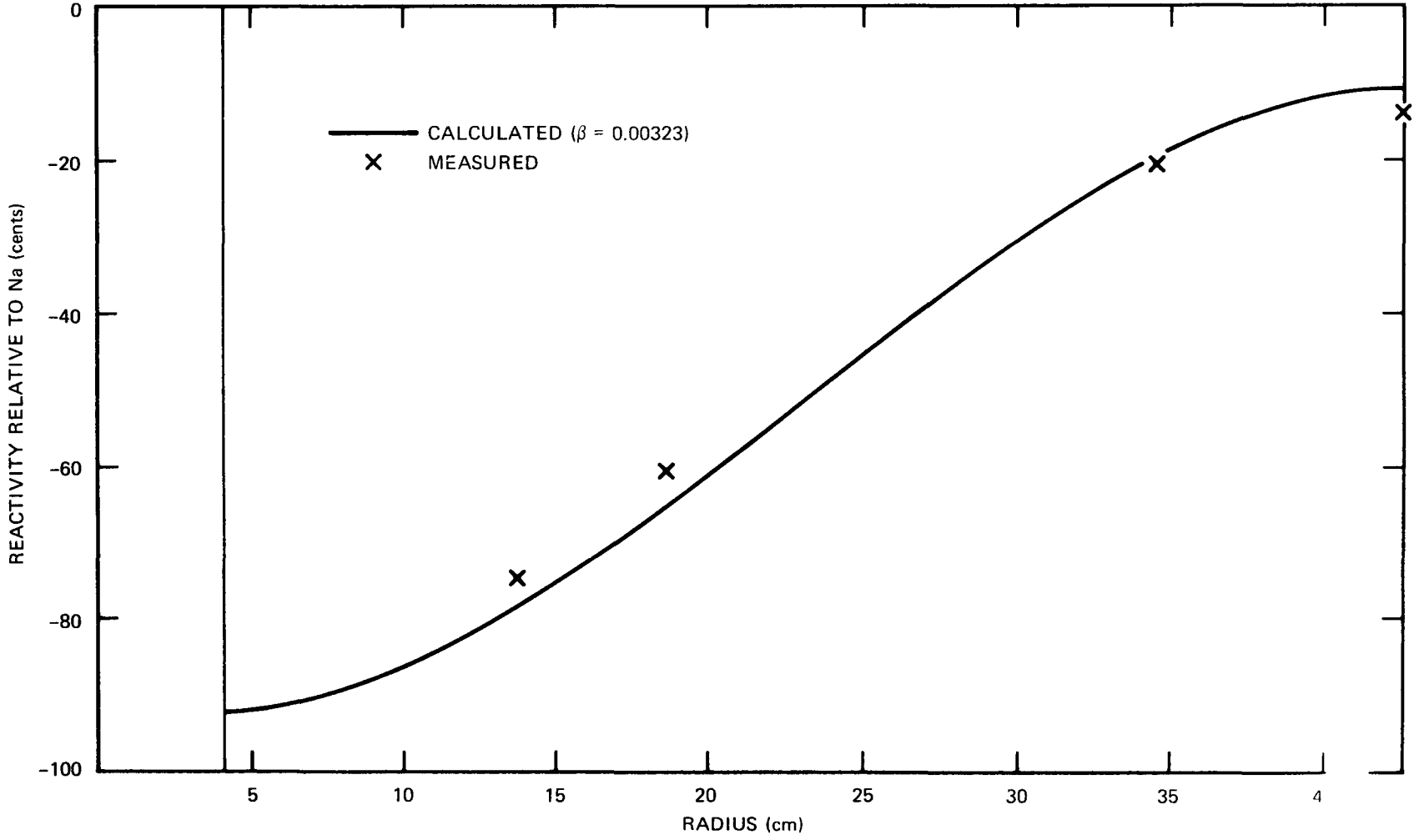
FIGURE 4-3. RADIAL DEPENDENCE OF B_4C ROD WORTH (ASSEMBLY I-B)
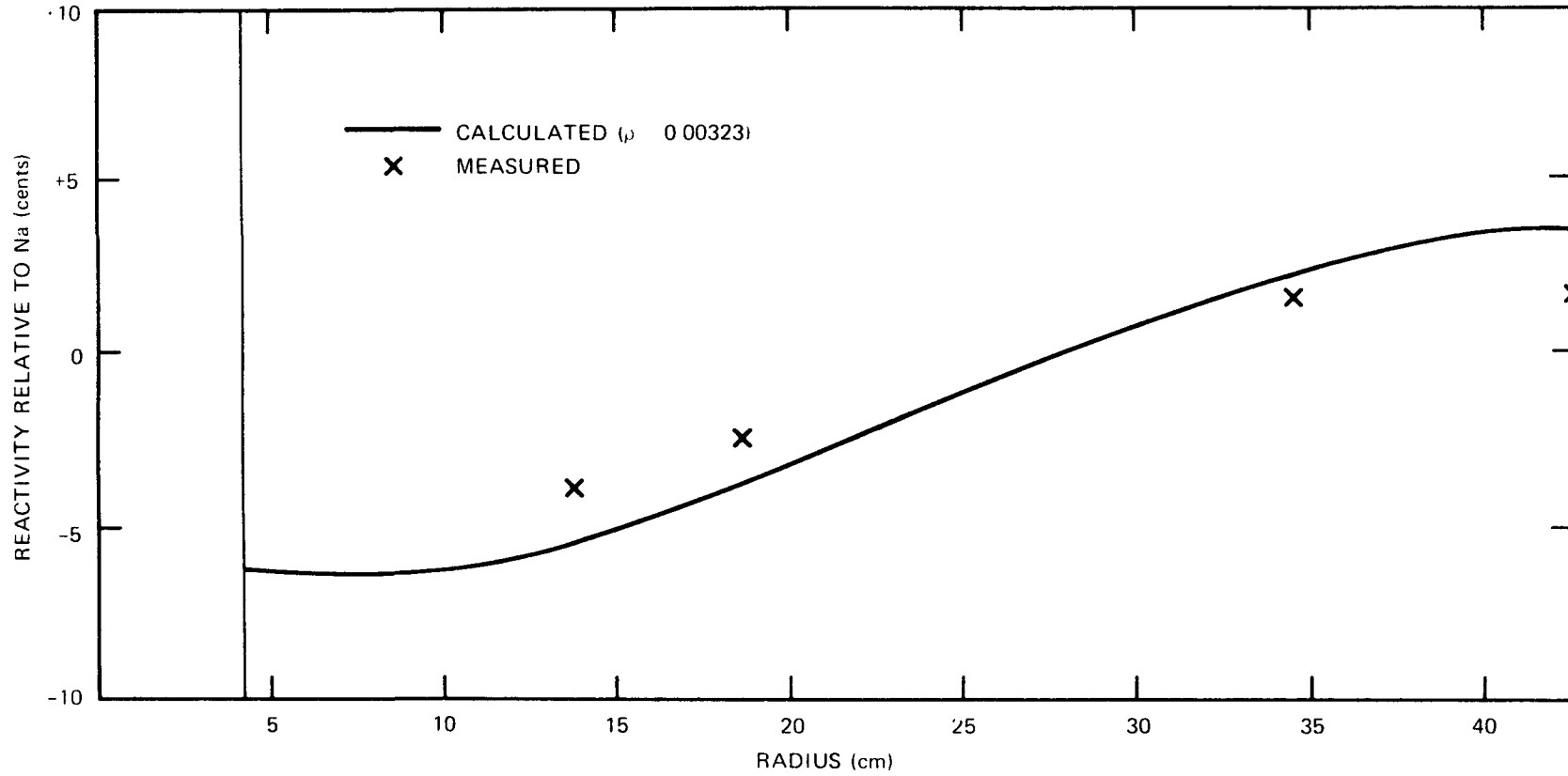
FIGURE 4-4. RADIAL DEPENDENCE OF STAINLESS STEEL ROD WORTH (ASSEMBLY I-B)

TABLE 4-1

MATERIAL REACTIVITY WORTH MEASUREMENTS

(ASSEMBLY I-B)

Measurement set Number	Core Location*	Type of Rod	Worth Relative to Sodium(cents)	
			Measured**	Calculated*** (β=0.00323)
1	W2.5-S5.0-B (Radius=42.7 cm)	Fuel (No.414)	+ 8.1	+ 8.8
		Fuel (No. 781)	+ 8.4	+ 8.8
		Stainless Steel	+ 1.7	--
		B_4C	-14.3	-14.9
2	W2.0-S4.0-B (Radius=34.6 cm)	Fuel (No.635)	+15.3	+16.6
		Fuel (No.781)	+15.7	+16.6
		Stainless Steel	+ 1.7	+ 2.5
		B_4C	-23.7	-23.0
3	W1.0-S2.0-B (Radius=18.6 cm)	Fuel (No.874)	+17.6	+37.4
		Fuel (No.781)	+30.5	+37.4
		Stainless Steel	- 2.5	- 3.3
		B_4C	-60.7	-69.8
4	E1.0-N2.0-B (Radius=13.8 cm)	Fuel (No.791)	+40.2	+42.4
		Fuel (No.781)	+39.3	+42.4
		Stainless Steel	- 3.9	- 4.4
		B_4C	-74.6	-83.8
	W4.0-S4.0 E4.0-N4.0 E5.0-S2.0 W5.0-N2.0 (Radius=42.6 cm)	4 BeO Tightener Rods	+16.0	+16.0

*   See Core loading Diagram - Figure 1-8, also Figure 4-1.

**   The estimated standard deviation in the measurement is approximately +0.5 cents (see Section 4.4).

*** Perturbation results of a two-dimensional synthesis calculation.

4.3   WORTH MEASUREMENTS IN ASSEMBLY I-D

The reactivity worth of fuel (18.7% fissile Pu), B_4C, stainless steel, guinea pig (25% fissile Pu), depleted UO_2, and BeO tightener rods were measured at several locations in Assembly I-D. The measurements were performed in the same manner, which is described above, as in Assembly I-B, with the addition that a guinea pig and a depleted UO_2 rod were substituted for the original fuel rod during the sequence of measurements. The worth of the BeO tightener rods in Assembly I-D were determined at four radial locations by replacing the original BeO rods in these locations with special stainless steel tightener rods. The positions within the core at which measurements were made are illustrated in Figure 4-5. The compositions of the various rods are discussed in Appendix I.

The measured values of fuel, B_4C, UO_2, and guinea pig rods are illustrated in Figures 4-6 through 4-9 along with calculated results, and measured values for all materials are tabulated in Tables 4-2 through 4-4. The data indicates that the measured worth of a fuel rod is higher at location E1.5 - N3.0-B (a radius of 21.8 cm) than at location W2.5 - N1.0-B (a radius of 20.6 cm). This may be due to the proximity of three B_4C rods at the latter location and the deficiency of B_4C rods in the N-E portion of the core (see Figure 4-5). However, a comparison of the measurement at E1.0 - N2.0-B with that at E1.0 - S2.0-D indicates that the proximity of a B_4C rod has little influence on fuel rod worth, and it is more probable that the indicated difference is a result of experimental variations.

The reactivity worths of the different materials were calculated from perturbations of one-dimensional diffusion and two-dimensional

● LOCATION OF IN-CORE B$_4$C RODS
⊕ FUEL, B$_4$C, UO$_2$, AND STEEL ROD WORTH MEASUREMENTS
⊙ FUEL AND GUINEA PIG ROD WORTH MEASUREMENTS
○ FUEL ROD WORTH MEASUREMENTS
○ BeO TIGHTENER ROD WORTH MEASUREMENTS
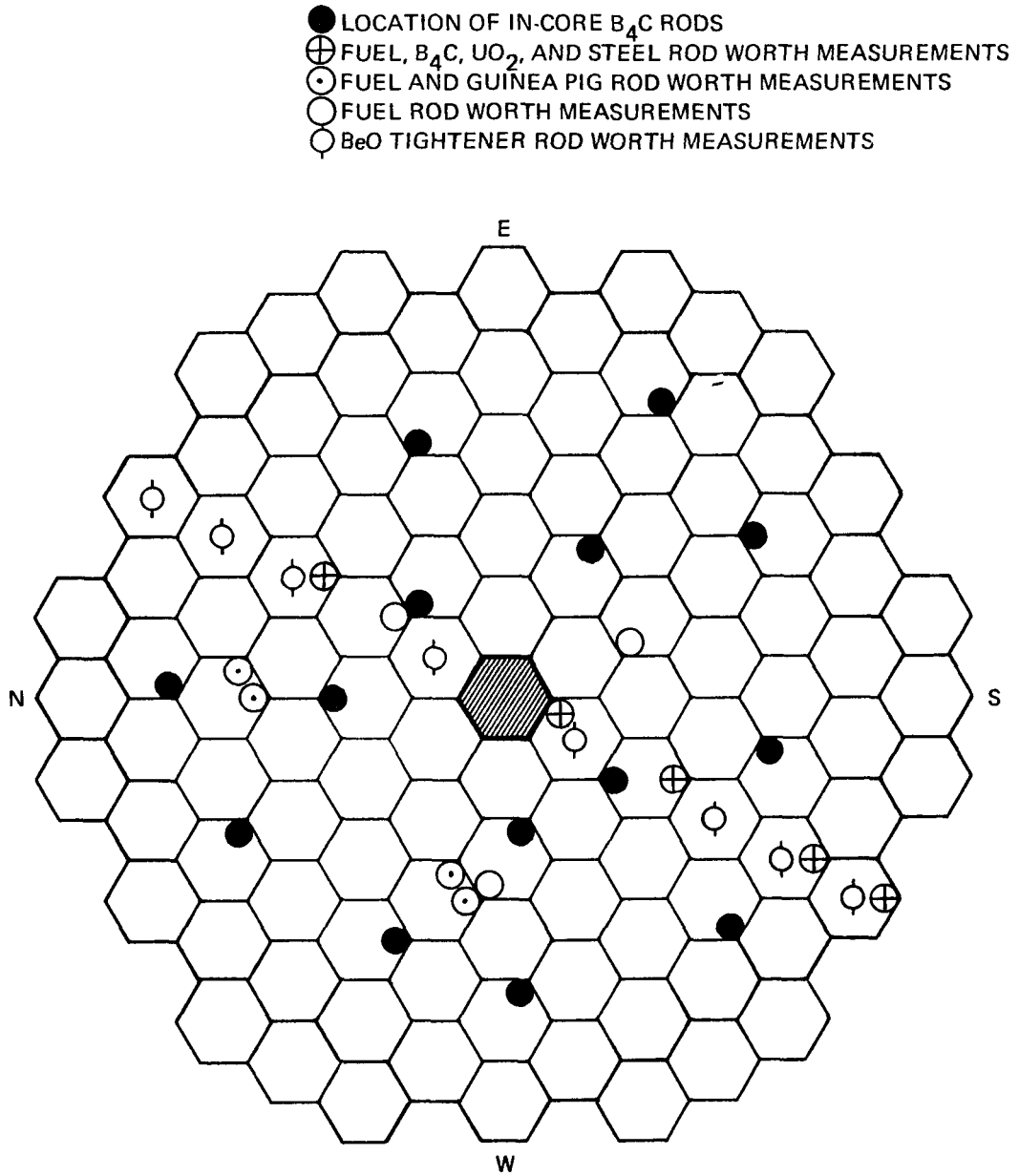
FIGURE 4-5. LOCATIONS OF MATERIAL WORTH MEASUREMENTS IN ASSEMBLY I-D
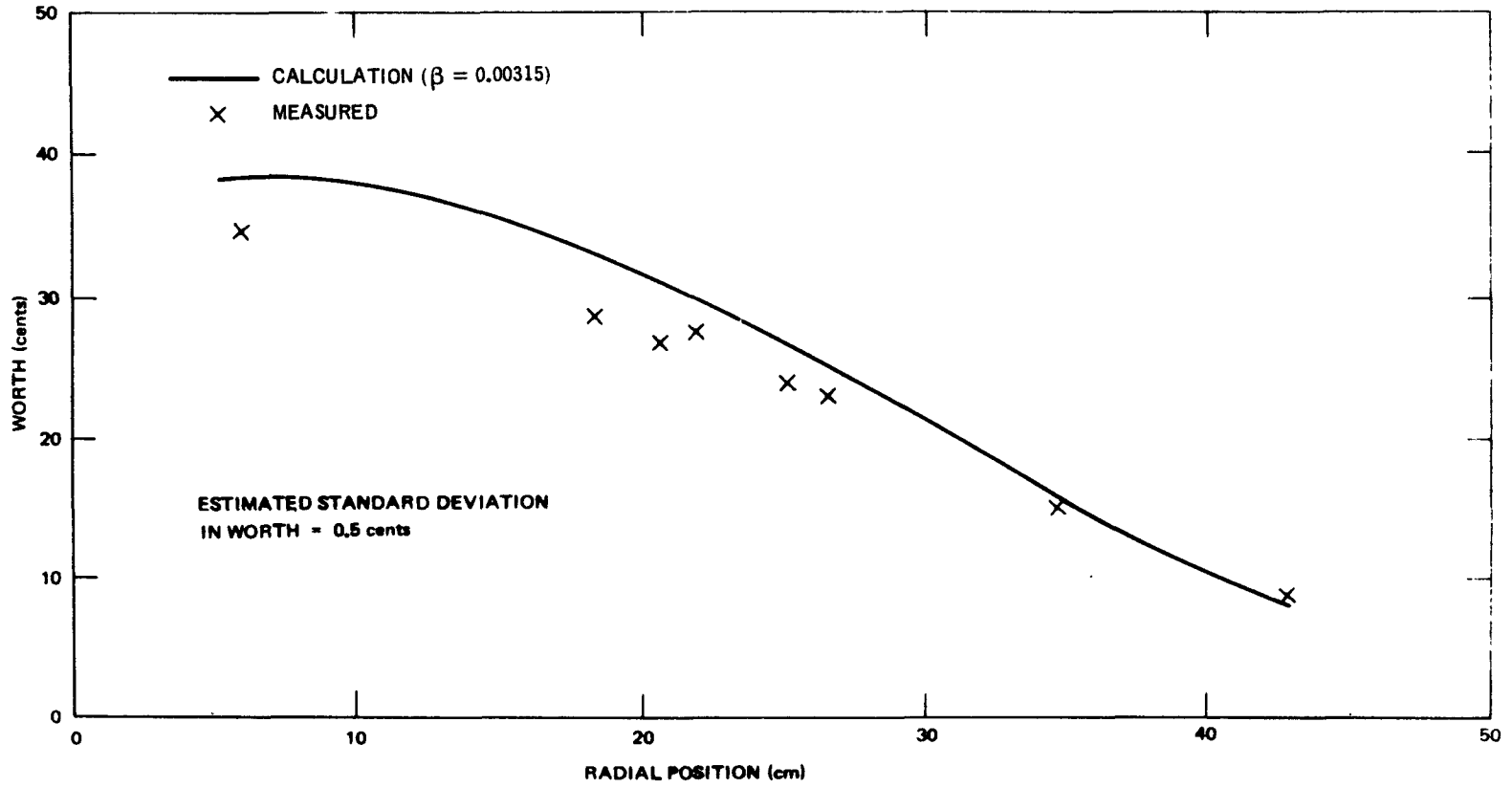
FIGURE 4-6. RADIAL DEPENDENCE OF FUEL ROD WORTH (ASSEMBLY I-D)
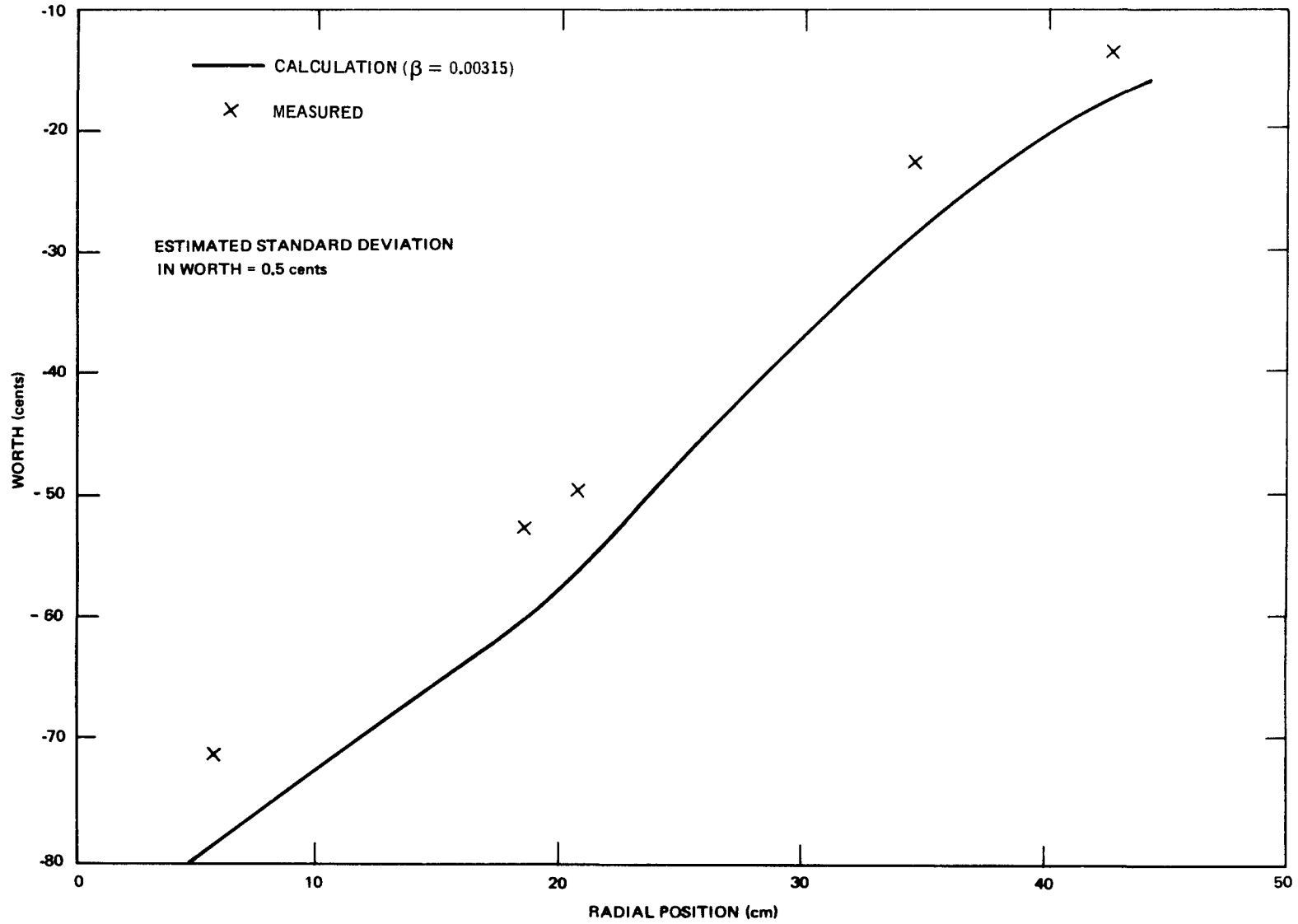
FIGURE 4-7. RADIAL DEPENDENCE OF B₄C ROD WORTH (ASSEMBLY I-D)
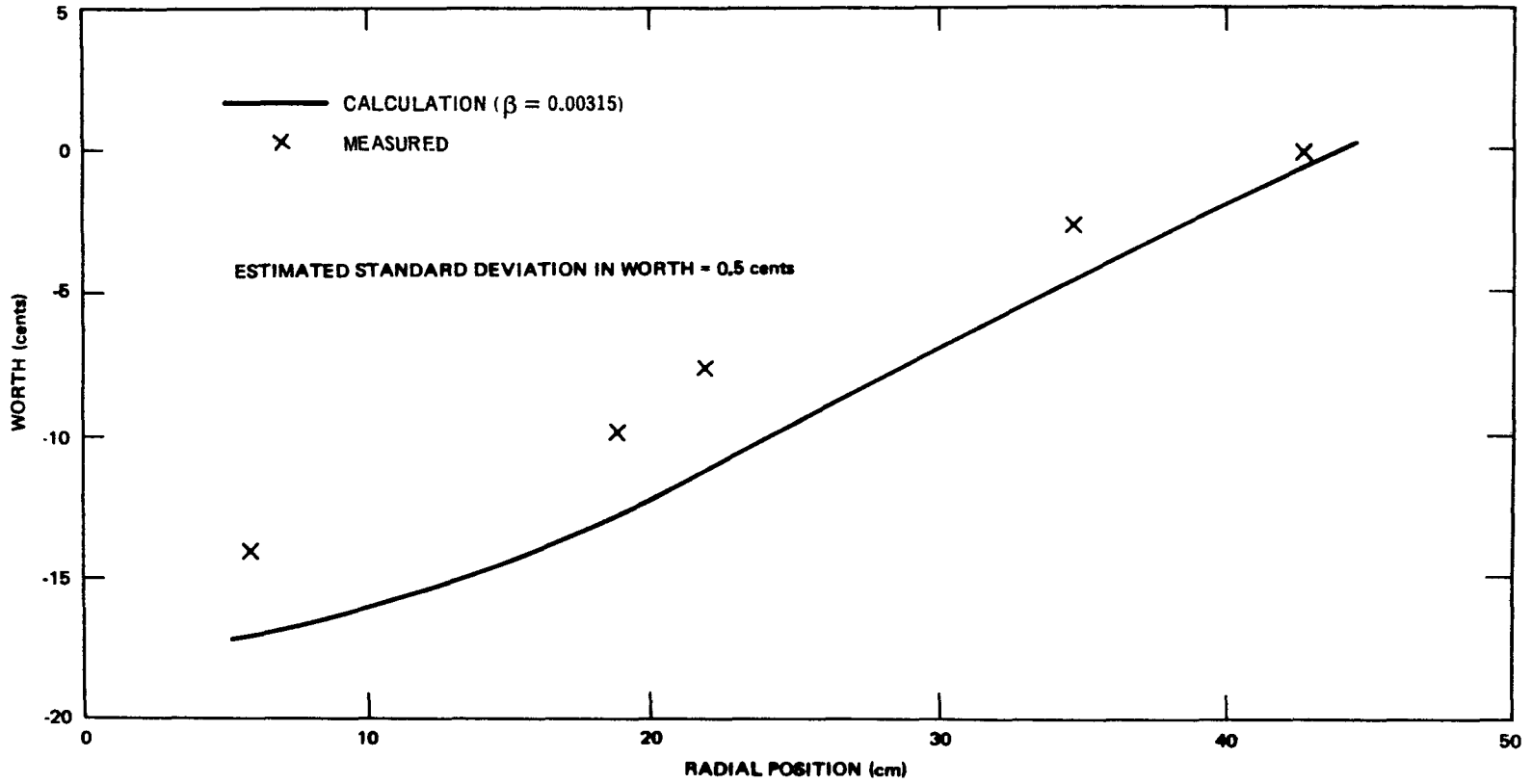
FIGURE 4-8. RADIAL DEPENDENCE OF DEPLETED UO$_2$ ROD WORTH (ASSEMBLY I-D)
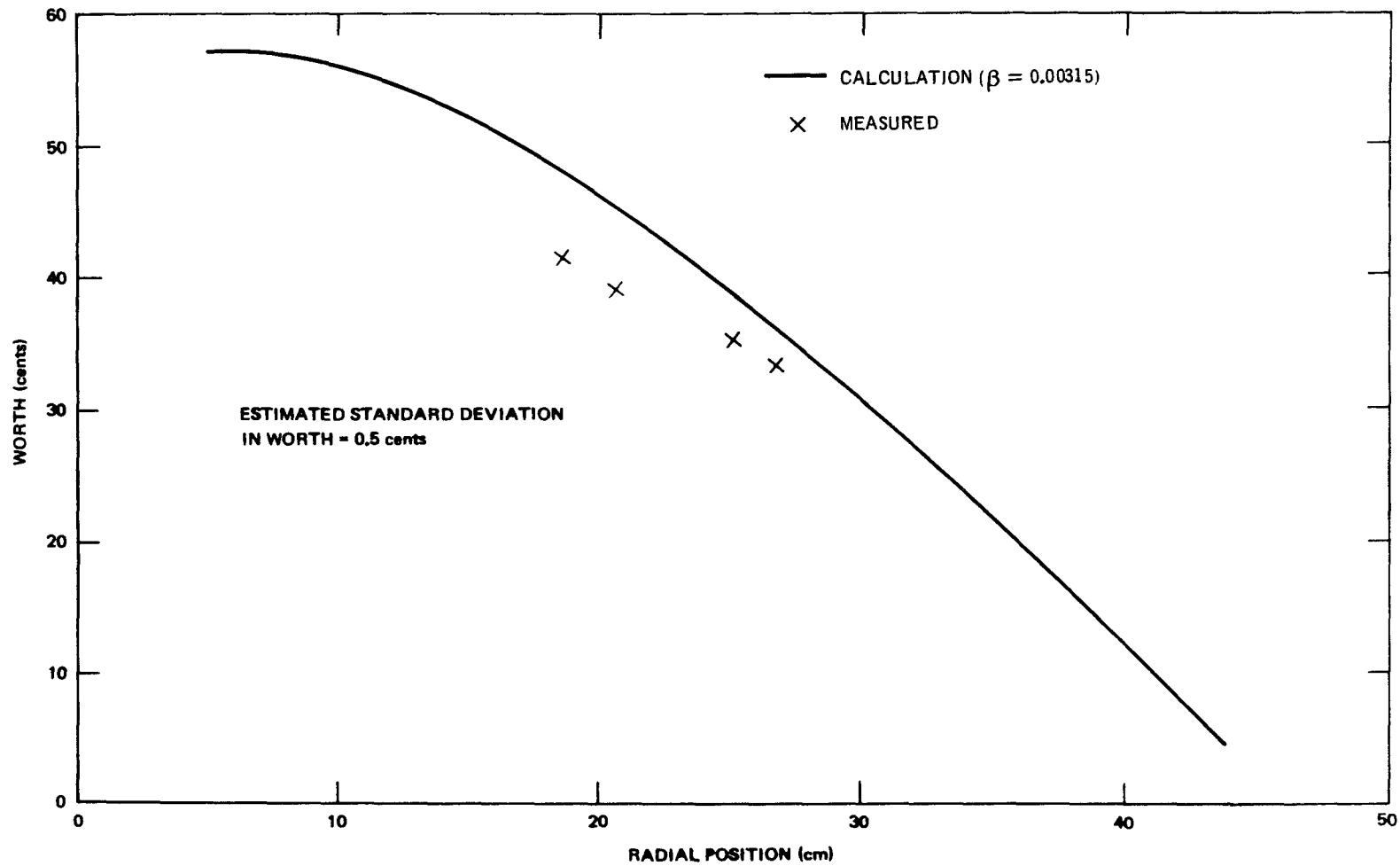
FIGURE 4-9. RADIAL DEPENDENCE OF GUINEA PIG ROD WORTH (ASSEMBLY I-D)

synthesis calculations and in addition, material worths were calculated
using a reactor model in which a portion of the original fuel rods in
a thin angular ring were replaced with sodium or one of the test rods
and the reactivity effect associated with this replacement was deter-
mined. The latter effects were calculated at a few locations using a
true two-dimensional diffusion[2] program. The results of these
calculations are compared with experiment in Table 4-5.

The two-dimensional calculations of fuel rod worth were in agree-
ment with the experiment (see Table 4-5). Calculated results at the
core periphery were essentially the same as experimental values, while
the calculated fuel rod worth near the center was approximately 10%
higher than the experimental value. The corresponding B_4C worth near
the core center was over-predicted by about 15%. The perturbation
calculations of the two-dimensional synthesis[3] solutions over-estim-
ated the magnitude of the worth for all materials by about 15 to 20%.
The discrepancies were the largest near the core center. This implies,
in agreement with the discrepancies in measured and calculated reaction
rates near the core boundaries (see Section V), that the calculated
synthesis flux distributions are not as flat as they should be.

Perturbation results of radial one-dimensional diffusion theory
calculations have shown that the calculated worths and radial flux
distribution in SEFOR, which has a high radial leakage, are strongly
influenced by the perpendicular bucklings which are used in the radial
regions outside the core. For a one-dimensional calculation which
provided reasonable agreement with experiment, (see Tables 4-2 through
4-4), the effect of the fuel gap on the non-core bucklings was eliminated
by using non-core bucklings obtained from calculations of the one-segment

TABLE 4-2

MATERIAL REACTIVITY WORTH MEASUREMENTS
(Assembly I-D)

Core Location*	Type of Rod	Worth Relative to Sodium (cents)	
		Measured**	Calculation*** (β=0.00315)
W2.5 - S5.0-B (Radius=42.7 cm)	Fuel (No. 121)	+ 8.7	+ 8.5
	Fuel (No. 781)	+ 9.2	+ 8.5
	Stainless Steel	+ 2.1	+ 0.8
	UO_2	0.0	- 1.1
	B_4C	-13.0	-17.5
W2.0 - S4.0-B (Radius=34.6 cm)	Fuel (No. 635)	+14.6	+16.2
	Fuel (No. 781)	+15.4	+16.2
	Stainless Steel	- 0.4	- 1.3
	UO_2	- 2.7	- 4.6
	B_4C	-22.1	-28.5
E1.5 - N3.0-B (Radius=21.8 cm)	Fuel (No. 695)	+27.8	+29.6
	Fuel (No. 781)	+27.6	+29.6
	Stainless Steel	- 1.6	- 5.0
	UO_2	- 7.6	-11.4
	B_4C	-49.1	-53.7
W1.0 - S2.0-B (Radius=18.6 cm)	Fuel (No. 783)	+28.4	+32.7
	Fuel (No. 781)	+28.8	+32.7
	Stainless Steel	- 2.8	- 6.0
	UO_2	- 9.8	-12.9
	B_4C	-52.3	-59.8
W0.5 - S1.0-F (Radius=5.8 cm)	Fuel (No.781)	+34.5	+38.7
	Stainless Steel	- 3.6	- 7.3
	UO_2	-13.0	-17.2
	B_4C	-70.9	-79.0

---

* See Core Loading Diagram Figure 1-8, also Figure 4-5.

** The estimated standard deviation in the measurements is approximately $\pm$0.5 cents (see Section 4.4).

*** Perturbation Results of a one-dimensional diffusion calculation.

TABLE 4-3

GUINEA PIG AND ADDITIONAL FUEL ROD
WORTH MEASUREMENTS   (ASSEMBLY I-D)

Core Location*	Type of Rod	Worth Relative to Sodium (cents)	
		Measurement**	Calculation*** (β=0.00315)
W0.0 – N4.0-A (Radius=26.6 cm)	Fuel (No. 781)	+23.1	+24.8
	Guinea Pig (No. A04)	+33.5	+36.0
W0.0 – N4.0-B (Radius=25.1 cm)	Fuel (No. 532)	+24.7	+26.3
	Fuel (No. 781)	+24.1	+26.3
	Guinea Pig (No. A04)	+35.4	+38.2
W2.5 – N1.0-B (Radius=20.6 cm)	Fuel (No. 666)	+26.7	+30.9
	Fuel (No. 781)	+27.0	+30.9
	Guinea Pig (No. A04)	+39.4	+45.2
W2.5 – N1.0-A (Radius-18.6 cm)	Fuel (No. 831)	+27.6	+32.7
	Fuel (No. 781)	+28.3	+32.7
	Guinea Pig (No. A04)	+41.8	+48.0
W2.0 – N0.0-D (Radius=18.6 cm)	Fuel (No. 774)	+27.9	+32.7
	Fuel (No. 781)	+27.9	+32.7
E1.0 – N2.0-B	Fuel (No. 791)	+33.7	+36.3
E1.0 – S2.0-D (Radius=13.8 cm)	Fuel (No. 626)	+32.7	+36.3

---

*   See Core Loading Diagram Figure 1-8, also Figure 4-5.

** The estimated standard deviation in the measurements is approximately ±0.5 cents (see Section 4.4).

*** Perturbation results of a one-dimensional diffusion calculation.

TABLE 4-4

TIGHTENER ROD REACTIVITY WORTH MEASUREMENTS

(ASSEMBLY I-D)

Core Location*	Type of Rod	Worth Relative to Stainless Steel (cents)	
		Measurement**	Calculation*** (β=0.00315)
W2.5 – S5.0 E2.5 – N5.0 (Radius=40.3 cm)	BeO BeO	4.6	5.4
W2.0 – S4.0 E2.0 – N4.0 (Radius=32.2 cm)	BeO BeO	5.7	5.0
W1.5 – S3.0 E1.5 – N3.0 (Radius=24.2 cm)	BeO BeO	6.1	5.2
W0.5 – S1.0 E0.5 – N1.0 (Radius=8.0 cm)	BeO BeO	4.5	6.0

* See Core Loading Diagram Figure 1-8, also Figure 4-5.

** The worth of substituting two rods simultaneously. The estimated standard deviation in the measurements is +0.5 cents (see Section 4.4).

*** Perturbation results of a one-dimensional diffusion calculation.

TABLE 4-5

COMPARISON OF CALCULATED AND EXPERIMENTAL
MATERIAL REACTIVITY WORTHS

	Worth from Synthesis perturbation calculation (¢)	Worth from one-dimensional perturbation calculation (¢)	Worth from two-dimensional diffusion calculation (¢)	Experimental Worth* (¢)
Fuel Rod Worth				
radius= 9.4 cm	43.0	39.2	39.7	36.0*
radius=40.4 cm	12.0	10.5	11.7	10.5*
B_4C Rod Worth				
radius= 9.4 cm	-83.0	-74.0	-78.0	-66.5*
radius=40.4 cm	-19.5	-20.0	--	-15.5*
UO_2 Rod Worth				
radius= 9.4 cm	-16.0	-16.3	--	-12.5*
radius=40.4 cm	- 1.4	- 1.4	--	- 0.5*
Guinea Pig Rod Worth				
radius= 19 cm	50.5	47.5	--	41.5*
radius= 26 cm	39.5	37.0	--	34.5*

*The experiments were actually performed at other radii (see Tables 4-2 and 4-3).
The values shown here were obtained by interpolation among the measured values.

mockup in ZPR-3 Assembly 47. The differences between the calculated axial flux distributions in the core and the axial distributions in the radial region outside the core near the fuel gap are illustrated in Figures 4-10 through 4-13. These curves show the axial distribution of four of the energy groups from a thirteen energy group two-dimensional calculation. For illustrative purposes the magnitude of the fluxes were normalized to unity at the axial location of the peak power in the core. The curves illustrate that the axial distributions outside of the core rapidly (within a very few centimeters) lose the two-segment gap characteristic of the core and assume a flatter shape which is more akin to a one-segment core. The effect of the gap in the outer radial non-fuel regions of the reactor is automatically eliminated in the two-dimensional calculations, where the agreement between experiment and calculation is in the 10 to 15% range. In the synthesis calculations however, the core axial flux shapes were extended out through the radial reflector region, and the resulting discrepancy between experiment and theory were of the order of 20% near the core center.

As was true with the results for Assembly I-B discussed in the previous section, generally better agreement between experiment and calculation would be obtained if the value of the calculated effective delayed neutron fraction (β=0.00315 for Assembly I-D) were increased by 6 to 10%.

RATIO OF FLUX INSIDE THE CORE TO
FLUX OUTSIDE THE CORE = 2.19 AT
PEAK POWER LOCATION

RELATIVE FLUX 3.75 CM INSIDE
RADIAL CORE BOUNDARY

RELATIVE FLUX 2.86 CM OUTSIDE
RADIAL CORE BOUNDARY

GAP
REGION

RELATIVE FLUX

HEIGHT (CM)
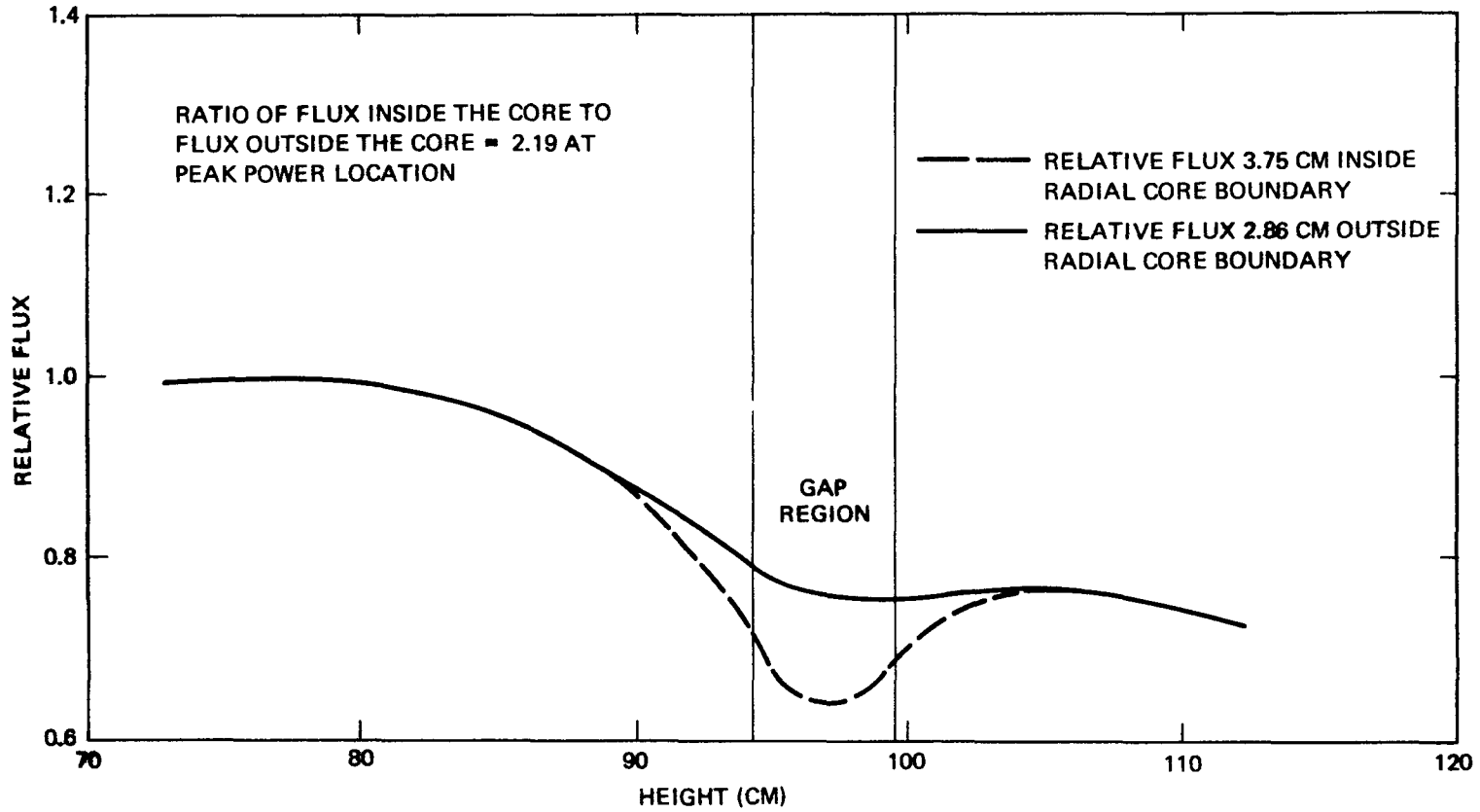
FIGURE 4-10.   AXIAL FLUX DISTRIBUTION FOR GROUP ONE (10.0 TO 2.2 MeV)

RATIO OF FLUX INSIDE THE CORE TO
FLUX OUTSIDE THE CORE = 1.68 AT
PEAK POWER LOCATION

RELATIVE FLUX 3.75 CM INSIDE
RADIAL CORE BOUNDARY

RELATIVE FLUX 2.86 CM OUTSIDE
RADIAL CORE BOUNDARY

GAP
REGION

HEIGHT (CM)
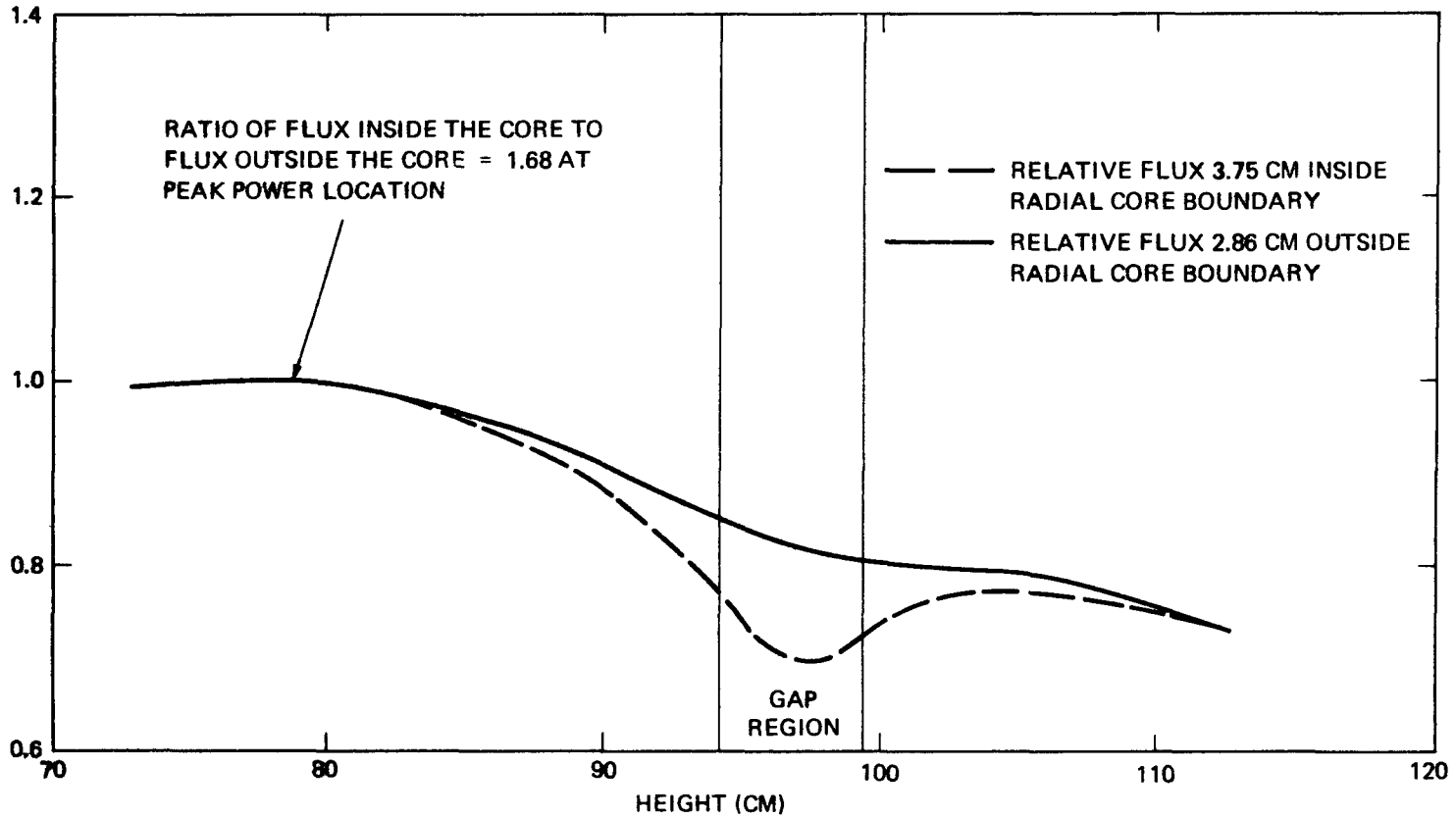
FIGURE 4-11. AXIAL FLUX DISTRIBUTION FOR GROUP TWO (2.2 TO 0.825 MeV)

RATIO OF FLUX INSIDE THE CORE TO
FLUX OUTSIDE THE CORE = 0.493 AT
PEAK POWER LOCATION

— — — RELATIVE FLUX 3.75 CM INSIDE
RADIAL CORE BOUNDARY

———— RELATIVE FLUX 2.86 CM OUTSIDE
RADIAL CORE BOUNDARY

GAP
REGION

RELATIVE FLUX

HEIGHT (CM)
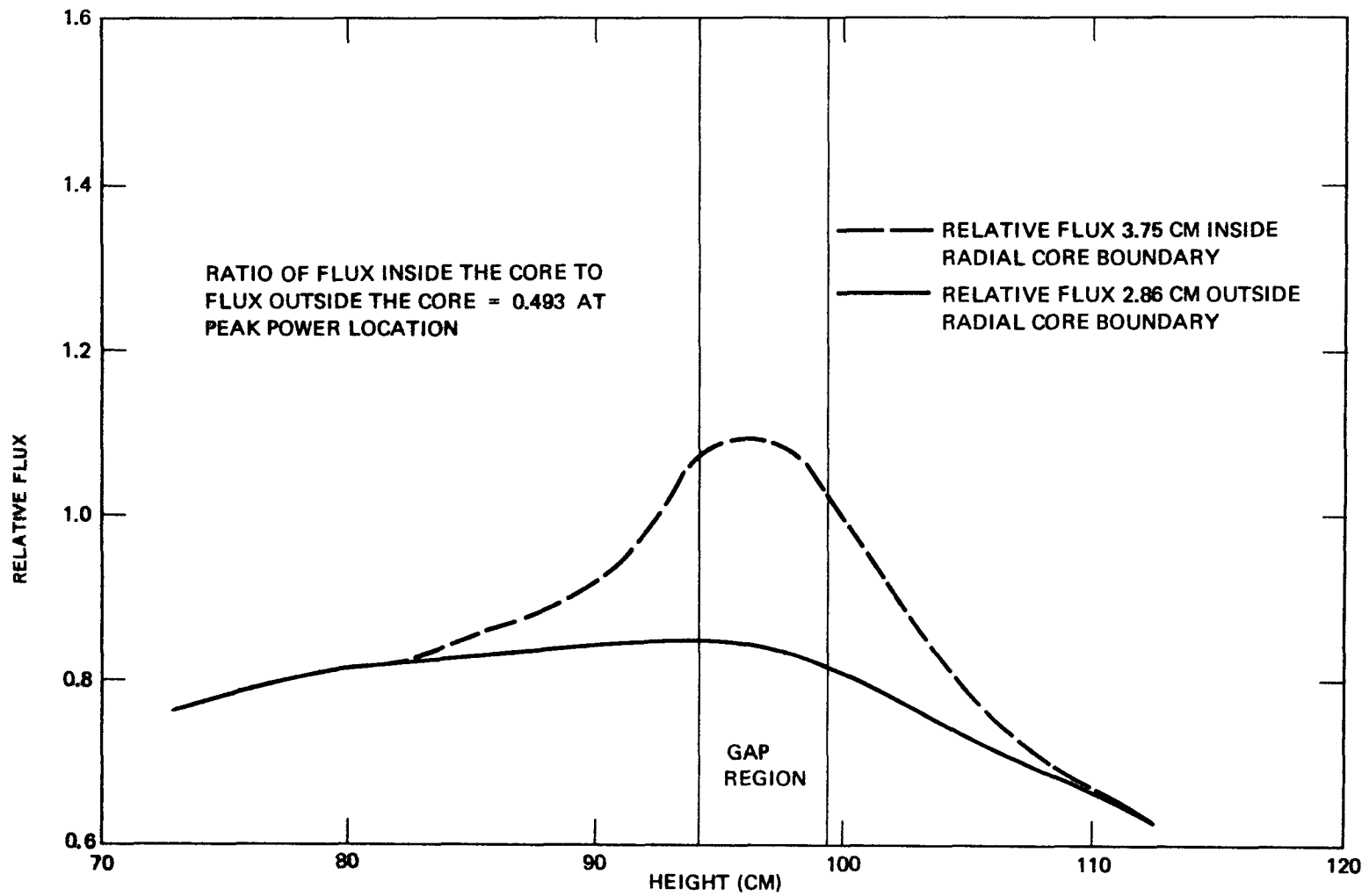
FIGURE 4-12.   AXIAL FLUX DISTRIBUTION FOR GROUP TWELVE (310 TO 91 eV)

RATIO OF FLUX INSIDE THE CORE TO
FLUX OUTSIDE THE CORE = 0.255 AT
PEAK POWER LOCATION

RELATIVE FLUX 3.75 CM INSIDE
RADIAL CORE BOUNDARY

RELATIVE FLUX 2.86 CM OUTSIDE
RADIAL CORE BOUNDARY

GAP
REGION

RELATIVE FLUX

HEIGHT (CM)
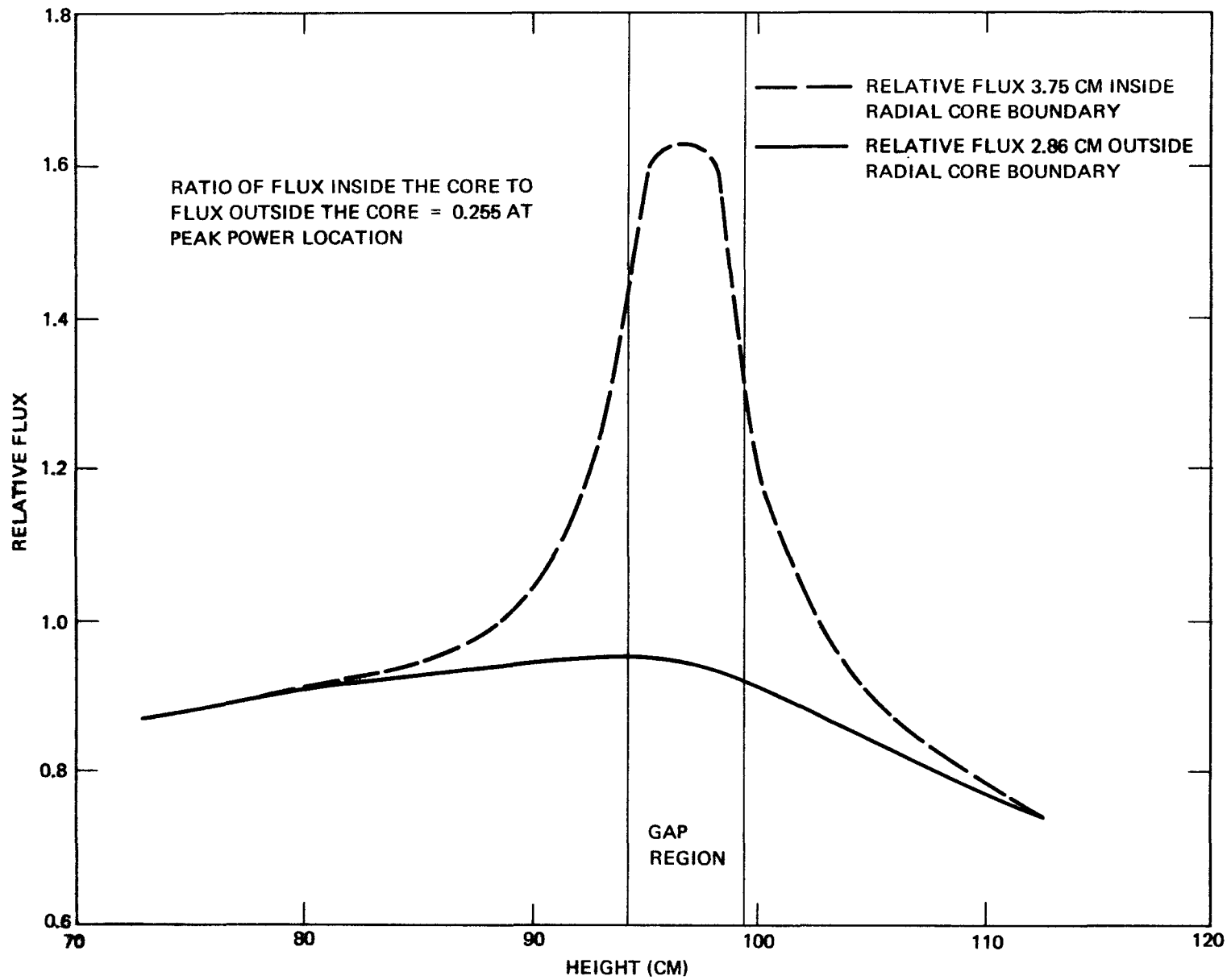
FIGURE 4-13. AXIAL FLUX DISTRIBUTION FOR GROUP THIRTEEN (LESS THAN 91 eV)

4.4   UNCERTAINTIES IN REACTIVITY MEASUREMENTS

Due to small variations in system temperatures, instrumentation, relative reflector-core configurations, etc., the measurement of the critical point (the system conditions for which the reactor is exactly critical) is inexact, and different measurements of the same point show small variations. Evidence for this variation is shown by the two sets of data in Tables 4-6 and 4-7, obtained from repeated measurements on two slightly different core configurations. (The core loading was changed slightly between the critical measurements on September 12 and September 13.) Although the mean reactivity is different for the two sets of data, because of the different core loadings, the individual deviation appears to be random. The estimated standard deviation, which is essentially the same for both cases, appears to be unaffected by changes in reactor configuration.

Based on the above measurements, the estimated standard deviation in a single measurement of a small reactivity change, calculated from the difference between two measurements of the critical point, is 0.37 $\sqrt{2}$ cents, or 0.5 cents.

Since the variations noted in Tables 4-6 and 4-7 appear to be random in nature, and, as noted in Section 3.3.4, the uncertainty due to reflector calibration errors in a 9 cent increment is (0.009) X 9 cents, or 0.08 cents, the estimated calibration uncertainty in a 90 cent reactivity change associated with movement of the reflector over ten consecutive increments, which were measured to be worth 9 cents each, would be expected to be $\sim 0.08\sqrt{10}$ cents, or 0.25 cents. Similarly,

the calibration uncertainty in any reactivity change of magnitude
Δk cents would be expected to be approximately $0.08 \sqrt{\Delta k/9}$ cents, and
the total uncertainty in any reactivity change would thus be
$[2(0.37)^2 + (0.08)^2 \Delta k/9]^{1/2}$. This relation is probably reasonable
for reactivity changes which are of the order of 30 cents or less.
For larger changes the reflector configuration changes considerably,
and the reflector interaction effects noted in Section 3.3 may increase
the uncertainties.

TABLE 4-6

SEFOR CRITICAL CHECKS
(September 1 to September 12)

Measurement Number	Date	Reflector #8 Position(cm)	Reflector #8 Relative Worth(Cents)*	Temperature Measured(°F)	Temperature Reactivity Effect** (Relative to 350°F)	X_i Relative Reactivity* at 350°F(cents)
1	9/1	51.66	73.24	350.0	0.0	73.24
2	9/2	50.78	71.65	347.5	+1.50	73.15
3	9/3	51.65	73.22	350.0	0.0	73.22
4	9/3	52.00	73.85	352.5	-1.50	72.35
5	9/4	52.09	74.02	352.0	-1.20	72.82
6	9/5	51.71	73.33	350.0	0.0	73.33
7	9/12	51.20	72.41	349.5	+0.30	72.71

$$\text{Average} = \bar{X} = 72.97$$

$$\text{Estimated standard deviation,} \left[\sum_{i=1}^{7} (X_i - \bar{X})^2/6 \right]^{\frac{1}{2}} = 0.36 \text{ cents}$$

* Relative to the worth with the reflector lowered.

** Using a temperature coefficient at 350°F of -0.60 cents/°F.

TABLE 4-7

SEFOR CRITICAL CHECKS

(September 13 to October 7)

Measurement Number	Date	Reflector #8 Position(cm)	Reflector #8 Relative Worth(cents)*	Temperature Measured(°F)	Temperature Reactivity Effect** (Relative to 350°F)	X_i Relative Reactivity* at 350°F(cents)
1	9/13	52.52	74.79	351.5	−0.90	73.89
2	9/14	52.25	74.30	351.5	−0.90	73.40
3	9/16	50.92	71.90	347.0	+1.80	73.70
4	9/16	52.78	75.27	352.5	−1.50	73.77
5	9/16	52.81	75.32	352.5	−1.50	73.82
6	9/17	51.88	73.64	349.0	+0.60	74.24
7	9/18	51.64	73.20	348.75	+0.75	73.95
8	9/18	52.00	73.85	349.25	+0.45	74.30
9	9/19	52.01	73.87	349.0	+0.60	74.47
10	9/20	53.09	75.83	353.0	−1.80	74.03
11	9/20	52.77	75.25	351.25	−0.75	74.50
12	9/20	51.87	73.62	349.75	+0.15	73.77
13	9/24	50.99	72.03	348.0	+1.20	73.23
14	10/7	52.04	73.93	350.0	0.0	73.93

Average = $\bar{X}$ = 73.93

Estimated standard deviation, $\left[\sum_{i=1}^{14} (X_i - \bar{X})^2 / 13\right]^{\frac{1}{2}}$ = 0.37 cents

* Relative to the worth with the reflector lowered.

** Using a temperature coefficient at 350°F of −0.60 cents/°F.

SECTION V

Foil Irradiation Data

F(

The spatial distri   .sotopes
Pu-239, U-238, and U-2:   can be
used to estimate the p   of an
absolute fission rate   me avail-
able, to provide an at   n, the
isotopic fission rati(from
relative activities o

5.1   DESCRIPTION ANI

5.1.1 Fission Rate

    Foils of three   re placed at
selected axial posit   These rods
were inserted into ⌐⌐⌐ ⌐⌐   and irradiated
for approximately 1 hour at a nominal reactor powei ⌐⌐ kw. After
removal from the core, the fission product gamma activity of each foil
was obtained with a Na-I crystal scintillation counter. The energy
window for the counting of all foils was the same, and covered the range
between 430 and 730 keV. This region included several gamma peaks which
are composites of fission product peaks.

    The specified isotopic compositions of the thin cylindrical foils
are listed in Table 5-1. The weight of the uranium foils was of the
order of 120 milligrams, while that of the Al-clad Pu foils (a Pu-Al
alloy of 99.01% Pu) was about 23 milligrams.

TABLE 5-1

FOIL ISOTOPIC COMPOSITIONS

Foil Type	Isotopic Composition	
	Isotope	Percent
Enriched	U-235	93.15
Uranium	U-238	6.85
Depleted	U-235	0.19
Uranium	U-238	99.81
Plutonium	Pu-238	0.036
	Pu-239	92.905
	Pu-240	6.444
	Pu-241	0.582
	Pu-242	0.033

The fissionable foils were placed in cylindrical Al "cans" that were 0.27 inches in height with an outer diameter of 0.475 inches. The fissionable foils within a given can were separated from each other and from the ends of the can by Al foils. The cans were positioned vertically within the special foil holder rod, (see Figure 5-1) by Al spacers*. The position of the cans and spacers within a foil holder rod is indicated in Table 5-2. The axial position of the foils above the bottom of the core (not including the lower uranium insulator pellet) is also shown in the table. In calculating the axial foil positions, it was assumed that all foils were 0.098 inches above the bottom of the foil can. In some instances the foil can was replaced with a 1/4" Al spacer. The effect on axial foil position of this slight difference in thickness (0.02 inches) was neglected.

Six of the standard fuel rods in core loading Assembly I-D were replaced by the special foil holder rods. Their location within the core is shown in Figure 5-2. With this core configuration the reactor was critical with reflector #8, which is close to the position of foil holder rod FE, at an intermediate height (at a position of ∿47 cm relative to a completely raised position of ∿98 cm) and all other reflectors were completely raised.

The measured specific activities for all the foils are tabulated in Tables 5-3 through 5-5. The corrections for background gamma events in the foils, small differences in foil weight, and activity decay during the counting process are included. The background corrections for U-238 and Pu-239 were about 5% of the observed count rate in the irradiated foils of lowest activity. Background corrections for the U-235 were negligible. The corrections for the time decay of the activity were determined from the measured time dependence of the specific activity

---

*These were of two thicknesses: 1/4" and 1".
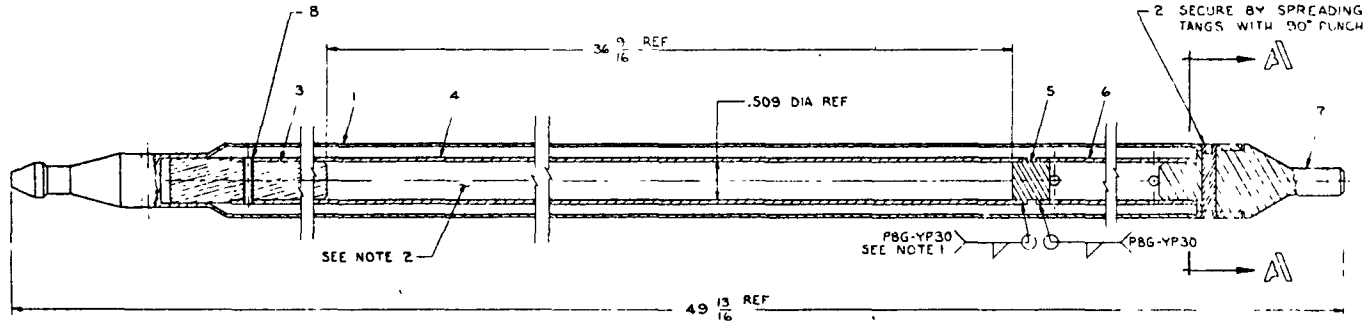
FIGURE 5-1. FOIL HOLDER ROD

ROD	LOCATION
FB	W0.5–S1.0E
FC	W2.0–S2.0B
FD	W4.0–S4.0B
FE	E4.5–S3.0F
FF	W4.5–N3.0C
FG	W2.5–N1.0F
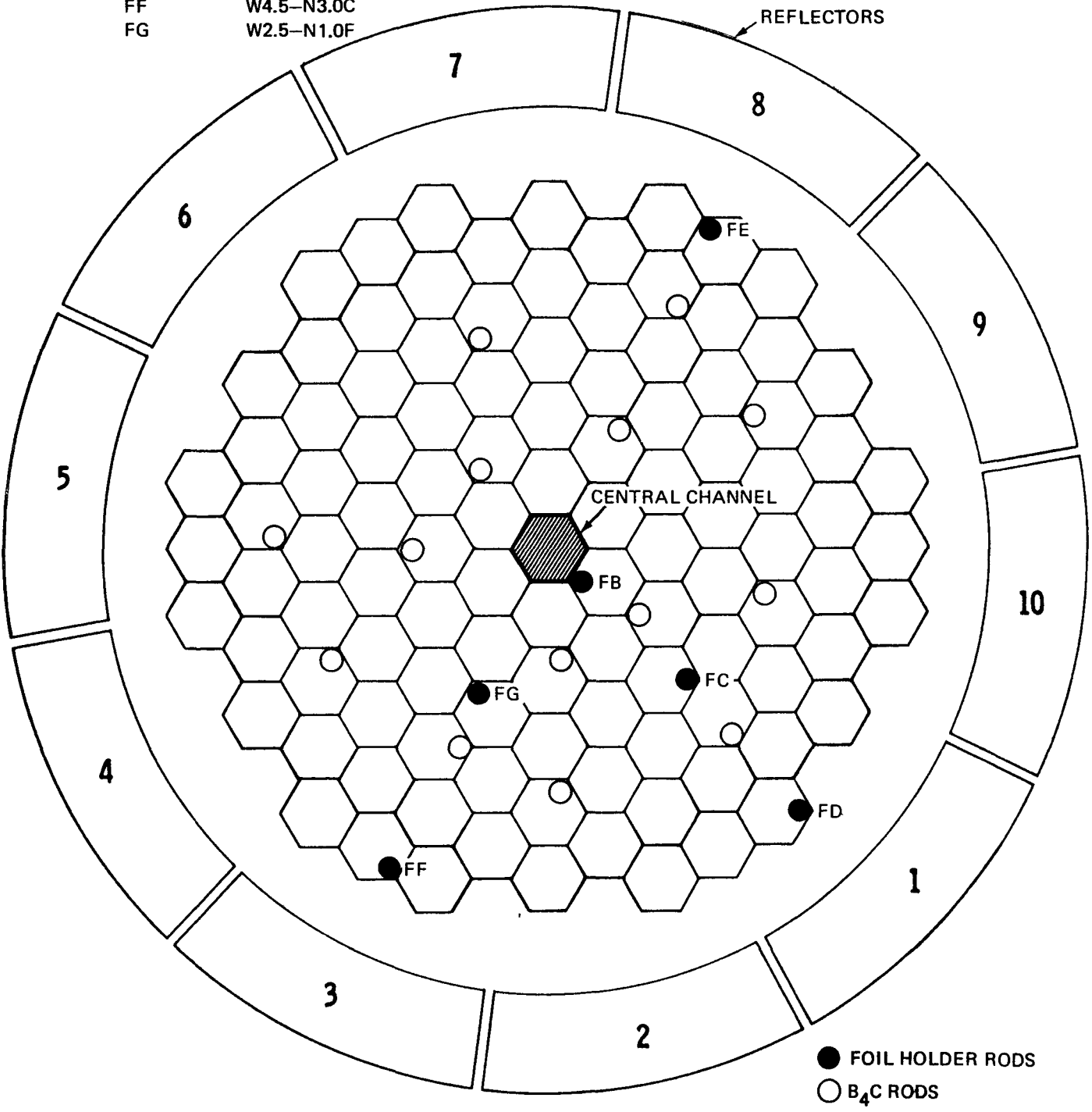
FIGURE 5-2. FOIL HOLDER ROD LOCATIONS (ASSEMBLY I-D)

TABLE 5-2

FOIL POSITIONS IN FOIL HOLDER RODS

Position Number	Height of Al Spacers Below Can at 70°F (inches)	Can Width* at 70° F (inches)	Foil Height** above bottom of core at 350°F (cm)
1	0.75	0.27	1.2
2	9.50	0.27	26.1
3	4.00	0.27	37.0
4	6.00	0.27	53.0
5	0.50	0.27	54.9
6	1.00	0.27	58.2
7	5.75	0.27	73.5
8	6.50	0.27	90.8

* In some rods a few cans were replaced with 1/4 inch spacers.

** Foils located 0.098 inches (at 70°F) above bottom of can. The bottom of the first can is 3/8 inches above the bottom of the core. A linear expansion coefficient of $1.3 \times 10^{-5}/°F$ was used for the aluminum. The core height at 350°F is 91.2 cm.

for each type of foil. These corrections were 3% or less for foils within the same rod but ranged up to ∿23% for foils in different rods.

5.1.2 Determination of Approximate Fission Ratios

In addition to the data described in the previous section, supplementary count rate data has been taken on the three foils near the core center (can number 3, rod FB) to determine approximate foil fission ratios. The 1.6 Mev La-140 fission product emission was counted for the depleted uranium, enriched uranium and plutonium foils in this can. The enriched uranium and plutonium foils were counted for one hour twenty minutes and the depleted uranium foil was counted for fifteen hours thirty seven minutes. The data was recorded on a multi-channel analyzer and the area under the total energy peak of the 1.6 gamma ray was integrated for each foil.

The area under the total energy peak consists of the 1.6 Mev events from the decay of La-140 plus background from other fission products. The background was assumed to have the same shape and magnitude as the spectrum just above the 1.6 Mev peak. This background was subtracted from the area of the total energy peak and the resulting count rate was then normalized to the foil weight to obtain the specific "La-140" activity for each type of foil.

No normalization was made for differences in counting time. The counts were treated as if they had been taken in the middle of the counting interval and the three count intervals were assumed to be at the same time after shutdown. The first assumption results in less than one percent error (Reference 1 p.49), while the second assumption results in less than 2% error as can be seen by using the daughter product relation

Activity of La $(\lambda_{La} N_{La}) =$

$$N_{La,o} \frac{\lambda_{Ba} \lambda_{La}}{\lambda_{La} - \lambda_{Ba}} \quad (e^{-\lambda_{Ba}t} - e^{-\lambda_{La}t})$$

for the times in question.

The foil fission ratios are as follows after accounting for count length, mass and yield

$$\frac{\sigma \text{ Depleted U}}{\sigma \text{ Enriched U}} = 0.0290$$

$$\frac{\sigma \text{ Pu Mixture}}{\sigma \text{ Enriched U}} = 0.9215$$

The actual isotopic fission ratios that were determined from these ratios are shown in the next section.

The estimated outside error limit ($\sim 2\sigma$) on these ratios is about 10%. This limit is due to a combination of uncertainties in La-140 yield, counting statistics, background subtraction, weigh normalization and counting geometry reproducibility.

TABLE 5-3

FISSION RATE MEASUREMENTS FOR Pu FOILS
(Relative Values)

Rod Number	FB	FG	FC	FF	FE	FD
Radial Distance*(cm)	5.8	19.6	23.2	43.3	43.3	44.5

Axial Position

No.	Distance** (cm)						
8	90.8	0.6013	–	–	–	–	–
7	73.5	0.7388	–	–	–	–	–
6	58.2	0.9198	–	–	–	–	–
5	54.9	0.9396	–	–	0.5769	–	0.5871
4	53.0	0.9423	–	–	–	–	–
3	37.0	1.0000$^+$	0.8564	0.8111	0.5543	–	0.5747
2	26.1	0.9419	–	–	–	–	–
1	1.2	0.6901	–	–	–	–	–

*Distance from core center

** Distance above bottom of core – core height = 91.2 cm

+ The specific activity at this point was 6398.3 counts/min/mg.

TABLE 5-4

FISSION RATE MEASUREMENTS
FOR ENRICHED URANIUM FOILS
(Relative Values)

Rod Number	FB	FG	FC	FF	FE	FD
Radial Distance*(cm)	5.8	19.6	23.2	43.3	43.3	44.5

Axial Position

No.	Distance** (cm)						
8	90.8	0.6240	0.5418	0.5018	–	–	–
7	73.5	0.7778	0.6629	0.6184	0.4311		0.4747
6	58.2	0.9515	0.8222	0.7807	0.5673		0.6055
5	54.9	0.9750	0.8679	0.8093	0.5979	0.5003	0.6114
4	53.0	0.9932	0.8806	0.7949	0.5953	–	0.6001
3	37.0	1.0000+	0.8599	0.8154	0.5703	0.5450	0.5782
2	26.1	0.9633	0.8524	0.7742	0.5275	–	0.5523
1	1.2	0.7191	0.6114	0.5739	–	–	–

*Distance from core center.

** Distance above bottom of core – core height=91.2 cm.

+ The specific activity at this point was 6410.2 counts/min/mg.

TABLE 5-5

FISSION RATE MEASUREMENTS
FOR DEPLETED URANIUM FOILS
(Relative Values)

Rod Number	FB	FG	FC	FF	FE	FD
Radial Distance*(cm)	5.8	19.6	23.2	43.3	43.3	44.5

Axial Position

No.	Distance** (cm)						
8	90.8	0.4156	0.3667	0.3453	–	–	–
7	73.5	0.7032	0.6503	0.6075	0.3185	–	0.2875
6	58.2	0.7873	0.7179	0.6607	0.3607	–	0.3485
5	54.9	0.7825	0.6976	0.6365	0.3638	0.3177	0.3360
4	53.0	0.7743	0.6976	0.6729	0.3684	–	0.3555
3	37.0	1.0000^{+}	0.8873	0.8345	0.4205	0.4151	–
2	26.1	0.9476	0.8713	0.8085	0.4051	–	0.3806
1	1.2	0.5165	0.4601	0.4200	–	–	–

*Distance from core center

** Distance above bottom of core – core height=91.2 cm.

+ The specific activity at this point was 230.8 counts/min/mg.

5.2   COMPARISON OF EXPERIMENTAL AND CALCULATED RESULTS

5.2.1   Comparison of Fission Rate Distributions

The calculated and measured fission rate distributions in a
number of rods are compared in Figures 5-3 through 5-10. The estimated
uncertainty in the measured values is +5% for the axial profiles and +10%
for the radial profiles. The agreement between the calculations, which
are discussed in more detail below, and the experiment is well within
the experimental uncertainties throughout the major portion of the
core, but differences of the order of 20% occur near the core boundaries.
Possible explanations for these discrepancies are discussed below.
In general, however, it appears that the actual fission rate, and
thus the power, distribution may be slightly flatter than calculated.

The calculations were performed with a core model for Assembly
I-D that had six radial core zones. The first (central dry well) core
zone is described in Appendix I. The second, fourth, and sixth cal-
culational zones contained 36, 108, and 288 fuel rods respectively.
The third zone contained 67 fuel and 5 B_4C rods, while the fifth zone
contained 135 fuel rods and 9 B_4C rods. The tightener rods, core
structure, and sodium were distributed uniformly as described in
Appendix I. The fuel and B_4C were assumed to be uniformly distributed
within their respective zones.

Calculations using the above model were performed in 13 energy
groups using two-dimensional synthesis,[2] as well as true two-dimensional
diffusion[3] programs. There were no significant differences between the
reaction rate distributions calculated with the two methods. Generally,
however the reaction rate profiles obtained from the true 2-D calculations
were somewhat flatter than those calculated with the synthesis program.
Infinitely dilute cross sections were used to calculate the fission rate
distributions. The results of the true two-dimensional calculations
as shown in Figures 5-3 through 5-10. The apparent effect of the lowered
reflector #8 on the axial uranium profile in rod FE is clearly demonstrated.
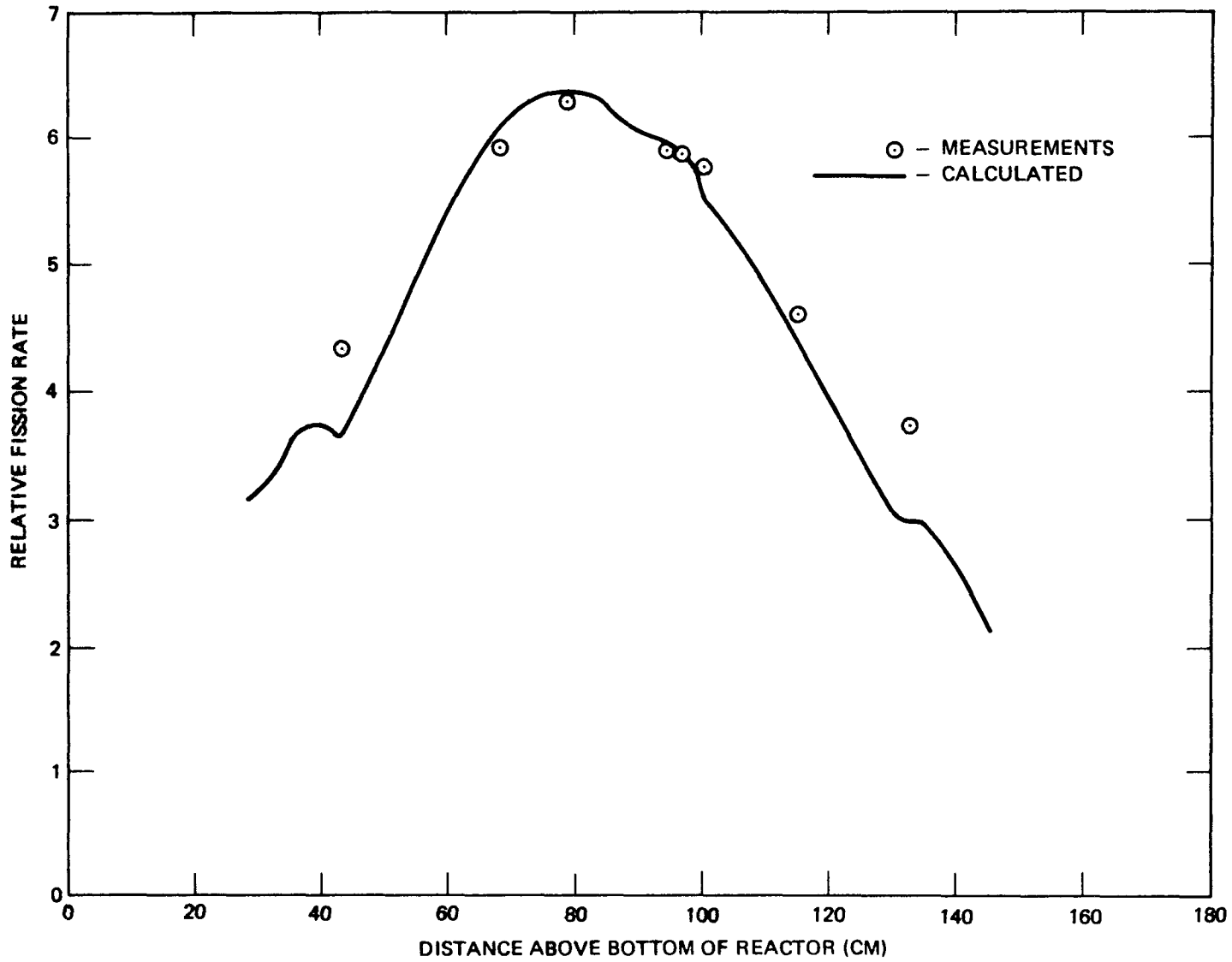
FIGURE 5-3. PU-239 FISSION DISTRIBUTION IN ROD FB
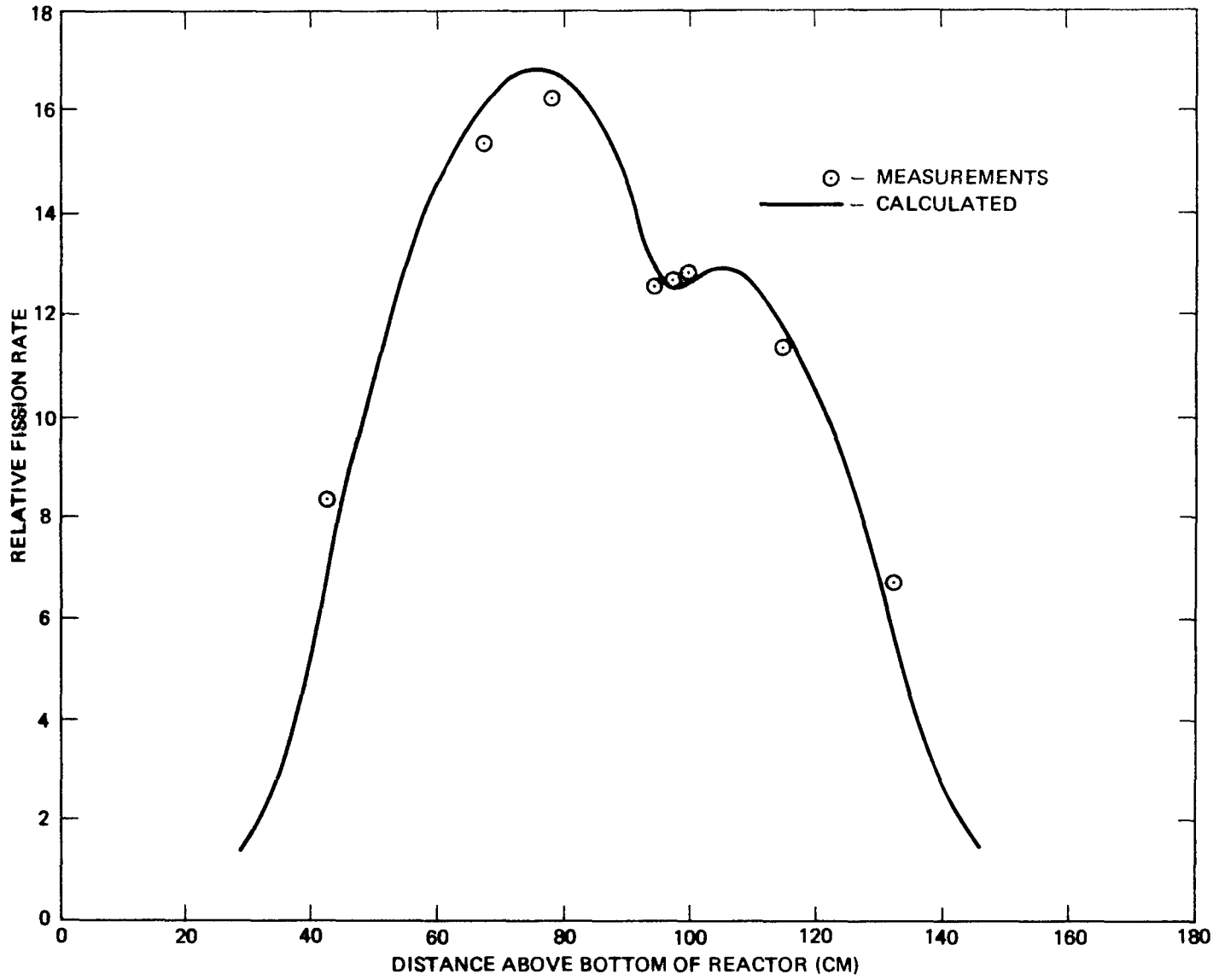
FIGURE 5-4. U-238 FISSION DISTRIBUTION IN ROD FB
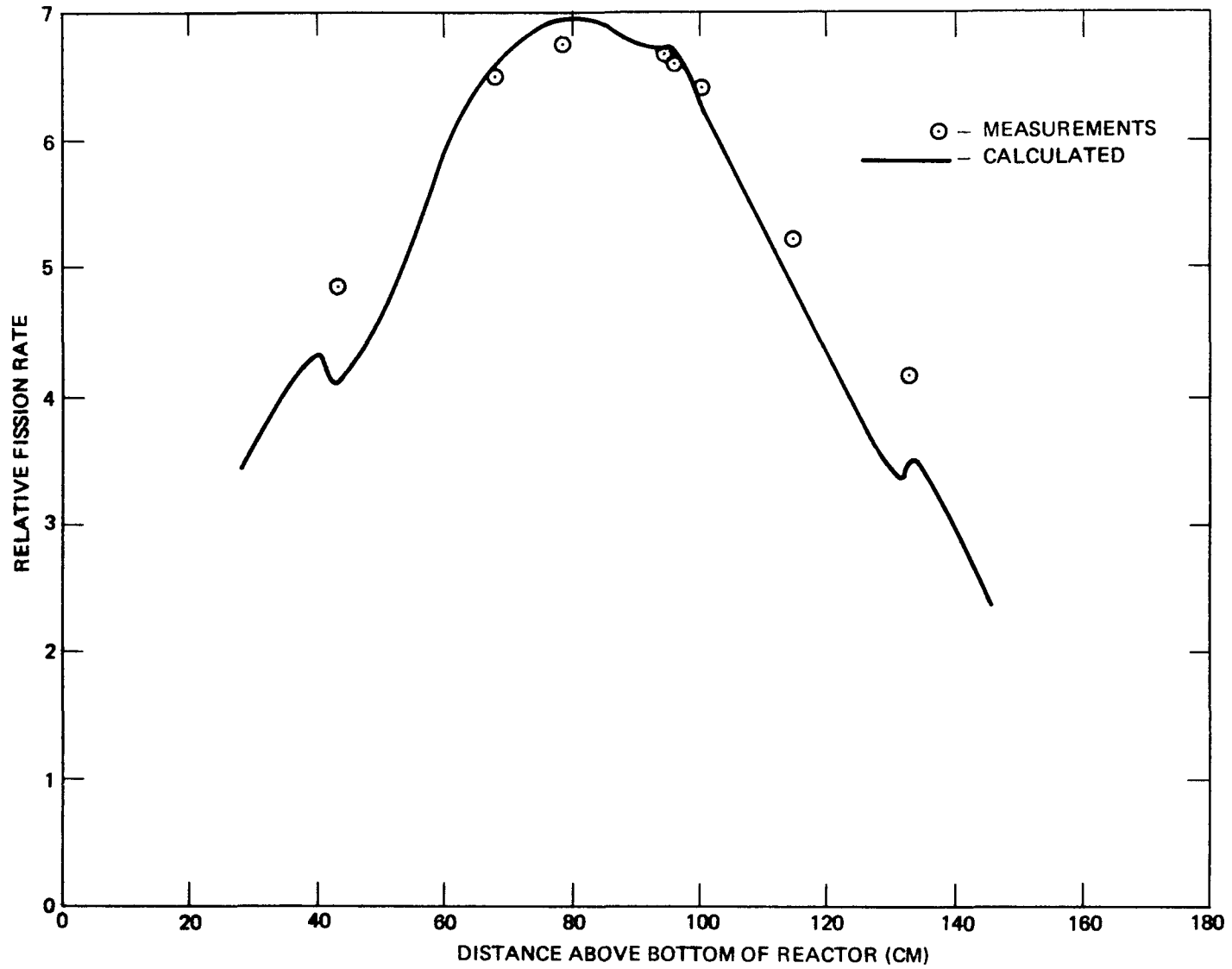
FIGURE 5-5. U-235 FISSION DISTRIBUTION IN ROD FB
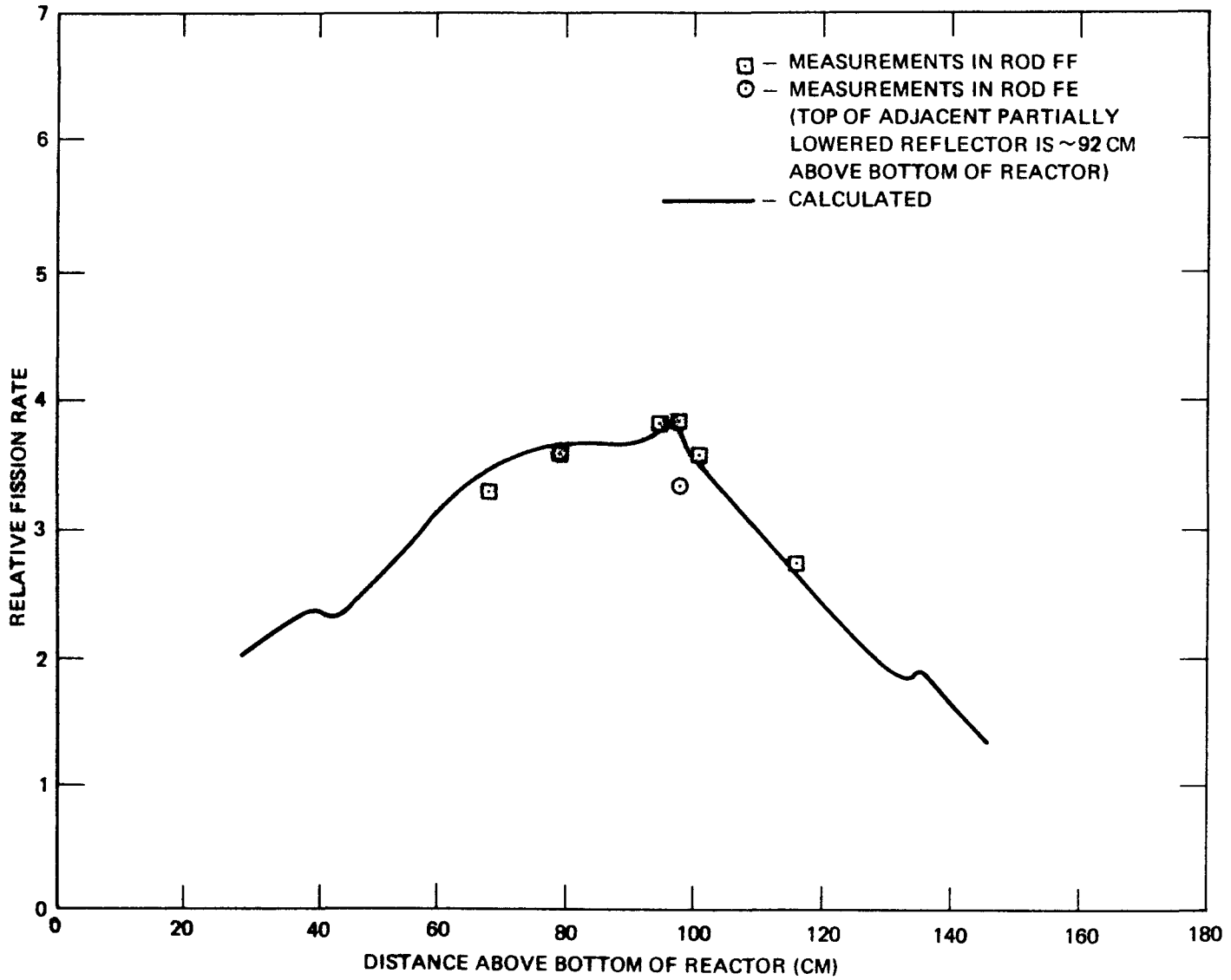
FIGURE 5-6. U-235 AXIAL FISSION DISTRIBUTION AT CORE RADIAL BOUNDARY
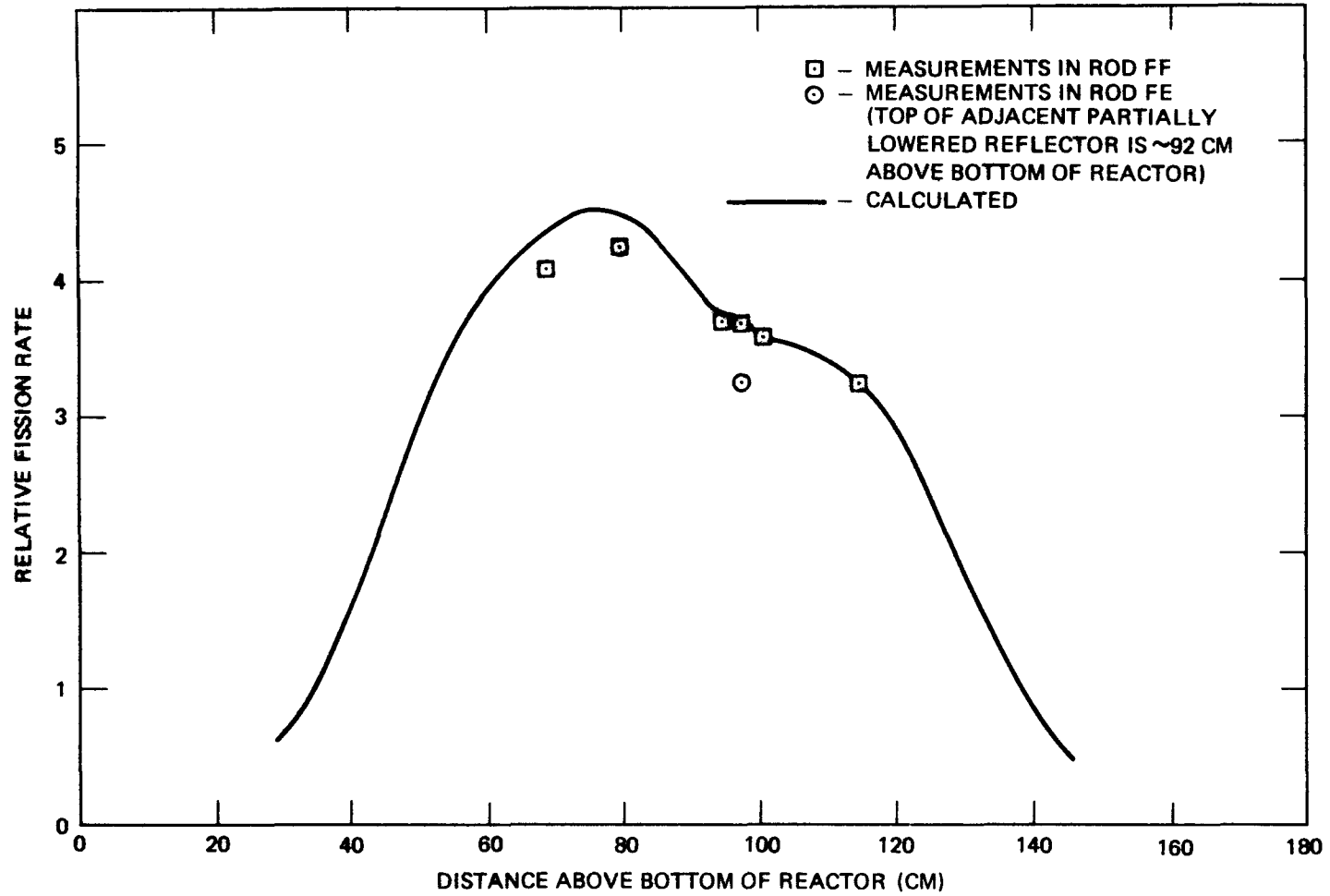
FIGURE 5-7. U-238 AXIAL FISSION DISTRIBUTION AT CORE RADIAL BOUNDARY
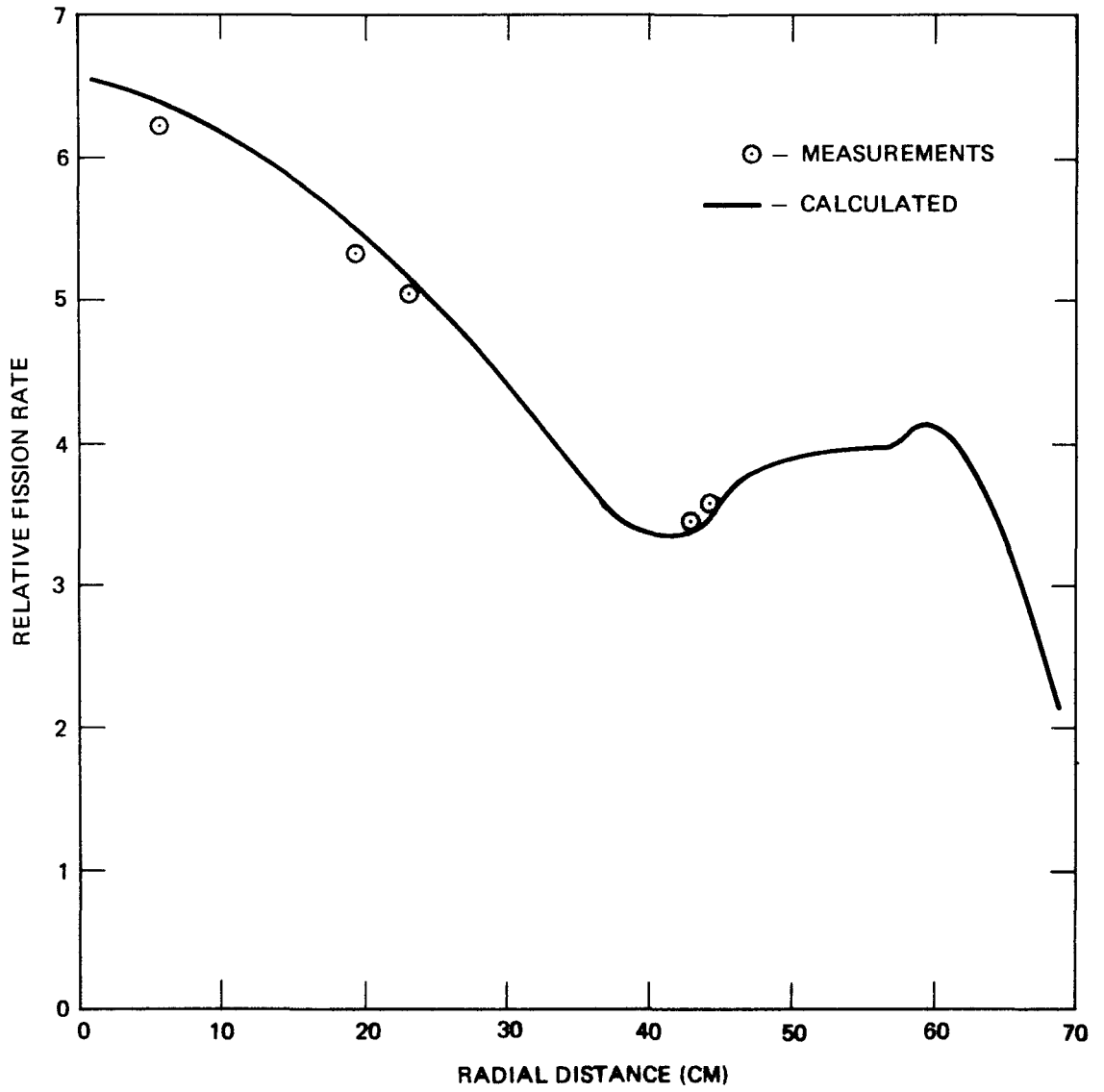
FIGURE 5-8. PU-239 RADIAL FISSION DISTRIBUTION AT AXIAL POSITION 3
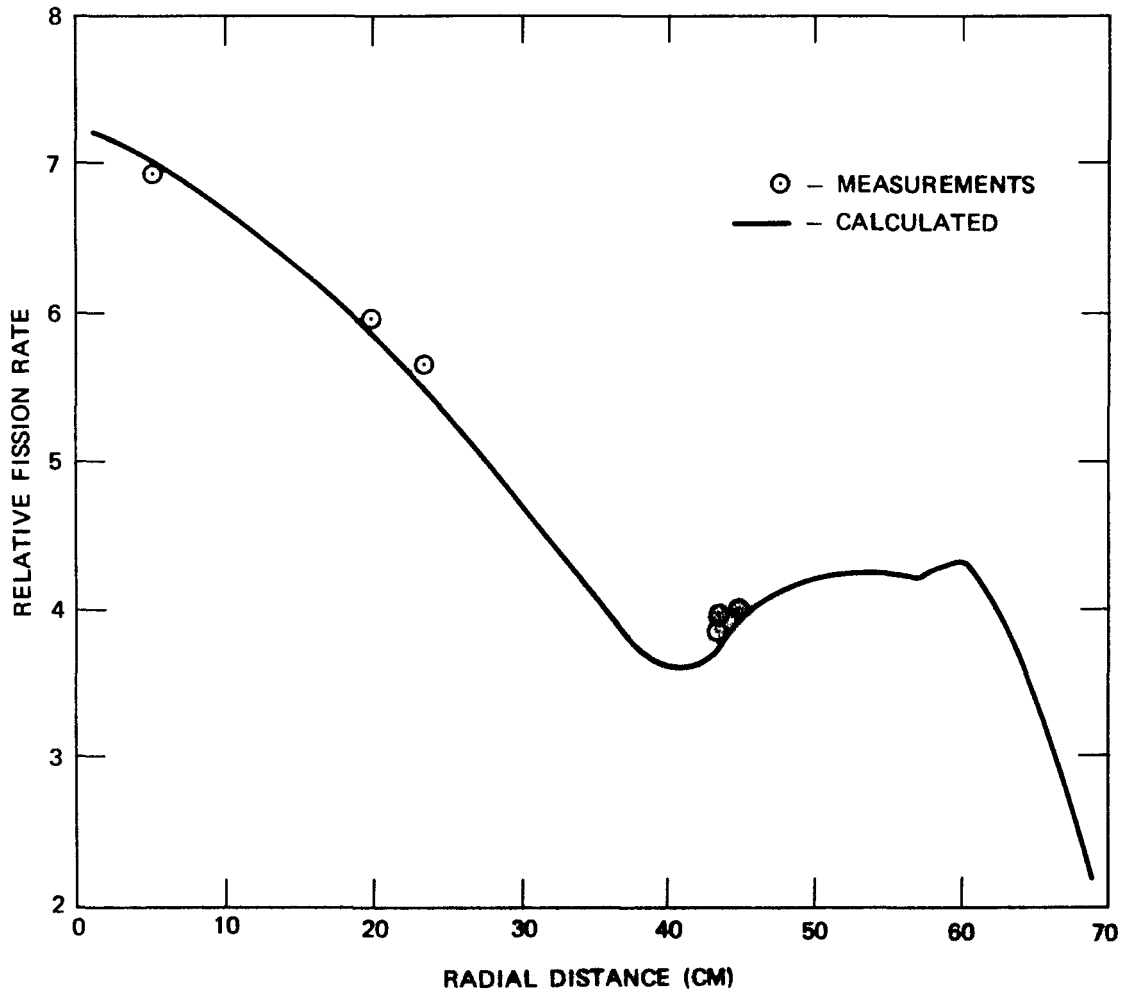
FIGURE 5-9. U-235 RADIAL FISSION DISTRIBUTION AT AXIAL POSITION 3
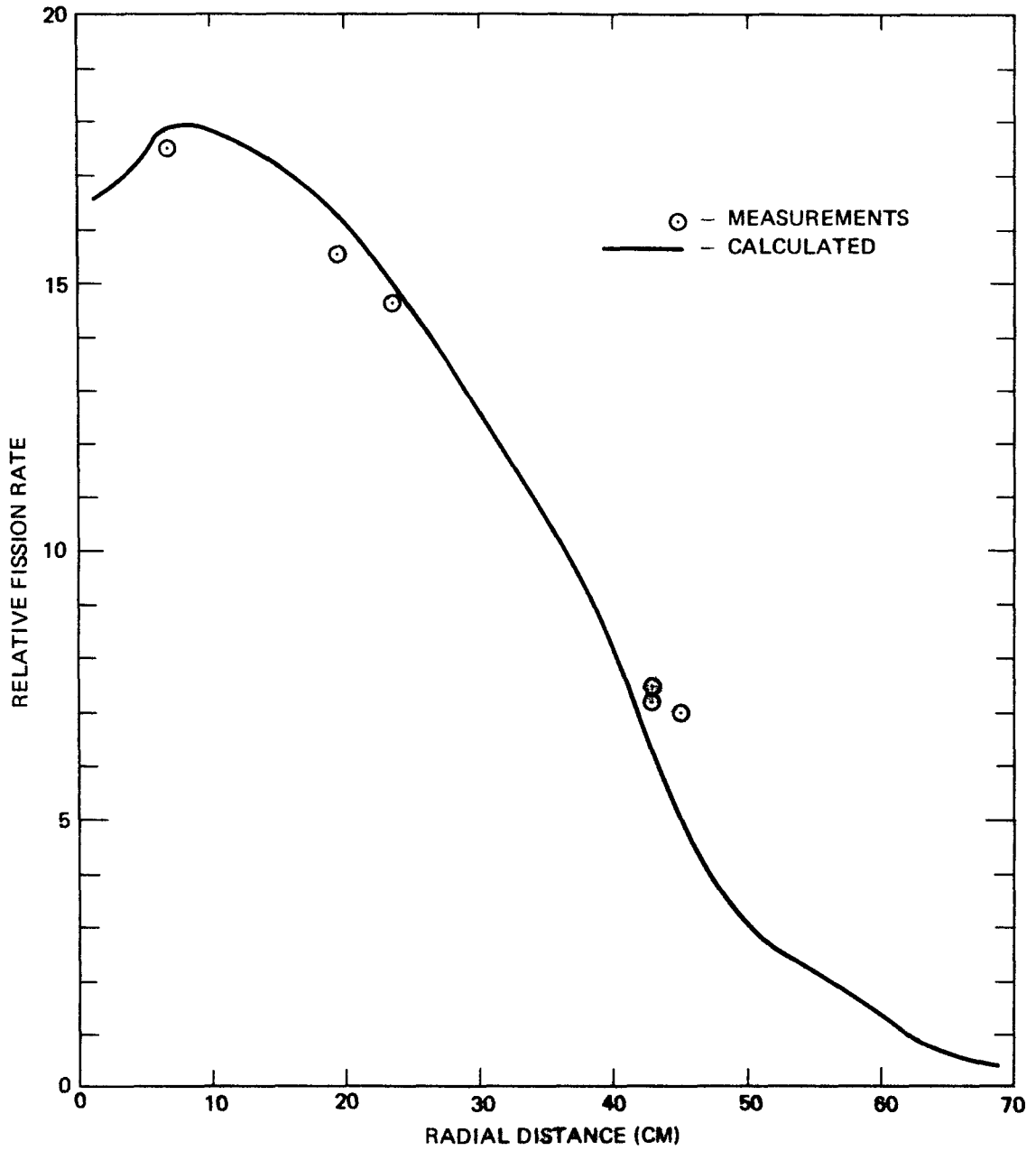
FIGURE 5-10. U-238 RADIAL FISSION DISTRIBUTION AT AXIAL POSITION 3

The calculations indicated that the U-238 fission rate within
the Al filled foil-holder rods may be about 5% lower (except in the
gap region) than in the adjacent fuel rods and they also indicated
that the axial profile within the foil holder rod is significantly
less depressed through the fuel gap region than is the U-238 fission
distribution within the fuel rods. This effect is apparently caused by
the sharp decrease in the high energy flux (and U-238 fissions) in
those core regions, such as the fuel gap, central channel, foil holder
rods, etc., that contain no fission source. The rapid change in high
energy flux shape in and around the gap region is shown in Figures
4-10 and 4-11 of Section 4. In addition, the difference between the
shape of the calculated axial U-238 fission distribution at a radius
of 3.17 cm (in the calculational model this is in a sodium steel
central channel region and is ∿1 cm. from the inner radius of the
fuel zone) and at 5.97 cm (or ∿1.7 cm within the fuel zone) is indicated
by the fission rate ratios shown in Figure 5-11. The calculations
indicate that this difference in axial shape occurs within a distance
of about 1 cm into the central channel and undergoes little additional
change at further distances into the channel. Since the shortest distance
between fuel rod centers is ∿2.8 cm, these calculations indicate that
corrections should be applied to the calculations of the U-238 fission
distribution to account for the absence of a fission source in the foil
holder rods. Such corrections were applied by using the curve in Figure
5-11 to obtain the calculated curves in Figure 5-5 and 5-7. Although
a cell calculation, perhaps with transport theory, may provide better
correction terms and closer agreement, the measured U-238 axial profiles
agree fairly well with the presently calculated profiles. Calculations
indicated that no corrections of this nature were required for the U-235
and Pu-239 distributions. Fissions in these isotopes are predominantly
the result of lower (<1Mev) energy neutrons which are not so directly
influenced by the lack of an in-rod fission source.

RATIO OF U-238 FISSION RATE 1 CM INTO THE CENTRAL
CHANNEL AND THE U-238 FISSION RATE 1.7 CM INTO
THE FUEL REGION – USED AS CORRECTION FOR U-238
FOILS IN Al FILLED FOIL HOLDER ROD.
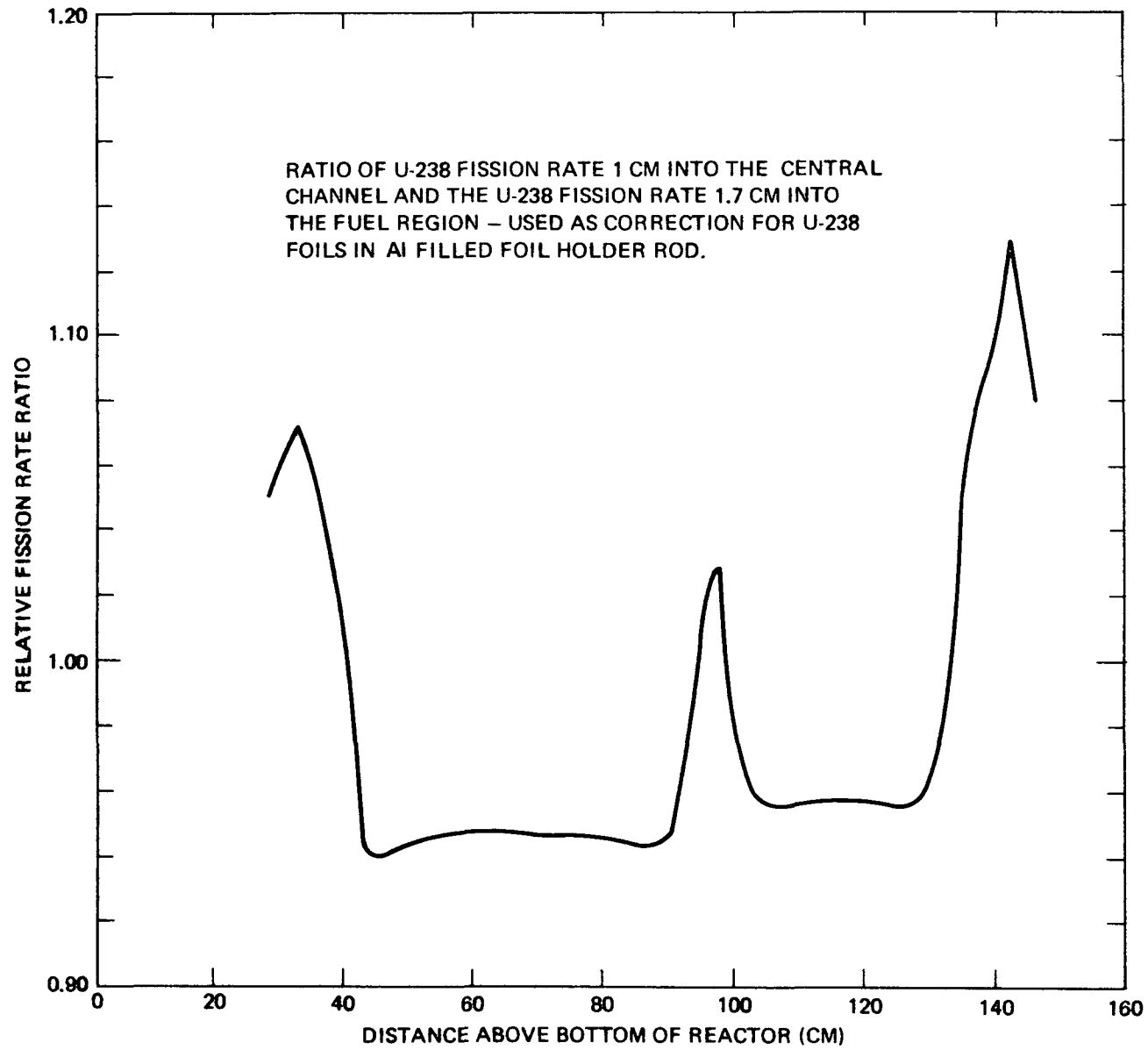
FIGURE 5-11. RATIO OF U-238 FISSION IN THE CENTRAL CHANNEL AND ADJACENT FUEL REGION

The measured relative radial fission rates near the core midplane are shown in Figures 5-8 through 5-10, and the axial distributions in the uranium near the radial core boundary are shown in Figures 5-6 and 5-7. The fission rates in these regions near the edge of the core are difficult to calculate because of the unusual geometry. The cylindrical model in which the volume of the core was preserved does not provide sufficient detail to accurately represent the geometry in and around the three foil holder rods on the edge of the core. With this model, for example, one of the foil holder rods (FD) is located at a radius (44.5 cm) outside the periphery (44.1 cm) of the core. In addition to geometrical deficiencies in the model, diffusion theory results in a more isotropic angular flux distribution than would be expected in such a region.

The measured values of the reaction rates in all the foils are higher, relative to the rates in the center, than the calculated values near the core reflector interfaces at the upper and lower boundaries of the core. Preliminary comparisons of two dimensional transport (S_4) and diffusion theory calculations indicate that corrections for transport effects would decrease these disparity by no more than $\sim 3\%$.

The general agreement between the calculated and measured reaction rate profiles throughout most of the core and the apparent (see above) underprediction of the reaction rates near the core boundaries indicate that the power (and thus fuel temperature) distribution may be somewhat flatter than calculated. Even if additional calculations do not remove the disparities, previous calculations[5,6] have indicated that the Doppler effect is relatively insensitive to the shape of the flux and temperature distributions and it is expected that the observed disparities in the power distribution will have only a small effect ($\lesssim 3\%$) effect on the calculated reactivity coefficients.

5.2.2 Comparison of Calculated and Measured Fission Ratios

The measured fission ratios in the foils at the core center were discussed in Section 5.1.2. The calculated fission ratios for all the fissionable isotopes were previously calculated and reported in reference 4. The measured (from La-140 decay) foil fission ratios of the previous section can be combined with the foil isotopic content given in Table 5-1 to obtain isotopic fission cross section ratios. These "measured" values are listed along with the previously calculated values in Table 5-6. The "measured" U-238 to U-235 fission ratio in Table 5-6 is obtained directly from the measured foil fission ratios and the isotopic composition in Table 5-1. The "measured" Pu-239 to U-235 ratio of Table 5-6 was obtained from the measured foil ratios by treating the small amount of Pu-241 (see Table 5-1) as if it were Pu-239, and by treating the other isotopes as Pu-240. In addition the calculated[4] Pu-240 to U-235 fission ratio of 0.206 was used to obtain a correction of 0.013 in the value of 0.905 in Table 5-6.

The measured and calculated fission cross section ratios are in very good agreement. Even if the measured U-238 to U-235 ratio is increased by approximately 5% to account for the apparent high energy flux depression in the foil holder rods (see Figure 5-11 and the discussion in the previous section) the agreement is still within ∿4%. In view of estimated uncertainty (∿10%) in the measurement, it is possible however that the true fission ratios are not calculated with the same accuracy as indicated by the table. It is expected that a more accurate measurement can be obtained from the proposed fission track-etch measurement.

TABLE 5-6

FISSION CROSS SECTION RATIOS NEAR CORE CENTER

Ratio	Measured	Predicted[4]
$\sigma_f^{238}/\sigma_f^{235}$	0.0252	0.0256
$\sigma_f^{239}/\sigma_f^{235}$	0.905	0.894

SECTION VI

ANALYSIS AND RESULTS OF NOISE MEASUREMENTS

The primary purpose of the Noise Measurement was to determine the ratio (ℓ/β) of the neutron lifetime to the delayed neutron fraction. This ratio will be used in the interpretation of the super-prompt critical transients. In addition, the experiment provides a means of determining the reactor power, independently of the detector efficiency, by using a calculated value for the delayed neutron fraction. Conversely, if the reactor power is accurately known, the effective delayed neutron fraction can be determined.

6.1   DESCRIPTION OF THE EXPERIMENT

6.1.1   Experimental Method and Instrumentation

In order to obtain a high efficiency for the detection of neutrons, the neutron noise was measured with two sensitive He-3 detectors* located in the central channel of the core. They were operated as ionization chambers (operating voltage: 300V). The fluctuating components of the chamber currents were amplified, digitized with a sampling frequency of 10^4 samples/sec, and recorded on magnetic tape using the data acquisition system. Since this system accepts only positive signals, batteries were used to provide a constant positive bias voltage so that the negative portion of the fluctuating signal could be recorded on the magnetic tape. The mean value of the current from each detector was measured with a pico ammeter. A high pass filter and

---

* Texas Nuclear, Model 9321
  Filling pressure 6 atm., outer diameter 1.0 inch.
  Active length 6 inches.
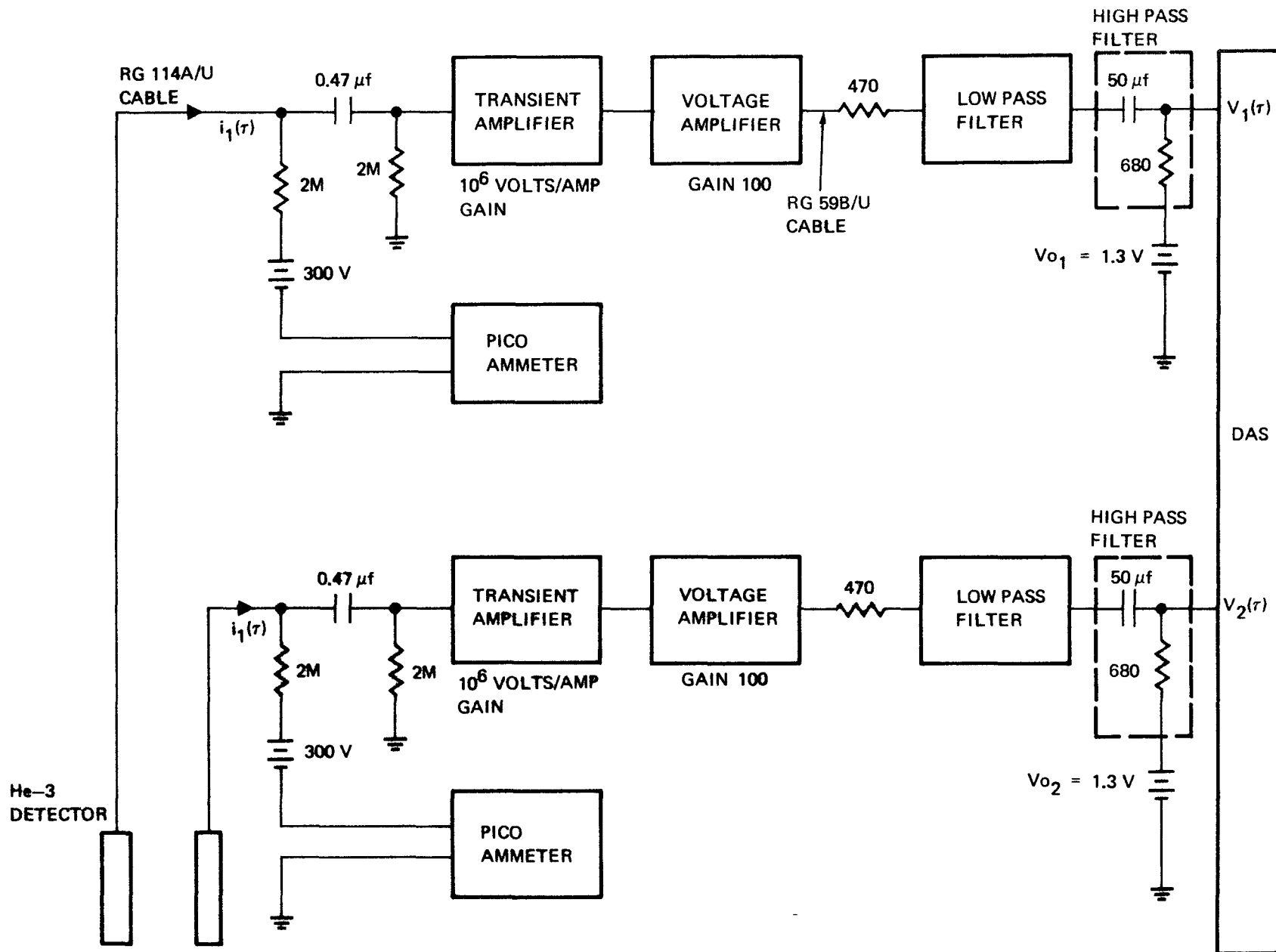
FIGURE 6-1. EXPERIMENTAL SET-UP FOR NOISE RECORDING

and low pass filter were included to avoid aliasing and to eliminate
low frequency induced noise respectively. Figure 6-1 shows a block
diagram of the experimental setup.

In order to determine the finite band width of the measuring
channel (ionization chamber plus amplifier), the frequency response
of the whole detection system, except for the He-3 chambers, was
measured with a sine wave generator. The results are plotted in
Figure 6-2. Measurements were also performed to determine the frequency
response of the He-3 chambers. Previously, satisfactory measurements
to determine the response of similar detectors had been performed in
the SEFOR mockup in ZPR-III[1] using "white" neutron noise. Because
of the difficulties in obtaining a "white" neutron source, the response
of the detectors was determined with the "white" noise of a 20 Curie -
Co^{60} source. These measurements indicated a cut-off frequency for
the detectors above 5 kH. Unfortunately, these measurements may not
provide an adequate description of the ionic component of the chamber
current produced by neutrons, because the gamma radiation is mainly
detected by electron release in the walls of.the chamber, while the
neutron detections occur as a result of the n-p reaction in He-3.

6.2   ANALYSIS AND CORRECTIONS

The analysis of the data has mainly been performed in the time
domain. A digital computer was used to calculate the auto correlation
functions $\psi_{11}(\tau)$ and $\psi_{22}(\tau)$ and the cross correlation of function
$\psi_{12}(\tau)$ from the digitized and amplified fluctuating components of the
two detector signals $V_1(\tau)$ and $V_2(\tau)$ that were recorded on magnetic tape. These
correlation functions are defined as follows:

$$\psi_{jj}(\tau) = \frac{1}{T} \int_o^T V_j(t) V_j(t + \tau)\, dt - \bar{V}_j^2 \qquad j=1,2 \qquad (6-1)$$

$$\psi_{12}(\tau) = \frac{1}{T} \int_o^T V_1(t) \, V_2(t + \tau) \, dt - \bar{V}_1 \bar{V}_2 \tag{6-2}$$

where:

$$V_1(\tau) = (I_1(\tau) - \bar{I}_1) \, y_1 + \bar{V}_1 \tag{6-3}$$

$$V_2(\tau) = (I_2(\tau) - \bar{I}_2) \, y_2 + \bar{V}_2 \tag{6-4}$$

I_j = time dependent current in chamber j

$\bar{I}_j$ = average current in chamber j

y_j = total gain of channel j

$\bar{V}_j$ = average (battery) voltage for channel j

The theoretical expression for the correlation functions as obtained from the point reactor kinetics model can be written[2] as follows:

$$\psi_{jj}(\tau) = \bar{I}_j y_j \frac{\overline{q^2}}{\bar{q}} \delta(\tau) + \bar{I}_j^2 \, y_j^2 \frac{\chi}{2\alpha F \Lambda^2} e^{-\alpha\tau} \tag{6-5}$$

$$\psi_{12}(\tau) = \bar{I}_1 \bar{I}_2 y_1 y_2 \frac{\chi}{2\alpha \, F\Lambda^2} e^{-\alpha\tau} \tag{6-6}$$

with

$\bar{q}$ = average charge collected for one neutron in He-3 chamber

$\chi = \dfrac{\overline{\nu(\nu-1)}_p}{\bar{\nu}^2} = 0.815 \, (1-\beta)^2$ - see reference (3).

ν = average number of neutrons produced per fission

$\Lambda = \dfrac{\ell}{k}$ - prompt neutron generation time

k = effective multiplication factor

F = total fission rate in the reactor

$\alpha = \dfrac{1-k \, (1-\beta)}{\ell}$ (=β/ℓ for a critical reactor)

The value for β/ℓ was determined from semi-logarithmic plots of the
correlation functions. To obtain statistical independent results,
each measurement of about 2.5 minutes total recording time was
divided into series of 20 sec intervals and each interval was analyzed
separately. From these results, the averages and standard deviations
were calculated to obtain the best experimental results and estimates
for the error.

A value F, which is proportional to the total reactor power, was
calculated with the following expression from the average detector
currents $\bar{I}$, and $\bar{I}_2$, and the total gain of all amplifiers by using the
values of ψ_{12} (o) and β/ℓ obtained from the cross correlation function
and calculated values for β and χ.

$$F = \bar{I}_1 \, \bar{I}_2 y_1 y_2 \frac{\chi \beta/\ell}{2\beta^2 \, \psi_{12} \, (o)} \qquad (6-7)$$

If an absolute and independent power calibration, either by fission
track counting or some other means, becomes available, it may be possible
to use the above relation to check the calculated value of β.

As a test of the recorded data, the amplitude distributions of the
measured ionization current fluctuations were checked. The total range
of the voltages between 0 and 2.5 volts was divided into 100 intervals
and the number of values of the digitized voltage occurring within each
interval was counted. This distribution was compared with a calculated
Gaussian distribution for which the mean value m and the variance σ^2 were
taken from the measured auto correlation functions ($m_j = \bar{V}_j$ and $\sigma_j^2 = \psi_{jj}$ (o)).
In all cases a good agreement was observed. There were some small
deviations from a Gaussian distribution near the mean values of the actually
observed distributions however. These may be due to an induced back-
ground.

The induced background was determined separately before and after each noise-record by measuring the current obtained without the high voltage supply for the He-3 chambers. In some cases corrections were made for this background.

To all correlation functions, corrections for the finite band width of the recording system have been applied. These corrections were calculated from the system frequency response $H_1(w)$ and $H_2(w)$, for channel 1 and 2 which were obtained from the measurements with a sine-wave generator. If the reactor spectral density is denoted by $\psi_0(w)$, the measured spectral density $\psi(w)$ would be

$$\psi(w) = H_1(w) \, H_2(w) \, \phi_0(w) = (1 + \psi(w)) \, \psi_0(w)$$

which is related to the measured correlation function $\psi(\tau)$ by a Fourier transform as follows:

$$\psi(\tau) = \psi_0(\tau) + \int_{-\infty}^{+\infty} \phi_0(w) \, \psi(w) e^{iw\tau} dw$$

The integral in the preceding relation is the correction for the finite band width which was subtracted from $\psi(\tau)$ to obtain the corrected values $\psi_0(\tau)$. These corrections were normally small and never larger than 5%.

The effect of delayed neutrons on the correlation function was estimated. The effect at the frequency range of interest is small and can be neglected.

As the He-3 detectors were used in the current mode, a discrimination against gamma rays was not possible. Prompt fission gamas and gammas from neutron capture and inelastic scattering are directly correlated with prompt neutrons and should increase the total detector efficiency without inducing systematic errors. The effect of completely uncorrelated

gammas from fission products, which contribute only 15% to the total
gamma energy, were eliminated by using the cross correlation technique
and by using longer delay times τ for evaluating β/ℓ from the auto
correlation function. However, since the detection of gammas from short
lived fission products might interfere with correlated neutron noise,
if their lifetimes are of the same order of magnitude as the prompt
neutron lifetime, their contribution to the total detector current
was estimated from a current measurement with a Co^{60} gamma source
and from an estimated gamma flux in the reactor. This effect was also
found to be negligible.

6.2   EXPERIMENTAL RESULTS

Four measurements have been made in the full size core (Assembly
I-D) at different power levels (i.e. at different subcritical reactivities)
between 0.2 and 6000 watts. The background level due to induced
noise was relatively high for the measurement at the lowest power level
of 0.2 watts and no reasonable information could be obtained from
this measurement. The results of the other three measurements are
listed in Table 6-1.

The wide range monitor readings, given in column one are proportioned
to the reactor power. The reactivities were obtained from the cali-
brated reflector readings and the different power levels were cal-
culated from equation (6-7). Except for the highest level of 6180.0
watts, this power calibration is in good agreement with the calibration
obtained from the subcritical measurements using the theoretical value
for the inherent neutron source (see Appendix VII). The values of $\psi(0)$
and ℓ/β in Table 6-1 are average values, determined by the method
described above, and the errors are the estimated standard deviations.

The difference between the values of ℓ/β measured at the two higher

power levels is probably due to saturation effects. The non-linearity of the average detector currents $\bar{I}$ with the WRM readings indicates saturation in the in-core He-3 detectors for power levels $P \geq 1$ kw, presumably caused by charge build-up in the He-3 tubes. Thus, the value for measurement number three is probably invalid. The difference in ℓ/β between measurements number 1 and 2 is about 10% larger than expected from the corresponding changes in the reactivity. Although the reason for this difference is not clearly defined, it may be the result of signal distortion or saturation, of a lower than anticipated cut off frequency, and of a higher than expected detector efficiency. As examples, the variances of the detector signals $\sigma_1^2 = \psi_{11}(0)$ and $\sigma_2^2 = \psi_{22}(0)$ are not proportional to the WRM values as they should be, and the ratio of the second to the first term in equation (6-5) due to correlated and uncorrelated events are much larger than calculated by using the estimated detector efficiency of 3×10^{-5} counts/fission. (The calculated value does not include any contribution from gamma radiation).

There is no indication of a peak in the auto correlation function caused by uncorrelated events (see Figure 6-4). However, a comparison between the auto and cross correlation functions shows that a relatively small contribution from uncorrelated events may be smeared out over the time interval of approximately $0 < \tau < 300$ μsec. This would be explained if the detector efficiency is larger than 3×10^{-5} counts/fission and if the cut off frequency of the detector tubes is lower than 5 kH. The first effect might be due to a relatively higher gamma sensitivity compared to the neutron sensitivity of the He-3 chambers, caused perhaps by partial saturation for neutron detection because of the longer collection time and therefore higher recombination probability for ions.

A lower cut off frequency of the He-3 tubes would not agree with the results of Morrell[1]. Also, the difference in gas pressure (6 atm.)

of the detectors used in SEFOR and those used by Morrell for the SEFOR
mockup in ZPR-III (10 atm.), should increase rather than decrease the cut
off frequency [4]. A lower cut off frequency would explain some of the
differences observed in SEFOR however, and if the tubes had a lower cut
off frequency, which would only be caused by the ionic component, and if
partial saturation occurred at $\bar{I} \sim 5$ µamp, the results from the measure-
ments No. 2 and 3 would be erroneous.

For more detailed investigations of these questions an analysis
was also made in the frequency domain. These investigations led to the
same suggestions. These investigations included the calculation of
the stochastic coherence function[5] (this is the ratio of the cross
power spectral density and the square root of the product of the auto-
spectral densities) to circumvent the problem of an unknown detector
frequency response. This is independent of the detector frequency response
and in principle it should be possible to evaluate ℓ/β from this
function without the knowledge of the detector frequency response.[5]
Unfortunately in the case of a relatively low cut-off frequency and
a high detector efficiency, as is indicated for the SEFOR data, the
method does not provide increased accuracy in the determination of ℓ/β.

Because of the apparent low cut-off frequency and high detector
efficiency, the measurements No. 2 and 3 at higher power levels should
be treated as invalid and measurement No. 1, made at the lowest power
level, must be regarded as the most reliable. Even for this measure-
ment however, the possibility of systematical errors cannot be completely
excluded, and clear answer can only be obtained by checking the chamber
characteristics, including the frequency response, in a "white" neutron
field of adequate intensity.
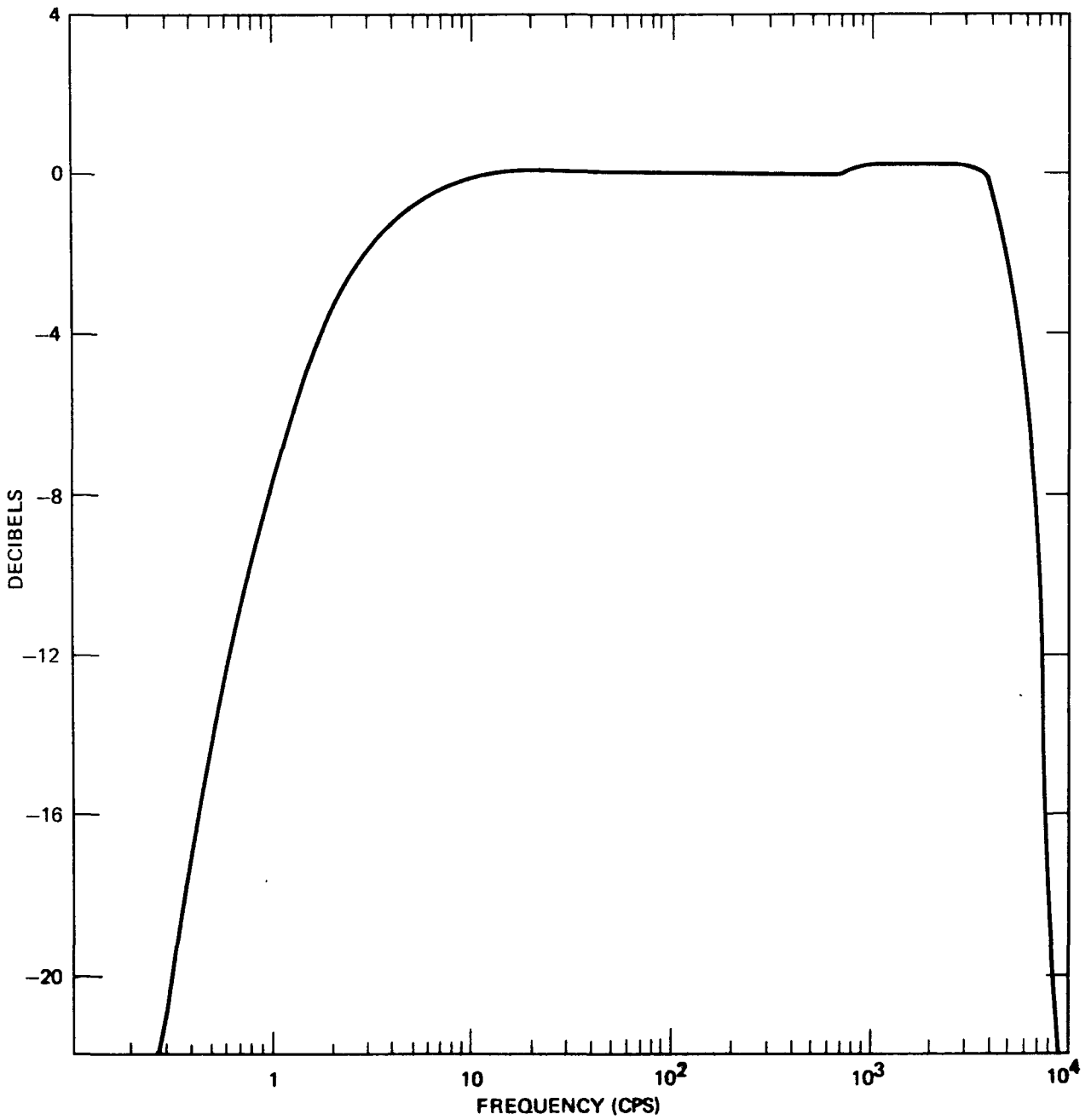
FIGURE 6-2. FREQUENCY RESPONSE FOR CHANNEL 1
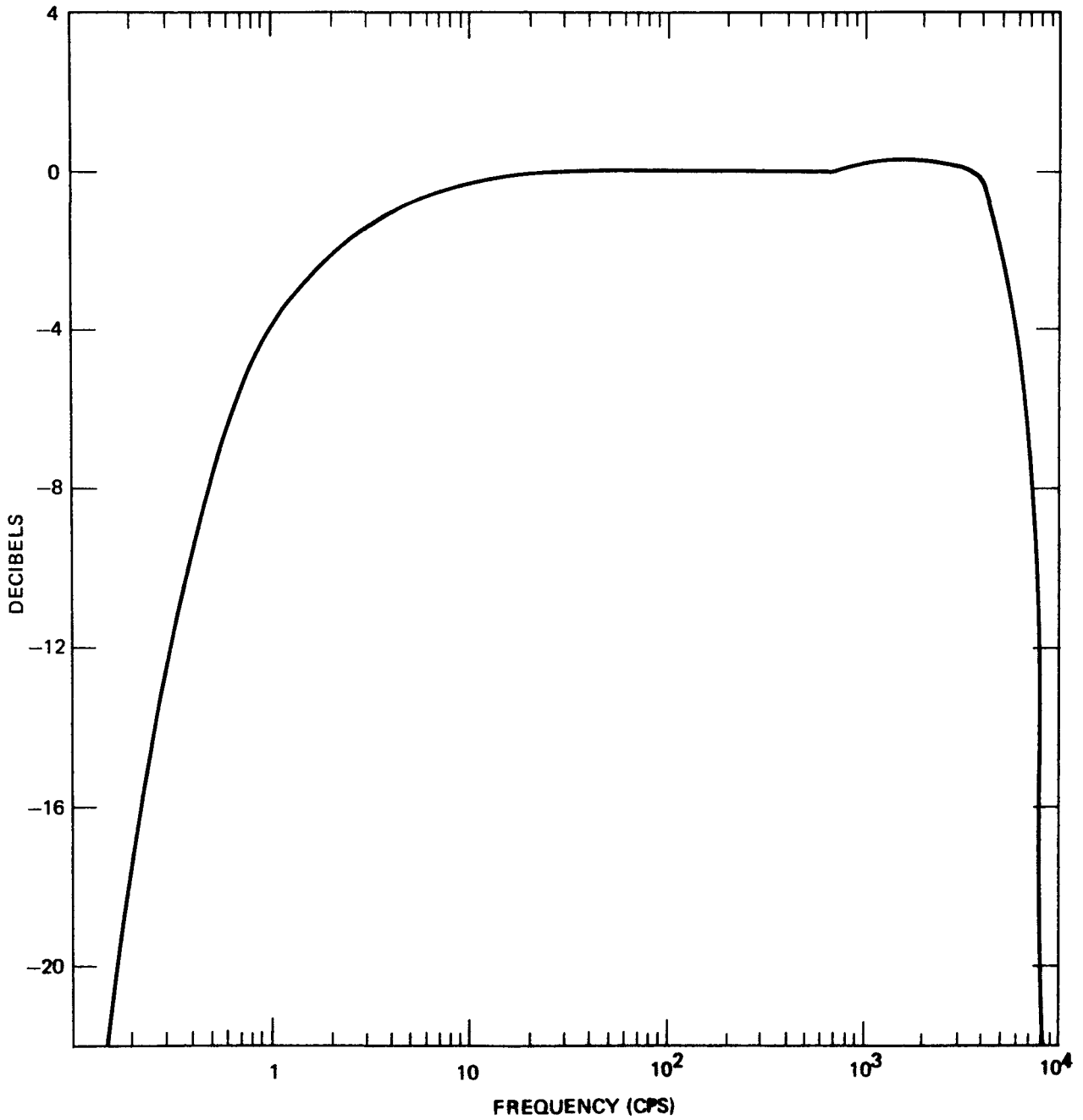
FIGURE 6-3. FREQUENCY RESPONSE FOR CHANNEL 2
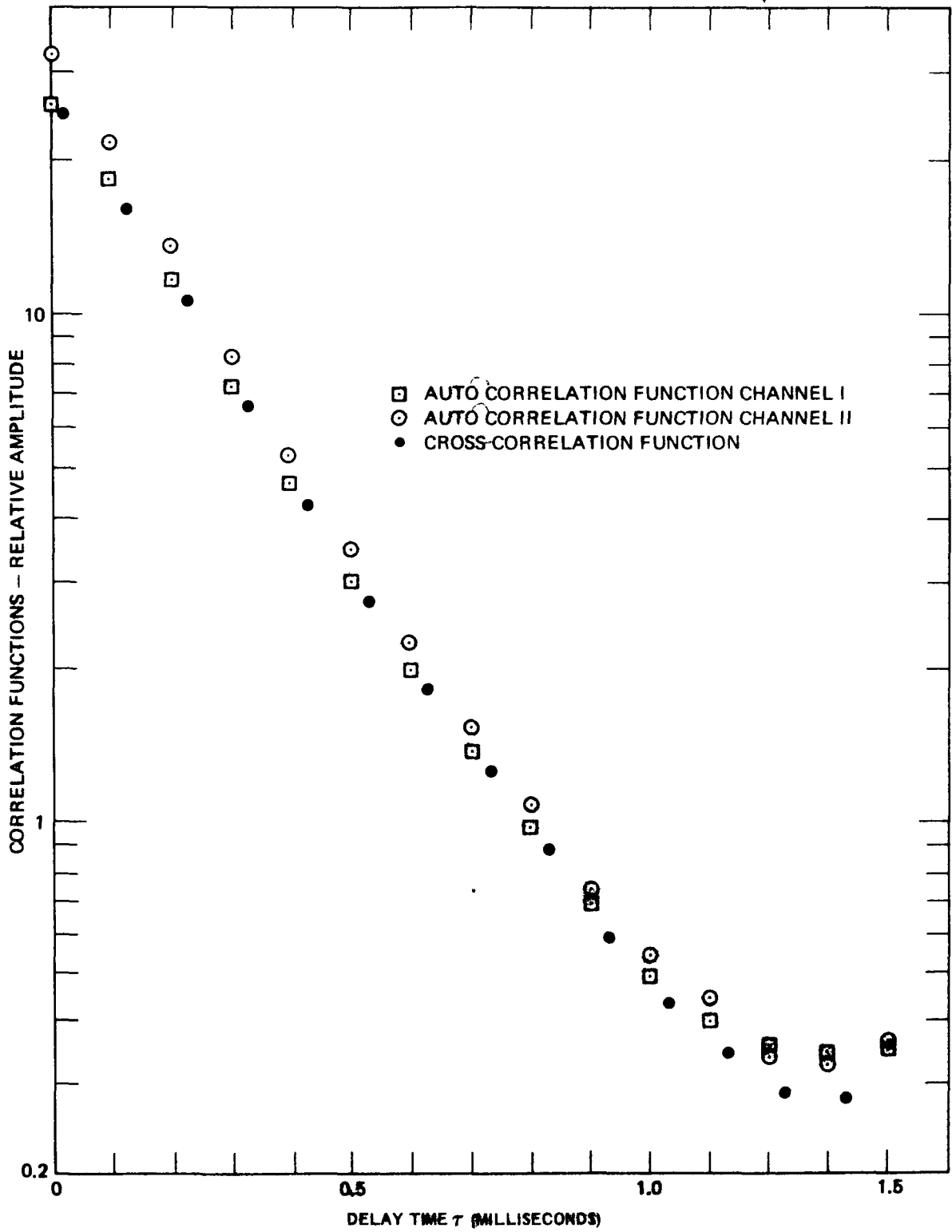
FIGURE 6-4. CORRELATION FUNCTIONS FROM MEASUREMENT NO. 2

6.3 CALCULATION OF ℓ/β AND COMPARISON WITH EXPERIMENT

The effective delayed neutron fraction β was calculated as des-
cribed in Appendix V. The lifetime ℓ was calculated with a two-
dimensional synthesis and with a two-dimensional diffusion program from
the reactivity effects resulting from the introduction of a 1/v absorber.
The results for ℓ/β are given in Table 6-1. In the synthesis method,
relatively high uncertainties are expected due to difficulties of getting
accurate axial flux distributions in the radial reflector regions.
Therefore, the result of the two-dimensional diffusion calculation must
be regarded as the best theoretical value. The influence of hetero-
geneity and transport effects on the lifetime calculations were estimated
from one-dimensional homogeneous and heterogeneous cell calcu-
lations, as well as from a comparison of two-dimensional diffusion S_4
transport calculations (with 4 energy groups). Both effects turned
out to be small (0.7% and 0.2% respectively).

It is possible that the point reactor kinetics model does not
provide an adequate description of a fast reflected system such as
SEFOR. Such a possibility is indicated by the analysis of the pulsed
measurements with the ZPR-III SEFOR mockup[6]. More sophisticated
methods for neutron lifetime calculations, such as modal or nodal
analyses might clarify this point.

A comparison between the best experimental and theoretical values
indicates that the measured prompt neutron lifetime is 11% bigger than
calculated. Although more detailed calculation or additional measure-
ments may decrease this difference, it is in agreement with previous
comparison of calculation[7] and experiment in the SEFOR mockup in
ZPR-3.

TABLE 6-1

RESULTS OF NOISE ANALYSIS

Measurement Number	Wide Range Monitor	Power obtained from Noise Analysis (watts)	Reactivity (¢)	$\bar{I}_1$ µamp.	$\bar{I}_2$ µamp.	$\psi_{12}(0)$ (volt)^2	$\psi_{11}(0)$ (volt)^2	$\psi_{22}(0)$ (volt)^2	ℓ/ρ (sec) measurement*
1	12×10^{-6}	22.28	-1.2 ± 0.5	0.101	0.114	0.0108	0.0105	0.0120	0.205×10^{-3}
2	50×10^{-5}	1036.	0.0	4.0	4.2	0.305	0.286	0.352	0.232×10^{-3}
3	25×10^{-4}	6180.	0.0	14.7	16.2	0.647	0.616	0.770	0.244×10^{-3}

* The estimated uncertainty in the measurements is $\pm$ 1%.

Calculated results:

2-dimensional synthesis program $\ell/\beta = 0.214 \times 10^{-3}$ sec.
True 2-dimensional diffusion program $\ell/\beta = 0.184 \times 10^{-3}$ sec.

SECTION VII

ZERO POWER REACTIVITY COEFFICIENT MEASUREMENTS

7.1 FLOW AND PRESSURE COEFFICIENTS OF REACTIVITY

The flow and pressure coefficients of reactivity in SEFOR are essentially zero. The reactivity effects that are associated with changes over the normal operating range of reactor vessel hydraulic pressure and primary coolant flow are of the order of the standard deviation (0.5¢) in reactivity difference measurements (see Section 4.4). These results are in agreement with expectations.[1]

In order to enable the ultimate determination of the Doppler reactivity coefficient, a number of experiments are performed in SEFOR to determine the relationship, if any, between reactivity (reflector position) and plant variables such as fuel temperature, reflector temperature, core inlet temperature, etc. The experiments discussed here were performed to determine the relationship between reactivity and coolant flow, and between reactivity and reactor vessel hydraulic pressure. In these experiments, the flow and the vessel cover gas pressure were separately and independently changed in increments between minimum and maximum values while the reflector position was adjusted to maintain a constant flux level. The variation in reactor temperature during these measurements was held to 20°F or less.

The data are tabulated in the sequential order of data collection in Tables 7-1 through 7-3 and the relative reactivity after corrections for the temperature variations are plotted versus the pressure in

Figure 7-1, and versus flow in Figures 7-2 and 7-3. Two sets of flow
coefficient measurements were performed on two different core loadings,
Assemblies I-E, and I-I. The first of these data sets was limited
by operational difficulties to flows of 4000 gpm or less. Flow rates
up to ∿100% flow (5000 gpm) were obtained in the measurements in
Assembly I-I. The reflector calibration curve for Assembly I-F (which
is similar to Assembly I-I) was used to determine the relative react-
ivity data in Assembly I-I. The slight differences, if any, in
reflector calibrations will not affect the results.

The data indicates little or no correlation between flow and
reactivity, or between pressure and reactivity. For example, even
though Figure 7-1 indicates that there may perhaps be a loss in re-
activity of 0.5 to 1.0¢ when the pressure is lowered from 5 psig to
0 psig, (the normal operating pressure is 20 psig), the maximum
difference between any of the reactivity values in Figure 7-1 or Table
7-1 is 1.15¢, while the maximum deviation from the mean of these values
is 0.82¢. These deviations are all of the same order of magnitude
as the estimated standard deviation (+0.5¢ – see Section 4.4) in the
reactivity measurements.

Similarly, the first set of flow-reactivity data, shown in
Figure 7-2 and Table 7-2, appears to be uncorrelated. The second set
of data; shown in Figure 7-3 and Table 7-3 indicates that there may
be a loss in reactivity of the order of one cent as the flow is in-
creased from 500 gpm to 3500 gpm and that this reactivity is regained
as the flow is increased to 4000 gpm. In view of the small magnitude
of this apparent change, the relatively large temperature changes
(∿20°F) which occurred during the second set of measurements, and the

evident lack of any such correlation in the first set, it appears that there is no appreciable correlation between flow and reactivity.

The data thus indicates that any reactivity effects which may accompany changes in flow or pressure are of the same order of magnitude as the 0.5¢ estimated standard deviation in reactivity measurements. Any effects of flow and pressure on reactivity are therefore negligible and can be neglected.

TABLE 7-1

PRESSURE-REACTIVITY MEASUREMENTS

(Assembly I-E)

Cover Gas Pressure (psig)	Reflector #8		Temperature (°F)	Relative System Reactivity at 350°F** (¢)	Deviation From Mean Reactivity (¢)
	Position (¢)	Worth* (¢)			
20	38.85	72.71	348.75	71.86	+0.17
15	38.85	72.71	348.75	71.86	+0.17
0	39.36	71.83	349.0	71.15	-0.54
20	39.03	72.40	349.25	71.89	+0.20
15	39.14	72.21	349.5	71.87	+0.18
10	39.13	72.23	349.5	71.89	+0.20
5	39.13	72.23	349.5	71.89	+0.20
0	39.21	72.09	349.0	71.41	-0.28
20	38.66	73.04	348.5	72.02	+0.33
0	39.23	72.06	348.25	70.87	-0.82
20	38.67	73.03	348.25	71.84	+0.15

Mean = 71.69

---

*Relative to worth in the completely raised position (∿98 cm)

**Using a temperature coefficient at 350°F of -0.68¢/°F.

***Estimated standard deviation in measurements is ±0.5¢.

TABLE 7-2

FLOW-REACTIVITY MEASUREMENTS

(Assembly I-E)

Coolant Flow (GPM)	Reflector #8 Position (cm)	Reflector #8 Worth* (¢)	Temperature (°F)	Relative System Reactivity at 350°F** (¢)	Deviation from*** Mean Reactivity (¢)
500	39.54	71.52	350.5	71.86	-0.20
1000	39.56	71.48	351.0	72.16	+0.10
1500	39.56	71.48	351.0	72.16	+0.10
2000	39.56	71.48	351.0	72.16	+0.10
2500	39.63	71.36	351.0	72.04	-0.02
3000	39.84	71.00	351.0	71.68	-0.38
3500	40.13	70.50	352.0	71.86	-0.20
4000	40.36	70.10	353.0	72.14	+0.08
370	38.66	73.04	348.75	72.19	+0.13
830	38.65	73.06	348.75	72.21	+0.15
1410	38.88	72.66	349.25	72.15	+0.09
2000	38.96	72.52	349.5	72.18	+0.12
2600	38.97	72.51	349.5	72.17	+0.11
3150	39.15	72.19	349.5	71.85	-0.21

Mean = 72.06

*Relative to worth in the completely raised position. (∿98 cm)

**Using a temperature coefficient at 350°F of -0.68 ¢/°F.

***Estimated standard deviation in measurements is ±0.5¢.

TABLE 7-3

FLOW-REACTIVITY MEASUREMENTS

(Assembly I-I)

Coolant Flow (GPM)	Reflector #8 Position (cm)	Reflector #8 Worth* (¢)	Temperature (°F)	Relative System Reactivity at 390°F** (¢)	Deviation from*** Mean Reactivity (¢)
500	54.09	46.99	389.0	46.31	+0.33
500	53.89	47.32	388.25	46.13	+0.15
500	53.68	47.67	387.75	46.14	+0.16
1000	53.55	47.89	387.0	45.85	-0.13
1000	53.15	48.55	386.25	46.00	+0.02
1000	52.90	48.97	385.5	45.91	-0.07
1500	52.76	49.20	385.0	45.80	-0.18
1500	52.55	49.55	384.5	45.81	-0.17
1500	52.38	49.84	384.0	45.76	-0.22
2000	52.31	49.96	383.75	45.71	-0.27
2000	52.15	50.22	383.25	45.63	-0.35
2000	52.01	50.46	383.0	45.70	-0.28
3000	51.93	50.59	382.5	45.49	-0.49
3000	52.09	50.32	382.75	45.39	-0.59
3000	52.22	50.11	383.0	45.35	-0.63
3500	52.19	50.16	382.75	45.23	-0.75
3500	52.25	50.06	382.75	45.13	-0.85
3500	52.15	50.22	382.5	45.12	-0.86

---

*Relative to worth in the completely raised position (∿98 cm) – using the reflector calibration curve for Assembly I-F.

**Using a temperature coefficient at 390°F of -0.68¢/°F.

***Estimated standard deviation in measurements is ±0.5¢.

TABLE   7-3 (Continued)

FLOW-REACTIVITY MEASUREMENTS

(Assembly I-I)

Coolant flow (GPM)	Reflector #8 Position (cm)	Reflector #8 Worth* (¢)	Temperature (°F)	Relative System Reactivity at 390°F** (¢)	Deviation from*** Mean Reactivity (¢)
4000	58.71	39.31	400.0	46.11	+0.13
4000	58.74	39.26	400.0	46.06	+0.08
4000	58.57	39.54	400.0	46.34	+0.36
4000	58.55	39.57	399.75	46.20	+0.22
4450	58.68	39.36	400.0	46.16	+0.18
4450	58.84	39.10	400.25	46.07	+0.09
4450	58.86	39.06	400.5	46.20	+0.22
4450	58.93	38.95	400.5	46.09	+0.11
4900	59.37	38.23	401.5	46.05	+0.07
4900	59.49	38.04	402.0	46.20	+0.22
4900	59.78	37.57	402.5	46.07	+0.09
4900	59.77	37.58	402.75	46.25	+0.27
500	57.69	40.98	399.25	47.27	+1.29
500	57.52	41.26	398.0	46.70	+0.72
500	57.35	41.55	397.25	46.48	+0.50
500	57.35	41.55	397.25	46.48	+0.50

Average = 45.98

---

*Relative to worth in the completely raised position (~98 cm) —using the reflector calibration curve for Assembly I-F.

**Using a temperature coefficient at 390°F of $-0.68¢/°F$.

***Estimated standard deviation in measurements is $\pm0.5¢$.
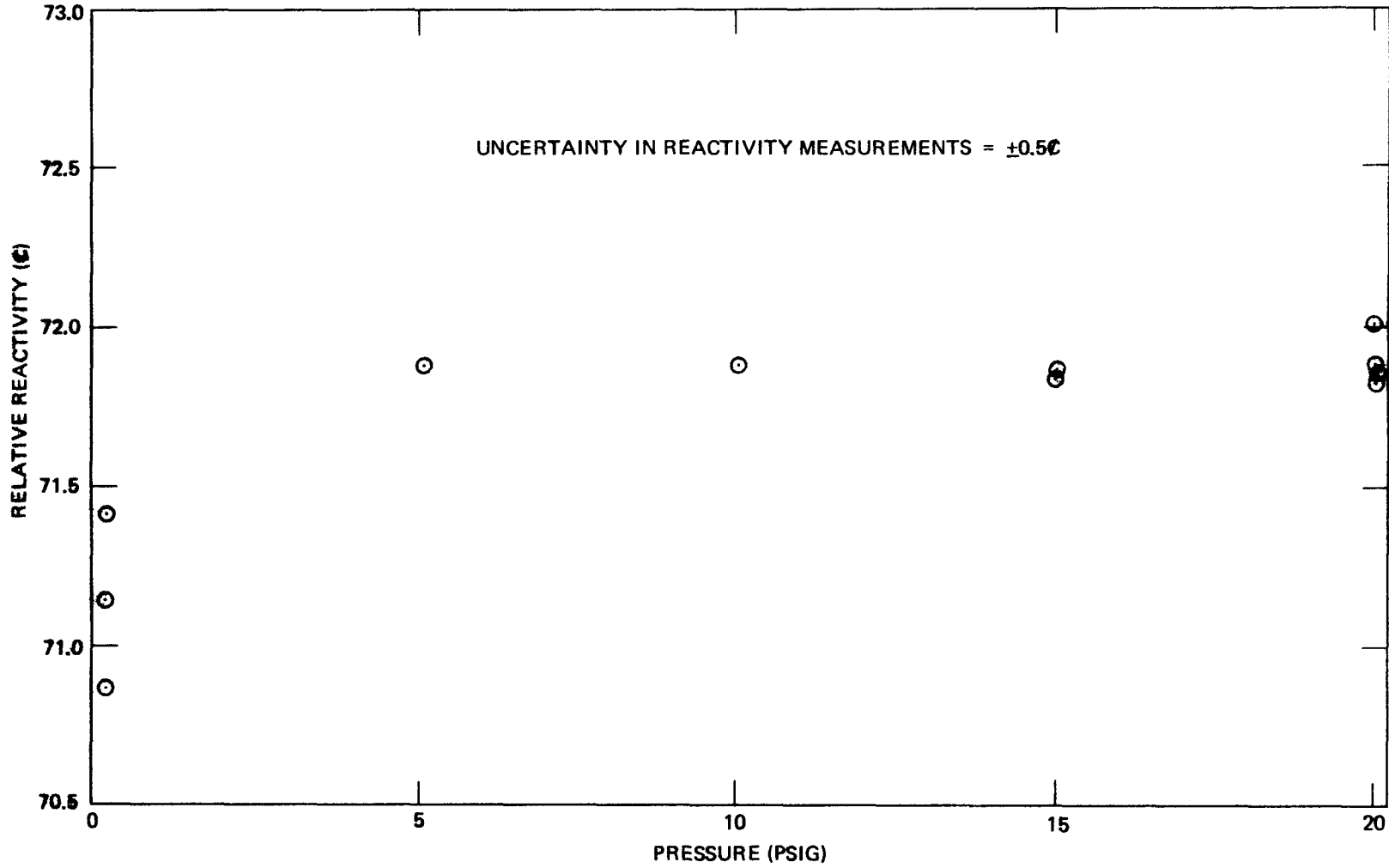
FIGURE 7-1. PRESSURE REACTIVITY MEASUREMENTS (ASSEMBLY I-E)

GEAP-13588
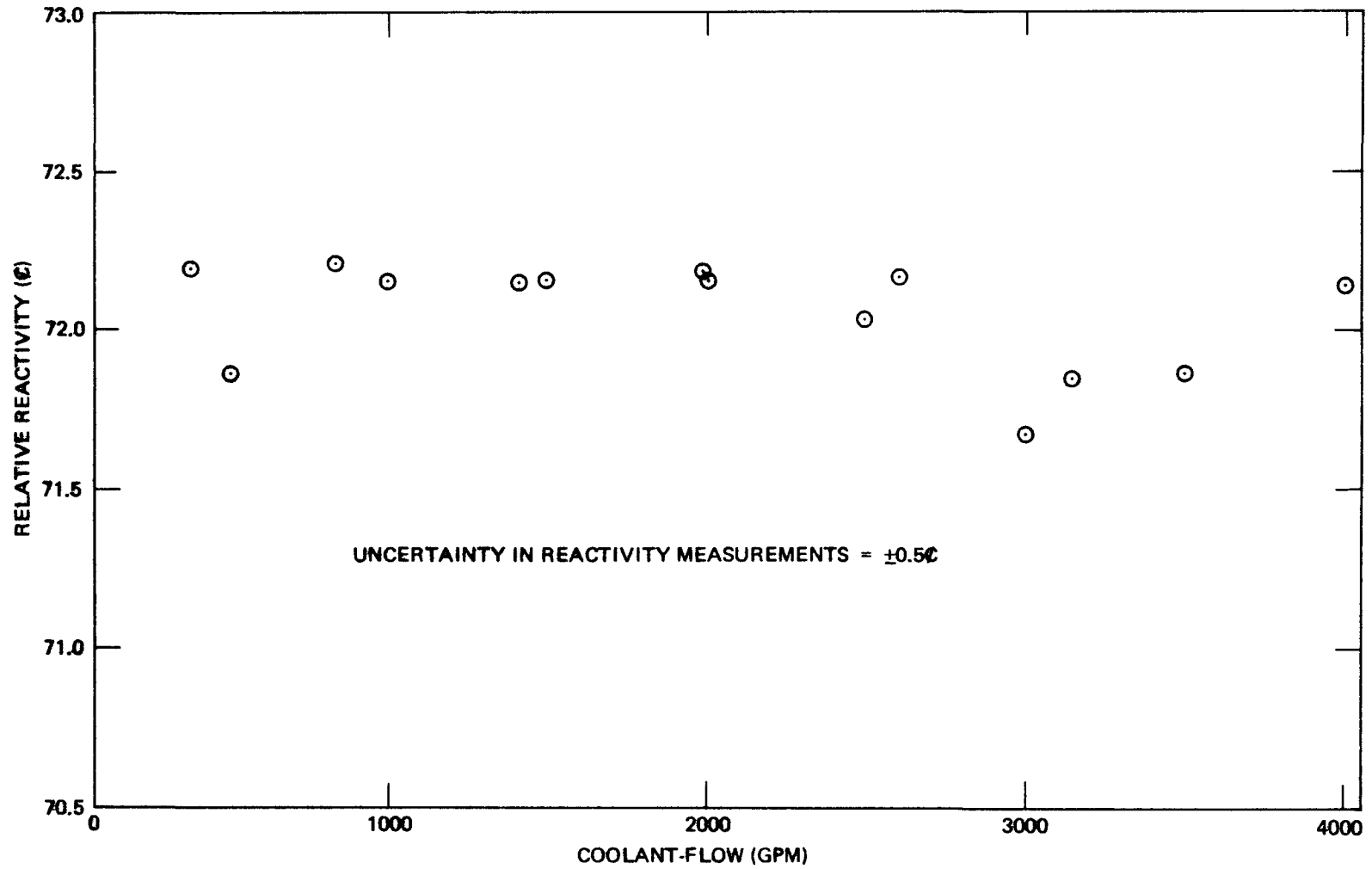
FIGURE 7-2. FLOW REACTIVITY MEASUREMENTS (ASSEMBLY I-E)
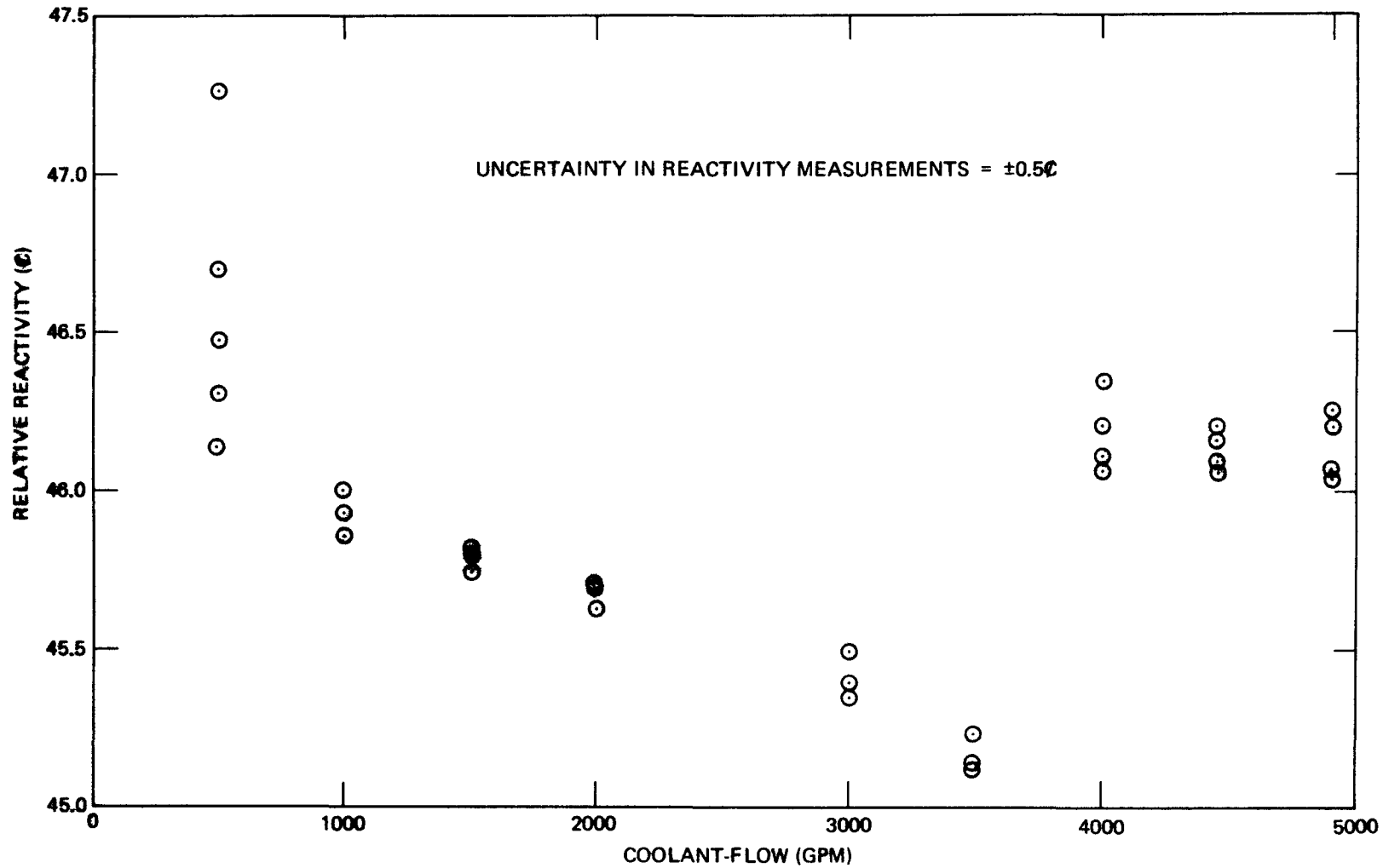
FIGURE 7-3. FLOW REACTIVITY MEASUREMENTS (ASSEMBLY I-I)

7.2   CALCULATION OF THE UNIFORM TEMPERATURE REACTIVITY COEFFICIENTS

The major components of the temperature dependent reactivity
feedback coefficients for the fully loaded SEFOR core were calculated,
and the influence of core B_4C content on these coefficients was in-
vestigated. In addition, the reactivity coefficients were also cal-
culated for the minimum critical core loading. Both of these cal-
culations were performed prior[2,3] to the actual[4,5] temperature
coefficient measurements. The calculated average Doppler coefficient
(T dk/dT) between fuel temperatures of 300°K and 1400°K was -0.0082
for a fully loaded core containing 19 uniformly distributed B_4C rods,
while the expansion coefficient was -0.36¢/°F. The magnitudes of the
Doppler and expansion coefficients were increased by only 5% and 3%,
respectively, for a core containing 12 uniformly distributed B_4C rods
instead of 19. Since the coefficients are relatively insensitive to
B_4C content, the values quoted here should be representative of the
feedback coefficients for any SEFOR full size core loading. The corres-
ponding Doppler $T\frac{dk}{dT}$ and total expansion coefficient for the minimum
critical core were -0.0086 and -0.44¢/°F, respectively.

The total calculated[3] feedback coefficient for the fully loaded
core, including Doppler, is -0.68¢/°F at 350°F and -0.58¢/°F at 700°F.
The corresponding total feedback coefficient for the minimum critical
core[2] is -0.77¢/°F at 350°F. The calculated Doppler coefficient
for the fully loaded core is in good agreement with previously cal-
culated values for the full size[6] core and is only 5% lower for the
fully loaded core containing 19 uniformly distributed B_4C rods than
for the minimum critical partially loaded core. The expansion
coefficient is ∿20% lower in the full size core than for the minimum

critical core, primarily because of the decreased sodium density effect between the core and vessel due to the smaller amount of sodium between the core and reflectors in the fully loaded core.

Calculations were performed for two fully loaded SEFOR cores; one containing 629 fuel rods and 19 B_4C rods distributed uniformly throughout the core and the other containing 636 fuel rods and 12 B_4C rods. In addition, calculations were performed for a partially loaded core containing 512 fuel rods and no B_4C rods. The calculational models, cross sections, and energy group structures are described in Appendix I.

The calculation for the 512 rod core was performed to provide a basis for correcting any reactivity measurements in a partially loaded core for undesired temperature variations. No temperature coefficient measurements were actually performed on a partially loaded core, but the close agreement between calculation and experiment for the fully loaded core allows the results for the partially loaded core to be used with a reasonable degree of confidence. A core model with 512 rods was used in the initial critical prediction, and was used for the reactivity coefficient calculations prior to the initial loading because it was nearly the size of the predicted minimum critical core.

7.2.1 Doppler Coefficient Calculations

The U-238 contribution to the Doppler coefficient was calculated using temperature dependent cross sections at 300°K, 700°K and 1400°K for the fully loaded core that were obtained from a cross section fitting routine. Similar temperature dependent cross sections at 300°K and 700°K were used in the 512 rod core. Results for the fully loaded cores

containing B_4C were calculated for a uniform fuel temperature change using 13 group cross sections and the two-dimensional synthesis code BISYN[7]. The results are summarized in Table 7-4. The Doppler reactivity effect for the partially loaded core was calculated by perturbation of a 60 energy group, one-dimensional radial diffusion theory calculation. In addition, the Doppler coefficient for this core was also evaluated from calculations using 13 energy groups and a two-dimensional synthesis program[7]. The results of the two methods of calculation are in good agreement as indicated in Table 7-4. The calculations indicate that for the fully loaded core the quantity defined as T dk/dT can be treated as a constant (within $\sim \pm 5\%$) over the temperature range between 300°K and 1400°K. The predicted Doppler T dk/dT is -0.0082 for a fully loaded core containing 19 uniformly distributed B_4C rods and -0.0086 for a partially loaded core containing 512 fuel rods and no B_4C rods. These values are composed of the U-238 contributions listed in Table 7-4 and a previously calculated[6] value of -0.0003 for the Pu-240 contribution. It was assumed that the Pu-239 contribution to the Doppler effect is zero. The predicted Doppler T dk/dT for a fully loaded core containing 12 B_4C rods (including a contribution from Pu-240 of -0.0003) is -0.0086.

TABLE 7-4

U-238 DOPPLER CALCULATIONS

Number of B_4C rods in Fully Loaded Core	Reactivity Effects for Fully Loaded Core (using 13 energy groups and synthesis (7) calculation)		
	300°K to 700°K Δk	700°K to 1400°K Δk	Average T dk/dT (300°K to 1400°K)
19	-0.00695	-0.00518	-0.0079
12	-0.00726	-0.00541	-0.0083

Method of Calculation	Reactivity Effects for 512 Rod Partially Loaded Core	
	300°K to 700°K Δk	Doppler $T \frac{dk}{dT}$ 300°K to 700°K
Perturbation of a 60-group radial problem	-0.00707	-0.00835
Change in reactivity from synthesis (7) calculations	-0.00692	-0.00817
	Average =	-0.0083

7.2.2 Definition and Calculation of Expansion Coefficients

The expansion coefficients for SEFOR have been previously defined in Reference 6, but are repeated here for convenience of the reader.

1. Axial Fuel Expansion: The reactivity effect due to increasing the length of the fuel segments with a corresponding reduction in fuel density and size of the gap.

2. Axial Fuel Clad Expansion: The reactivity effect due to axial expansion of the fuel clad. Most of this reactivity effect is due to the upper fuel segment moving with the fuel clad and there is a smaller contribution due to the reduction in clad density.

3. BeO Axial Expansion: The reactivity effect due to extending the length of the BeO in the tightener rods with a corresponding reduction in BeO density.

4. Structure Axial Expansion: The reactivity effect due to extending the length of the channels, steel side rods, tightener rod cladding, tightener sleeve, axial reflectors, and the inner vessel wall with a corresponding reduction in the respective material densities.

5. Structure Radial Expansion: The reactivity effect caused by radial expansion of the channels. Since the structure temperature change is accompanied by the same change in fuel and BeO clad temperatures, core volume fractions remain unchanged during radial expansion. Displacement of sodium surrounding the core is included in this effect. Change of sodium density is not included; this appears in a separate coefficient.

6. Sodium Density Effect in Core and Axial Reflectors: The reactivity effect due to a change of sodium density in the core and axial reflectors.

7. Sodium Density Effect Between Core and Vessel: The reactivity effect due to a change of sodium density in the region between the core and the vessel wall.

8. B_4C Axial Expansion: The reactivity effect due to extending the length of the B_4C rods with a corresponding reduction in B_4C density.

The coefficients for fuel axial expansion and fuel clad axial expansion were taken directly from Reference 6. All other expansion coefficients were calculated from the results of a series of 13 group BISYN[7] problems. All expansion reactivity effects are assumed to vary linearly with respect to the dominating variable, i.e. change in height, radius, etc. The expansion reactivity coefficients obtained from the BISYN calculations are summarized in Tables 7-5 and 7-6.

The total expansion coefficient for the fully loaded core in Table 7-5 is ∿20% lower than the expansion coefficient for the minimum critical core given in Table 7-6. The primary reason for this is the decreased volume of sodium between the core and radial reflector in the fully loaded core. Because of the smaller amount of sodium, the sodium density effect in this region is reduced from -0.122 to -0.056. Another effect, although of smaller magnitude, is the decreased magnitude of the core sodium density coefficient in the fully loaded core.

TABLE 7-5

EXPANSION REACTIVITY COEFFICIENTS FOR FULLY LOADED SEFOR CORE

Effect	Percentage Change** per degree Fahrenheit (%/°F)	Reactivity Effects* for Core with 19 B_4C Rods (¢/°F)
Fuel Axial Expansion	+0.000461	-0.009[+]
Fuel Clad Axial Expansion	+0.000980	-0.072[+]
BeO Axial Expansion	+0.000580	-0.003
Structure Axial Expansion	+0.000980	-0.014
Structure Radial Expansion	+0.000980	-0.135
Sodium Density in Core and Axial Reflector	-0.015789	-0.072(-0.076)
Sodium Density Between Core and Vessel	-0.015789	-0.056(-0.059)
B_4C Axial Expansion	+0.000250	+0.002(+0.001)
		-0.359(-0.367)

*If different, the reactivity effect for a core containing 12 B_4C rods is enclosed in parenthesis.

**This represents the percentage change in length, density, etc.

+Based on the calculated coefficients in Reference 2 of -19.27¢/% $\Delta h/h$ for fuel axial expansion and -73.31¢/% $\Delta h/h$ for fuel clad axial expansion

TABLE 7-6

EXPANSION REACTIVITY COEFFICIENTS FOR 512 ROD CORE

Effect	Percentage change** per degree Fahrenheit(%/°F)	Reactivity Effect (¢/°F)
Fuel Axial Expansion	+0.000461	-0.009*
Fuel Clad Axial Expansion	+0.000980	-0.072*
BeO Axial Expansion	+0.000580	-0.004
Structure Axial Expansion	+0.000980	-0.014
Structure Radial Expansion	+0.000980	-0.130
Sodium Density in Core and Axial Reflector	-0.015789	-0.093
Sodium Density Between Core and Vessel	-0.015789	-0.122
B_4C Axial Expansion	+0.000250	0.0
		-0.444

---

*Based on the calculated coefficients in Reference 2 of -19.27¢/% Δh/h
 for fuel axial expansion and -73.31¢/% Δh/h for fuel clad axial expansion

**This represents the percentage change in length, density, etc.

7.3   TEMPERATURE COEFFICIENT MEASUREMENTS

7.3.1   Temperature Coefficient Measurement in Assembly I-D

A preliminary measurement of the temperature coefficient was performed in a fully loaded core Assembly I-D (see Figure 1-4) in order to determine an appropriate fuel loading for the normal operating temperature (760°F), and to obtain a preliminary value for use in correcting other zero power reactivity test data for undesired changes in temperature.

The primary sodium was heated from 350°F to 400°F by the primary loop trace heating system. The temperature was maintained at 400°F for about two hours and the primary system was then cooled down to 350°F. This process was repeated to establish the reproducibility of the data. The reactor was shut down during the actual heating and cooling periods, but steady state critical reflector positions were recorded at both temperature extremes.

The data obtained during the experiment are shown in Table 7-7. A least squares fit of a straight line to the data in the table gives a value of -0.59 $\pm$ 0.01 ¢/°F for the temperature coefficient.

TABLE 7-7

TEMPERATURE COEFFICIENT MEASUREMENTS IN ASSEMBLY I-D

Temperature (°F)	Reflector #3 Position (cm)	Worth* (¢)	Reflector #8 Position (cm)	Worth* (¢)	Reactivity Change Relative to 350°F (¢)
352.0	0.75	0.19	52.09	74.02	-0.88
398.5	0.75	0.19	69.07	101.60	-28.46
397.5	0.75	0.19	68.88	101.33	-28.19
397.0	0.75	0.19	68.67	101.03	-27.89
350.0	0.44	0.00	51.71	73.33	0.00
398.25	0.44	0.00	69.27	101.88	-28.55
398.25	0.44	0.00	69.27	101.88	-28.55
398.25	0.44	0.00	69.15	101.71	-28.38
398.25	0.44	0.00	69.15	101.71	-28.38

*Relative to the worth with the reflector lowered.

7.3.2 Temperature Coefficient Measurements in Assembly I-E

In order to determine the temperature coefficient of reactivity
in Assembly I-E (see Figure 1-5), the reactor was heated from 350°F
to 760°F with the primary loop trace heating system, cooled to about
700°F and then reheated to 760°F. The reactor power level was held
constant at about 600 watts throughout the heating and cooling periods
by adjusting the reflector positions to compensate the reactivity feed-
back effects. Resistance-Temperature Detectors (RTD's) were used to
monitor the main and, over the last portion of the experiment, the
auxilary primary reactor inlet and outlet temperature. In addition,
the temperatures indicated by a thermocouple located inside the re-
actor vessel were recorded. The RTD readings had an estimated un-
certainty at any point of $\pm$ 2.5°F, while the estimated uncertainty
in the thermocouple reading at any point was $\pm$0.25°F.

The temperatures and reflector positions were recorded approxi-
mately every 15 minutes. The primary sodium temperature was stabilized
for two to three hours at temperatures of approximately 450°F, 550°F,
650°F, and 760°F to ensure that both thermal and nuclear equilibrium
were attained at these points. The time dependent behavior of the
temperatures are shown in Figures 7-4 through 7-10 and the reactivity
feedback as a function of temperature indicated by the thermocouple
is shown in Figure 7-11.

Although the indicated auxilary primary inlet temperature is
somewhat erratic, the thermocouple and the main primary RTD's show a
nearly constant difference of about 15°F (which can be corrected by
recalibration), and the indicated changes in temperature are nearly

identical. The data indicates that the relationship between react-
ivity and temperature is independent of the heating rate, for rates of
about 20°F per hour or less. This demonstrates that the reactivity
feedback contains no major components with long time constants and that
reactivity transient effects are insignificant for heating rates up
to ∿20°F/hour.

The close agreement between the experimental reactivity feedback
and the feedback calculated using the predicted values of −0.0082 for
the Doppler T $\frac{dk}{dT}$, and −0.36¢/°F for the combined expansion – sodium
density coefficient is shown in Figure 7-11. The actual data taken
during the experiment are tabulated in Appendix VII.
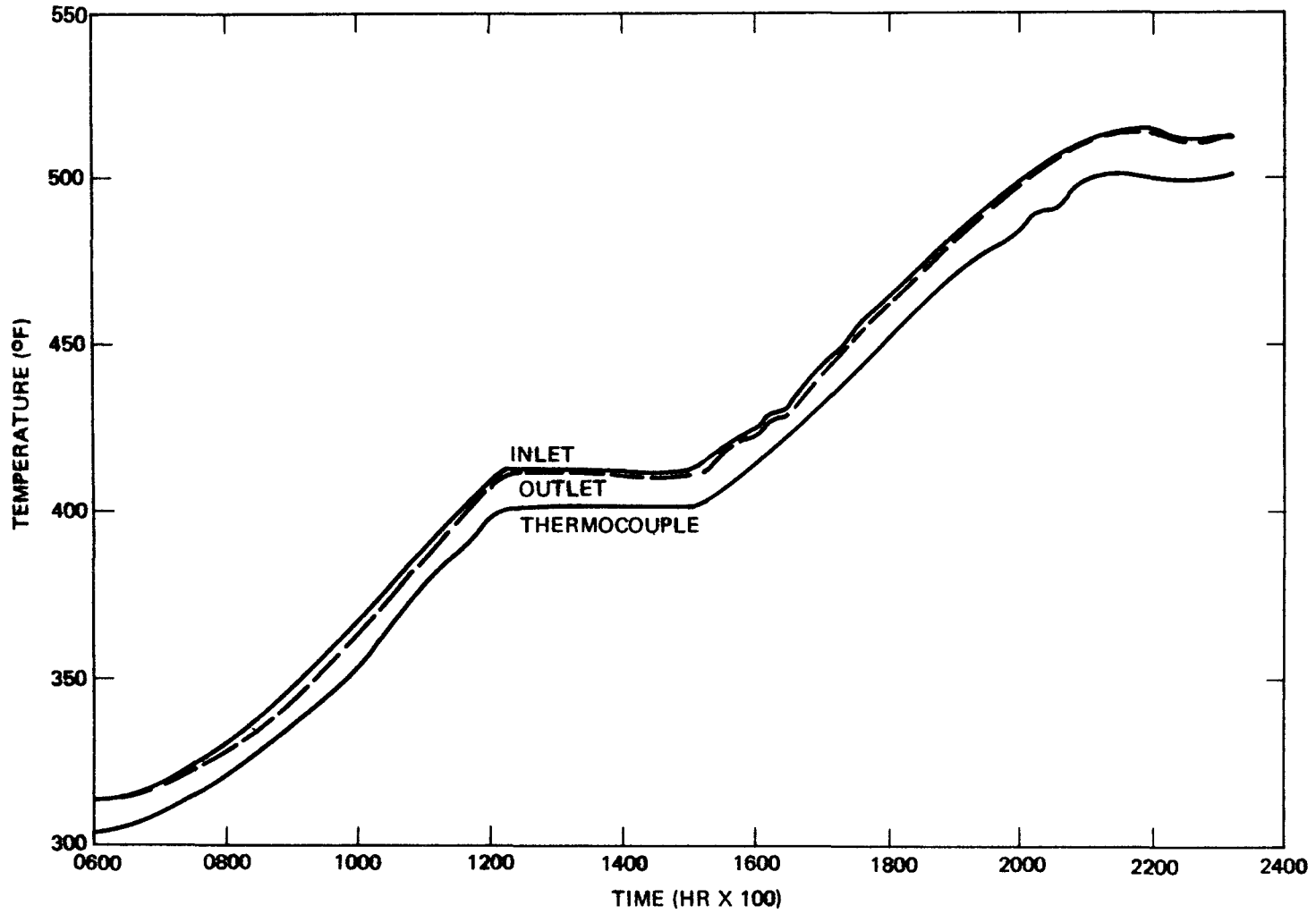
FIGURE 7-4. IN CORE THERMOCOUPLE AND MAIN PRIMARY RTD'S (10/22/69)
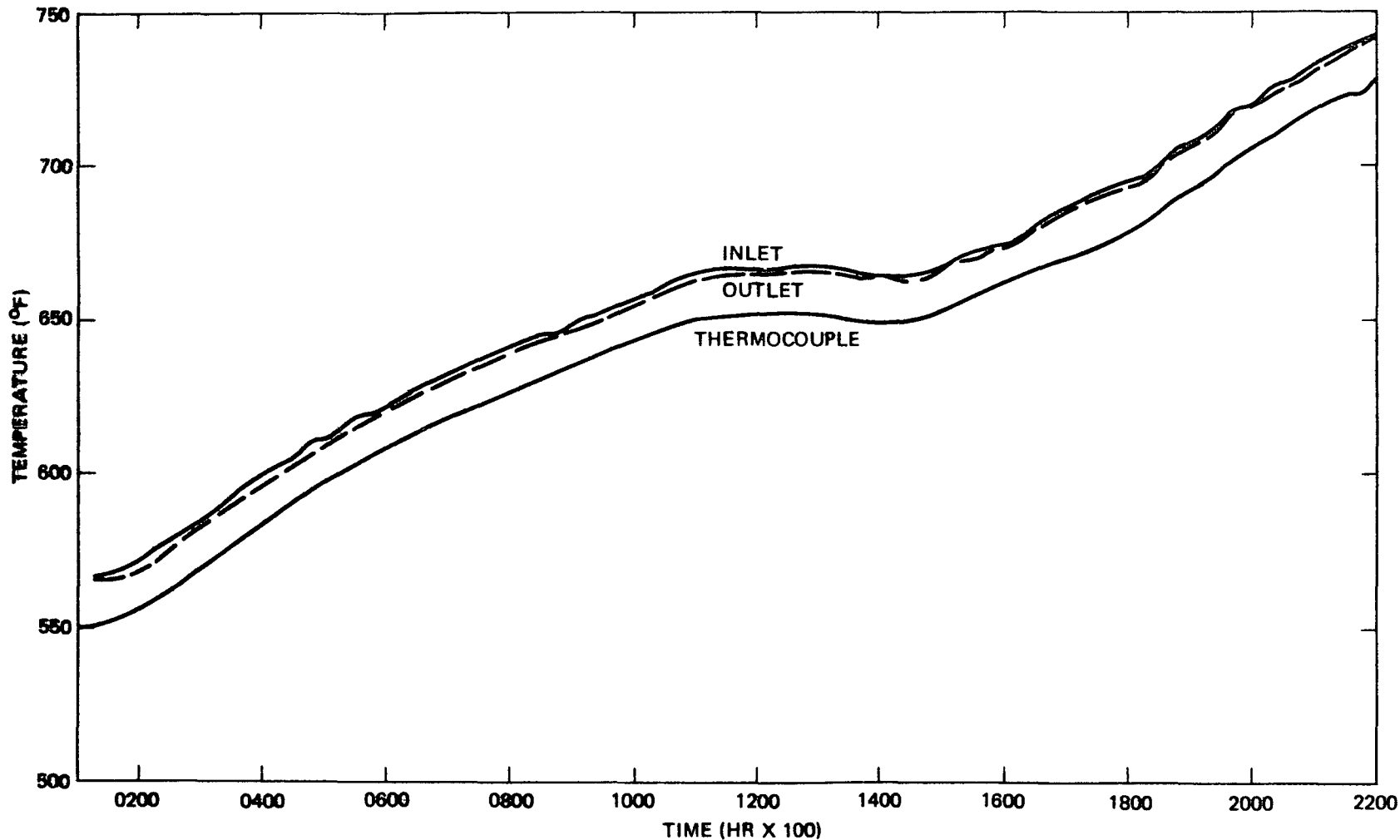
FIGURE 7-5. IN CORE THERMOCOUPLE AND MAIN PRIMARY RTD'S (10/25/69)
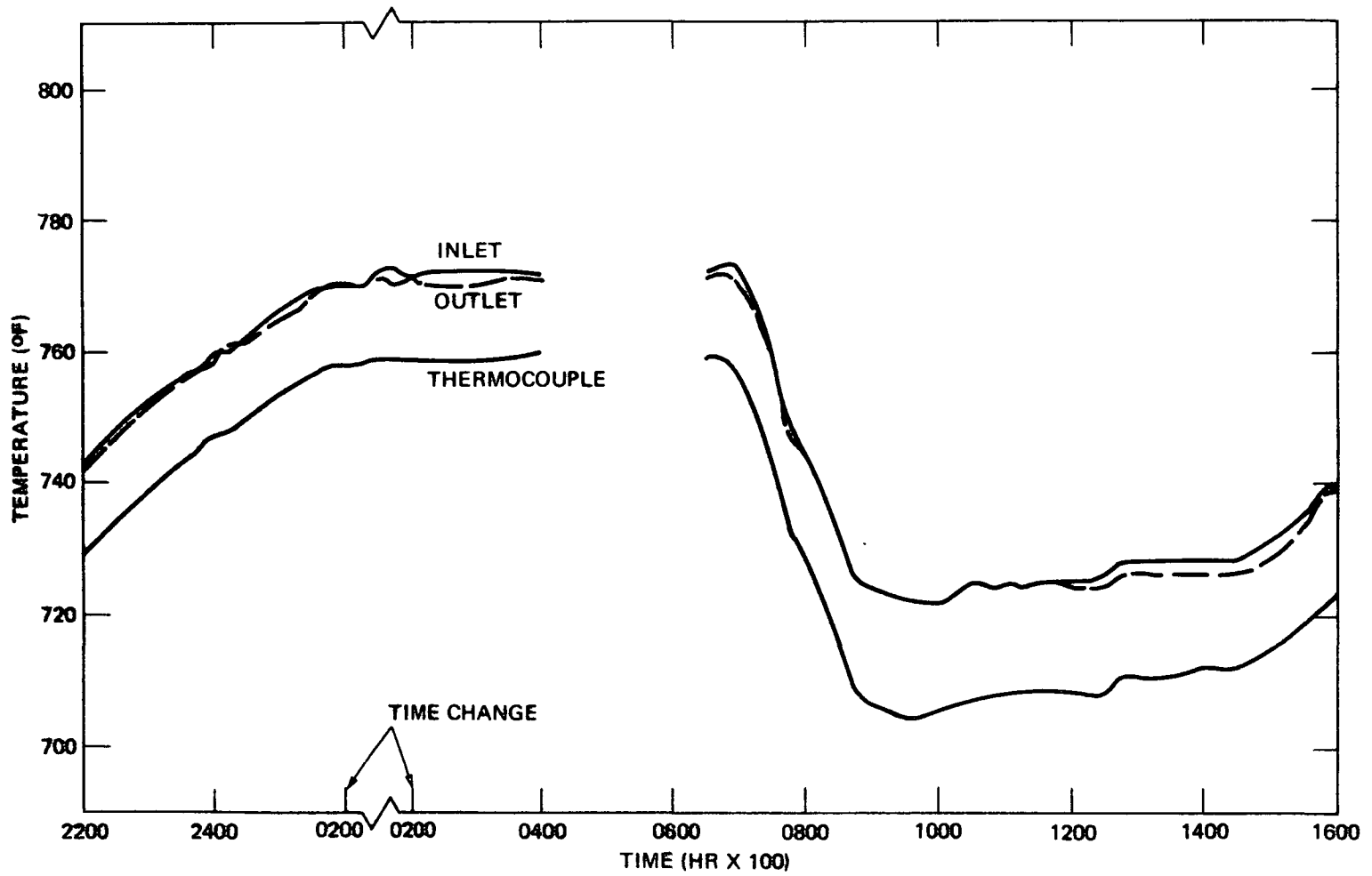
FIGURE 7-6. IN CORE THERMOCOUPLE AND MAIN PRIMARY RTD'S (10/25/69 - 10/26/69)

GEAP-13588
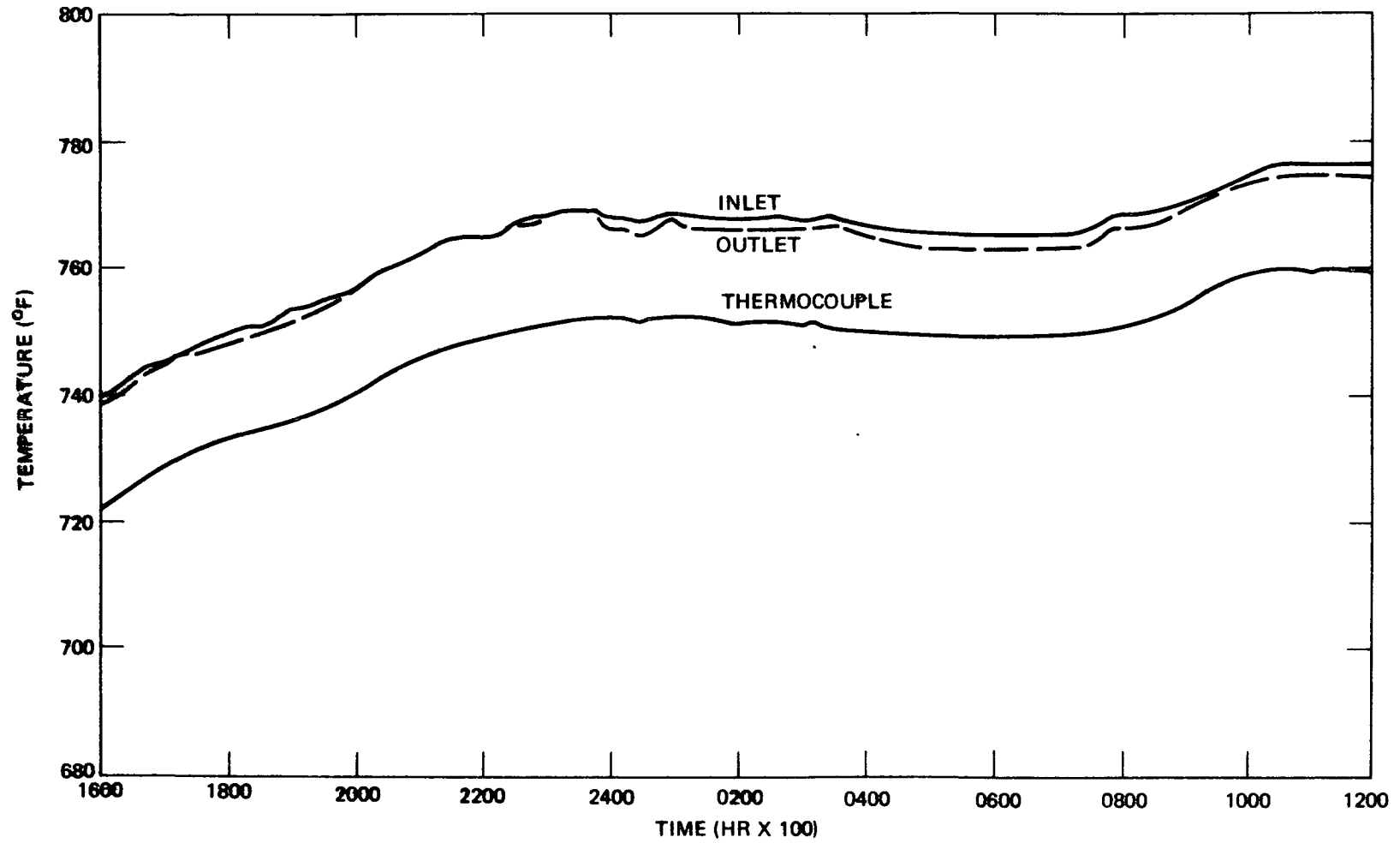
FIGURE 7-7. IN CORE THERMOCOUPLE AND MAIN PRIMARY RTD'S (10/26/69 - 10/27/69)
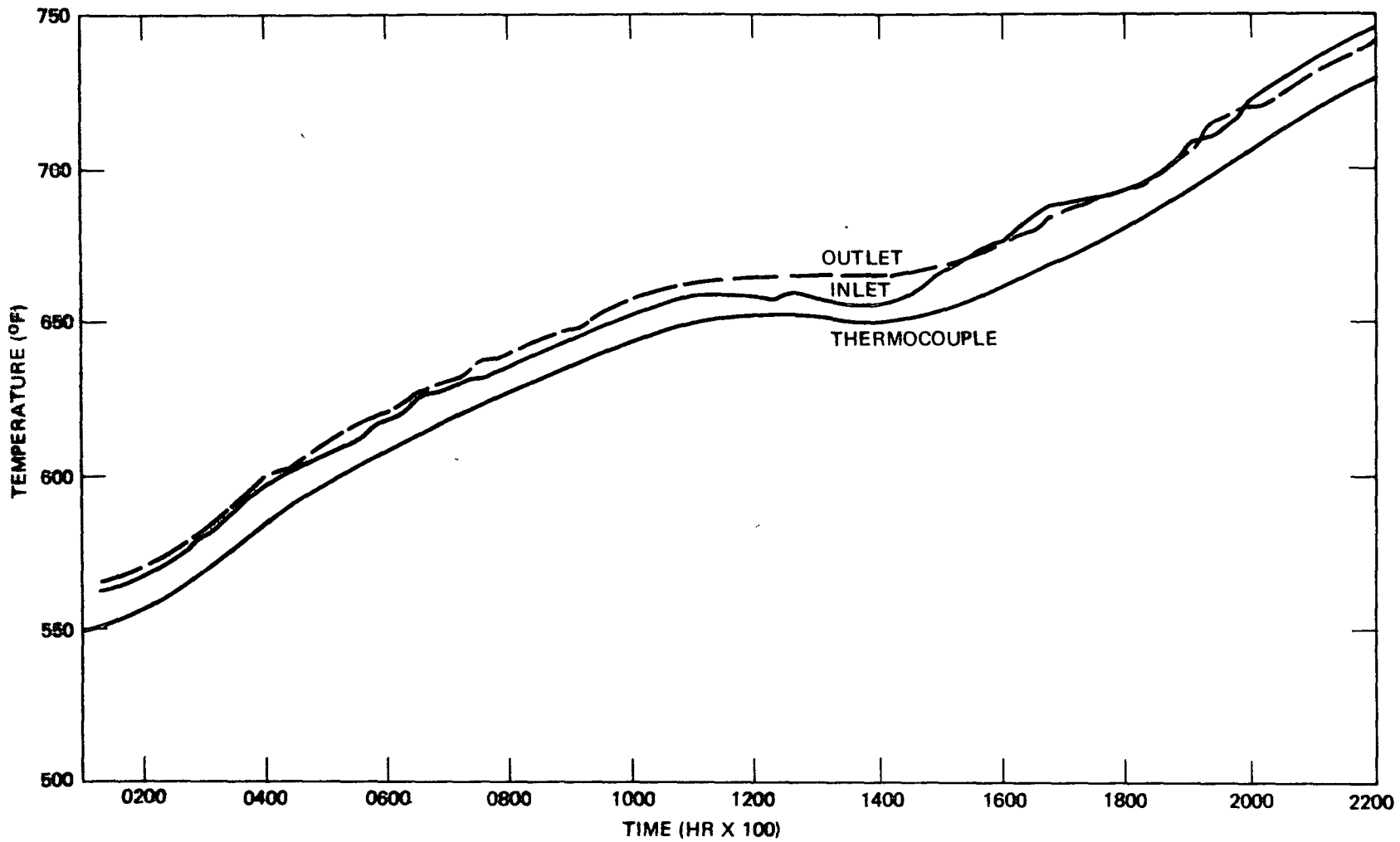
FIGURE 7-8. IN CORE THERMOCOUPLE AND AUXILIARY PRIMARY RTD'S (10/25/69)
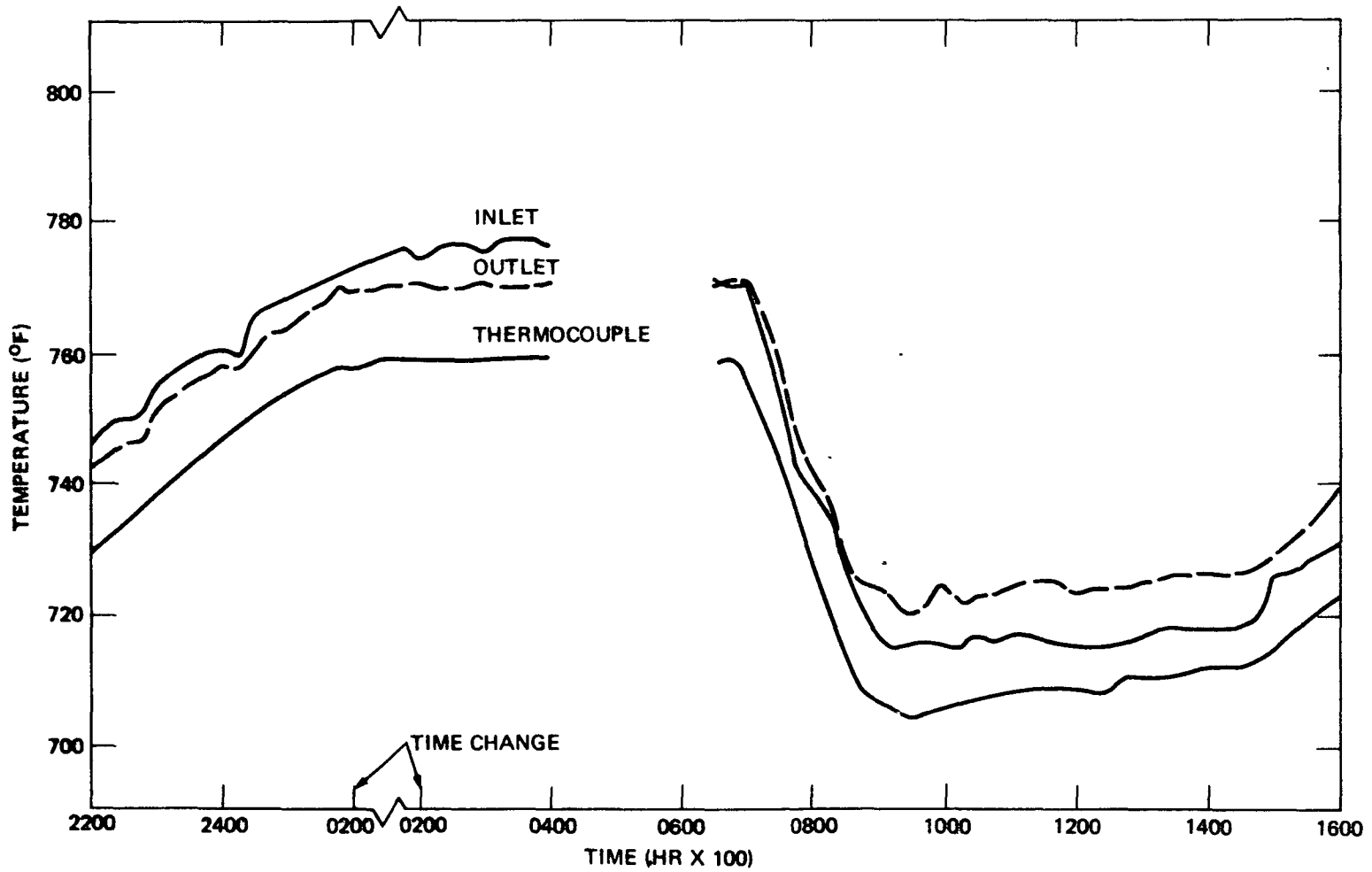
FIGURE 7-9. IN CORE THERMOCOUPLE AND AUXILIARY PRIMARY RTD'S (10/25/69 - 10/26/69)
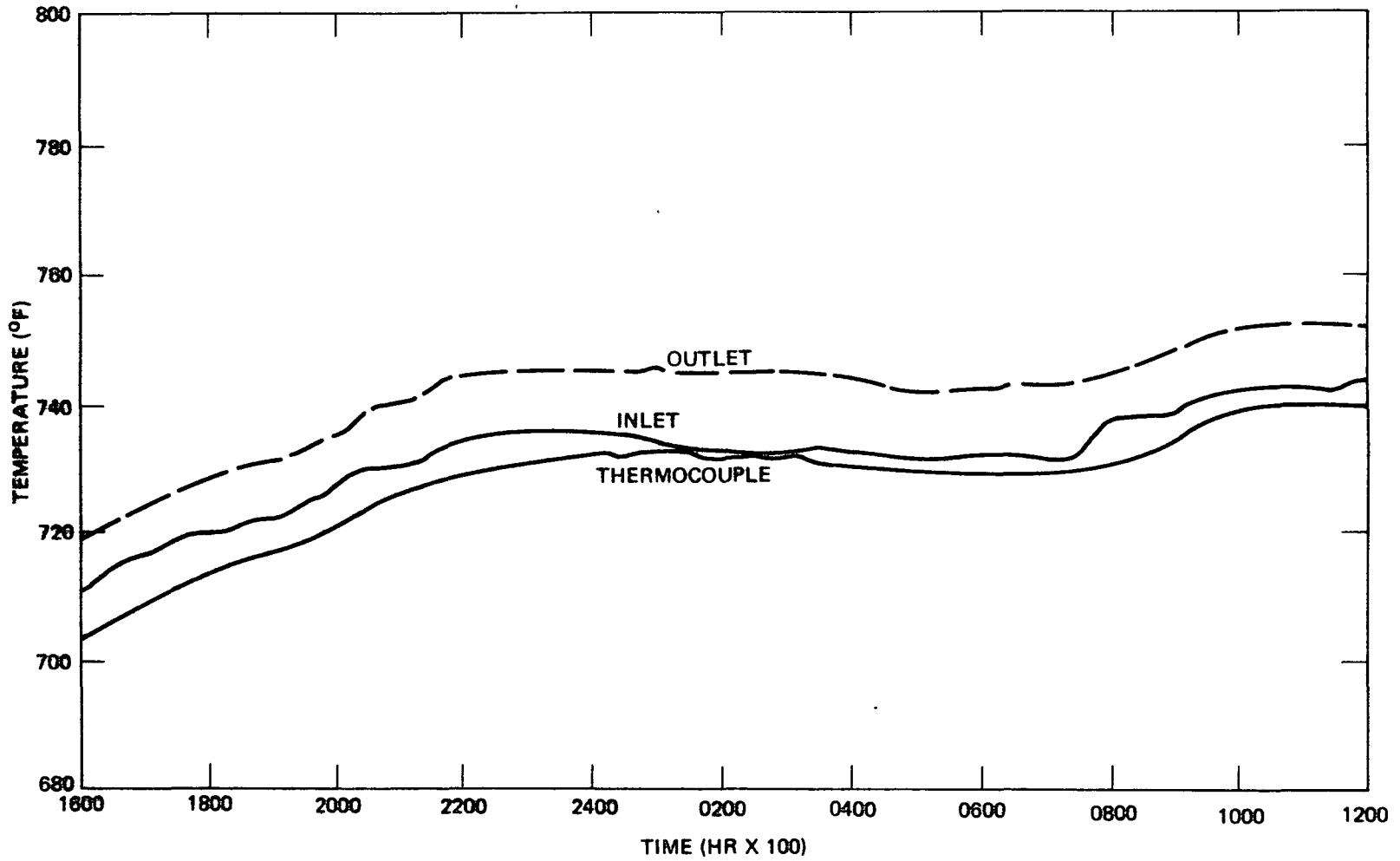
FIGURE 7-10. IN CORE THERMOCOUPLE AND AUXILIARY PRIMARY RTD'S (10/26/69 - 10/27/69)

7.4   COMPARISON OF EXPERIMENTAL AND CALCULATED RESULTS

The flow and the pressure coefficients of reactivity are essentially zero (see Section 7.1). The reactivity effects, if any, that occur as a result of changes within their normal operating ranges in reactor vessel hydraulic pressure or primary coolant flow are of the order of the ±0.5¢ standard deviation in reactivity difference measurements. This is in agreement with expectations[1].

Figure 7-11 illustrates the excellent agreement between the predicted[3] temperature dependent reactivity feedback, and the experimentally determined reactivity feedback for Assembly I-E. This agreement is further illustrated in Table 7-8 where the reactivity coefficients calculated from the previously predicted[4] total expansion coefficient of -0.36¢/°F and the predicted Doppler $T\frac{dk}{dT}$ of -0.0082 is compared with the coefficients determined from a least squares fit of a parabola to the experimental data in Appendix VII. Since the prediction was based (see Section 7.2) on a reactor model containing 19 B_4C rods, while Assembly I-E contained 14 B_4C rods, the calculated values should be modified to reflect this difference. Using the calculated results in Section 7.2 as a basis for extrapolating to a core with 14 B_4C rods results in about a 4% increase in the calculated total coefficient. This in turn results in approximately a 6% difference between the calculated and measured uniform temperature coefficient, rather than the ∿2% difference in Table 7-8. Regardless of which calculated coefficients are used, the agreement between calculation and experiment is quite good .

The approximately 12% difference the reactivity coefficient of -0.59¢/°F (in the range 350°F to 400°F) that was measured in Assembly

I-D, and the corresponding value of -0.67¢ that was measured in Assembly
I-E is unexplained. Although the core loadings, and thus the reflector
arrangements, were different in the two cases, two-dimensional synthesis[7]
calculations which were performed to estimate the influence of reflector
density on the temperature coefficients of reactivity indicate that
only a one or two percent change in the total coefficient might be
expected between the two assemblies*. Because of the large amount of
data obtained in Assembly I-E versus the rather limited data in Assembly
I-D, and the calculated small influence* of the reflectors on the
temperature feedback, the results obtained in Assembly I-E are considered
to be the most reliable. The estimated uncertainties in the measured
reactivity changes are estimated to be ±0.5¢ (see Section 4.4) or
±4% (due to "shadowing" – see Appendix VIII), whichever is larger.

The rather limited range of these measurements, in terms of absolute
temperature, does not provide for a good experimental separation
of the Doppler from the expansion effects. However, since the Doppler
effect contributes about 40% of the calculated uniform temperature
coefficient in the 350°F to 760°F temperature range, the close agree-
ment between the calculated and measured total temperature coefficient
is an indication that the Doppler effect is not drastically different
from its predicted value.

---

*Preliminary analysis of recent measurements in Assembly I-I, which
 has yet a third core loading and reflector configuration, substantiate
 the results obtained in Assembly I-E.
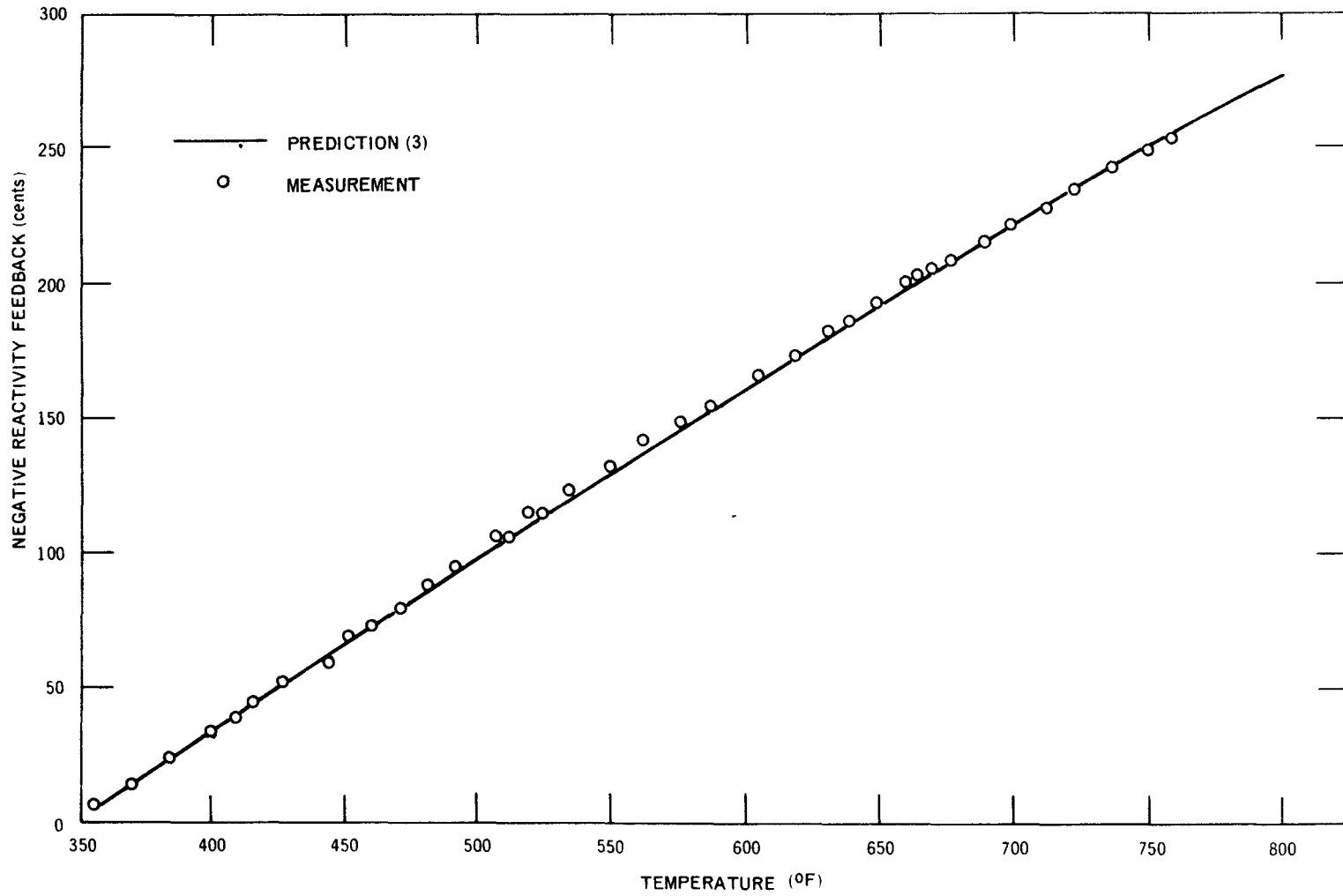
FIGURE 7-11. TEMPERATURE REACTIVITY FEEDBACK (ASSEMBLY I-E)

TABLE 7-8

UNIFORM TEMPERATURE COEFFICIENT OF REACTIVITY BETWEEN 350°F and 760°F

Temperature Range (°F)	Average Temperature Reactivity Coefficient in indicated Temperature Range (¢/°F)	
	Measured**	Predicted*
350 to 450	-0.67	-0.66
450 to 550	-0.64	-0.63
550 to 650	-0.60	-0.61
650 to 760	-0.57	-0.58

---

*The expression[3] for the coefficient at a given temperature T (in degrees Rankin) is $-(0.36 + 260/T)$ ¢/°F. (see discussion and Section 7.2 for the influence of B_4C content on the calculated coefficients).

**A fit to the experimental data yields a coefficient at a given temperature T (in degreees Fahrenheit) of the form – $[0.692 - 0.000357(T-350)]$ ¢/°F.

APPENDIX I

SEFOR CALCULATIONAL MODEL AND CROSS SECTION DATA

CALCULATIONAL MODEL

A typical cross section of a SEFOR fuel channel is shown in Figure I-1, and the SEFOR two-segment fuel design is illustrated in Figure I-2. A calculational model for the core was obtained by homogenizing all materials within a unit cell containing a fuel channel and additional sodium associated with a spacing between channels of 0.010 inches.

Because of the construction of the core and the fuel and tightener rods, the core was divided into four compositionally different regions which are labled in Figure I-3 as lower core, core, gap, and central channel. The combined length of the lower core, core, and gap is equal to the height of the fuel (P_uO_2 - UO_2) pellet column (exclusive of the UO_2 insulator pellets at each end of the fuel column - these are homogenized into the axial reflectors) within the fuel rods. The gap region includes the actual physical gap (void), as well as the springs, spacers, and UO_2 insulator pellets on each side of the gap. The length of the lower core region is determined by the length of the low-BeO portion of the tightener rods. The central channel contained He-3 detectors during the critical approach and will contain a dry well for operation at higher power levels.

The radial dimensions of the core were chosen to yield right circular cylinders of volumes equal to those of the various core regions.

The homogenized composition of the various rods which are inserted into the core from time to time are summarized in Table I-1 and the

composition of the unit cells and the over-all reactor model given in
Tables I-2 through I-3. The material densities corresponding to this
reactor model are given in Table I-4.

During the initial critical loading the outer radial region of the
core contained only sodium and the steel from the channels and side
rods, and from the tightener sleeve. A homogenized composition for
this region is readily obtained from Table I-3 by replacing all fuel,
BeO and SS-316 in Composition 1 with sodium. The height of this region
(which contains 13.11% SS-304 and 86.89% Na) is the same as that of a
fuel rod. (i.e., it extends through both axial reflectors.) The comp-
osition of any core loading can be obtained in a straight forward manner
from the data in Tables I-1 through I-4.

Most of the calculations were performed with either thirteen or
four energy groups. These group structures were selected according
to the recipe in reference 1 and are shown in Table I-5. The group
cross sections were obtained from a condensation of 60 group one-
dimensional diffusion calculations which used perpendicular bucklings
obtained from previous calculations[2]. The sources of the cross sections
for the 60 group calculations are discussed below.

Self-shielding calculations for the fuel isotopes were performed
(in the sixty group structure mentioned above) using a cross section
fitting routine with a Bell[3] approximation for resonance region
heterogeneity. In addition, the cross sections for the movable nickel
segments in the radial reflector zones were self-shielded using tables
in Bondarenko[4] and factors generated with the ENDRUN code[5].

CROSS SECTION DATA

Data Sources

The cross section values which were used are essentially those in
the ENDF/B file, Version 1, distributed by Brookhaven National Laboratory
in the summer of 1968[6] with the exception of the following changes:

a) Pu-239. The $\bar{\nu}$ values were increased by 0.77% (to 2.89 at
    low energy) to agree more with current evaluations. The
    fission cross section between 20 and 100 keV was increased
    to ignore the dip in the White data.[7] Below 15 keV the
    fission cross section was lowered to be consistent with
    higher alpha values used at these energies, while a slight
    decrease was made in σ_f above 2 MeV. The alpha value below
    15 keV was increased to agree with the measured values of
    ORNL-RPI,[8] and the infinitely dilute cross sections computed
    on the basis of an analysis which accounts for rapid energy
    variations in both the strength function and the fission
    width.[9]

b) U-238. The capture cross section was lowered by about 4%
    over the energy range at the peak of the neutron flux
    ($\sim$200 keV), and from 5 to 10 percent between 4 and 20 keV.
    This resulted in values which agree with the Garg data,[10]
    plus some additional p-wave contribution around 1 keV, in
    the resolved resonance range; Pönitz's values[11] from 3
    to about 100 keV; and a compromise between Barry, Bunce
    and White values[12] and the much lower Pönitz data above
    100 keV. The fission cross section above 2 MeV was also
    slightly decreased.

c) <u>Pu-240.</u> The fission cross section at energies below
several hundred keV was modified to agree with the Petrel
results.[13] The primary difference from ENDF/B is an
increase to about 0.3 barns at 1 keV. Capture cross
sections were reduced at all energies to account for
lower values of Γ_γ, as indicated by the analysis of
Pitterle.[14] The reduction factor was a constant
0.83, corresponding to a decrease in Γ_γ from 0.030
to 0.025 eV.

Indicated Further Data Adjustments

In Section 2.1 it was seen that the directly computed multiplication
factor for the ZPR-III and SEFOR minimum critical assemblies was from 0.5
to 1.5 percent low. Cross section changes which could account for these
low values and are most probable from differential measurements are:
a) decreases in σ_c and inelastic scattering for U-238, and b) an increase
in σ_f for Pu-239. Studies by Pitterle,[14] Küsters,[15] Kato,[16]
Hummel,[17] and Zolotar[18] show that similar substantial changes from
Version 1 ENDF/B data are required to obtain good agreement between
calculated and measured integral quantities. Although the cross sections
used for this analysis have already been adjusted in some of these direc-
tions, additional changes could be made and still be consistent with
differential data.

The value of σ_c for U-238 from 20 to several hundred keV is uncertain.
Independent absolute measurements disagree by as much as 30%. Below
20 keV there is weak indication from results obtained by Glass, et.al[19]
that Γ_γ is 20% lower than obtained by Garg[10]. Zolatar's[18] calcu-
lations show variations of several percent in the multiplication factors

of fast assemblies due to the inelastic scattering cross section. A large uncertainty in σ_f of Pu-239 results from normalization of the experimental results. Hummel[17] shows a variation of 5% in the multiplication factor of ZPR-III, Assembly 48 due to this difference in normalization. Thus, a reasonable increase in the values used for the current calculations could also increase k on the order of 1 percent.

Differences from Data Used in Earlier Design Calculations

A comparison of the nuclear data used for these calculations and that used for the original SEFOR computations shows the following major differences.

a) Pu-239. There have been two major changes in Pu-239 nuclear data since the generation of the original SEFOR values. These are: 1) the identification of extremely broad fission resonances, associated with the J = 0 spin state; and 2) differential measurements indicating that the alpha value below 15 keV is from 30 to 70 percent higher than that assumed earlier. These two changes result in group constants for Pu-239 which have a 30 to 50 percent higher alpha value below 10 keV, but one which decreases with self-shielding of the Pu-239.

The fission cross sections used in both the earlier and present calculations are based on the measurements of White[7] above 10 keV. However, the dip in White's data between 20 and 100 keV has been smoothed out in the new set, making the present data as much as 8% higher than the old SEFOR values in this range. Below 10 keV the new values tend to be somewhat lower than the original data set, as a result of the recent analysis of the Pu-239 alpha value, although both are close to James' values.[20]

b) <u>U-238.</u> In the energy range above 40 keV, the capture cross section has been reduced below the values of Barry, Bunce and White[12] used originally due to more recent measurements by Pönitz,[11] and others. Between 10 and 40 keV, the present values are significantly higher than the old SEFOR values. The resolved resonance data of Garg[10], used previously, have been augmented by a p-wave contribution, which increases the capture cross section, but is still significantly lower than that of the ENDF/B file.[6]

Ineleastic scattering by U-238 is increased, and produces a much softer spectrum of secondary neutrons in the current file. This is a result of level data measured by Barnard, et al.[21]

c) <u>Pu-240.</u> The major change in Pu-240 cross sections is a substantial reduction in the capture cross section. Between 20 and 200 keV the reduction has been about 50 percent, while it is somewhat less at lower energies. The inclusion of non-zero σ_f values at sub-threshold energies is also a difference.

d) <u>Other Materials.</u> There have been no significant changes in the basic cross sections of Be, Na, 0, Fe, Cr, and Ni.

FUEL PELLET 0.875 ±0.001 DIA.

FUEL CLAD SST
0.890 ±0.0015 I.D.
0.040 ±0.002 WALL

SIDE ROD
SST—0.250 ±0.001 DIA.

TIGHTENER SLEEVE
0.960 ±0.005 INSIDE

ACROSS FLATS X
0.035 ±0.004 WALL

CENTRAL BeO PELLETS
0.777 ±0 003 O.D.

CENTRAL BeO CLAD
0.875 ±0.002 O.D. X
0.040 ±0.002 SST WALL

FUEL ROD CENTERS
LOCATED ON 2.190 DIA.

0.060 ±0.002 WALL SST

3.150 ±0.003
HEX. CHANNEL

3.160
HEX.
MEAN CELL
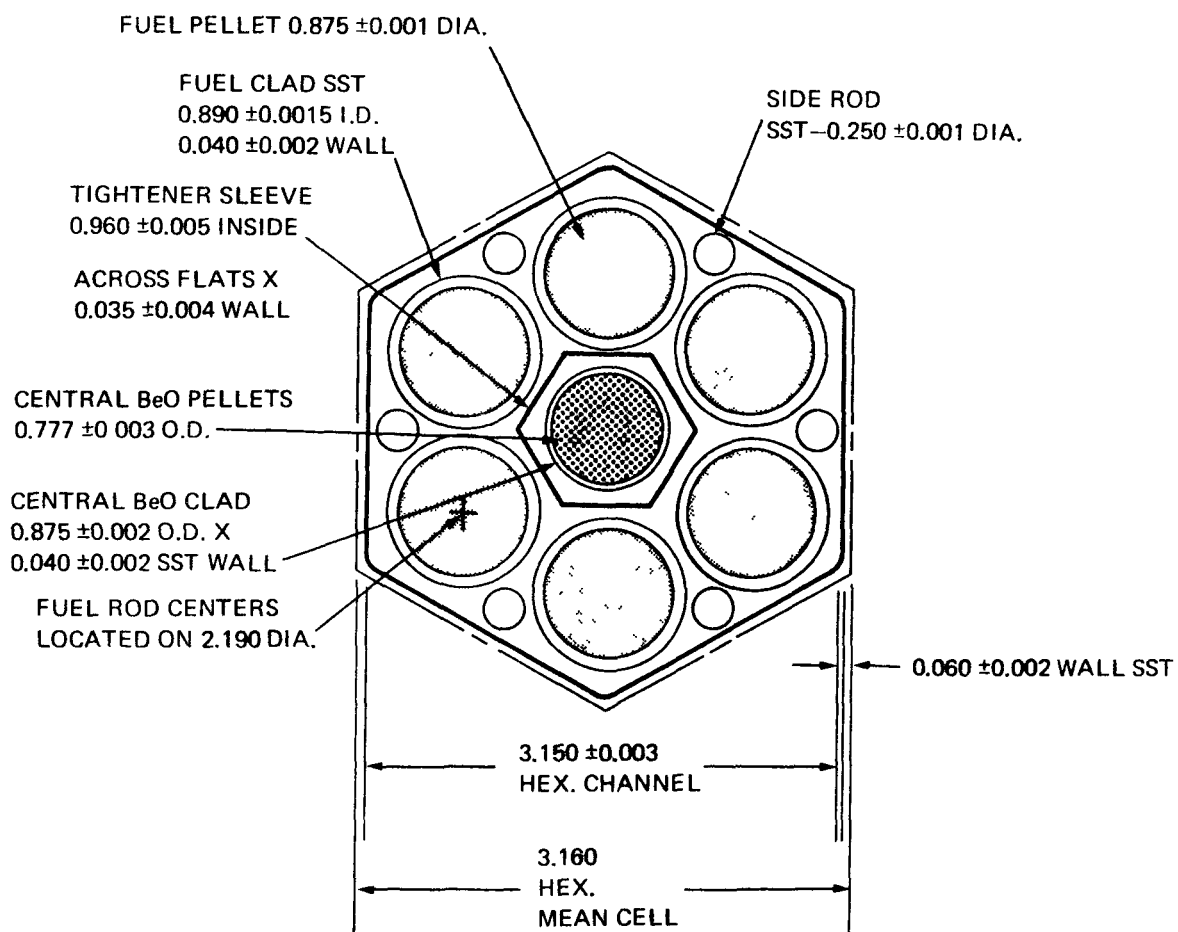
FIGURE I-1. SEFOR FUEL CHANNEL

FIGURE I-2. SEFOR FUEL ROD

CLADDING O.D.	0.970
CLADDING MATL.	STN. STL.
CLADDING THICKNESS	0.040
CORE LENGTH	36.56
FUEL LENGTH	33.81
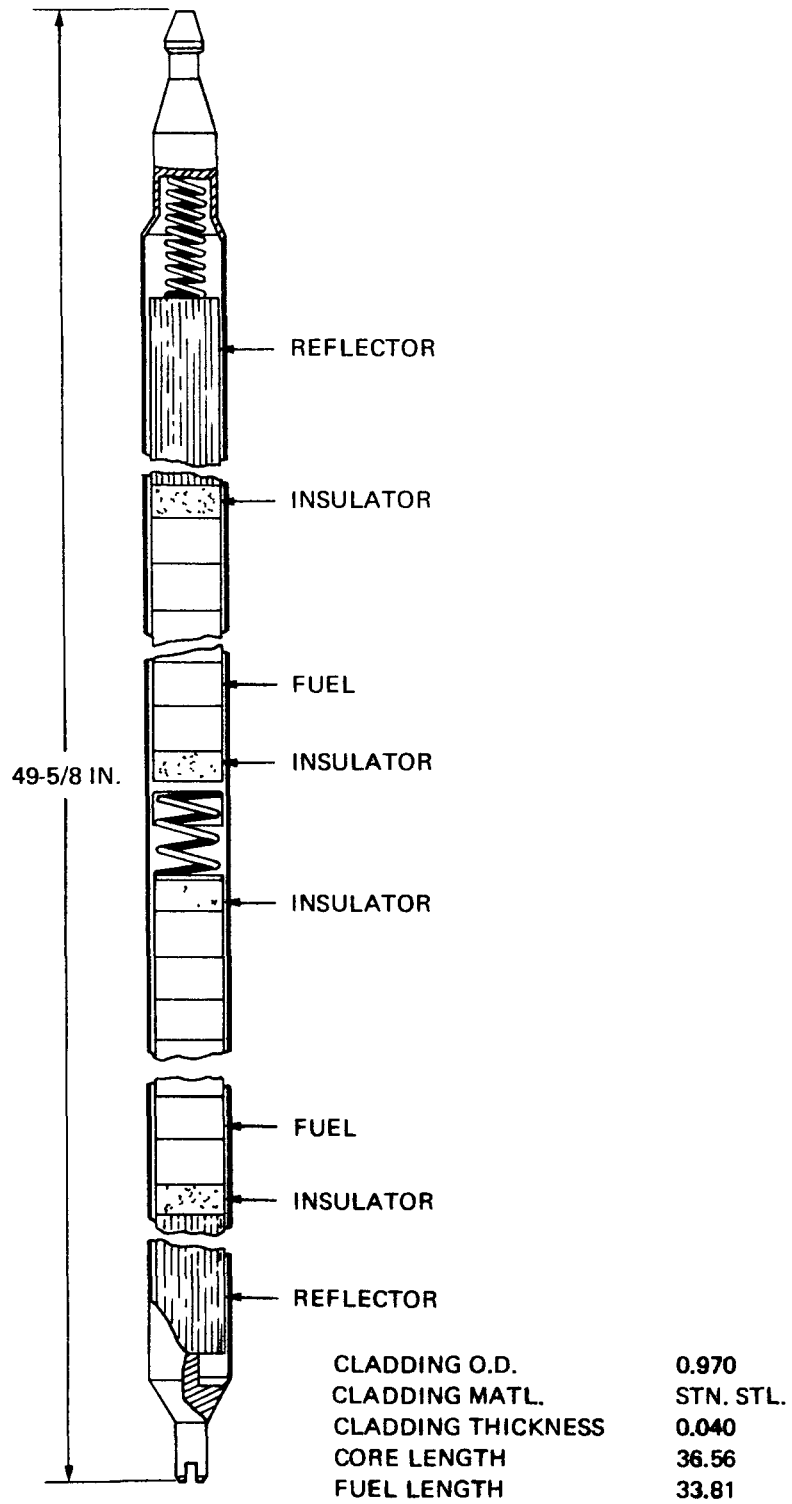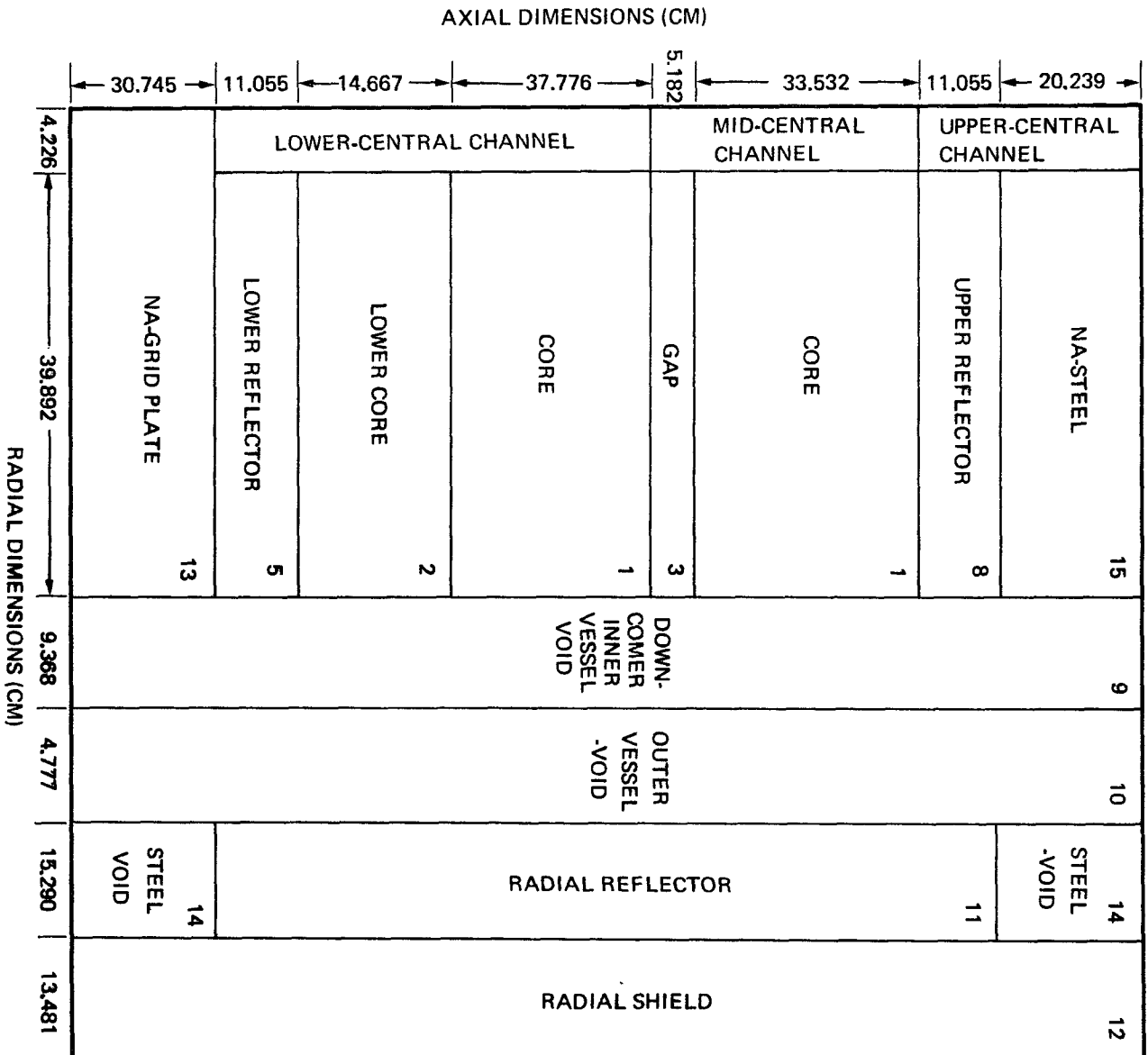
FIGURE I-3. SEFOR FULL CORE GEOMETRY (3500°F)

TABLE I-1

ROD COMPOSITIONS

Material	Material Volume Fractions in the Core Region of the Reactor					
	Fuel[1] and Guinea Pig[1] Rod	Tightener Rods[4] Upper Portion of Core	Lower Portion of Core	Core Poison Rod	Stainless Steel Rod	UO_2 Rod
Fuel[1]	0.8384[2]	-	-	-	-	-
UO_2	-	-	-	-	-	0.8384
Cladding(SS-316)	0.1616	0.1745	0.3229[3]	0.1616	0.1616	0.1616
BeO	-	0.8255	0.5868	-	-	-
SS-304(in Steel Rod)	-	-	-	0.4982	0.8103	-
Void	-	-	0.0903	-	0.0281	-
Central Shaft(SS-304) inside Poison Rod	-	-	-	0.3402	-	-

(1) $(Pu\text{-}239 + Pu\text{-}241)/(U + Pu) = \begin{cases} 0.187 \text{ for standard fuel rods} \\ 0.250 \text{ for guinea pig rods} \end{cases}$, $Pu\text{-}240/Pu = 0.0824$

(2) Exclusive of gap regions where the fuel is replaced by a smeared composition of 37.5% UO_2, 3.1% inconel, 15.1% SS-304, and 44.3% void.

(3) Includes additional SS-316 inside the cladding.

(4) In the special tightener rods used for material reactivity worth measurements the BeO and void was replaced with SS-304 at a smeared density of 7 g/cc.

TABLE I-1   (Continued)

ROD COMPOSITIONS

Material	Fuel[1] and Guinea Pig[1] Rods	Tightener Rod Upper Reflector	Tightener Rod Lower Reflector	Core Poison Rod Upper Reflector	Core Poison Rod Lower Reflector	Stainless Steel Rod	UO_2 Rod
			Material Volume Fractions in the Axial Reflector Regions of the Reactor				
UO_2	0.0725	–	–	–	–	–	0.0725
Ni	0.7659	0.4223	0.4730	0.8128	0.7897	–	0.7659
SS-316	0.1616	0.1609	0.1873	0.1616	0.1616	0.1616	0.1616
BeO	–	0.0710	0.0507	–	–	–	–
Void	–	0.3458	0.2890	–	0.0487	0.0281	–
Central Shaft(SS-304) inside Poison Rod	–	–	–	0.0256	–	–	–
SS-304 (in Steel Rod)	–	–	–	–	–	0.8103	–

(1)   (Pu-239 + Pu-241)/(U + Pu) = $\begin{cases} 0.187 \text{ for standard fuel rods} \\ 0.250 \text{ for guinea pig rods} \end{cases}$,   Pu-240/Pu = 0.0824

TABLE I-2

UNIT CELL COMPOSITION

Composition	Cell Volume Fraction		
	Standard Core Unit Cell	Unit Cell in lower portion of Core	Gap Region in Core
Fuel / UO_2	0.4316	0.4316	0.1619
BeO	0.0574	0.0408	0.0574
Fuel Clad(SS-316)	0.0832	0.0832	0.0832
BeO Clad(SS-316)	0.0121	0.0224*	0.0121
Tightener Sleeve(SS-304)	0.0178	0.0178	0.0178
Channel and Side Rods (SS-304)	0.1133	0.1133	0.1784**
Sodium	0.2846	0.2846	0.2846
Inconel	–	–	0.0133
Void	–	0.0063	0.1913

* Includes extra cladding around BeO

** Includes extra SS-304 in the gap portion of six fuel rods.

TABLE I-3

SEFOR FULL-CORE (648 FUEL ROD) VOLUME FRACTIONS

Volume Fraction by Region

Composition	1	2	3	4	5	6	7	8
Fuel	0.4316	0.4316	–	–	–	–	–	–
UO_2	–	–	0.1619	–	0.0373	–	–	0.0373
SS-316	0.0953	0.1056	0.0953	–	0.0962	–	–	0.0944
SS-304	0.1311	0.1311	0.1962	0.3056	0.1215	0.1177	0.1812	0.1383
Inconel	–	–	0.0133	–	–	–	–	–
BeO	0.0574	0.0408	0.0574	–	0.0035	–	–	0.0049
Sodium	0.2846	0.2846	0.2846	0.6944	0.2908	0.6944	0.6944	0.2871
Ni(Fuel Rod)	–	–	–	–	0.3943	–	–	0.3943
Ni(Tightener Rod)	–	–	–	–	0.0330	–	–	0.0294
Void	–	0.0063	0.1913	–	0.0236	0.1879	0.1244	0.0145

TABLE I-3 (Continued)

SEFOR FULL-CORE (648 FUEL ROD) VOLUME FRACTIONS

Volume Fraction by Region

Composition	9	10	11	12	13	14	15
SS-316	–	–	–	–	–	–	–
SS-304	0.2855	0.1563	0.0338	0.12	0.244	0.150	0.325
Inconel	0.0202	–	–	–	–	–	–
Sodium	0.6203	–	–	–	0.706	–	0.565
Ni	–	–	0.8078	–	–	–	–
Void	0.0740	0.6461	0.1227	0.36	–	0.850	0.110
Al-Mg	–	0.1976	0.0357	0.13	–	–	–
B_4C	–	–	–	0.39	0.050	–	–

TABLE I-4

SEFOR MATERIAL DENSITIES @ 350°F

Material	Density* (g/cc)

Fuel - Pu - U Oxide
   Oxygen/metal = 1.99
   (Pu-239 + Pu-241)/(Pu+U) = 0.1870
   Pu-240/Pu = 0.0824
   U-235/U = 0.0022
	9.587

Uranium in insulator pellets and special UC_2 rod (Oxygen/metal = 2.01)	9.786
Stainless Steel 316 and 304	7.961
Inconel	8.288
BeO	2.731
Na	0.9131
B_4C in special poison core rod B-10/B = 0.199	1.415
B_4C in radial shield	1.600
Ni in radial reflector	8.833
Ni in axial reflector	8.433
Al-Mg (96% Al, 4% Mg)	2.669

---

*Some of these densities are "smeared" to include void regions and should be used only with the volume fractions indicated in Tables I-1 through I-3.

TABLE I-5

SEFOR THIRTEEN AND FOUR GROUP STRUCTURE

13 Group Structure

Group Number	Lethargy Interval	Lower Energy of Group
1	1.500	2.23 MeV
2	1.000	0.821 MeV
3	0.500	0.498 MeV
4	0.500	0.302 MeV
5	0.500	0.183 MeV
6	0.600	0.101 MeV
7	0.800	45.2 KeV
8	1.100	15.0 KeV
9	1.333	3.96 KeV
10	1.367	1.01 KeV
11	1.167	315 eV
12	1.233	91.7 eV
13	–	thermal

4 Group Structure

Group Number	Lethargy Interval	Lower Energy of Group
1	3.000	0.498 MeV
2	1.300	0.136 MeV
3	2.533	10.8 KeV
4	–	thermal

APPENDIX II

HETEROGENEITY EFFECTS IN SEFOR AND
IN ZPR-III, ASSEMBLY 47 ON REACTIVITY

Heterogeneity effects on reactivity may be decomposed into four contributions:

1. **High Energy Heterogeneity Effect**

    This effect is caused by an increased fission probability of fission neutrons in the fuel plates or rods, which may be described by a fuel flux peak in the spatial distribution of high energy neutrons. The high energy heterogeneity effect is the most important one in the reactor considered and will be estimated below.

2. **Heterogeneity Effect on Resonance Self-shielding**

    This effect is caused by flux depressions in the fuel at resonance energies. It was taken into account in calculating the self-shielding factors by applying Bell's[3] approximation, which assumes a flat flux distribution throughout the cell between resonances.

3. **"Smooth Shielding" of Fuel Cross Sections in the Lattice Cell**

    This is caused by low energy fuel flux depression between resonances, and is not taken into account by using Bell's[3] approximation for self-shielding factors.

4. Heterogeneity Effects on Leakage

They are caused by the relatively large mean free neutron paths in certain regions of the lattice cell and generally result in increased effective diffusion coefficients for the lattice.

Results of estimation of the effects 1, 3, and 4 for SEFOR and ZPR-III, Assembly 47 are listed in the following table:

	High Energy Effect	"Smooth" Shielding Effect	Leakage Effect	Total
ZPR-ᵀII, Assembly 47	+0.008	-0.002	-0.002	+0.004
SEFOR	+0.006	-0.002	-0.001	+0.003

The estimates are based on calculated and measured effects in ZPR-III, Assembly 48 and SNEAK, Assembly 3A-1 and 3A-2. Extrapolation to SEFOR and ZPR-III, Assembly 47 was done by use of two-region models for the cells and simple transport models.

The model used for comparative estimation of the dominating high energy heterogeneity effects was based on the following considerations:

a) The contributions to the high energy effects (roughly above 0.5 MeV) are energy dependent, but the energy dependence is similar in the considered reactors.

b) The main contributions stem from the energy region around 2 MeV. The neutron optical parameters of the lattice cell should be compared at that energy.

c) For a given energy group, the contribution to the increased reactivity is roughly proportional to the relative change in the flux weighted fuel cross sections, compared to the homogeneous case:

$$\frac{\Delta k_{eff}}{k_{eff}} \sim \frac{\Sigma_{fuel}(\phi_{fuel} - \bar{\phi})V_{fuel}}{\Sigma_{fuel}\bar{\phi}V_{fuel}} = \frac{\phi_{fuel} - \bar{\phi}}{\bar{\phi}}$$

$\bar{\phi}$ is the average cell flux, which is assumed to be the same as in the homogeneous case. V_{fuel} is the Volume of the fuel material.

d) Multiple collison probability equations, using Wigner's rational approximation for single collision probabilities, yield:

$$\frac{\phi_{fuel}}{\bar{\phi}} \sim \frac{1 + \dfrac{V_{fuel}}{V_s}}{1 + \dfrac{V_{fuel}}{V_s} \dfrac{1 + \Sigma_{rem,fuel}L_{fuel}Q_s/(Q_{fuel} + Q_s)}{1 + \Sigma_{rem,s}L_sQ_{fuel}/(Q_{fuel} + Q_s)}}$$

Subscript s denotes the second region of the cell (structural and coolant material), L is a symbol for the average chord length of the respective region, and Q is a symbol for the source strength (fission sources plus downscattering sources). Subscript rem denotes removal.

e) The sources Q are usually concentrated in the fuel region
of the two-medium cell; an approximation that takes into account
downscattering sources in the non-fuel region is:

$$\frac{Q_{fuel}}{Q_{fuel} + Q_s} = \frac{1}{1 + C\ \dfrac{(\Sigma_{rem,s} - \Sigma_{a,s})V_s}{(\Sigma_{rem,fuel} - \Sigma_{a,fuel})V_{fuel}}}$$

Subscript a denotes absorption.

The parameter C may be adjusted to reproduce results of multi-group cell calculations.

The estimation of the smooth shielding effect at low energies
was done by use of the same formula for $\phi_{fuel}/\bar{\phi}$, which was used
for the high energy heterogeneity effect. The source ratio
Q_{fuel}/Q_s was assumed to be proportional to $\Sigma_{rem,fuel}V_{fuel}/
\Sigma_{rem,s}V_s$. (At low energies, Q_{fuel}/Q_s is close to 0 instead
of close to 1 as at high energies.) The effect of differences
in the global form of the spectrum of the reactor was neglected.

The estimation of heterogeneity effects on leakage was based on
a single formula for a correction of the diffusion coefficients
at high energies:

$$\frac{D_{het} - D_{hom}}{D_{hom}} \sim \left[1 + \frac{1}{\Sigma_{fuel}L_{fuel}} + \frac{1}{\Sigma_s L_s}\right]^{-1} \times \frac{\dfrac{\Sigma_{fuel}}{\Sigma_s} + \dfrac{\Sigma_s}{\Sigma_{fuel}} - 2}{\dfrac{L_{fuel}}{L_s} + \dfrac{L_s}{L_{fuel}} + 2}$$

This formula was derived from Benoist's[22] expression for
the diffusion coefficient in a two medium cell:

$$3D_{het} (V_1 + V_2) = \phi_1 V_1 \left(\frac{P_{11}}{\Sigma_1} + \frac{P_{12}}{\Sigma_2} \right) + \phi_2 V_2 \left(\frac{P_{21}}{\Sigma_1} + \frac{P_{22}}{\Sigma_2} \right)$$

Again, Wigner's rational approximation was used for calculating
the collision probabilities P_{ik}. Differences between ϕ_1 and ϕ_2
were neglected.

Cell transport theory calculations were done using the one-
dimensional SN1D code[23] with 24-energy groups, 16 angles
and anisotropic scattering. Table II-1 shows results for the
ZPR-III Assembly 47 plate lattices and for the SEFOR rod lattice
based on analysis of the cell transport calculations. It is
seen that the overall high energy and low energy "smooth shielding"
heterogeneity effects deduced from the transport calculations
are in good agreement with estimates based on the formulas
described above. The largest difference between the values
obtained using the formulas and those deduced from the transport
calculations is an appreciably smaller low energy "smooth shielding"
effect for SEFOR obtained from the transport calculations. This
may be explained because the above formulas do not take into
account the spectral difference between the SEFOR minimum critical
configuration and the ZPR-III critical assembly mockup, with the
latter having a somewhat softer spectrum because of a higher
BeO content and a lower leakage.

TABLE II-1

HETEROGENEITY EFFECTS ON REACTIVITY FOR SEFOR & ZPR-III

(ASSEMBLY 47), BASED ON SN1D$^{(23)}$ - RESULTS

LATTICE PROBLEM	SEFOR	ZPR-III, ASSEMBLY 47	
		INNER CORE ZONE	OUTER CORE ZONE
High Energy Heterogeneity Effect[a]	+0.005	+0.0056	+0.0171
"Smooth" Low Energy Heterogeneity Effect[a]	-0.0004	-0.0015	-0.0041
Sum	+0.0047	+0.0041	+0.0130
Statistical Weight of the Lattice Zone[b]	0.82	0.64	0.18
Weighted Reactivity Contribution	+0.0038	+0.0026	+0.0024
Sum for the Reactor	+0.0038	+0.0050	

(a) For the corresponding unreflected critical lattice.

(b) The statistical weight of the total core is not one because
     the lattice does not extend to the extrapolated boundary
     (core dimension plus reflector savings).

APPENDIX III

COUNTING RATE CORRECTIONS AND EFFECTS OF DETECTOR LOCATION

COUNT RATE CORRECTIONS

The count rate data obtained during the initial approach to critical are summarized in Tables III-1 through III-3. The count rates on each in-core counting channel were generally repeated at least five times to accumulate a total of 10,000 counts, in order to obtain better than 1% statistical accuracy. As discussed in Section 2.2.1, the fuel was loaded with the reflectors completely lowered. Count rates were taken with the reflectors lowered; a specified number of fuel rods were loaded, the reflectors were raised, and count rates were recorded again. The counting rates were monitored throughout the fuel loading however, and some of the count rates obtained during a loading increment are shown in Tables III-1 and III-2. As discussed in Section 2.2.1, the first loading increment was broken into two steps 1(a) and 1(b) to allow insertion of the in-core detectors. The corrections for the count rates on the in-core detectors became quite large with the reflector raised after approximately 520 rods had been loaded, and they were switched to the current mode of operation for loading step number thirteen.

As the initial SEFOR loading approached the critical size, the count rates on the He-3 in-core detectors became very high, (see Table III-1 for example) and two indications of a need for dead time correction were observed. One, the ratio of the observed count rates on the two He-3 detectors did not remain constant, but instead exhibited a definite trend with increasing count rate. This is demonstrated in Figure III-1

and can be observed from the uncorrected count rate data in Tables
III-1 and III-2. Two, the ratio of the count rates in the He-3
detectors to the count rates in the source range monitors (SRM's)
also exhibited a definite trend with increasing count rate (see
Figure III-2 which was obtained from the data in the tables).

Because of the relatively low count rates in the source range
monitors, it was felt that no dead time corrections were required for
these detectors. This assumption appears to be born out by the data
shown in Figure III-3 and Table III-3. Although there is some scatter,
the ratio of the count rates in the two source range monitors appears
to be independent of the absolute counting rate and no definite trend
with increasing count rate is indicated.

In order to estimate the appropriate dead time corrections for
the two He-3 detectors, a paralyzable type[24] relationship between
the observed He-3 counting rate y and the true He-3 counting rate x
of the form

$$y = x \ \exp \ (- \tau x)$$

was assumed, where τ is the dead time. In addition, it was assumed
that with the reflectors raised* the ratio of the true He-3 counting
rate x to the true average SRM count rate z is, at lease on the average,
constant; i.e.,

$$x/z = C = \text{constant}$$

---

*The data obtained with the reflectors in the raised, rather than lowered,
position was used in order to emphasize the difference between the "true"
and "observed" counting rates and thus the effect of the dead time
correction.

Although this latter assumption simplifies the analysis and provides
for a reasonable correlation of results, it is not a unique choice
and other, perhaps equally valid, assumptions could be postulated.

From these two assumptions, an expression of the form

$$\ln (y/z) = \ln C - (\tau C) z$$

was used to determine the parameters "$\ln C$" and "τC", and thus the
dead time τ from a least squares fit to the observed values of $\ln$
(y/z). The experimental values, as well as the fitted curves, are
shown in Figure III-2.

The dead times obtained from the fit were 12.23 μ-sec for de-
tector #1 and 7.91 μ-sec for detector #2. These dead times were used
with the expression for the paralyzable type (24) system to obtain
estimates of the true He-3 counting rates. The corrected ratio of count
rates between the two He-3 detectors is shown in Figure III-1 along
with the uncorrected ratio. As would be expected for the true counting
rate ratio, the corrected ratio appears to be essentially constant
and does not exhibit the previously noted trend demonstrated by the
raw data. The fitted dead times thus appear to provide for an ade-
quate description of the true counting rates. The corrected count
rates are tabulated in Tables III-1 and III-2.

EFFECT OF DETECTOR LOCATION

When the reflectors were raised, the counting rates on the two
source range monitors located below the core increased by a larger
factor than did the counting rates on the two in-core detectors. This
effect is demonstrated by the data in Figure III-4. Although the

corrected data shows a much smaller change than the raw data, the ratio of the reflector up to reflector down count rates in the SRM's divided by the corresponding ratio for the He-3 detectors increases slightly with increasing core size to a value of ~ 1.4 for the critical core.

The fact that the reflector up-to-down count rate ratio is different for detectors located in different positions and that this ratio is a function of core size should not be surprising. Even the simple one group model described in Appendix IV shows both of these effects when reflector-up-to-reflector down flux ratios at the center are compared to the corresponding flux ratios at different radial locations. This effect, although interesting, does not, of course, influence reflector calibrations by period measurements, power calibrations, etc.

TABLE III-1

COUNT RATES ON IN-CORE He-3 DETECTOR #1

Loading Step Number	Number of Fuel Rods in Core	Average Count Rate (counts/sec.)			
		Reflectors Down		Reflectors Up	
		Observed	Corrected*	Observed	Corrected*
1(a)	36	113.3	113.4	138.6	138.8
1(b)	42	130.7	130.9	-	-
1(b)	48	147.0	147.3	-	-
1(b)	54	161.3	161.6	-	-
1(b)	66	192.9	193.3	-	-
1(b)	108	346.0	347.5	392.4	394.3
2	216	926.2	936.8	1067	1081
3	264	1267	1287	-	-
3	282	1417	1442	1706	1742
4	288	1480	1507	-	-
4	306	1691	1727	-	-
4	348	2245	2310	2921	3031
5	402	3085	3210	4423	4684
6	456	4415	4676	7528	8336
7	486	5575	5999	11380	13400
8	504	6603	7212	16090	20730
9	516	7567	8385	21670	32080
10	524	8060	8997	24970	41460
11	531	8492	9543	-	-
12	534	8647	9742	-	-

*Using a paralyzable type dead time of 12.23 μ sec.

TABLE III-2

COUNT RATES ON IN-CORE He-3 DETECTOR #2

Loading Step Number	Number of Fuel Rods in Core	Average Count Rate(counts/sec.)			
		Reflectors Down		Reflectors Up	
		Observed	Corrected*	Observed	Corrected*
1(a)	36	133.9	134.0	164.4	164.6
1(b)	42	153.1	153.2	-	-
1(b)	48	172.9	173.1	-	-
1(b)	54	192.0	192.3	-	-
1(b)	66	230.2	230.6	-	-
1(b)	108	417.0	418.4	469.8	471.5
2	216	1120	1131	1288	1302
3	264	1536	1555	-	-
3	282	1712	1735	2065	2099
4	288	1786	1812	-	-
4	306	2052	2086	-	-
4	348	2727	2788	3551	3655
5	402	3748	3865	5390	5636
6	456	5409	5657	9294	10070
7	486	6868	7275	14220	16160
8	504	8109	8686	20430	24870
9	516	9304	10080	28370	38460
10	524	9918	10800	33710	50100
11	531	10410	11390	-	-
12	534	10640	11670	-	-

*Using a paralyzable type dead time of 7.91 μ sec.

TABLE III-3

COUNT RATES ON START-UP CHANNELS

(SOURCE RANGE MONITORS)

Loading Step Number	Number of Fuel Rods in Core	Counts per Minute			
		SRM No. 1		SRM No. 2	
		Reflectors		Reflectors	
		Down	Up	Down	Up
1(a)	36	18	24	18	24
1(b)	108	71	104	76	103
2	216	200	305	205	326
3	282	302	507	326	529
4	348	488	874	507	932
5	402	660	1355	715	1436
6	456	960	2432	1047	2616
7	486	1253	3900	1341	4203
8	504	1459	5907	1602	6309
9	516	1728	9108	1823	9614
10	524	1834	11950	1959	12800
11	531	1958	15980	2056	16980
12	534	1986	18320	2122	19580
13	540	2111	26150	2232	27580
14	545	2266	78960	2366	82360
15	546	2292	95640	2382	99950
16	547	2281	142300	2458	148900
17	548	2274	271100	2406	281900
18	549	2454	690300	2700	753500
19	550		Critical		Critical
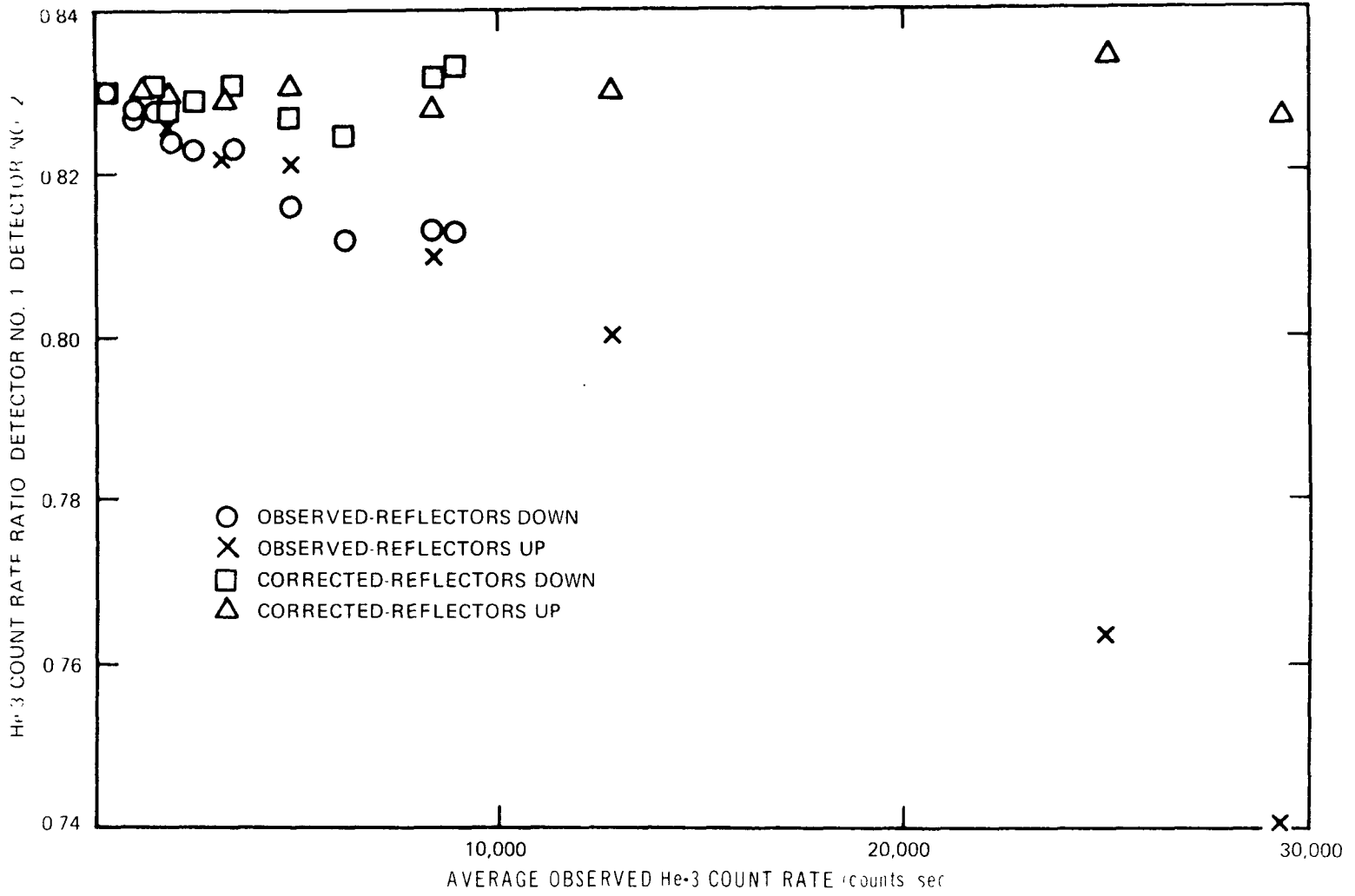
FIGURE III-1. RATIO OF COUNTING RATES IN HE-3 DETECTORS
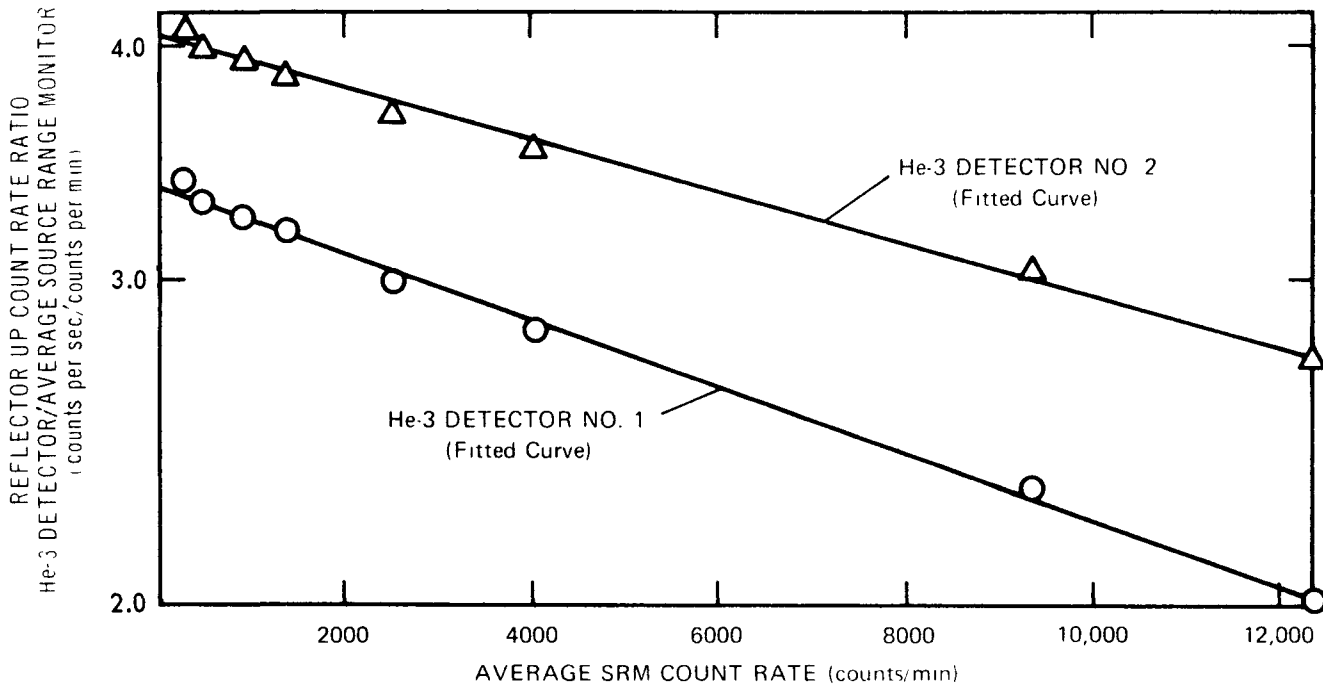
FIGURE III-2. COUNT RATE RATIO BETWEEN HE-3 DETECTOR AND SOURCE RANGE MONITORS
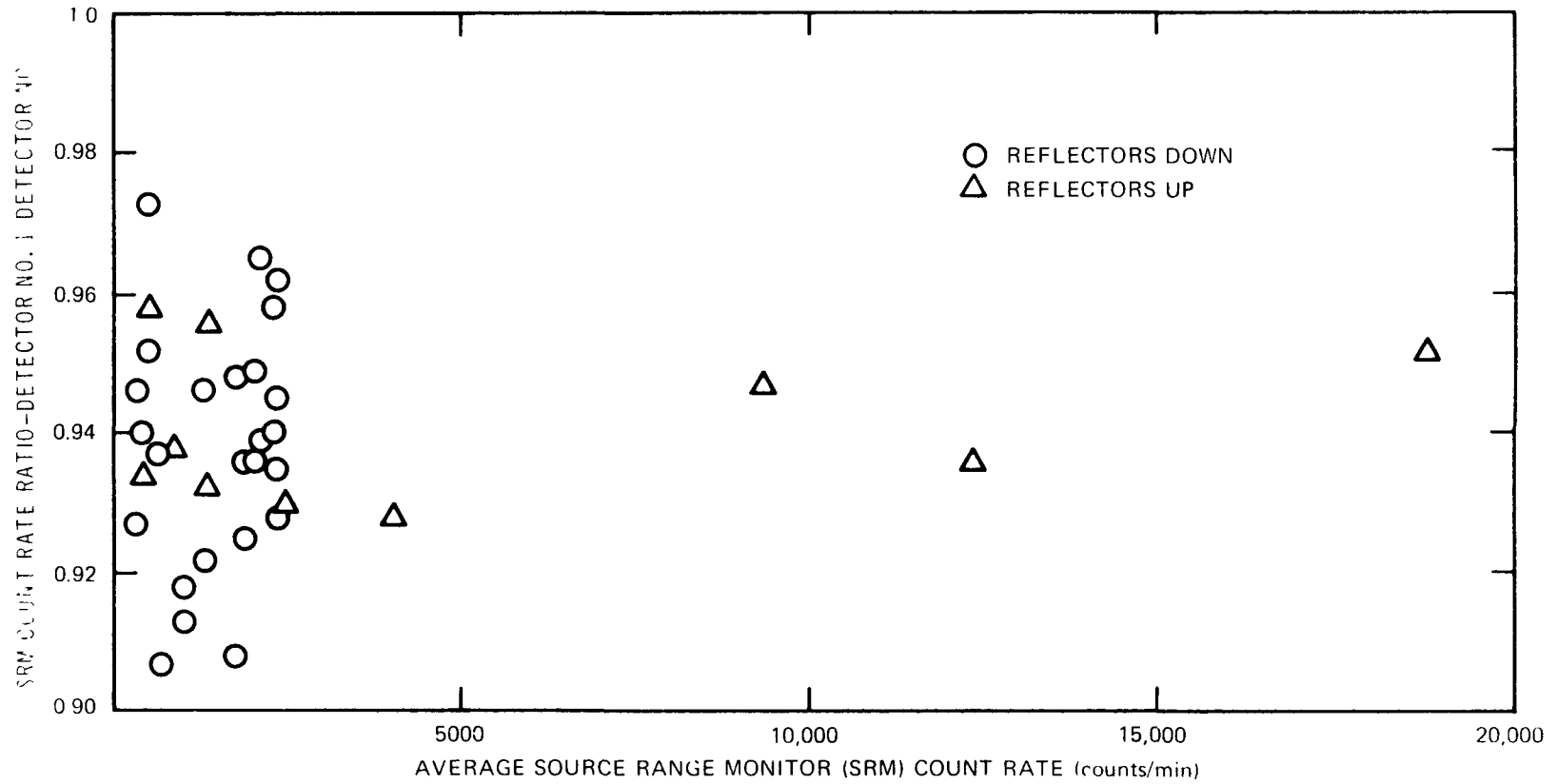
FIGURE III-3. RATIO OF COUNT RATES IN SOURCE RANGE MONITORS
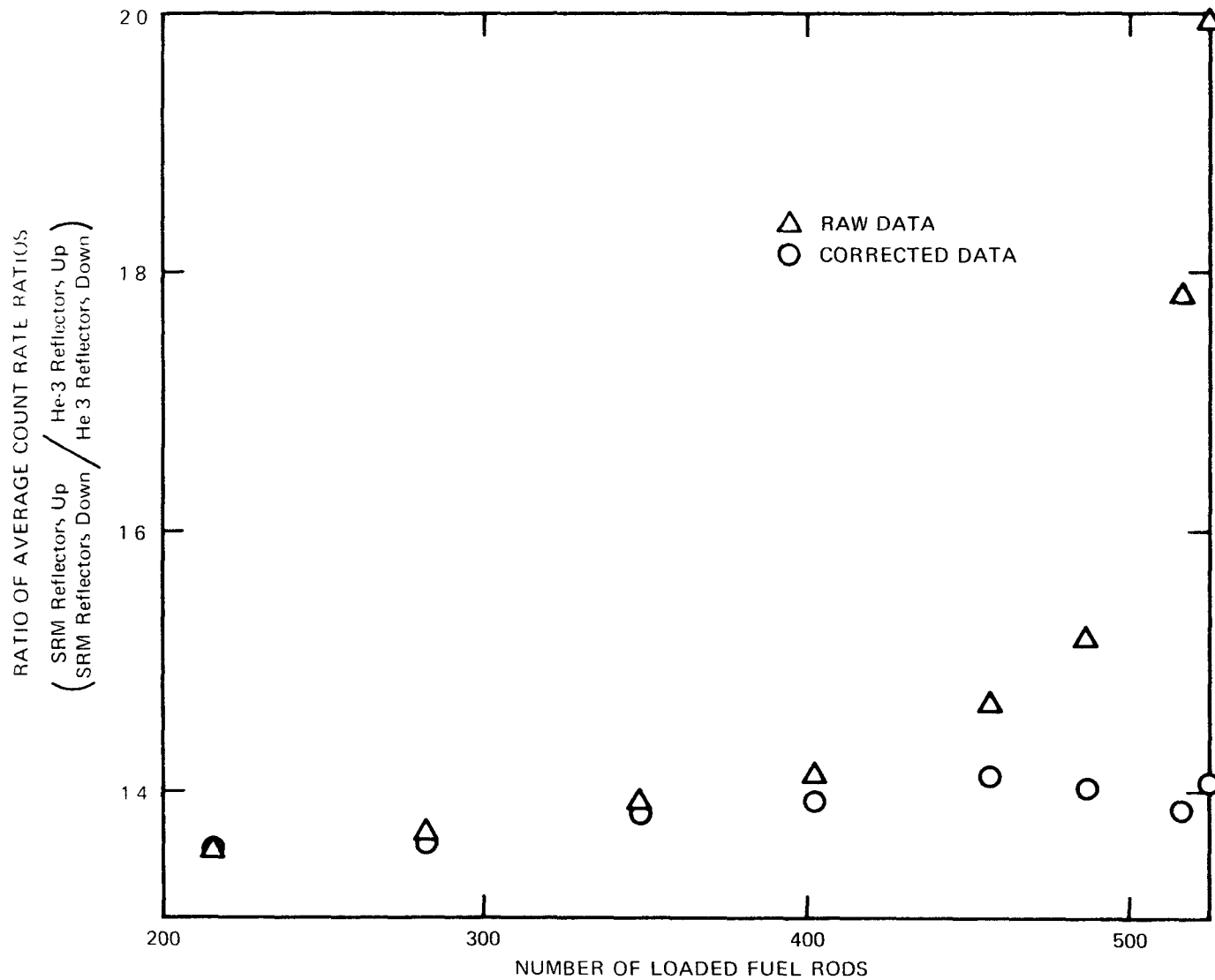
FIGURE III-4. EFFECT OF REFLECTOR POSITION ON COUNTING-RATE RATIOS

APPENDIX IV

A SIMPLE ONE-GROUP MODEL FOR THE PARTIALLY LOADED CORE

A simplified model for the SEFOR reactor is sketched in Figure
IV-1. For simplicity it was assumed that the reactor is infinite in
height and that it contains a central void, a core with fissionable
material and a constant source of neutrons per unit volume, a source
free sodium-steel region, and a reflector. It was further assumed that
all material properties of the core and sodium-steel region are constant,
and that all radii except R_1 in Figure IV-1 are fixed. Within the core,
the flux solution of the one group diffusion equation with a constant
source in the core, and conventional boundary conditions can be expressed
as follows.

$$\phi(r) = \sum_{n=1}^{\infty} \phi_n F_n (\alpha_n r)$$

The eigen functions, $F_n(\alpha_n r)$ are defined in terms of Bessel functions
of the first and second kinds by

$$F_n(\alpha_n r) = J_o(\alpha_n r) - Y_o(\alpha_n r) J_1(\alpha_n R_o)/Y_1(\alpha_n R_o)$$

and the expansion coefficients ϕ_n can be expressed as

$$\phi_n = \frac{1}{D_1(\alpha_n^2 - B^2)} \left[\frac{2S(CR_1/D_1) F_n(\alpha_n R_1)}{(\alpha_n^2 R_1^2 + C^2 R_1^2/D_1^2)F_n^2(\alpha_n R_1) - \alpha_n^2 R_o^2 F_n^2(\alpha_n R_o)} \right]$$

where B^2 is the critical buckling of the system with reflectors raised
(i.e., $B^2 = \alpha_1^2$ when the reactor is critical), and S is the value of the
constant neutron source. Except for the parameter C, which is defined
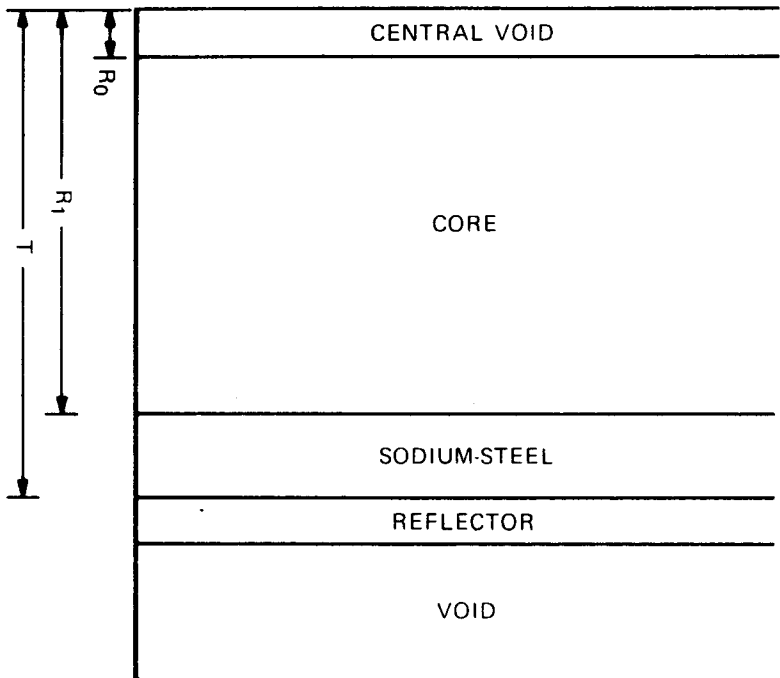
FIGURE IV-1. SIMPLIFIED SEFOR MODEL

below, conventional notation is used with dimension symbols defined
by Figure IV-1, with α_n^2 denoting the core bucklings, D_1 the core
diffusion coefficient, etc. The bucklings are the solutions α_n of
the following expression

$$-D_1 F_n' (\alpha_n R_1)/F_n(\alpha_n R_1) = C \tag{1}$$

where F_n' denotes the derivate of F_n with respect to r, and C is the
neutron current to flux ratio at the outer core boundary. The para-
meter C may be written interms of the modified Bessel functions of the
first and second kinds (the solution of the diffusion equation in the
sodium-steel region) as follows:

$$C = \frac{D_2 \beta \ [K_1(\beta R_1) + A \ I_1 \ (\beta R_1)]}{K_0 \ (\beta R_1) - A \ I_0(\beta R_1)} \tag{2}$$

where D_2 is the diffusion coefficient and β is the reciprocal of the
diffusion length in the sodium-steel region, and where A is defined
as follows:

$$A = \frac{b \ K_0(\beta T) - D_2 \beta K_1(\beta T)}{b \ I_0(\beta T) + D_2 \beta \ I_1(\beta T)} \tag{3}$$

The parameter b in the above expression is the neutron current to flux
ratio at the inner edge, T, of the reflector region, and is thus an
indicator of reflector position (raised-reflection; lowered-no reflection).
From equation (3) it is seen that the parameter A is independent of
core radius and depends only on reflector configuration (i.e. the para-
meter A takes on one value when the reflectors are in the raised
position and a second value when the reflectors are lowered: these
two values are _independent of core size_).   For constant material
properties in the sodium-steel region, the parameter C is dependent

only on the outer core radius, R_1, and the parameter A which indicates the position of the reflectors. Thus, for constant material properties, the complete solution can be obtained by specifying the parameter A and the core radius R_1. These two values are used to calculate the parameter C with Equation (2), and C is in turn used in Equation (1) to determine the α_n, and the preceding expressions are used to determine the flux.

The flux at the core center was calculated using the values shown in Table IV-1. The diffusion coefficients and the reciprocal diffusion length of the sodium-steel region are representative one group values for the critical SEFOR reactor. The value for the parameter A in the reflector-lowered condition represents a case with little neutron reflection at the outer edge of the sodium-steel region, and was calculated from Equation (3) for a value of T=58.26 cm and a value for the parameter b of slightly less than 0.5. The value of A in the reflector raised condition was not calculated from Equation (3) but was determined from the experimental data as described below.

NORMALIZATION OF THE MODEL

A best fit of the fundamental mode description of the flux at the core center to the experimental count rate data observed on the He-3 detectors located in the core was used to select the value of the parameter A in the reflector-raised condition and to normalize the calculated flux to the observed count rates. The selection was based on the assumption that there should be a constant relationship, independent of core size and reflector configuration, between the calculated flux at the core center and the observed He-3 count rates.

With the value of A for the reflector lowered condition and the
actual critical size (550 fuel rods) held constant, a value of A in
the reflector raised condition was selected (by trial and error) to
provide the best fit to the data between core sizes of ∿200 and 550
rods. The value listed in Table IV-1 (0.506) provided the best fit.
Only the fundamental mode was used to represent the flux at the core
center. The calculations showed that the second and higher modes
contribute only a small correction to the fundamental mode solution-
over the range of interest. The contribution of the higher modes
was ≲3% even for fuel rod loadings as low as 20 rods.

TABLE IV-1

PARAMETERS IN MODAL EXPANSION OF FLUX

Parameter	Symbol	Value
Core Diffusion Coefficient	D_1	1.200 cm
Na–Steel Region Diffusion Coefficient	D_2	2.728 cm
Reciprocal Diffusion Length in Na–Steel Region	β	0.010325 cm^{-1}
Inner Core Radius	R_o	4.226 cm
Critical Core Buckling (550 fuel rods with a critical radius of 40.678 cm)	B^2	$2.2107 \times 10^{-3} cm^{-2}$
Indicator of reflector position		
1) reflectors raised	A	0.506
2) reflectors lowered	A	0.620

APPENDIX V

IN-HOUR RELATION FOR SEFOR

The in-hour equation was used to convert the measured reflector position versus period relationships into a relationship between position and reactivity. The relation between asymptotic period (T) and reactivity (K) for SEFOR is illustrated in Figure V-1. The relationship was calculated from the in-hour equation taking into account 24 delayed neutron groups, 6 each for Pu-239, Pu-240, U-238, and U-235. The resulting expression may be written as follows:

$$K = (\frac{1}{T})(\frac{\ell}{\beta}) + \sum_{i=1}^{6} \sum_{j=1}^{4} \frac{\bar{\beta}_{ij}/\beta}{1 + \lambda_{ij}T}$$

with

$$\bar{\beta}_{ij} = \frac{\beta_{ij} \int d^3r \int dE' \int dE\ f_{ij}(E')\ \phi(E', \not{r})\ \nu_j(E) \Sigma_{fj}(E, \not{r}) \phi(E, \not{r})}{\sum_{j=1}^{4} \int d^3r \int dE' \int dE\ \chi(E')\ \phi(E', \not{r}) \nu_j(E)\ \Sigma_{fj}(E, \not{r}) \phi(E, \not{r})}$$

and with the effective delayed neutron fraction, β, defined by

$$\beta = \sum_{i=1}^{6} \sum_{j=1}^{4} \bar{\beta}_{ij}$$

where:

k = reactivity in dollars

ℓ = neutron lifetime

$f_{ij}(E)$ = energy spectrum for delay group i and isotope j

$\chi(E)$ = energy spectrum of prompt neutrons

$\nu_j(E)$ = prompt neutrons per fission for isotope j

$\Sigma_{fj}(E, \underset{\sim}{r})$ = fission cross section for isotope j

$\quad$ i = index for delayed neutron group

$\quad$ j = index for isotope

$\quad$ $\phi(E, \underset{\sim}{r})$ dE d^3r = neutron flux

$\quad$ $\phi^+(E, \underset{\sim}{r})$ dE d^3r = adjoint flux

$\quad$ β_{ij} = delayed neutron fraction for delay group i
$\quad\quad\quad$ and isotope j

$\quad$ λ_{ij} = decay constant for delay group i and isotope j.

The effective delayed neutron fractions by group and by isotope, $\bar{\beta}_{ij}$, were calculated from the above expression with the BISYN[25] program. The values for λ_{ij}, β_{ij}, and $f_{ij}(E)$ were taken from Keepin[26]. The calculated $\bar{\beta}_{ij}$ as well as the λ_{ij} taken from Keepin[26] are shown in the table. The value of the lifetime, ℓ, inferred from the measured ratio $\ell/\beta = 2.0 \times 10^{-4}$ sec, and the calculated effective delayed neutron fraction β are also shown.

TABLE V-1

DELAYED NEUTRON PARAMETERS

Delay Group Index	Pu-239		Pu-240		U-238		U-235	
	$\bar{\beta}_{1j} \times 10^4$	λ_{1j} (Sec.$^{-1}$)	$\bar{\beta}_{2j} \times 10^4$	λ_{2j} (Sec.$^{-1}$)	$\bar{\beta}_{3j} \times 10^4$	λ_{3j} (Sec.$^{-1}$)	$\bar{\beta}_{4j} \times 10^4$	λ_{4j} (Sec.$^{-1}$)
1	0.62	0.0129	0.01	0.0129	0.18	0.0132	0.02	0.0127
2	4.63	0.0311	0.13	0.0313	1.94	0.0321	0.10	0.0317
3	3.53	0.134	0.09	0.135	2.26	0.139	0.09	0.115
4	5.41	0.331	0.16	0.333	5.48	0.358	0.19	0.311
5	1.70	1.26	0.06	1.36	3.17	1.41	0.06	1.40
6	0.57	3.21	0.01	4.04	1.06	4.02	0.01	3.87

$\bar{\beta}_{ij}$ = effective delayed neutron fraction (based on Keepin's[26] data)

λ_{ij} = decay constants (taken from Keepin[26])

$\beta = \sum_i \sum_j \bar{\beta}_{ij} = 0.003148$

lifetime $(\ell) = 6.3 \times 10^{-7}$ sec.
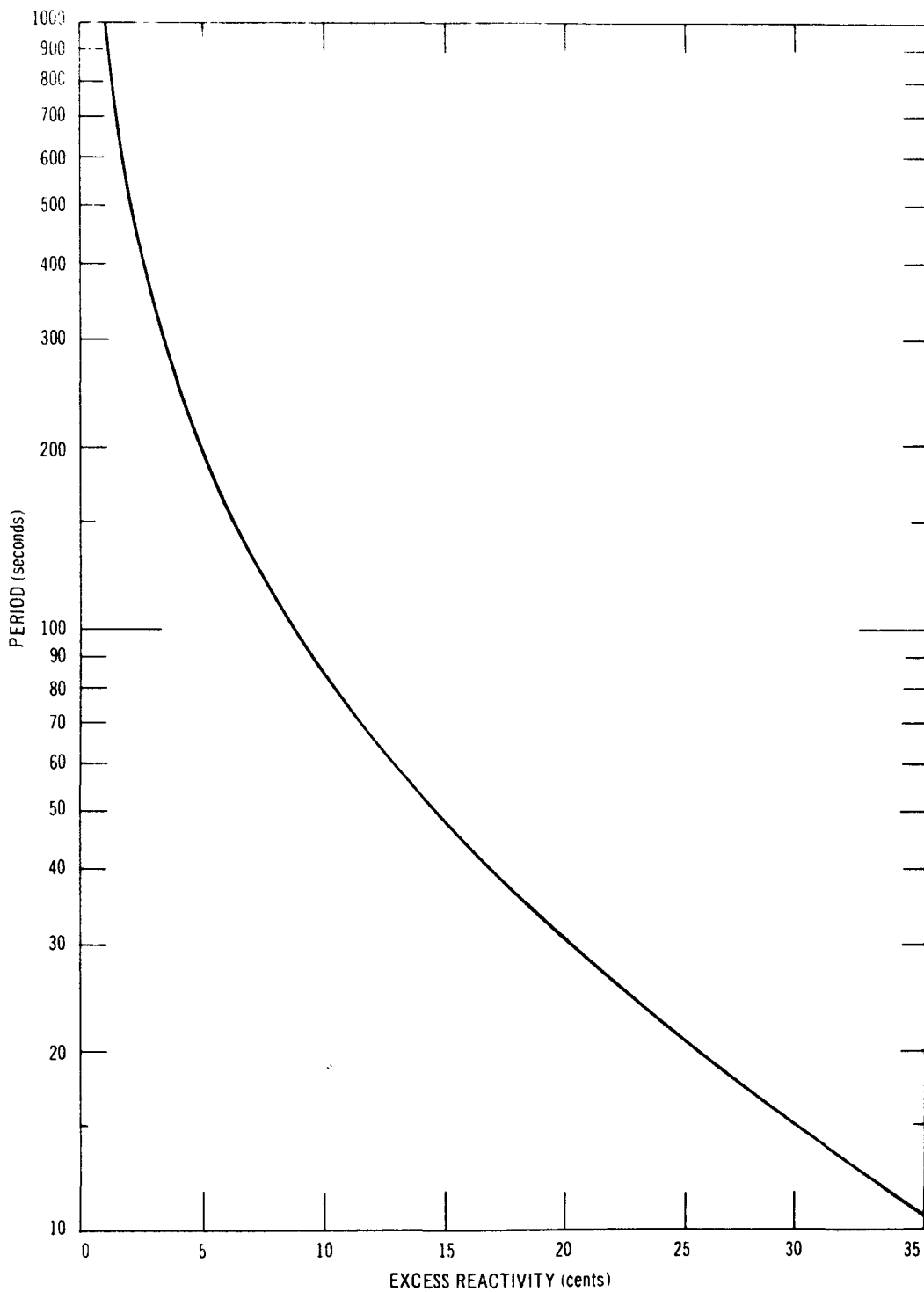
FIGURE V-1. ASYMPTOTIC REACTOR PERIOD FOR SEFOR

APPENDIX VI

FINE REFLECTOR CALIBRATION DATA

The two fine reflectors (#3 and #8) were calibrated by means of period measurements according to the procedure outlined in Section 3.3.2. The in-hour relation that was used to convert the measured periods into reactivities is described in Appendix V. The positions of the coarse reflectors during these calibrations are discussed at the end of Section 3.3.2.

The results of the calibrations of both reflectors in Assemblies I-B and I-D, and in Assembly I-E at two different temperatures, 350°F and 650°F are summarized in Tables VI-1 through VI-8. The calibration data for reflector #8 in Assembly I-F at 350°F is summarized in Table VI-9.

TABLE VI-1

REFLECTOR #3 CALIBRATION - ASSEMBLY I-B

Reflector No. 3 (cm)		Period (sec)	Reactivity * (¢)
From	To		
0.46	10.11	115.41	7.847
10.11	18.18	95.07	9.152
18.18	25.15	85.11	9.967
25.15	31.18	85.11	9.967
31.18	36.27	98.68	8.889
36.27	41.19	94.92	9.163
41.19	46.22	93.77	9.250
46.22	50.94	99.69	8.818
50.94	55.61	104.59	8.490
55.61	60.56	104.88	8.471
60.56	65.74	104.45	8.499
65.74	71.97	98.68	8.889
71.97	78.98	102.43	8.632
78.98	86.56	132.29	7.021
86.56	94.47	230.83	4.362
94.47	97.66	1180.12	0.945

*Estimated uncertainty in individual measured reactivities is ±1% of tabulated values.

TABLE VI-2

REFLECTOR #8 CALIBRATION - ASSEMBLY I-B

Reflector No. 8 (cm)		Period (sec)	Reactivity (¢)
From	To		
0.65	9.52	127.42	7.241
9.52	18.52	82.83	10.176
18.52	26.11	78.07	10.642
26.11	32.23	83.98	10.070
32.23	36.31	131.60	7.052
36.31	41.48	92.35	9.361
41.48	46.54	94.66	9.183
46.54	51.73	92.64	9.338
51.73	56.50	107.65	8.292
56.50	61.51	108.22	8.263
61.51	66.54	116.88	7.768
66.54	71.63	136.36	6.848
71.63	76.56	160.46	5.976
76.56	83.46	136.36	6.848
83.46	87.40	387.16	2.731
87.40	95.18	256.13	3.976
95.18	98.16	1080.72	1.029

TABLE VI-3

REFLECTOR #3 CALIBRATION - ASSEMBLY I-D

Reflector No. 3 (cm)		Period (sec)	Reactivity (¢)
From	To		
00.44	10.31	117.89	7.727
10.31	19.30	82.39	10.233
19.30	25.46	97.69	8.974
25.46	30.67	105.77	8.429
30.67	35.59	105.05	8.475
35.59	40.49	101.29	8.722
40.49	45.16	103.17	8.596
45.16	50.10	94.08	9.242
50.10	54.75	104.47	8.512
54.75	59.84	97.69	8.974
59.84	65.44	96.82	9.036
65.44	72.19	90.05	9.560
72.19	81.53	77.23	10.745
81.53	90.19	146.82	6.450
90.19	97.67	367.14	2.873

TABLE VI-4

REFLECTOR #8 CALIBRATION - ASSEMBLY I-D

Reflector No. 8 (cm)		Period (sec)	Reactivity (¢)
From	To		
0.64	8.19	174.17	5.582
8.19	16.13	105.19	8.460
16.13	22.03	119.19	7.660
22.03	27.04	120.92	7.569
27.04	32.13	103.31	8.587
32.13	37.10	101.87	8.683
37.10	42.10	95.95	9.100
42.10	47.14	92.64	9.353
47.14	52.22	94.08	9.241
52.22	57.46	92.92	9.331
57.46	62.24	115.15	7.875
62.24	67.95	103.89	8.549
67.95	75.45	86.72	9.841
75.45	82.22	136.01	6.871
82.22	89.36	190.62	5.165
89.36	98.17	309.09	3.363

TABLE VI-5

REFLECTOR #3 CALIBRATION - ASSEMBLY I-E
(350°F)

Reflector No. 3 (cm)		Period (sec)	Reactivity (¢)
From	To		
0.44	8.10	159.42	6.019
8.10	16.00	147.44	6.428
16.00	23.05	85.7	9.932
23.05	29.01	89.02	9.646
29.01	34.46	87.21	9.799
34.46	40.00	79.35	10.529
40.00	45.07	85.12	9.983
45.07	49.94	87.14	9.806
49.94	55.01	89.45	9.610
55.01	60.16	91.61	9.434
60.16	65.47	97.39	8.996
65.47	71.51	89.59	9.598
71.51	77.11	122.63	7.484
77.11	85.94	99.98	8.812
85.94	97.66	153.36	6.219

TABLE VI-6

REFLECTOR #8 CALIBRATION - ASSEMBLY I-E
(350°F)

Reflector No. 8 (cm)		Period (sec)	Reactivity (¢)
From	To		
01.03	09.10	161.29	5.960
09.10	17.03	110.51	8.139
17.03	23.72	101.13	8.733
23.76	29.04	114.41	7.916
29.04	34.01	110.66	8.131
34.01	39.17	99.69	8.832
39.17	44.13	102.72	8.626
44.13	48.71	106.76	7.987
48.71	53.98	96.08	9.091
53.98	58.89	113.40	7.973
58.89	64.15	110.08	8.165
64.15	70.02	107.63	8.313
70.02	76.03	125.23	7.357
76.03	82.87	147.16	6.438
82.87	90.03	201.26	4.928
90.03	98.18	317.68	3.280

TABLE VI-7

REFLECTOR #3 CALIBRATION - ASSEMBLY I-E
(650°F)

Reflector No. 3 (cm)		Period (Sec)	Reactivity (¢)
From	To		
0.43	8.52	132.03	7.044
8.52	15.98	100.00	8.811
15.98	22.98	78.93	10.571
22.98	29.05	78.49	10.615
29.05	34.32	83.54	10.126
34.32	39.16	87.59	9.767
39.16	43.71	93.93	9.253
43.71	48.20	96.24	9.079
48.20	52.66	98.98	8.882
52.66	57.20	102.02	8.673
57.20	62.00	100.72	8.761
62.00	67.00	110.10	8.163
67.00	72.20	115.00	7.883
72.20	78.01	123.52	7.440
78.01	84.01	165.22	5.839
84.01	91.01	212.12	4.706
91.01	97.66	462.48	2.319

TABLE VI-8

REFLECTOR #8 CALIBRATION - ASSEMBLY I-E
(650°F)

Reflector No. 8 (cm)		Period (sec)	Reactivity (¢)
From	To		
01.03	10.17	117.58	7.743
10.17	16.38	130.28	7.122
16.38	21.91	120.61	7.585
21.91	26.00	155.67	6.141
26.00	30.97	109.36	8.208
30.97	34.83	140.95	6.674
34.83	39.85	94.35	9.221
39.85	44.01	120.61	7.585
44.01	48.77	103.73	8.560
48.77	53.60	101.42	8.713
53.60	58.55	103.88	8.550
58.55	63.72	106.90	8.358
63.72	69.40	108.35	8.269
69.40	75.55	118.59	7.690
75.55	82.38	135.04	6.915
82.38	90.09	187.84	5.231
90.09	98.18	448.97	2.384

TABLE VI-9

REFLECTOR #8 CALIBRATION - ASSEMBLY I-F
(350°F)

Reflector No. 8 (cm)		Period (sec.)	Reactivity (¢)
From	To		
1.03	9.14	99.2	6.588
9.14	17.73	66.6	9.090
17.73	24.35	67.3	9.016
24.35	30.30	68.5	8.892
30.30	35.36	70.5	8.693
35.36	40.18	71.4	8.606
40.18	44.93	70.4	8.702
44.93	49.53	77.4	8.070
49.53	54.06	83.2	7.613
54.06	59.88	61.8	9.633
59.88	66.27	60.4	9.804
66.27	72.64	70.7	8.673
72.64	80.02	74.7	8.303
80.02	88.50	95.1	6.823
88.50	98.18	186.8	3.805

APPENDIX VII

INHERENT SOURCE MEASUREMENT

A series of measurements were performed in the initial critical core Assembly I-A and in the fully loaded core, Assembly I-D to determine the relationship between steady-state detector readings (power) and reflector position (subcritical reactivity) in a near critical core. These measurements served two purposes. They experimentally established flux levels (instrument readings) for which the source contribution was insignificant and the reactor could be considered critical when the steady state flux levels were greater than or equal to the established value. In addition the measurements provided a means for determining the strength of the inherent source - or conversely of estimating the absolute power level. The results are shown in Table VII-1 and VII-2. (The indicated subcritical reactivity of the systems were obtained from the respective reflector calibration data using a four point difference formula.)

The data show that both systems are critical for all steady-state wide range monitor (WRM) readings greater than $\sim 50 \times 10^{-5}$ and that the product of the WRM reading and the subcritical reactivity is essentially constant. The latter result is in agreement with theory and provides a means of relating the WRM readings to the reactor power and the inherent source of neutrons resulting from the spontaneous fission of Pu-240 and the alpha-neutron reaction in oxygen from Pu-239 and Pu-240 alpha decay.

A modal one-energy-group analysis (Appendix IV) for a system containing a constant source of neutrons per unit core volume provides

the following relationship between the total power, P, in watts, the
total source of neutrons per second, S, and the subcritical reactivity
k (in cents) in a near critical core:

$$P = \frac{100 \, S}{\nu k \beta C} \, F$$

where ν = 2.94 is the average number of neutrons per fission, β = 0.0032
is the effective delayed neutron fraction, C = 3 x 10^{10} fissions per
W-sec, and F is the square of the core average of the fundamental flux
shape divided by the average of the square of the fundamental flux
shape. For SEFOR, F $\simeq$ 0.9, and the above expression can be written as

$$P = 3.2 \times 10^{-7} \, \frac{S}{k}$$

where the power P, source S, and subcritical reactivity are in units of
watts, neutrons/sec, and cents, respectively.

The above expression corresponds to the measured relations (Table
VII-1 and VII-2) between WRM reading, ϕ, and reactivity k:

$$\phi = A/k$$

where A = 11.6 x 10^{-6} for Assembly I-A and has a value of 9.8 x 10^{-6}
for Assembly I-D.

Thus, if the source strength is known, the relation between WRM
reading and power can be determined. Conversely, if the relation between
WRM reading and power is known, the inherent source can be determined.
It may be possible to determine the latter relation after the heat
balances have been performed and the instruments have been calibrated.

An approximate value for the source strength can be calculated.

According to a previous study[27] the source is given (within an estimated uncertainty of a factor of 1.5) by:

$$S = (1.29 \times 10^6 M_1 + 7.8 \times 10^4 M_2) N$$

where N is the number of fuel rods; M_1 = 0.0493 kg/rod is the Pu-240 mass per rod; and M_2 = 0.5489 kg/rod is the Pu-239 mass per rod. For the 550 rod core, $S = 5.9 \times 10^7$ neutrons/sec and the calculated power level for a WRM reading of 50×10^{-5} is 810 watts. If the values from the 634 rod Assembly I-D are used, $S = 6.8 \times 10^7$ neutrons/sec and the calculated power level for a WRM reading of 50×10^{-5} is 1100 watts.

TABLE VII-1

INHERENT SOURCE MEASUREMENT (ASSEMBLY I-A)

Wide Range Monitor Reading	No. 3 Reflector Position (cm)	Temperature (°F)	Subcritical Reactivity** at 351.25°F (Cents)	Product of Subcritical Reactivity and Wide-Range-Monitor Reading [(cents) x 10^6]
40×10^{-8}	62.36	351.5	26.90	10.8
8×10^{-7}	71.10	351.5	13.70	11.0
15×10^{-7}	75.61	351.5	7.84	11.8
42×10^{-7}	79.70	351.0	2.76	11.6
8.3×10^{-6}	80.93	351.0	1.49	12.3
14.5×10^{-6}	81.35	350.75	0.88	12.8
28×10^{-6}	81.99	351.0*	0.44	12.4
53×10^{-6}	82.44	351.25	0.20	10.4
25×10^{-5}	82.60	351.25	0.05	11.8
50×10^{-5}	82.65	351.25	0.00	--
7.5×10^{-4}	82.65	351.25	0.00	--

Average = 11.6

*Adjusted to provide agreement with theory. The recorded value of 351.25°F gives a value for the product in the last column of 17.5

**Using the estimated temperature coefficient for this assembly of -0.74¢/°F.

TABLE VII-2

INHERENT SOURCE MEASUREMENT (ASSEMBLY I-D)

Wide Range Monitor Reading	No. 8 Reflector Position (cm)	Temperature (°F)	Subcritical Reactivity** at 375.0°F (cents)	Product of Subcritical Reactivity and wide=Range-Monitor Reading [(cents) x 10^6]
39×10^{-8}	45.60	375.0	25.87	10.1
50×10^{-8}	48.56	375.0	20.42	10.2
6.2×10^{-7}	51.64	375.0	14.83	9.2
8.0×10^{-7}	53.26	375.0	11.90	9.5
18.0×10^{-7}	57.00	375.0	5.25	9.5
24.4×10^{-7}	57.73	375.0	3.99	9.7
34.0×10^{-7}	58.29	375.0	3.04	10.3
48.0×10^{-7}	58.90	374.75	1.86	8.9
7.5×10^{-6}	59.24	374.75	1.29	9.7
15.0×10^{-6}	59.59	374.75	0.71	10.7
29.0×10^{-6}	59.82	374.75	0.33	9.6
49.0×10^{-6}	59.83	374.5	0.16	7.8
20.0×10^{-5}	59.93	374.5*	0.0	-----
32.0×10^{-5}	60.11	375.0	0.0	-----
49.0×10^{-5}	60.11	375.0	0.0	-----
44.0×10^{-4}	60.11	375.0	0.0	-----

Average = 9.8

*Adjusted to provide agreement with theory. The recorded value of 374.75°F gives a value for the product in the last column of 30.0.

**Using the measured temperature coefficient for this assembly of -0.60¢/°F.

APPENDIX VIII

TEMPERATURE DEPENDENT REACTIVITY DATA IN ASSEMBLY I-E

The recorded values of the reflector positions and the coolant temperature as indicated by the in-core thermocouple are tabulated in Tables VIII-1 through VIII-10. The temperatures recorded with the other temperature detectors are compared with the in-core thermocouple in Section 7.3.2. The reactivity feedback was determined from the positions of the calibrated fine reflectors and is listed in the last column of the tables.

During the performance of the experiment, one of the coarse reflectors had to be completely raised and another had to be partially raised. This required the use of different fine reflector calibration curves during different portions of the experiment. The calibration curves for Assembly I-E at 350°F were used for reflector #8 between reading number 1 and reading number 33 and for reflector #3 between reading number 34 and reading number 43. The calibration curve for Assembly I-E at 650°F was used for reflector #8 between reading number 34 and reading number 283, since the calibration of reflector #8 at 650°F was performed with reflector #10 in the same position – completely raised – (see Section 3.3.2) as these measurements were performed. This choice of calibration curves should minimize the "shadowing" effects discussed in Section 3.

The differential worth of a fine reflector near the midpoint of its stroke, or 1.9¢/cm, was used to adjust the reactivities for the drift of reflector #5 away from 50.0 cm between some of the measurements subsequent to reading number 117. Since these corrections

are small (< 1¢), the exact differential worth of reflector #5 is not required.

In order to obtain one composite set of integral reactivity feedback data such as that listed in Tables VIII-1 through VIII-10, the reactivity data obtained from the fine reflector calibration curves had to be renormalized whenever the coarse reflector configuration was changed. Such renormalizations were required between reading number 33 and 34, and again between reading number 116 and 117. These normalizations were performed by requiring that a fitted curve (a straight line in this case) describe a continuous relationship between reactivity and temperature through the change over point between the different coarse reflector configurations. In addition to the normalizations just described, the composite integral set of data was normalized to a temperature of 350°F by adjusting the data so that the linearly extrapolated reactivity at 350°F was zero.

TABLE VIII-1

TEMPERATURE - REACTIVITY MEASUREMENTS

Reading Number	Reflector Positions*(cm) #8	Coolant Temperature (°F)	Negative Reactivity** Feedback (cents)
1	40.80	353.5	2.5
2	41.00	354.75	2.8
3	41.72	356.5	4.1
4	42.78	359.5	5.9
5	43.67	360.5	7.4
6	44.58	363.75	9.0
7	45.98	366.75	11.5
8	46.66	370.0	12.7
9	48.76	373.0	16.3
10	49.65	379.0	17.9
11	51.63	381.0	21.3
12	52.56	384.25	22.9
13	54.86	389.25	26.8
14	55.95	393.75	28.6
15	58.19	398.5	32.2
16	60.34	403.5	35.6
17	62.73	409.0	39.3
18	65.48	415.5	43.4
19	68.21	421.25	47.3
20	70.79	426.75	50.8
21	74.00	432.75	54.8
22	77.40	437.5	58.6
23	81.06	443.5	62.1
24	84.74	448.0	65.0
25	88.03	450.75	67.3
26	88.94	451.75	67.9
27	89.24	452.0	68.1
28	89.24	451.75	68.1
29	89.10	451.75	68.0
30	88.98	451.75	67.9

* Reflectors #5 and #10 were down, all other reflectors were up.
** Relative to 350°F.

TABLE VIII-2

TEMPERATURE - REACTIVITY MEASUREMENTS

Reading Number	Reflector Positions*(cm) #3	#8	Coolant Temperature (°F)	Negative Reactivity Feedback (cents)
31	up	89.12	451.75	68.0
32	up	89.12	451.75	68.0
33	up	89.12	451.75	68.0
34*	75.55	1.03	451.75	67.9
35	75.64	1.03	451.75	68.0
36	75.74	1.03	453.0	68.1
37	78.82	1.03	456.75	71.8
38	80.61	1.03	461.0	73.8
39	84.21	1.03	466.0	77.2
40	86.04	1.03	469.25	78.7
41	88.78	1.03	472.5	80.7
42	94.07	1.03	476.25	83.6
43	up	3.99	483.0	87.0
44	up	7.77	488.0	90.3
45	up	11.88	492.5	94.4
46	up	15.16	497.75	98.2
47	up	16.65	502.75	100.1
48	up	20.29	507.0	105.0
49	up	20.29	511.5	105.0
50	up	22.28	516.25	107.9
51	up	26.21	519.75	113.8
52	up	26.57	524.5	114.4
53	up	28.55	528.25	117.6
54	up	28.55	530.0	117.6
55	up	31.45	535.0	122.5
56	up	32.50	539.5	124.3
57	up	33.40	540.25	125.8
58	up	34.95	546.75	128.6
59	up	35.90	549.5	130.3
60	up	36.41	551.0	131.2

* Reflectors #5 and #10 were both down prior to Reading Number 34.
  For Reading Number 34, reflector #5 was down and reflector
  #10 was up. All other reflectors were up.
** Relative to 350°F.

TABLE VIII-3

TEMPERATURE - REACTIVITY MEASUREMENTS

Reading Number	Reflector Positions*(cm) #8	Coolant Temperature (°F)	Negative Reactivity** Feedback (cents)
61	36.89	551.5	132.1
62	36.89	551.25	132.1
63	36.54	550.0	131.5
64	36.38	549.5	131.2
65	36.19	549.0	130.8
66	36.35	549.5	131.1
67	36.57	550.0	131.1
68	36.57	550.5	131.5
69	36.76	551.25	131.9
70	37.55	554.0	133.3
71	38.66	556.25	135.4
72	39.65	559.5	137.2
73	40.61	562.75	139.0
74	41.55	567.5	140.7
75	42.78	569.75	142.9
76	43.99	573.75	145.1
77	45.13	577.0	147.2
78	45.97	581.0	148.7
79	47.23	584.25	151.0
80	48.64	588.0	153.5
81	49.60	591.25	155.2
82	50.84	594.75	157.5
83	51.62	597.75	158.9
84	52.73	600.5	160.9
85	53.84	603.75	162.9
86	54.79	606.25	164.5
87	55.40	608.75	165.6
88	56.52	611.25	167.5
89	57.01	613.75	168.4
90	58.24	616.25	170.5

* Reflector #5 was down, all other reflectors were up
** Relative to 350°F.

TABLE VIII-4

TEMPERATURE - REACTIVITY MEASUREMENTS

Reading Number	Reflector Positions*(cm) #5	#8	Coolant Temperature (°F)	Negative Reactivity* Feedback (cents)
91	down	59.00	618.75	171.7
92	down	59.79	621.25	173.1
93	down	60.34	623.25	174.0
94	down	61.12	625.0	175.2
95	down	62.13	627.75	176.8
96	down	63.18	629.75	178.5
97	down	64.18	631.5	180.1
98	down	65.00	634.0	181.3
99	down	65.35	635.5	181.8
100	down	66.00	637.75	182.8
101	down	67.47	639.75	184.9
102	down	68.46	641.75	186.3
103	down	69.56	--	187.8
104	down	69.56	645.0	187.8
105	down	70.96	--	189.7
106	down	71.35	649.0	190.2
107	down	72.03	650.25	191.1
108	down	72.64	651.0	191.8
109	down	72.63	651.5	191.8
110	down	72.63	651.5	191.8
111	down	72.86	652.0	192.1
112	down	73.00	652.0	192.3
113	down	73.14	652.0	192.5
114	down	73.23	652.75	192.6
115	down	73.13	652.25	192.4
116	down	72.4	650.0	191.5
117	50.0	28.07	649.5	190.5
118	50.0	28.07	650.25	190.5
119	50.0	28.49	650.25	191.2
120	50.0	29.1	652.0	192.2

* All other reflectors were up
** Relative to 350°F.

226

TABLE VIII-5

TEMPERATURE - REACTIVITY MEASUREMENTS

Reading Number	Reflector Positions*(cm) #5	#8	Coolant Temperature (°F)	Negative Reactivity** Feedback (cents)
121	50.0	29.8	653.5	193.4
122	50.0	30.77	656.25	195.0
123	50.0	31.40	657.5	196.1
124	50.0	32.14	659.5	197.4
125	49.5	32.60	661.25	197.2
126	49.5	33.58	663.5	198.9
127	49.5	34.77	666.25	201.0
128	49.5	35.33	669.0	202.0
129	49.2	36.21	670.5	203.0
130	49.0	36.94	672.75	204.0
131	50.0	36.24	675.25	204.6
132	49.9	37.24	677.5	206.2
133	49.9	38.01	678.75	207.7
134	49.8	39.11	682.5	209.5
135	50.0	39.83	685.0	211.2
136	49.9	41.17	690.0	213.5
137	50.0	42.40	693.0	215.9
138	49.9	43.55	696.0	217.8
139	49.9	44.58	700.0	219.7
140	49.9	45.45	703.5	221.3
141	49.7	46.44	706.75	222.7
142	50.0	47.05	709.5	224.3
143	50.0	47.84	712.25	225.7
144	50.0	48.93	716.0	227.7
145	50.0	49.76	718.75	229.2
146	49.8	50.69	721.75	230.5
147	49.7	51.61	724.5	232.0
148	49.9	51.61	724.5	232.4
149	49.9	52.94	729.5	234.8
150	49.9	53.67	731.5	236.1

* All other reflectors were up
** Relative to 350°F

TABLE VIII-6

TEMPERATURE - REACTIVITY MEASUREMENTS

Reading Number	Reflector Positions*(cm) #5	#8	Coolant Temperature (°F)	Negative Reactivity** Feedback (cents)
151	49.9	54.94	734.5	238.3
152	49.9	55.54	736.75	239.3
153	49.9	56.38	739.0	240.8
154	49.9	56.85	740.75	241.6
155	49.7	57.68	743.0	242.6
156	50.0	56.38	744.5	241.0
157	50.0	58.18	747.0	244.1
158	50.0	58.74	747.5	245.0
159	50.0	59.32	750.0	246.0
160	50.0	60.03	751.25	247.1
161	50.0	60.58	752.75	248.0
162	50.0	61.44	755.0	249.4
163	49.9	61.89	756.0	250.0
164	49.8	62.67	757.75	251.0
165	50.0	62.31	757.5	250.8
166	50.0	62.31	758.25	250.8
167	50.0	63.36	759.0	252.5
168	50.0	63.28	758.75	252.4
169	50.0	62.52	759.0	251.2
170	50.0	62.56	758.75	251.2
171	50.0	62.76	758.75	251.5
172	50.0	62.86	758.5	251.7
173	50.0	63.09	759.0	252.1
174	49.9	63.30	759.0	252.2
175	50.0	62.88	759.0	251.7
176	50.0	63.00	759.25	251.9
177	50.0	63.11	758.75	252.1
178	50.0	63.55	759.0	252.8
179	50.0	63.19	759.25	252.2
180	50.0	62.76	757.0	251.5

---

* All other reflectors were up
** Relative to 350°F.

TABLE VIII-7

TEMPERATURE – REACTIVITY MEASUREMENTS

Reading Number	Reflector Positions* (cm) #5	#8	Coolant Temperature (°F)	Negative Reactivity** Feedback (cents)
181	50.0	59.94	750.0	247.0
182	50.0	57.41	744.25	242.7
183	50.0	55.44	733.25	239.4
184	50.0	53.29	727.50	235.6
185	50.0	51.21	722.0	231.8
186	50.0	50.00	715.25	229.6
187	50.0	47.97	708.25	226.0
188	50.0	46.76	706.75	223.8
189	50.0	47.00	705.5	224.2
190	50.0	46.00	704.25	222.4
191	50.0	46.00	704.5	222.4
192	50.0	46.40	705.25	223.2
193	50.0	47.00	706.5	224.2
194	50.0	47.00	707.0	224.2
195	50.0	47.00	707.0	224.2
196	50.0	47.44	708.0	225.0
197	50.0	47.81	708.25	225.7
198	50.0	47.81	708.5	225.7
199	50.0	47.30	708.25	224.8
200	50.0	47.53	708.0	225.2
201	50.0	47.79	708.0	225.7
202	50.0	47.79	708.0	225.7
203	50.0	48.13	710.5	226.3
204	50.0	48.13	710.5	226.3
205	50.0	47.81	710.5	225.7
206	50.0	47.98	711.0	226.0
207	50.0	.48.24	711.25	226.5
208	50.0	48.34	711.75	226.6
209	50.0	48.43	711.75	226.8
210	50.0	48.43	711.75	226.8

* All other reflectors were up
** Relative to 350°F.

TABLE VIII-8

TEMPERATURE - REACTIVITY MEASUREMENTS

Reading Number	Reflector Positions*(cm) #5	#8	Coolant Temperature (°F)	Negative Reactivity** Feedback (cents)
211	50.0	48.94	712.75	227.7
212	50.0	49.00	714.5	227.8
213	50.0	49.45	716.75	228.6
214	50.0	50.05	718.5	229.7
215	50.0	50.96	720.5	231.4
216	50.0	51.47	722.5	232.3
217	50.0	52.10	724.75	233.4
218	50.0	52.70	726.0	234.5
219	50.0	53.30	727.5	235.6
220	50.0	53.74	729.0	236.4
221	49.9	54.11	730.25	236.8
222	50.0	54.66	731.25	238.0
223	50.0	54.28	732.5	237.3
224	50.0	54.53	733.25	237.8
225	50.0	55.00	733.75	238.6
226	50.0	55.31	734.5	239.1
227	50.0	55.71	735.75	239.8
228	50.0	55.96	736.5	240.3
229	49.9	56.41	736.75	240.8
230	49.9	56.81	738.0	241.5
231	49.9	57.21	739.5	242.2
232	50.0	57.31	740.5	242.6
233	50.0	57.91	742.0	243.6
234	49.9	58.48	743.5	244.4
235	49.8	59.12	745.0	245.3
236	50.0	59.03	746.0	245.5
237	50.0	59.26	746.5	245.9
238	50.0	59.61	748.0	246.4
239	49.9	60.02	748.5	246.9
240	49.9	60.36	749.0	247.5

* All other reflectors were up
** Relative to 350°F.

TABLE VIII-9

TEMPERATURE - REACTIVITY MEASUREMENTS

Reading Number	Reflector Positions*(cm) #5	#8	Coolant Temperature (°F)	Negative Reactivity** Feedback (cents)
241	49.9	60.73	749.5	248.1
242	49.9	61.03	750.0	248.6
243	49.9	61.33	750.5	249.1
244	49.7	61.44	751.25	248.9
245	50.0	60.87	751.75	248.5
246	50.0	60.99	752.0	248.7
247	50.0	61.03	752.0	248.8
248	50.0	61.40	752.0	249.4
249	50.0	61.20	752.5	249.0
250	50.0	61.2	751.5	249.0
251	50.0	61.5	752.5	248.7
252	50.0	61.5	752.5	249.5
253	50.0	61.6	752.5	249.7
254	49.6	61.81	752.5	249.3
255	50.0	60.68	751.75	248.2
256	50.0	60.80	751.25	248.4
257	50.0	60.98	752.0	248.7
258	50.0	60.98	752.0	248.7
259	50.0	60.98	752.0	248.7
260	50.0	61.10	751.25	248.9
261	50.0	61.10	752.0	248.7
262	49.9	61.23	750.5	248.9
263	50.0	60.45	750.25	247.8
264	50.0	60.37	750.0	247.7
265	50.0	60.37	749.25	247.7
266	50.0	60.25	749.5	247.5
267	50.0	59.96	749.5	247.0
268	50.0	60.08	749.25	247.2
269	50.0	60.36	749.75	246.7
270	50.0	60.19	749.75	247.4

---

* All other reflectors were up
** Relative to 350°F.

TABLE VIII-10

TEMPERATURE - REACTIVITY MEASUREMENTS

Reading Number	Reflector Positions*(cm) #5	#8	Coolant Temperature (°F)	Negative Reactivity** Feedback (cents)
271	50.0	60.88	750.5	248.5
272	50.0	61.11	751.25	248.9
273	50.0	62.17	753.5	250.6
274	50.0	63.24	757.0	252.3
275	50.0	63.76	758.75	253.1
276	50.0	64.03	759.25	253.5
277	50.0	64.27	760.0	253.9
278	50.0	63.56	759.5	252.8
279	50.0	63.91	759.5	253.3
280	50.0	63.98	759.75	253.4
281	50.0	64.16	759.75	253.7
282	50.0	64.16	759.5	253.7
283	50.0	64.31	759.5	253.9

---

* All other reflectors were up.
** Relative to 350°F

REFERENCES

SECTION I

1. G. R. Pflasterer, "SEFOR Experimental Program Planning, Volume 1 Specifications for the Plant and Experimental Equipment" GEAP-5092, August 1966.

2. G. R. Pflasterer and L. Caldarola, "SEFOR Experimental Program Planning, Volume II Descriptions of Planned Tests, GEAP-5092, August 1966.

3. L. D. Noble, G. R. Pflasterer, C. D. Wilkinson, and L. Caldarola, "Recent Developments in the SEFOR Experimental Program" Proceedings of the International Conference on Fast Critical Experiments and Their Analysis October 10-13, 1966; ANL-7320.

4. L. D. Noble and C. D. Wilkinson, "Final Specifications for the SEFOR Experimental Program"; GEAP-5576, January 1968.

5. G. Billuris, et.al., "SEFOR Plant Design" Fast Reactors National Topical Meeting, San Francisco, April 1967, ANS-101.

6. R. A. Meyer, et al., "Design and Analysis of SEFOR Core I", (GEAP to be issued)

7. "Southwest Experimental Fast Oxide Reactor Development Program, Ninth Quarterly Report, May-July 1966"; GEAP-5208, August 1966.

8. "Southwest Experimental Fast Oxide Reactor Development Program, Tenth Quarterly Report, August-October 1966"; GEAP-5301, November 1966.

9. "Southwest Experimental Fast Oxide Reactor Development Program, Eleventh Quarterly Report, November 1966-January 1967"; GEAP-5442, February 1967.

10. "Southwest Experimental Fast Oxide Reactor Development Program, Nineteenth Quarterly Report, November 1968-January 1969"; GEAP-5754, February 1969.

11. A.B. Reynolds and S. L. Stewart, "Analysis of the SEFOR Mockup Critical Experiments in ZPR-3", GEAP-5294, March 1967.

12. "Southwest Experimental Fast Oxide Reactor Development Program, Twelfth Quarterly Report, February-April 1967"; May 1967.

13. "Southwest Experimental Fast Oxide Reactor Development Program, Twenty-First Quarterly Report, May-July 1969", GEAP-10010-21, August 1969.

REFERENCES (Continued)

SECTION I (Cont'd)

14. G. R. Pflasterer, et.al., "Investigation of Low Plutonium Content in SEFOR Fuel", (GEAP-13576 to be issued).

15. E. R. Craig, "SEFOR Instrumented Fuel Assembly Design and Development", GEAP-5615, April 1968.

SECTION II

1. R. L. McVean, et.al., "Critical Studies of the Southwest Experimental Fast Oxide Reactor (SEFOR) in ZPR-3 (Assembly 47)", ANL-7248, March 1967.

2. A. B. Reynolds and S. L. Stewart, "Analysis of the SEFOR Mockup Critical Experiments in ZPR-3", GEAP-5294, March 1967.

3. H. Küsters, et.al., "Analysis of Fast Critical Assemblies and Large Fast Power Reactors with Group Constant Sets Recently Evaluated at Karlsruhe", Winter Meeting of ANS, Washington, D. C. Nov. 10-15, 1968.

4. W. Y. Kato, et. al., "Measurement of Reaction Ratio and Neutron Spectra in a Soft Spectrum Fast Reactor", Winter Meeting of A.N.S., Washington, D. C. Nov. 10-15, 1968.

5. H. H. Hummel, "Correlation, Evaluation and Interpretation of Integral Data", ANL Reactor Physics Division, Progress Report for September 1968.

6. "ENDF/B Summary Documentation", ENDF Newsletter, Volume 3, No.2, Brookhaven National Laboratory, National Neutron Cross Section Center, October 2, 1967.

7. R. Protsik and E. G. Leff, "Users Manual for DOT2DB: A Two-Dimensional Multigroup Discrete Ordinates Transport/Diffusion Code with Anisotropic Scattering", GEAP-13537, September 1969.

8. P. Greebler, et.al., "BISYN - A Two-Dimensional Synthesis Program", GEAP-4922, July 1965.

REFERENCES (Continued)

SECTION II (Cont'd)

9. R. Protsik, "Transport vs. Diffusion Theory in Large Fast Reactor Calculations", Conference on Review of the Discrete Ordinates S_N Method for Radiation Transport Calculations, Oak Ridge National Laboratory, March, 1968, ORNL-RSIC-19.

10. R. Protsik and J. M. Kelley, "SN1D - A One-Dimensional Discrete Ordinates Transport Code with General Anisotropic Scattering", GEAO-0064, September 1964.

11. R. A. Harris, "A Preliminary Study of the Heterogeneous Effects in the FTR and FTR Critical Mockup", BNWL-CC-963, Battelle-Northwest Laboratories (1967).

12. D. Wintzer, Kernforschungzentrum, Karlsruhe, Germany, Private Communication.

13. S. L. Stewart, G.E. - BRDO, Private Communication.

14. L. P. Abagyan, et al., "Group Constants for Nuclear Reactor Calculations", Consultants Bureau, New York, 1964.

15. B. A. Hutchins, "The ENDRUN Code - General Description", G.E. - BRDO memo, June 11, 1968.

16. G. R.Pflasterer, et. al., "Investigation of Low Plutonium Content in SEFOR Fuel", (GEAP-13576 to be issued).

SECTION III

1. "Southwest Experimental Fast Oxide Reactor Development Program, Nineteenth Quarterly Report, November 1968-January 1969", GEAP-5754, February 1969.

2. L. D. Noble and C. D. Wilkinson, "Final Specifications for the SEFOR Experimental Program", GEAP-5576, January 1968.

3. A. B. Reynolds and S. L. Stewart, "Analysis of the SEFOR Mockup Experiments in ZPR-III", GEAP-5294, March, 1967.

4. R. Protsik and E. G. Leff, "Users Manual of DOT2DB: A Two-Dimensional Multigroup Discrete Ordinates Transport/Diffusion Code with Anisotropic Scattering", GEAP-13537, September 1969.

REFERENCES (Continued)

SECTION III (Continued)

5. "Southwest Experimental Fast Oxide Reactor Development Program, Eighth Quarterly Report, February-April, 1966, GEAP-5160, May 1966.

6. G. R. Keepin, "Physics of Nuclear Kinetics", Addison-Wesley, Palo Alto, 1965.

SECTION IV

1. G. R. Pflasterer, et. al., "Investigation of Low Plutonium Content in SEFOR Fuel (GEAP-13576 to be issued).

2. R. Protsik, "Users Manual for DOT2DB: A Two-Dimensional Multigroup Discrete Ordinates Transport/Diffusion Code with Anisotropic Scattering", GEAP-13537, September 1969.

3. P. Greebler, et.al., "BISYN - A Two-Dimensional Synthesis Program", GEAP-4922, July 1965.

SECTION V

1. W. F. Welsh, "Determination of Absolute Power in SNAP-50 Critical Assemblies by Ba-140 Fission Product Measurements,"PWAC 474, July, 1965.

2. P. Greebler, et.al, "BISYN - A Two-Dimensional Synthesis Program", GEAP-4922, July 1965.

3. R. Protsik and E. G. Leff, "Users Manual for DOT2DB: A Two-Dimensional Multigroup Discrete Ordinates Transport/Diffusion Code with Anisotropic Scattering", GEAP-13537, September 1969.

4. "Southwest Experimental Fast Oxide Reactor Development Program, Twenty-First Quarterly Report, May-July, 1969"; GEAP-10010-21, August 1969.

5. "Southwest Experimental Fast Oxide Reactor Development Program, Tenth Quarterly Report, August-October 1966", GEAP-5301, November 1966.

6. "Southwest Experimental Fast Oxide Reactor Development Program, Twelfth Quarterly Report, February-April 1967", GEAP-5498, May, 1967.

REFERENCES (Continued)

SECTION VI

1. R. P. Morrell,"SEFOR β/ℓ Measurements by Noise Analysis Techniques IDO-17210 August 1966.

2. J. P. Dragt, "Reactor Noise, A Study of Neutronic Fluctuations in Low Power Nuclear Reactors with Special Emphasis on Accurate Time Domain Analysis", RCN Report RCN-101.

3. B. C. Diven et.al.,"Multiplicities of Fission Neutrons," Phys. Rev. 1956, Vol. 101., No. 3.

4. A. I. Mogilner et.al., "Experimental Study of Neutron Detectors Frequency Responses ", RCN-REport 98, July 1968.

5. W. Seifritz, " The Polarity Correlation of Reactor Noise in the Frequency Domain", Nuclear Applications & Technology Vol.7, Dec. 1969.

6. G. S. Brunson and R. I. Huber, " Precision Pulsed Measurements with Reflected Fast Critical Assemblies", ANL-7320, Proc. of the Int. Conf. on Fast Critical Exp. and Their Analysis, Oct.10-13, 1966.

7. A. B. Reynolds and S. L. Stewart, "Analysis of the SEFOR Mockup Critical Experiments in ZPR-3", GEAP-5294, March 1967.

SECTION VII

1. L. D. Noble and C. D. Wilkinson, "Final Specifications for the SEFOR Experimental Program", GEAP-5576, January 1968.

2. "Southwest Experimental Fast Oxide Reactor Development Program Twentieth Quarterly Report, February-April 1969", GEAP-10010, May 1969.

3. "Southwest Experimental Fast Oxide Reactor Development Program, Twenty-First Quarterly Report, May-July, 1969", GEAP-10010-21, August 1969.

4. "Southwest Experimental Fast Oxide Reactor Development Program, Twenty-Second Quarterly Report, August-October 1969, GEAP-10010-22, December 1969.

5. "Southwest Experimental Fast Oxide Reactor Development Program, Twenty-Third Quarterly Report, November 1969-January 1970", GEAP-10010-23, February 1969.

REFERENCES (Continued)

SECTION VII (Cont'd)

6. R. A. Meyer, et al., "Design and Analysis of SEFOR Core I",
    (GEAP to be issued)

7. P. Greebler, et.al., "BISYN - A Two-Dimensional Synthesis
    Program", GEAP-4922, July 1965.

APPENDICES

1. "Sodium-Cooled Reactors Fast Ceramic Reactor Development Program,
    Twenty-Seventh Quarterly Report, May-July 1968", GEAP-5671,
    August 1968.

2. S. L. Stewart, G.E. -BRDO, Private Communication.

3. G. I. Bell, "A Single Treatment for Effective Resonance Absorption
    Cross Sections in Dense Lattices", Nuc. Sec. and Eng. 5, Pg.138,
    (1959)

4. L. B. Abagyan, et.al., "Group Constants for Nuclear Reactor
    Calculations", Consultants Bureau, New York, 1954.

5. B. A. Hutchins', The ENDRUN Code - General Description", G.E. -
    BRDO Memo, June 11, 1968.

6. "ENDF/B Summary Documentation, "ENDF Newsletter, Vol.3, No. 2.,
    Brookhaven National Laboratory, National Neutron Cross Section
    Center, October 2, 1967.

7. P. H. White, J. G. Hodgkinson, G. L. Wall, "Measurements of Fission
    Cross Sections for Neutrons of Energies in the Range 40-500 keV",
    Proc. Conf. on Physics and Chemistry of Fission, IAEA, Salzburg,
    Austria, EANDC(UK) 535, (1964).

8. R. Gwin, et al., "Measurements of the Neutron Fission and Absorption
    Cross Section of Pu-239 Over the Energy Region 0.01 eV to 30 keV",
    NPD Annual, May 15, 1968.

9. R. N. Evatt, "Pu-239 Resonance Parameters in the Unresolved Region,"
    G. E. Memo to B. A. Hutchins, November 8, 1968.

REFERENCES (Continued)

APPENDICES (Cont'd)

10. J. B. Garg, et al, *Phys. Rev. 135*, B985 (1964)

11. K. H. Beckurts, et al, "Neutron Capture and Fission Cross Section Data in the keV Energy Range,"Fast Reactor Physics Conf., Karlsruhe, Germany, October 30 - November 3, 1967, SM-101/9.

12. J. F. Barry, J. Bunce, P.H. White, "Cross Section for the Reaction $^{238}U(n, \gamma)^{239}U$ in the Energy Range 0.12-7.6 MeV," *J. Nucl. Energy 18*, 481 (1964).

13. D. H. Byers, et al., "Fission Cross Sections from Petrel", LA-3586, p. 59 (1966).

14. T. A. Pitterle, E. M. Page, M. Yamamoto, "Analysis of Sodium Reactivity Measurements," Volumes I and II, Atomic Power Dev. Associates, Inc., APDA-216, June 1968.

15. H. Küsters, et al., "Analysis of Fast Critical Assemblies and Large Fast Power Reactors with Group Constant Sets Recently Evaluated at Karlsruhe", Winter Meeting of American Nuclear Society, Washington, D. C., November 10-15, 1968.

16. W. Y. Kato, et al., "Measurement of Reaction Ratios and Neutron Spectra in a Soft Spectrum Fast Reactor," Winter Meeting of American Nuclear Society, Washington, D. C., November 10-15, 1968.

17. H. H. Hummel, "Correlation, Evaluation and Interpretation of Integral Data," ANL Reactor Physics Division, Progress Report for September, 1968.

18. B. A. Zolotar, B. R. Gehgal, J. M. Kallfetz, "Fast Reactor Integral Studies of Modifications to ENDF/B U-238 Inelastic Scattering", American Nuclear Society Winter Meeting, San Francisco, December 1969.

19. N. W. Glass, et al., "U-238 Neutron Capture Results from Bomb Source Neutrons", Conf. of Neutron Cross Sections and Technology, Washington, D. C., March 4-7, 1968.

20. C. D. James, TRDWP/P30, 1965; or AERE-PR/NP6, 1964.

21. E. Barnard, et al, "Scattering of Fast Neutrons by U-238", International Conference on Study of Nuclear Structure with Neutrons, Antwerp, Belgium, EANDC-50-S, P/26 (1965).

REFERENCES (Continued

APPENDICES (Cont'd)

22. P. Benoist, "Theorie du Coefficient de Diffusion des Neutrons dans un Reasau Comportant des Cavites", CEA-R-2278 (1964)

23. R. Protsik and J. M. Kelley, "SN1D - A One-Dimensional Discrete Ordinates Transport Code with General Anisotropic Scattering", GEAO-0064, September 1964.

24. Robley D. Evans, "The Atomic Nucleus", McGraw-Hill, New York, (1955).

25. P. Greebler, et al, "BISYN - A Two-Dimensional Synthesis Program", GEAP-4922, July 1965.

26. G. R. Keepin, "Physics of Nuclear Kinetics", Addison-Wesley, Palo Alto, 1965.

27. L. D. Noble and C. D. Wilkinson, "Final Specifications for the SEFOR Experimental Program", GEAP-5576, January 1968.

ACKNOWLEDGEMENTS

The work reported here is based on the
contributions of several people. The authors
especially wish to acknowledge the contributions
of the following people:

J. Arterburn

P. Greebler

J. H. Haar

B. Hutchins

M. L. Johnson

R. Protsik

C. Russell

S. Stewart

DISTRIBUTION

Division of Technical Information Extension U.S. Atomic Energy Commission P. O. Box 62 Oak Ridge, Tennessee	15
Director Research and Development Division U. S. Atomic Energy Commission Richland Operations Office P. O. Box 550 Richland, Washington 99352	1
Mr. G. Vendryes Cen Saclay Boite Postale 2 Gif-Sur-Yvette (S et O) France	10
Dott, Ing. F. Pierantoni CNEN Viz Mazzini 2 Bologna, Italy	4
Chief Fuel Fabrication Branch DRD&T, USAEC Washington, D. C. 20545	1
Mr. F. W. Lewis, President Lousiana Power and Light Company 142 Delaronde Street New Orleans, Louisiana 70114	1
Mr. R. C. Green, President Missouri Public Service Co. 10700 East 50 Highway Kansas City, Missouri	1
Mr. L. J. Cucullu, President New Orleans Public Service Inc. 317 Baronne Street New Orleans, Louisiana 70160	1
Mr. B. S. Jeffrey, President Kansas Power and Light Company 808 Kansas Avenue Topeka, Kansas 66601	1
Mr. J. Robert Welsh Chairman of the Board Southwestern Electric Power Company P. O. Box 1106 Shreveport, Louisiana 71102	1
Power Reactor Development Company 1191 First Street Detroit, Michigan 48226	1

Project Manager FFTF Project Pacific Northwest Laboratory Richland, Washington 99352	5
Chief, Fuels and Materials Branch DRD&T, USAEC Washington, D. C. 20545	1
Assistant Director for Reactor Projects Division of Reactor Licensing DRD&T, USAEC Washington, D. C. 20545	1
Director Los Alamos Scientific Laboratory Los Alamos, New Mexico 87544	3
Dr. John C. Woodhouse 21 Woodbrook Circle Wilmington, Delaware 19803	1
Senior Representative U.S. Mission to EURATOM Communities c/o U. S. Embassy Brussels, Belgium	3
Chief, Liquid Metal Project Branch DRD&T, USAEC Washington, D. C. 20545	1
Asst. Director for Nuclear Safety DRD&T, USAEC Washington, D. C. 20545	1
Director, Contracts Division U. S. Atomic Energy Commission San Francisco Operations Office 2111 Bancroft Way Berkeley, California 94704	2
F. W. Thalgott Associate Director, Idaho Division Argonne National Laboratory Box 1096 Idaho Falls, Idaho 83401	1
Director, Argonne National Laboratory 9800 South Cass Avenue Argonne, Illinois 60439	2

Chief,	1
Reactor Physics Branch	
DRD&T, USAEC	
Washington, D. C. 20545	

Mr. C. C. Czeschin, President	1
Arkansas-Missouri Power Company	
104 South Fifth Street	
Blytheville, Arkansas 72316	

Mr. T. Flynn — 1
Ebasco Services, Inc.
2 Rector Street
New York City 6, N. Y.

USAEC — 1
Office of RDT Site Representative
310 DeGuigne Drive
Sunnyvale, California 94086
Attn: J. Levy

Director — 1
Liquid Metals Information Center
P. O. Box 309
Canoga Park, California 91305
(Topicals only)

Mr. S. Golan, Project Manager — 2
1000 MWe LMFBR Follow-On Study
Atomics International
P. O. Box 309
Canoga Park, California 91304

Mr. M. W. Croft, Project Manager — 2
1000 MWe LMFBR Follow-On Study
The Babcock & Wilcox Company
5061 Fort Avenue
P. O. Box 1260
Lynchburg, Virginia 24505

Dr. W. P. Staker, Project Manager — 2
1000 MWe LMFBR Follow-On Study
Combustion Engineering, Inc.
P. O. Box 500
Windsor, Connecticut 06095

Mr. C. A. Anderson, Project Manager — 2
1000 MWe LMFBR Follow-On Study
Westinghouse Electric Corporation
Advanced Reactors Division
Waltz Mill Site
P. O. Box 158
Madison, Pennsylvania 15663

Mr. L. W. Fromm, Manager — 2
1000 MWe LMFBR Follow-On Study Project
Building 208
Argonne National Laboratory
9800 South Cass Avenue
Argonne, Illinois 60439

USAEC Scientific Representative — 1
United States Embassy, Box 40
FPO
New York, N. Y. 09510

General Directorate — 10
Research and Training
EURATOM
51-53 Rue Belliard
Brussels, Belgium
Attn: A. DeStordeur

Mr. F. H. Coughlin, Chairman of Board — 1
Central Louisiana Electric Co., Inc.
P. O. Box 111
Alexandria, Louisiana 71301

Mr. John Stewart, President — 1
The Central Kansas Power Company
111 East 11th Street
Hays, Kansas 67601

Mr. Reeves Ritchie, President — 1
Arkansas Power and Light Company
Ninth and Louisiana Street
Little Rock, Arkansas 72203

Mr. J. T. Jones, President — 1
The Empire District Electric Co.
602 Joplin Street
Joplin, Missouri 64802

Mr. Harold E. Mortimer — 1
Vice President
Assistant to Chairman of the Board
Gulf States Utilities Company
P. O. Box 2951
Beaumont, Texas 77704

Mr. C. F. Edwards, Vice President — 1
Western Power Division
Central Telephone & Utilities Corp.
P. O. Box 170
Great Bend, Kansas

Gesellschaft fur Kernforschung m.b.H. — 10
Projekt Schneller Bruter
75) Karlsruhe, Germany
Postfach 947

Director, — 1
LMFBR Program Office
Argonne National Laboratory
South Cass Avenue
Argonne, Illinois 60439

Asst. Director for Plant Engineering — 2
DRD&T, USAEC
Washington, D. C. 20545

243

Asst. Director for Reactor Engineering DRD&T, USAEC Washington, D. C. 20545	2
Brookhaven National Laboratory Associated Universities, Inc. Upton, Long Island, N. Y. 11973 Attn: Dr. C. H. Raseman	1
Project Manager Special Projects Branch DRD&T, USAEC Washington, D. C. 20545	1
Mr. G. W. Evans, President Kansas Gas and Electric Company 201 North Market Street Wichita, Kansas 67201	1
Mr. L. F. C. Reichle Ebasco Services, Inc. 2 Rector Street New York 6, New York	1

Mr. R. B. Wilson, President Mississippi Power and Light Company Electric Building Jackson, Mississippi 39205	1
Mr. Ray W. Call, President Missouri Utilities Company 400 Broadway Cape Girardeau, Missouri 63701	1
Mr. W. A. Parker, President Oklahoma Gas and Electric Company 321 North Harvey Street Oklahoma City, Oklahoma 73101	1
Mr. D. J. Tuepker, Chairman Public Service Company of Oklahoma 600 South Main Street Tulsa, Oklahoma 74102	1